DEVELOPMENT AND APPLICATION OF PROTEOMIC TOOLS TO STUDY PLATELET FUNCTION IN THE CONTEXT OF CARDIOVASCULAR DISEASE

by

Chengcheng Zhang

B.Sc., Shanghai Jiao Tong University, 2008

A THESIS SUBMITTED IN PARTIAL FULFILLMENT OF
THE REQUIREMENTS FOR THE DEGREE OF

DOCTOR OF PHILOSOPHY

in

THE FACULTY OF GRADUATE AND POSTDOCTORAL STUDIES
(Experimental Medicine)

THE UNIVERSITY OF BRITISH COLUMBIA

(Vancouver)

October 2014

Abstract

Cardiovascular diseases (CVDs) are the leading cause of death worldwide. Recent evidence suggests that activated platelets play an important role in promoting the recruitment of leukocytes, particularly monocytes, to damaged endothelium, which leads to formation of atherosclerotic plaques. Lysophosphatidic acid (LPA) accumulates in atherosclerotic plaques, activates additional platelets and amplifies immune response. Therefore, understanding the molecular mechanism of how platelets are activated and the effect of platelet-monocyte aggregate (PMA) formation is key to the design of intervention strategies for CVDs. To achieve this, two novel proteomics tools, i.e. *in silico* protein interaction analysis and quantitative multiplexed small GTPase activity assay, were developed and applied to study platelet functions. Using the former approach, a core network involved in platelet aggregation was identified that consists of integrin αIIb, integrin β3, talin1, fibrinogen α and β chains, Rap1b and other cytoskeletal proteins. Using the latter method, time-resolved activation profiles of ten small GTPases, i.e. Ras, Rho, Rap and Rac isoforms, in platelets in response to thrombin, ADP and LPA were generated. The addition of PI3K inhibitors only reduced the activation levels of Rap1A and Rap1B without affecting other small GTPase isoforms in LPA-induced platelet activation. Moreover, the small GTPase Rac and calcium, but not PI3 kinase or the small GTPase Rho, were found to be key regulators for LPA-induced platelet secretion. Furthermore, PMA formation was significantly increased in THP-1 monocytic cells incubated with thrombin- or LPA-activated platelets. To investigate the signaling changes in this process systematically, a quantitative phosphoproteomics strategy was adapted and optimized for a two-cell system, which revealed several key biological processes in monocytes, including leukocyte activation, small

GTPase activation and cytoskeleton organization. In summary, the research in this thesis has furthered our understanding of platelet function in the context of cardiovascular disease, which might serve as a basis for designing more targeted approaches for antiplatelet therapies. In addition, the proteomics tools we have developed and validated now enable the exploration of new avenues of research, as demonstrated by their successful application to study biological systems.

Preface

A version of section 1.2 has been published. Zhang, C.-C. and Kast, J. (2010) Applications of Current Proteomics Techniques in Modern Drug Design. Curr. Comput. Aided Drug Des. 6(3):147-164. This literature review was primarily written by me, with editing help from my supervisor JK.

A version of chapter 2 has been published. Zhang, C.-C., Rogalski, J. C., Evans, D. M., Klockenbusch, C., Beavis, R. C., and Kast, J. (2011) *In silico* Protein Interaction Analysis Using the Global Proteome Machine Database. J Proteome Res. 10(2): 656-668. I was the primary researcher involved in this project. I developed the method for the *in silico* protein interaction analysis, and tested the method on different biological systems. JCR provided intellectual input on optimization of the method, DME and RCB integrated the method into the Global Proteome Machine Database and CK conducted the integrin β1 pull down experiment validating the method. The manuscript was written primarily by me, with editing help from JCR and JK.

A version of chapter 3 has been submitted for publication. Zhang, C.-C., Lin, S.J., Liu, K., Rogalski, J. C. and Kast, J. Development and Application of Quantitative Multiplexed Small GTPase Activity Assay Using Targeted Proteomics. I was the primary researcher involved in this project. I developed the method for the multiplexed active small GTPase pull-down assay, developed targeted proteomic approaches targeting twelve small GTPase isoforms, and tested the method on platelet activation and aggregation. SJL conducted preliminary targeted proteomic experiment targeting one small GTPase peptide, KL helped conducted experiments testing

platelet functions using inhibitors, JCR provided intellectual input on optimization of the method. The manuscript was written primarily by me, with editing help from JK.

Ethical approval for platelet isolation from whole blood from healthy blood donors was obtained from the Clinical Research Ethics Board at University of British Columbia (H12-00757) and written consent was granted by the blood donors.

Table of Contents

List of Tables

List of Figures

List of Abbreviations

2D-PAGE	two-dimensional polyacrylamide gel electrophoresis
AC	adenylate cyclase
AD	activation domain
ADP	adenosine diphosphate
AP-MS	Affinity Purification Mass Spectrometry
BD	binding domain
CalDAG-GEF1	calcium and DAG-regulated guanine exchange factor 1
cAMP	cyclic adenosine monophosphate
CCL2	Monocyte chemoattractant protein-1
CCL5	regulated on activation, normal T cell expressed and secreted
CE	collision energy
CID	collision-induced dissociation
co-IP	co-immunoprecipitation
COX	cyclooxygenase
CV	coefficient of variation
CVD	Cardiovascular disease
CXCL4	platelet factor 4
DAG	diacylglycerol
DHB	2,5-dihydroxy benzoic acid
DIGE	differential in-gel electrophoresis
ECD	electron capture dissociation
ESI	electrospray ionization
ETD	electron transfer dissociation
f	frequency of occurrence
FBS	Fetal bovine serum
FT-ICR	fourier transform ion cyclotron resonance
FV	fragmentor voltage
GAP	GTPase-activating protein
GDI	guanine nucleotide dissociation inhibitor
GEF	guanine nucleotide-exchange factor
GO	gene ontology
GDP	guanosine diphosphate
GPCR	G-protein coupled receptor
GPIb-IX	glycoprotein Ib-IX
GPMDB	Global Proteome Machine Database
GPVI	glycoprotein VI
GTP	guanosine triphosphate

IC50	50% inhibitory concentration
ICAT	Isotope-coded affinity tags
IL-1β	Interleukin 1beta
IL-8	Interleukin 8
IMAC	Immobilized Metal Affinity Chromatography
IP3	Inositol triphosphate
IPA	Ingenuity Pathway Analysis
IPI	International Protein Index
iTRAQ	Isotope tags for relative and absolute quantification
JAK-STAT	Janus kinase-Signal Transducer and Activator of Transcription
LB	Lysogeny broth
LC	liquid chromatography
LIT	linear ion trap
LPA	Lysophosphatidic acid
m/z	mass-to-charge
MALDI	matrix-assisted laser desorption/ionization
MAPPIT	mammalian protein–protein interaction trap
MCP-1	Monocyte Chemoattractant Protein-1
mDHFR	dihydrofolate reductase
MLC-p	myosin light chain phosphorylation
MRM	multiple reaction monitoring
mRNA	Messenger RNA
MS	mass spectrometry
MS/MS	tandem mass spectrometry
MW	molecular weight
NO	nitric oxide
$P2Y_1$	purinergic receptor P2Y1
$P2Y_{12}$	purinergic receptor P2Y12
PAR1	proteinase-activated receptor 1
PAR4	proteinase-activated receptor 4
PCA	Protein-fragment Complementation Assay
PF4	platelet factor 4
pI	isoelectric point
PI3K	phosphoinositide 3-kinase
PKA	protein kinase A
PKB/Akt	protein kinase B
PKC	protein kinase C
PLC	phospholipase C
PMA	Platelet-monocyte aggregate
ProDis	protein distribution

PSGL-1	P-selectin glyocoprotein ligand-1
PTM	posttranslational modification
PVDF	Polyvinylidene fluoride
QQQ	triple quadrupole
rcf	relative centrifugal force
RANTES	regulated on activation, normal T cell expressed and secreted
RefSeq	Reference Sequence
RIAM	Rap1-interacting adaptor molecule
ROCK	Rho-associated protein kinase
RPMI	Roswell Park Memorial Institute medium
RTA-Y2H	repressed transactivator Y2H
rY2H	reverse Y2H
SCX	strong cation exchange
SILAC	stable isotope labeling by amino acids in cell culture
Std	standard deviation
TAP-MS	Tandem affinity purification mass spectrometry
Thr	thrombin
TiO_2	Titanium Dioxide
TP	thromboxane receptor
TRAP	Thrombin Receptor Activating Peptide
TXA_2	thromboxane A_2
VWF	Von Willebrand factor
Y2H	Yeast Two Hybrid
Y3H	Yeast three hybrid

Acknowledgements

I would like to thank my supervisor Dr. Juergen Kast for his guidance that helped me become an independent scientist. He taught me everything from critical thinking, experimental design to scientific writing. I appreciate his trust in me to pursue my own ideas, his support for my research projects and send me to many international and national conferences.

Also, I would like to thank my supervisory committee members, Dr. Leonard J. Foster, Dr. Kelly McNagny and Dr. Vincent Duronio, for being very supportive of my research and PhD studies. Particularly Dr. Leonard J. Foster for providing me thousands of hours of instrument time on the triple quadrupole and the Orbitrap mass spectrometers.

Throughout my PhD studies, I was extremely lucky to be surrounded by many brilliant scientists and wonderful people, the research in this thesis would not have been possible without their help. Thank-you to Jason C. Rogalski, who has been an awesome teacher and friend, he taught me mass spectrometry inside and out, revised our manuscripts with me side by side and gave me great advice about life; Dr. Geraldine Walsh, one of the most cheerful people I have ever met, for bringing me to the world of platelet biology, showing me how to handle these delicate cell fragments and constantly encouraging me during these six years; Dr. Cordula Klockenbusch for teaching me all the fundamentals about wet-lab work and helping me with experimental design, which set a high standard for my research; Dr. Iris Egner for recruiting blood donors for my research and never let me down; Shujun Lin for technical assistance and patiently training me on how to use various instruments; my platelet team and fellow PhD students Jiqing Huang and Ru Li, and research assistant Kate Liu for their help with my projects, which proved the importance of teamwork, they were an inspiration to me and I have learned a

lot from each one of them; and all other members of our lab for their help and support; also, Dr. Koshi Imami, Dr. Nikolay Stoynov, Dr. Joost Gouw, Jenny Moon, Sarah Michaud and Dr. Lindsay Rogers from Foster Lab for helpful discussion and assistance for my research, they were an amazing group of scientists and made me feel welcomed whenever I was there. As always, thank-you to all blood donors that made the research possible.

I would also like to thank everyone that I got to know and interacted with during courses, seminars, research days and conferences, which has inspired and motivated me and got me to do a lot of extra work.

In addition, I was very grateful and fortunate to receive financial support from Strategic Training Program in Transfusion Science Scholarship from the Centre for Blood Research and funding from the Experimental Medicine Program, which helped me tremendously.

At last but not least, I would like to thank my family, especially my parents, for always being there when I needed, and being patient and believing me unconditionally. Also my wife, Xinchi, for following me to Canada, her courage and understanding means the world to me and will always be cherished.

Dedication

To my parents and my wife

Chapter 1 Introduction

Cardiovascular diseases (CVDs) are the leading cause of death globally, accounting for 17.3 million deaths or 30% of all deaths in 2008 [1]. Coronary heart disease and stroke are the top CVDs, representing 7.3 and 6.2 million deaths, respectively [2]. CVDs are projected to remain the most common cause of death through 2030 [3].

CVDs refers to any disease that affects the cardiovascular system, i.e. heart and blood vessels. Blockage of blood vessels via thrombus formation leads to lack of oxygen and nutrients in downstream tissues or organs. Sudden occlusion of myocardial arteries results in myocardial infarction (heart attack); similarly, disturbance in blood supply to the brain leads to cerebral infarction (stroke). Atherosclerosis contributes to thrombus formation, and is considered the major cause of CVDs [4-6]. Although the symptoms and signs occur in the advanced stages of disease and usually affect older adults, atherosclerosis can be found in youths and remains asymptomatic for decades [4, 7]. Atherosclerosis is a chronic inflammatory process that involves the development of atherosclerotic plaques that accumulate and restrict blood flow. It is clinically silent until rupture of the plaque occurs, exposing coagulation factors and extracellular matrix which leads to immediate thrombus formation.

Several risk factors, e.g. diet, smoking, physical activity and environment, have been associated with CVDs. However, the root cause for the development of atherosclerosis is largely unclear. Therefore, understanding the molecular mechanisms that lead to atherosclerosis is key to prevention of CVDs.

The development of atherosclerosis is initiated by a dysfunctional endothelium that recruits leukocytes. Recent evidence suggests that activated platelets play an important role in promoting

the recruitment of leukocytes [8-10], including neutrophils [11], lymphocytes [12], and monocytes [13, 14]. Monocytes in particular have received much attention, not only because monocytes are directly involved in the formation of atherosclerotic plaques, but circulating platelet-monocyte aggregates in blood have also been established as an early marker for acute cardiovascular events, e.g. stroke [15], stable coronary artery disease [16] and hypertension [17].

Platelets play a pivotal role in the development of atherosclerosis. Activated platelets can directly interact with monocytes to form platelet-monocyte aggregates (Figure 1.1). They can also interact with monocytes indirectly by releasing soluble factors, proteins and microparticles. These interactions promote a pro-inflammatory state of monocytes and increase adhesion of monocytes to endothelial cells. Subsequently, monocytes transmigrate across the endothelial layer and become resident macrophages, which gradually become foam cells upon ingestion of lipid deposits. The cells in these lesions secrete cytokines, chemokines, and lipids that trigger additional platelet and monocyte recruitment, amplify immune response and lead to formation of atherosclerotic plaques. Upon plaque rupture, thrombus formation is accompanied by activation of additional platelets and formation of platelet-monocyte aggregates. The involvement of platelets in atherosclerosis is further highlighted by the use of antiplatelet drugs for the treatment of CVDs [18].

Lysophosphatidic acid (LPA), a phospholipid, has been implicated in atherogenesis in that LPA accumulates in atherosclerotic plaques, activates platelets, and facilitates adhesion of monocytes to the endothelium [19-21]. LPA also promotes platelet-monocyte aggregate formation [22]. Although LPA signaling has been established in different cell types [23, 24], the role of LPA in platelet activation is not well characterized. In this chapter, platelets and the mechanisms through which they are activated by different agonists, including LPA, are

discussed. Regulations of platelet secretion and aggregation, and formation of platelet-monocyte aggregates is also discussed. In later sections, the tools and techniques used to study platelet function in the context of atherosclerosis is described.

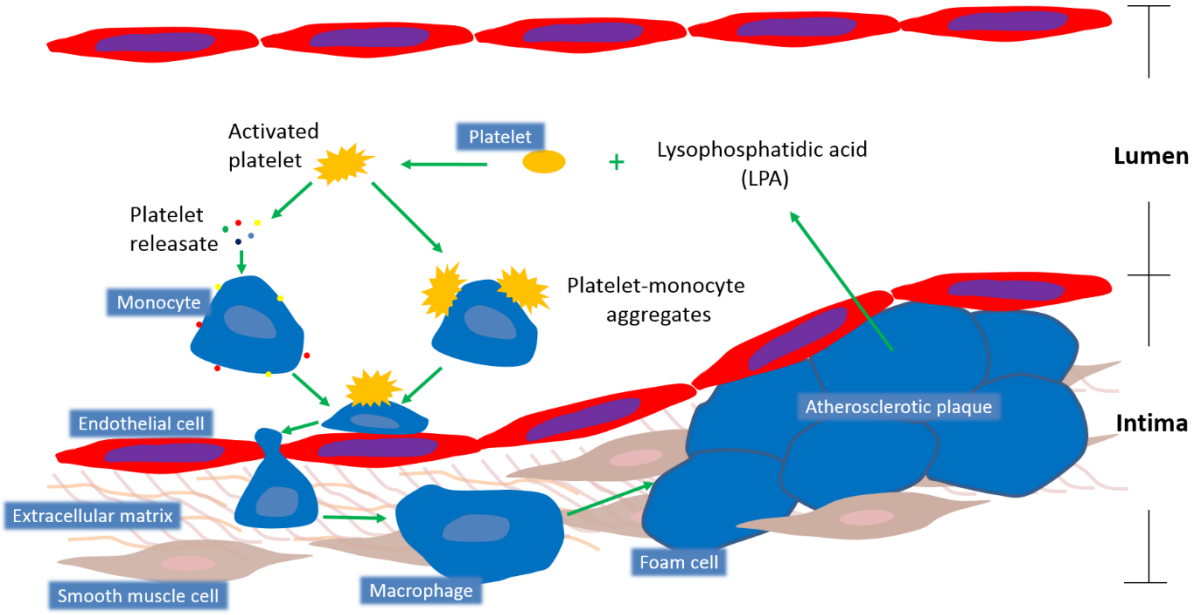

Figure 1.1 Activation of platelets and interaction between platelets and monocytes are crucial for the development of atherosclerotic plaques. The development of atherosclerosis is initiated by a dysfunctional endothelium that recruit leukocytes, particularly monocytes. Recent evidence suggests activated platelets plays an important role in promoting the recruitment of monocytes. Activated platelets can directly interact with monocytes by forming platelet-monocyte aggregates. They can also interact with monocytes indirectly by releasing soluble factors, proteins and microparticles, i.e. platelet releasate. These interactions promote a pro-inflammatory state of monocytes and increase adhesion of monocytes to endothelial cells. Subsequently, monocytes transmigrate across the endothelial layer and become resident macrophages, which gradually become foam cells upon ingestion of lipid deposits. The cells in these lesions secrete cytokines, chemokines, and lipids (e.g. lysophosphatidic acid (LPA)), that trigger additional platelets and monocytes recruitment, amplify immune response and lead to formation of atherosclerotic plaques.

1.1 Platelets

Platelets are derived from the cytoplasm of their progenitor cells, megakaryocytes, in the bone marrow of mammals. Human platelets are small, disc shaped non-nucleated cells that measure 2 to 5 μm in diameter and 0.5 μm in thickness [25]. Platelets lack genomic DNA [26], but

messenger RNA (mRNA) and the machinery required for protein synthesis was found in platelets [27]. After budding from megakaryocytes, these cell fragments circulate in blood for up to 10 days [28] before being destroyed by the reticuloendothelial system. About 100 billion platelets are produced by the human body every day [25], but only a fraction of these cells take part in hemostatic or thrombotic processes in a healthy state. In the event of vascular injury, a large amount of platelets will be rapidly recruited, activated and aggregated to form a blood clot at the site of the injury to prevent excessive bleeding. However, it is becoming more evident that platelets also play an important role in initiating and regulating inflammatory processes and immune responses [29]. For instance, platelets exert pathological pro-inflammatory functions in atherosclerosis development [30-32], where platelets are activated in response to inflamed endothelium and release interleukin 1beta (IL-1β), which enhances monocyte recruitment [33].

At the site of vascular injury, platelets bind to Von Willebrand factor (VWF) and collagen. After the initial adhesion, platelets are activated by various agonists, including thrombin, adenosine diphosphate (ADP), epinephrine, thromboxane A_2 (TXA_2) and in the case of atherosclerosis, LPA. Activated platelets release pro-coagulant molecules that are stored in α-granules and dense bodies (δ granules), recruit circulating platelets and further activate them to form aggregates. Platelet aggregation is achieved by the activation of glycoprotein IIb/IIIa (integrin αIIbβ3), which binds to fibrinogen, fibrin or VWF and forms bridges between platelets. During activation, platelets undergo dramatic shape change to spread over the damaged site, and facilitate platelet aggregate formation.

1.1.1 Platelet activation: a molecular view

In healthy blood vessels, platelet activation is inhibited by mediators produced by the

endothelium, i.e. nitric oxide (NO), prostacyclin, and ecto-ADPase [34]. NO limits platelet adhesion to endothelial cells even when platelets are pre-activated [35]. Prostacyclin elevates intracellular cyclic AMP (cAMP) level, which prevents platelet activation [36]. Ecto-ADPase lowers the level of plasma ADP and ATP, and abrogates secondary activation of platelets by ADP [37].

Once vascular injury occurs, extracellular matrix is exposed, and platelets are rapidly recruited to the damaged site. The initial adhesion of platelets is mainly mediated by VWF-glycoprotein Ib-IX (GPIb-IX) and collagen-glycoprotein VI (GPVI) interactions. The VWF-GPIb-IX interaction is strong enough to withstand high shear stress [38], and initiates signals for platelet activation [39]. This interaction is required for subsequent collagen-GPVI binding [40], which triggers further activation of platelets and the release of agonists from platelet granules, for instance, ADP. In addition, biochemical synthetic pathways are activated and produce thromboxane A2, another potent platelet activator. These second wave agonists act as positive feedback mediators that amplify activation signals and recruit more platelets. Firm adhesion is achieved when integrin αIIbβ3 and α2β1 are activated and bind to VWF and collagen [40].

When platelets adhere to the injured vessel wall, they can be activated locally by collagen or by factors released from damaged cells or activated platelets, including ADP, thrombin, TXA_2 and LPA. In general, agonist-stimulated platelet activation is achieved through G-protein coupled receptors (GPCRs) [41]. Downstream of these GPCRs, three types of Gα subunits, i.e. G_q, G_{i2} and $G_{12/13}$, are involved in distinct pathways (Figure 1.2). 1) G_q leads to the activation of β isoforms of phospholipase C (PLC) [42], which results in the formation of inositol trisphosphate (IP_3) and diacyl glycerol (DAG). IP_3-induced increase in cytosolic Ca^{2+}, and DAG-induced activation of protein kinase C (PKC) are required for activation of integrins, e.g.

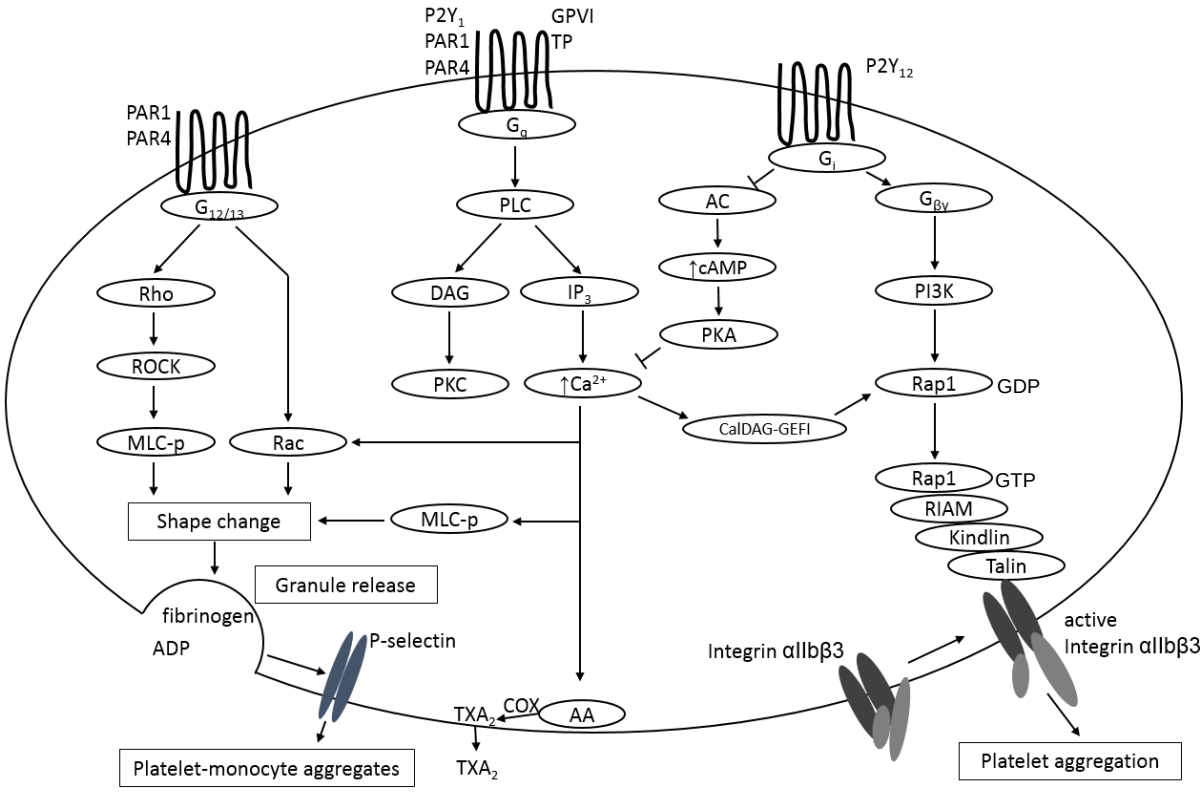

Figure 1.2 Main signaling pathways mediating platelet activation.AC, adenylate cyclase; ADP, Adenosine diphosphate; CalDAG-GEF1, calcium and DAG-regulated guanine exchange factor 1; cAMP, cyclic adenosine monophosphate; COX, cyclooxygenase; DAG, diacylglycerol; GDP, guanosine diphosphate; GPVI, glycoprotein VI; GTP, guanosine triphosphate; IP_3, Inositol triphosphate; MLC-p, myosin light chain phosphorylation; $P2Y_1$, purinergic receptor $P2Y_1$; $P2Y_{12}$, purinergic receptor $P2Y_{12}$; PAR1, proteinase-activated receptor 1; PAR4, proteinase-activated receptor 4; PI3K, phosphoinositide 3-kinase; PKA, protein kinase A; PKC, protein kinase C; PLC, phospholipase C; RIAM, Rap1-interacting adaptor molecule; ROCK, Rho-associated protein kinase; TP, thromboxane receptor; TXA_2, thromboxane A_2. This illustration does not exclude additional receptors or pathways involved in platelet functions.

integrin αIIbβ3 [43]. Both Ca^{2+} and PKC determine secretion level of 5-hydroxytryptamine from platelets [44]. 2) G_{i2} activation causes the release of βγ complexes [45], which regulates two main effectors in platelets: one being inhibition of adenylyl cyclase that in turn reduces cAMP level, the other being activation of phosphatidylinositol 3-kinases (PI3Ks), which subsequently activates protein kinase B (PKB/Akt) [46]. Finally, 3) $G_{12/13}$ has been found to activate Rho/Rho-kinase pathway by directly interacting with and activating Rho-specific activators, i.e. guanine

nucleotide exchange factors [47, 48]. Platelet shape change is regulated by Rho and Rac small GTPases, which will be discussed in section 1.1.2.

The final step of platelet activation is aggregation, which is mediated by the activation of integrin αIIbβ3. These integrins bind to fibrinogen and VWF to bridge activated platelets and form a platelet plug. Platelet aggregation is regulated by Rap1 small GTPases, and discussed in detail in section 1.1.3.

1.1.1.1 Platelet activation induced by ADP

ADP is released by damaged cells at the injured vessel wall, and also secreted from the dense granules in activated platelets. Therefore, ADP acts as an autocrine and paracrine platelet stimulus for recruitment and activation of additional platelets, and stabilization of the platelet plug [49]. Although ADP is a weak platelet activator, other stimuli are dependent on secondary activation by the secreted ADP to reach maximal platelet aggregation [50, 51].

Two ADP receptors, $P2Y_1$ and $P2Y_{12}$, are expressed on human and mouse platelets [52-55]. Both of these receptors are GPCRs, but they utilize distinct downstream pathways (Figure 1.2). Activation of $P2Y_1$ by binding to ADP signals through the G_q α subunit, which leads to the increase of cytosolic Ca^{2+} and activation of PKC as previously mentioned. In addition, the $P2Y_1$-G_q signaling is also responsible for platelet shape change mediated by small GTPase Rac [56]. In contrast, activation of $P2Y_{12}$ leads to formation of lipid raft- associated $P2Y_{12}$ oligomers [57], which couple to downstream G_{i2} α subunits [58]. This coupling is critical for activation of PI3K isoforms [51, 59]. Among the four PI3K isoforms, PI3Kα-δ, PI3Kβ and PI3Kγ were found to be required for ADP-induced platelet aggregation [60, 61], which is achieved by the activation of

the small GTPase Rap1 and integrin αIIbβ3 activation [62-65]. ADP-induced platelet aggregation is independent of activation of PKC [63].

1.1.1.2 Platelet activation induced by thrombin

Thrombin is the main effector protease for the coagulation cascade and the most potent activator of platelets. Thrombin generation is regulated by a series of coagulation factors [66]. Conversion of prothrombin to active thrombin occurs on cellular surfaces, including that of activated platelets [67].

Thrombin activates platelets by cleaving and activating the protease-activated receptor (PAR) family of GPCRs [68]. Three out of four members of the PAR family can be activated by thrombin, i.e. PAR1, PAR3 and PAR4. PAR1 and PAR4 are expressed on human platelets, whereas PAR3 and PAR4 are found in mouse platelets [69]. This makes mouse platelets not an ideal system to study human platelet functions. When thrombin cleaves the PAR receptors, a short N-terminal receptor fragment / peptide is released. A newly formed N-terminus is exposed that starts with the sequence SFLLRN, which in turn activates PAR receptors [68, 70]. Chemically synthesized peptide SFLLRN (Thrombin Receptor Activating Peptide or TRAP) is also able to activate the PAR receptors.

Signaling pathways downstream of PAR1 and PAR4 have been well established (Figure 1.2) [68, 71-73]. Both PAR receptors trigger downstream $G_{12/13}$ and G_q signaling. Activation of $G_{12/13}$ leads to Rho/Rho-kinase-mediated platelet shape change [74]. Activation of G_q results in strong activation of PLCβ, which in turn increases cytosolic Ca^{2+} concentration, activates PKC, and triggers integrin αIIbβ3 activation and platelet degranulation. Although PAR1 and PAR4 do not couple to G_i directly, they activate the G_i pathway by releasing the secondary mediator ADP

from platelet dense granules (Figure 1.2) [51, 73]. The ADP-induced $P2Y_{12}$/PI3K pathway is critical for PAR1-mediated irreversible platelet aggregation [75]. Interestingly, activation of PAR1 leads to a transient influx of Ca^{2+}, while a prolonged Ca^{2+} signal is mediated by PAR4 activation [73]. Furthermore, PAR1-induced platelet aggregation is transient and reversible, and requires additional signaling from ADP or PAR4 to reach maximum platelet aggregation [76]. PAR4 has been shown to be responsible for platelet aggregation at low level of thrombin, whereas PAR4-induced irreversible platelet aggregation is ADP independent [76].

1.1.1.3 Platelet activation induced by LPA

LPA accumulates in human atherosclerotic plaques and evidence suggests that LPA plays a role in aggravating cardiovascular disease [19, 20, 77, 78]. At the site of atherosclerotic plaques, LPA can be released by activated cells, particularly platelets [79]. LPA in turn induces further platelet activation and aggregation [80]. Similar to ADP, LPA can also be considered a secondary platelet mediator in an autocrine fashion.

Different forms of LPA exist which vary in the type of fatty acid and the type of linkage to the glycerol backbone. These LPA molecules differ greatly in their potency of platelet activation, e.g. alkyl ether-linked LPA has much stronger aggregating activity than acyl-LPA [22, 81]. However, it is unclear which receptor(s) LPA activates in platelets. There are six LPA receptors identified, i.e. LPA_1-LPA_6, which are all GPCRs [82-85]. A few other LPA receptors were proposed, but require more validation, i.e. GPR87 [86], $P2Y_{10}$ [87], GPR35 [88], and PPARγ [89]. The mRNA for all six LPA receptors can be found in human platelets, with LPA4 and LPA5 having the most abundant mRNA levels [90]. LPA-induced platelet activation can be inhibited by LPA1 and LPA3 antagonists [77]; however, the ligand specificities showed in LPA-

induced platelet aggregation is not accounted for LPA_{1-3}, which showed no preference in binding with either alkyl- or acyl-LPA [80, 81, 91, 92]. This suggests that other receptor(s) are involved in LPA-induced platelet aggregation. Moreover, the downstream signaling pathways mediated by LPA are not very well characterized. LPA-induced platelet aggregation can be inhibited by ADP receptor antagonist [22], suggesting LPA acts on platelets by activating ADP receptors. Moreover, LPA-induced platelet shape change is mediated by $G_{12/13}$-Rho pathway, as seen with other platelet agonists [22, 93].

Interestingly, individual heterogeneity was observed in platelet response to LPA in that platelets from 20% of healthy donors do not aggregate in response to LPA treatment [94]. The high LPA_4 mRNA level in nonresponsive platelets suggests LPA_4 regulates inhibitory pathway(s) that block platelet aggregation [94]. However, this inhibitory pathway might not involve cAMP, since cAMP level was not significantly changed in LPA-induced platelet aggregation [90]. Furthermore, LPA-induced platelet aggregation may be species-specific. Only human and cat platelets have showed LPA response [95], and mouse platelets cannot be activated by LPA, which seems to inhibit other agonist-induced aggregation [96, 97].

1.1.2 Platelet shape change and secretion regulated by the small GTPase Rho and Rac

Platelet shape change and secretion of granules is one of the hallmarks of platelet activation. Mature platelets form a surface-connected open canalicular system, which allows transportation of substances into the cells, as well as secretion of granule contents out of the cells [98]. The open canalicular system consists of surface membrane that does not only expand the total surface area, but also enables platelets to spread rapidly upon activation [99]. When vascular injury occurs, platelets adhere, spread over the damaged sites, secret granule contents and initiate the

following processes: 1) reorganization of platelet cytoskeleton proteins to change shape; 2) release of second wave agonists to recruit and activate additional platelets; and 3) relocation of adhesive and inflammatory molecules from the granules to the platelet surface to attract and activate leukocytes.

Platelet cytoskeleton reorganization plays an important role in triggering release of granules [100, 101]. Current evidence suggests that these two events are mainly regulated by the small GTPase Rho and Rac, myosin light chain kinase and Ca^{2+}/calmodulin interaction (Figure 1.2). Inhibition of the Rho/ROCK pathway using the ROCK inhibitor, Y-27632, led to impaired myosin light chain phosphorylation as well as decreased granule secretion [102, 103]. Similarly, inhibition of myosin light chain kinase also inhibited granule secretion [104]. Independent of the Rho/ROCK pathway, Ca^{2+}/calmodulin has also been shown to mediate myosin light chain phosphorylation and therefore platelet shape change [105, 106]. In addition, Rac activation has been shown to be involved in platelet secretion. Human and mouse platelets treated with Rac1 inhibitor, NSC23766, showed diminished relocation of P-selectin to the platelet membrane and decreased secretion of ATP [107]. These effects of Rac1 inhibition were also observed in atherosclerotic plaque-stimulated platelets [108]. Furthermore, PKC might be another regulator of platelet shape change; however, the effect has been shown to be PKC isoform dependent [103, 109-111].

Platelet secretion involves the release of three types of granules: α-granules, dense granules and lysosomes. More than 300 proteins that are released by α-granules have been identified [112, 113]. These α-granule proteins include: 1) membrane proteins, e.g. integrin αIIbβ3, GPVI and P-selectin; 2) coagulation factors: e.g. factor V, factor IX and factor XIII; 3) adhesion proteins: fibrinogen, VWF and thrombospondin; 4) chemokines: e.g. CXCL4 (platelet factor 4), CCL5

(RANTES) and CCL2 (MCP-1); 5) growth factors: e.g. epidermal growth factor, insulin-like growth factor and transforming growth factor β. Most of the membrane proteins in the α-granules can be found on resting platelets [114]; however, P-selectin translocates from α-granules to the platelet surface membrane when activated, which recruits leukocytes via P-selectin and P-selectin glyocoprotein ligand-1 (PSGL-1) interaction [115, 116]. The second type of platelet granules, dense granules, contain high concentrations of cations and nucleotides, e.g. 2.2 M calcium and 653mM ADP [117], which are critical for platelet activation. Dense granules also contain bioactive amines including serotonin and histamine [118]. The third type of platelet granules, lysosomes, mainly contain enzymes that are involved in protein degradation.

Interestingly, platelet shape change and secretion of coagulation factors, adhesion proteins and agonists facilitate platelet aggregation; however, platelet shape change and secretion is not a prerequisite for aggregation, and these processes might occur independently [119].

1.1.3 Platelet aggregation regulated by integrin αIIbβ3 and the small GTPase Rap1

Platelet aggregation is achieved primarily by activation of integrin αIIbβ3, which in turn binds to fibrinogen or VWF that bridges platelets to form platelet aggregates [120]. Blockade of integrin αIIbβ3 using antibody or peptide inhibits platelet aggregation [121], and inhibitors targeting integrin αIIbβ3 have been developed into antiplatelet agents to prevent cardiovascular events [18, 122, 123]. Integrin αIIbβ3 is one of the major platelet membrane receptors, approximately 80,000 copies per platelet [124, 125]. A substantial amount of the αIIbβ3 is stored in the platelet α-granules, and these integrins translocate to the platelet surface membrane upon activation [126, 127].

Cellular signals leading to the activation of integrin αIIbβ3 are referred to as "inside out signaling", which mainly consist of the G_q-PLC and G_i-PI3K-Rap1 pathways (Figure 1.2). Downstream of the G_q-PLC pathway, formation of DAG and elevation of cytosolic Ca^{2+} results in the activation of CalDAG-GEFI, a guanine nucleotide exchange factor for the small GTPase Rap1 [128-130]. CalDAG-GEFI- or Rap1b-deficient mice lead to compromised αIIbβ3 activation [130, 131]. In addition, Rap1-mediated αIIbβ3 activation can also be achieved through the G_i-PI3K pathway [132, 133]. Rap1 plays a vital role in mediating integrin αIIbβ3 activation. Activated Rap1 binds to Rap1-GTP-interacting adaptor molecule (RIAM), which recruits the cytoskeletal protein talin to the plasma membrane, and in turn activates integrin αIIbβ3 [134]. However, evidence suggests that talin itself might not be sufficient to activate integrin αIIbβ3 [135, 136]. Kindlin-3 has been found as a co-activator with talin for integrin αIIbβ3 activation [136-138]. Apart from talin and kindlin-3, additional interacting partners might also be involved integrin αIIbβ3 activation [139, 140].

1.1.4 Platelet-monocyte aggregate formation via P-selectin / PSGL-1 binding

As previously discussed, platelet-monocyte aggregate formation, which was found in various CVDs, is a direct result of platelet activation. LPA, which accumulates at the sites of atherosclerotic plaques, stimulates the formation of platelet-monocyte aggregates [22]. This formation is mainly mediated by the interaction of P-selectin on the surface of activated platelets and PSGL-1 on monocytes. The interaction can be abolished by blockage of PSGL-1 alone, and no further reduction of platelet-monocyte aggregates was observed by the addition of integrin αIIbβ3 and αMβ2 antagonists in combination with PSGL-1 inhibition [116].

P-selectin / PSGL-1 binding is not unique to platelet-monocyte interaction. For instance, neutrophils also express PSGL-1 and can bind to platelets; however, preferential interaction of platelets to monocytes over neutrophils has been shown *in vitro* [141]. In addition, clinical studies showed that platelet-neutrophil aggregates have a shorter half-life than platelet-monocyte aggregates [142]. Moreover, monocytes can bind to P-selectin on the surface of endothelial cells. Platelet-monocyte interaction may be favored due to the vast number of P-selectin molecules on activated platelets, i.e. 10,000 per cell [143]. This is among the most abundant membrane proteins after integrin αIIbβ3 (80,000 per cell) [125] and glycoprotein Ib (20,000 per cell) [144].

Signals initiated by P-selectin / PSGL-1 binding in monocytes trigger the expression and activation of β1 and β2 integrins, and increase their adhesiveness and ability to transmigrate across the endothelium [145]. In addition to direct binding to monocytes, platelets release soluble factors, i.e. RANTES and PF4 (platelet factor 4), that amplify the recruitment of monocytes to endothelium and accelerate atherosclerosis [146].

Soluble P-selectin shed from activated platelets may have biological implications in atherosclerosis [147]. Although translocation of P-selectin is not reversible in activated platelets *in vitro* [148], P-selectin on platelet surface can be shed to produce a soluble form of P-selectin *in vivo* [149]. Shedding of P-selectin occurs rapidly (within a few hours), and does not cause a defect in platelet function and circulation [150]. Therefore, P-selectin levels may not be an ideal marker for platelet activation *in vivo*, which might be better represented by circulating platelet-monocyte aggregates [142, 151].

Platelet-monocyte aggregates might be a potential target for the prevention of CVDs without affecting hemostatic functions of platelets. However, formation of platelet-monocyte aggregates induced by LPA is insensitive to aspirin treatment [22], which is a widely used antiplatelet drug

inhibiting COX-1 and production of TXA_2 [152]. Clearly, a better understanding of how platelets are activated and how platelet-monocyte aggregates are formed in the context of atherosclerosis would help identify possible pathways or even drug targets for the development of intervention strategies for CVDs.

1.2 Proteomics

1.2.1 Mass spectrometry-based proteomics

Proteomics, defined as the comprehensive analysis of the proteins that are expressed in cells or tissues [153, 154], has seen dramatic technical advances in the past few years [155]. The credit for the advancement of proteomics is largely given to the development of more powerful mass spectrometers [156]. For example, the linear ion trap (LIT) provides wide dynamic range, high sensitivity and speed, and the capability to analyze posttranslational modifications (PTMs) [157]. Other examples include the triple quadrupole (QQQ), which enables reliable quantification of low abundant proteins using the multiple reaction monitoring (MRM) technique [158]; the fourier transform ion cyclotron resonance (FT-ICR) mass spectrometer, which excels in high mass accuracy and high resolution [159, 160], and a recently developed mass spectrometer, the Orbitrap, which offers similar mass accuracy and resolution to FT-ICR without the need of a superconducting magnet [161, 162]. These technologies have increased the ability of mass spectrometry (MS)-based proteomics to identify and quantify thousands of proteins from complex samples, in a single experiment, which has already made an impact on biology and medicine [155, 163].

1.2.2 General workflow in mass spectrometry

In a general MS-based proteomics workflow, protein samples are appropriately isolated from their biological source, optionally separated by one dimensional (1D)/two dimensional (2D) gel electrophoresis or 1D/2D liquid chromatography (LC) techniques, followed by either in-gel or in-solution digestion, and additional peptide separation by LC if needed, and subsequently introduced to an ion source for ionization (Figure 1.3). Two popular techniques are utilized to generate peptide/protein ions: electrospray ionization (ESI) [164] and matrix-assisted laser desorption/ionization (MALDI) [165]. ESI is commonly applied to complex peptide/protein samples due to its ability to be coupled online with LC for further fractionation. MALDI is hampered by the sample complexity and is thus less popular; however, it is a valuable alternative for analyzing simple biological samples since it is more tolerant than ESI to the presence of salts and detergents.

The ionized peptides/proteins can then be directly analyzed in a mass spectrometer that measures the mass-to-charge (m/z) ratio and intensity of each peptide/protein (Figure 1.3). The real strength of this methodology appears when the ionized peptides/proteins are analyzed by tandem mass spectrometry (MS/MS), which allows the determination of their amino acid sequence and/or the type and site of PTMs [166]. To achieve this, a fragmentation step is introduced between two mass analysis steps, allowing determination of the masses of each of the intact ions, as well as the fragmentation pattern of each individual ion. These fragmentations can be induced in many different ways, including collision-induced dissociation (CID) [167], electron capture dissociation (ECD) [168] and electron transfer dissociation (ETD) [169, 170]. CID, where the peptide/protein ions are collided with neutral gas molecules for fragmentation, is currently the most widely used method. ECD involves the direct introduction of low energy

electrons into trapped gas phase ions, and ETD involves the transfer of electrons between the peptide/protein cations and reagent anions. Each of these fragmentation modes is controllable and produces predictable fragmentations. Tens of thousands of these experiments can be performed per sample, producing an enormous amount of data that requires computational approaches to fully decipher.

The identities of peptides/proteins are obtained from this data by comparing the acquired MS or MS/MS spectra to those predicted from a protein or genomic database using search algorithms (Figure 1.3). Genomic databases can be *in silico* transcribed to produce databases of possible proteins. Due to the completeness, accuracy and quality of genomic sequence annotation, the most widely used databases are Entrez Protein, Reference Sequence (RefSeq), Swiss-Prot and International Protein Index (IPI). The protein sequences in these databases can then be computationally converted into peptides and peptide fragments, the calculated masses of which can be used to compare to the input peptide spectrum. A number of database search algorithms are available for this comparison, including SEQUEST [171], MASCOT [172], ProteinProspector [173], TANDEM [174] and OMSSA [175]. These spectral matching search engines rank the possible peptide matches for each of the input spectra by measuring the degree of similarity between the input spectrum and the theoretical spectrum. However, due to high contaminant rate, low quality spectra, presence of homologous peptides, sequence variants and novel peptides, performance of the MS and the size of the database, the error rate might vary significantly, and even top-scoring peptides assignment could be incorrect. Therefore, statistical validation of peptide and protein assignment should be carried out [176].

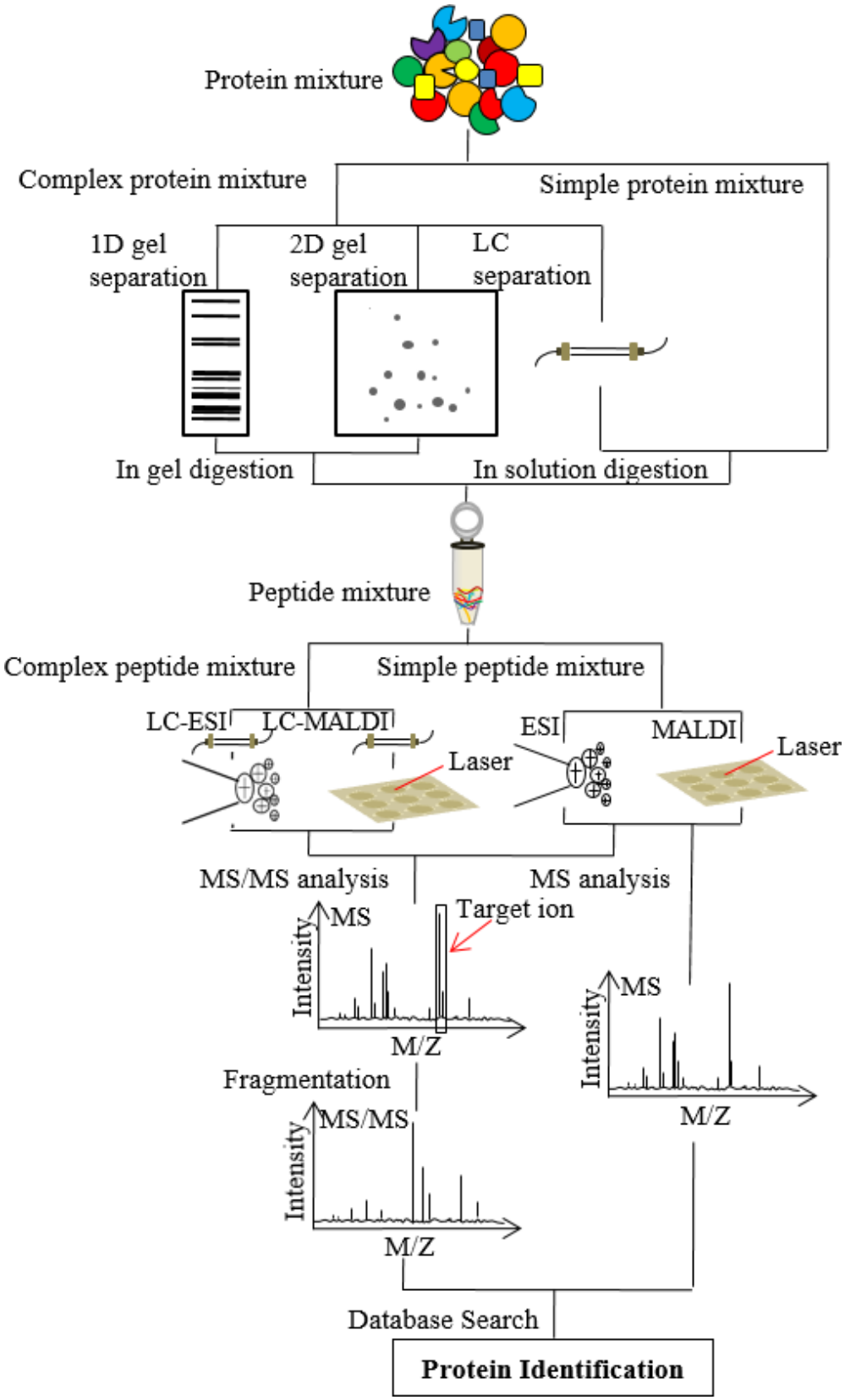

Figure 1.3 General workflow for mass spectrometry-based proteomics

1.2.3 Bottom-up or top-down proteomics

MS-based proteomics can be divided into two workflows based on the size of the analyte that enters the mass spectrometer: bottom-up analyses focus on enzymatically digested samples with peptides about 25 amino acids or less, while top-down analyses tend to focus on large peptides and intact proteins. Top-down mass spectrometry is an effective tool to monitor modifications for small proteins (<30kDa) [177], which is typically performed using ESI-ECD/ETD-FT-ICR/quadruple ion trap or the traditional CID setups. Although the mass range of this method has been extended to more than 200 kDa by Han et al. in 2006 [178], its lack of the ability to analyze complex sample makes top-down proteomics less popular than bottom-up proteomics [179]. However, top-down proteomics remains a potentially powerful technique, particularly in analyzing PTMs of proteins by measuring them intact rather than the indirect method of measuring peptides from the proteins [180].

1.2.4 Quantitative proteomics

The ability of quantifying the differences in protein expression between two or more physiological states of a biological sample has been greatly improved over the past decade (for recent reviews, see Ref. [181, 182]). While methods for label-free quantification have also been developed [183, 184], most of the current quantitative proteomics techniques require differential stable isotope labeling to be able to quantify small differences. In order to test an experimental variable, one state is given a light isotopic label, the other a heavy label, then the samples are mixed and analyzed simultaneously using LC-MS or LC-MS/MS. The chemical and physical properties of the heavy and light stable isotope-labeled peptides remain the same, the only difference lies in their mass, making these peptides distinguishable using MS. The relative

intensities of the peptide ions in the mass spectra directly reflect the relative quantities of the peptide under different physiological conditions, and thus the differences in the amounts of the proteins that incorporate the label can be deduced. The most accurate and widely used techniques are discussed below.

1.2.4.1 Metabolic incorporation of stable isotopes

Mann and coworkers introduced stable isotope labeling by amino acids in cell culture (SILAC) in 2002 [185]. In this technique, cells are cultured in either normal medium (i.e. "light") or $^{13}C_6$-arginine and/or $^{13}C_6$-lysine containing medium. Since trypsin, the most commonly used protease in proteomics, cleaves the amide bonds next to the carbonyl group of either an arginine or lysine residue, $^{13}C_6$-arginine and $^{13}C_6$-lysine labeling ensures that the trypsin cleaved peptides contain at least one heavy-labeled amino acid, leading to at least one mass increment over the non-labeled counterpart. The heavy amino acids can be incorporated into more than 95% of proteins in 6-8 passages [185].The advantage of SILAC is that the heavy and light labeled samples can be combined at intact cell level, which excludes errors that may otherwise be introduced by subtle variations of parallel purification and sample handling procedures. Therefore, SILAC is the most accurate quantitative proteomics technique to date, and it is suitable for tracking small changes and PTMs [186-191]. Currently, up to five conditions can be compared in a single SILAC experiment using different forms of heavy arginine and/or lysine, which is particularly useful in time-course and multiple drug treatment studies [192]. Interestingly, although SILAC is routinely performed in cell culture systems, it has recently also been applied to *in vivo* studies in mice [193]. However, SILAC cannot be done on

humans and is prohibitively expensive to do on mice, thus non-metabolic quantitative methods, i.e. chemical tagging approaches, are needed as well.

1.2.4.2 Chemical tagging approaches

Chemical labeling methods are based on the reaction of isotope labeled mass tags with cysteines, amino groups or carboxylic groups [194]. The reaction can be carried out on the protein level; however, it is more often employed at the peptide level after proteolytic digestion. Isotope-coded affinity tags (ICAT) were introduced by Aebersold and coworkers in 1999 [195], in which cysteines first react with a mass tag containing zero or eight deuterium atoms and a biotin group, and proteins are mixed and digested. The cysteine-derivatized peptides are then purified by the affinity of the biotin group in the mass tag and subsequently analyzed by MS. As cysteine is a less common amino acid, and ICAT enriches cysteine-containing peptides in the mixture, ICAT can be used to analyze highly complex peptide mixtures. However, proteins that only contain a few (or not any) cysteine residues can be difficult to characterize using ICAT.

More recently, another chemical labeling method was introduced. Isotope tags for relative and absolute quantification (iTRAQ) [196] utilize isobaric amine-specific tandem mass tags that consist of a reporter and a balance group. The isobaric labeled peptides are indistinguishable in the MS spectra; however, each tag generates a unique reporter ion upon fragmentation, which allows the simultaneous determination of both identity and relative abundance of the peptides. Commercially available iTRAQ reagents enable up to eight different conditions to be analyzed in a single experiment, which is useful for studying multiple time points and comparing multiple drug treatments. Although chemical tagging approaches are not as accurate as SILAC due to the

sample handling required prior to joining the samples, ICAT and iTRAQ can be directly applied to tissue samples, and therefore directly to human health research.

1.2.4.3 Computer tools for quantitative proteomics

Tens of thousands of spectra can be generated in a single experiment, and the mass shift introduced by the stable isotopes or mass tags makes these spectra more complicated. Therefore, a number of computer tools for protein quantification have been developed to automate their interpretation, such as MSQuant [197] and XPRESS [198] for SILAC and ICAT analysis, MaxQuant [199] for SILAC analysis, RelEx [200] for ICAT analysis, as well as Libra [201], Multi-Q [202] and i-Tracker [203] for iTRAQ isobaric labeling analysis.

1.2.5 Comparative proteomics

Comparative proteomics techniques have been adopted in this discovery-driven process to identifiy potential drug targets (for recent reviews, see [204, 205]), which typically involve sample preparation, separation/fractionation, MS analysis, protein identification and quantification.

Sample preparation should be tailored to the hypothesized potential protein targets. In the case of membrane proteins, differential centrifugation steps may be incorporated for isolating membranes from the sample. In the case of serum and plasma where levels of different proteins vary by up to 10 orders of magnitude, high abundance protein depletion is needed [206]. However, in many cases, little is known about the potential protein targets, therefore global proteomics techniques should be used to characterize as many proteins in the sample as possible.

Due to the complexity of biological samples that potentially contain many thousands of proteins, low abundance proteins can be masked by those of high abundance, and thus be difficult to detect by MS. Therefore, it is critical to do appropriate, usually extensive, sample separation and/or fractionation prior to MS analysis. Because of the high resolving power and its large sample loading capacity, two-dimensional polyacrylamide gel electrophoresis (2D-PAGE) has been adopted to compare proteomes from normal versus disease samples [207]. In 2D-PAGE, proteins are separated based on their mass and isoelectric point (pI). The relative abundances of proteins from different samples can be compared by the intensity of the protein staining. A number of mathematical–statistical methods have been developed for decoding the complex maps of 2D-PAGE [208-210].

Similarly, differential in-gel electrophoresis (DIGE) is also used to separate and compare proteins from different samples [211]. In DIGE, up to three different protein samples can be labeled with fluorescent dyes (Cy2, Cy3 and Cy5) and mixed together prior to two-dimensional electrophoresis. Changes in protein abundances can be observed by different colors of the protein spots. DIGE uses only one 2D gel, circumventing the limitation of inter-gel variation in traditional 2D electrophoresis.

However, both 2D-PAGE and DIGE are limited by the extreme complexity of biological samples, where subtle changes between two different conditions of the same sample are difficult to characterize. In this case, sample fractionation of protein digests is used as an alternative, i.e. strong cation exchange (SCX) followed by reversed-phase LC, which can be performed online using a bi-phasic column. SCX is based on the electrostatic interaction of positively charged peptides/proteins to the negatively charged particles on the SCX column. The pH and ionic

strength of the buffers determine the sequential elution of the bound molecules from the SCX column.

After appropriate sample preparation and separation/fractionation, MS or MS/MS analysis and database search tools are generally employed for the identification of critical proteins that are expressed differently under normal versus disease conditions, which could be potential drug targets.

1.2.6 Functional proteomics

Living cells rely on the interplay of thousands of proteins to maintain their cellular integrity and execute biological functions. These protein-protein interactions can be indirectly affected by external stimuli and/or inhibitors, which lead to changes in the biological state of cells. Thus studying protein-protein interactions in normal versus disease or disease versus inhibitor-treated conditions can help identify disease-related sub-networks [212-216], to clarify indirect inhibitor effects at the cell level.

Functional proteomics aims to identify and quantify changes in protein interactions in response to a specific biological condition, and seeks to address the complex protein interaction networks in an integrative and physiologically relevant fashion [217-220]. Here, several state-of-the-art functional proteomics techniques are discussed.

Yeast Two Hybrid (Y2H) The Y2H system was introduced by Fields and Song in 1989 [221], to detect direct interaction between two proteins, in which the two proteins are fused to either the DNA-binding domain (BD) or the activation domain (AD) of a transcriptional activator in the yeast *Saccharomyces cerevisiae*). If a physical interaction occurs between the two proteins, then the AD and BD are indirectly connected, allowing the activation of a downstream reporter gene,

the expression of which changes the cell phenotype. The Y2H method estimates the possibility of protein interactions regardless of the protein localization, expression level, protein processing, possible PTMs and competition with other alternative interacting partners in living cells. The high false positive rates that usually occur can be minimized when combined with Tandem affinity purification mass spectrometry (TAP-MS) [222], while the protein localization issue can be avoided using computational approaches [223-225].

Variant Y2H methodologies have been developed [226], including reverse Y2H (rY2H) [227] and repressed transactivator Y2H (RTA-Y2H) [228] systems to monitor the disruption of protein-protein interactions, and yeast three hybrid (Y3H) to detect direct binding of small molecules to proteins [229]. Moreover, mammalian protein–protein interaction trap (MAPPIT), an Y2H variant based on mammalian cells, has also been developed. MAPPIT relies on a variant JAK-STAT (Janus kinase-Signal Transducer and Activator of Transcription) signaling pathway [230]. The bait protein is fused to a signaling-deficient receptor that cannot recruit STAT, and the prey protein is fused to a functional receptor containing STAT-binding sites. The bait-prey interaction results in the phosphorylation of STAT and in turn activates a reporter gene.

Protein-fragment Complementation Assay (PCA) Michnick and coworkers developed PCA as an *in vivo* screen for protein-protein interactions [231, 232]. In their recent study on yeast protein interaction networks using the PCA approach [233], two proteins of interest were fused to complementary fragments of mutated murine dihydrofolate reductase (mDHFR), which is insensitive to the DHFR inhibitor methotrexate but retains full catalytic activity. The interaction between the two proteins allows the two fragments of mDHFR to fold and form the functional enzyme so that the yeast can survive the treatment with methotrexate. They identified 2770 interactions among 1124 yeast proteins, most of which were novel, and unraveled an unexplored

subspace of the yeast protein interactome. PCAs based on reporter proteins other than mDHFR have also been developed, including glycinamide ribonucleotide transformylase [234], aminoglycoside kinase [234], hygromycin B kinase [234], TEM1 β-lactamase [235, 236] and green fluorescent protein [237]. PCA can be used not only to identify protein-protein interactions, but also to characterize the localization of protein complexes, and the temporal and spatial protein interaction dynamics [238].

Affinity Purification Mass Spectrometry (AP-MS) AP-MS allows the isolation of multiprotein complexes from cell lysates through one or more affinity purification steps [239]. In contrast to Y2H and PCA, AP-MS can be performed under physiological conditions and coupled to quantitative proteomics methods to probe dynamic changes. TAP-MS was developed by Séraphin and coworkers to identify both direct and indirect protein interactions among protein complexes *in vivo* [240]. In TAP-MS, the C- or N-terminus of the protein of interest is fused to a TAP tag which consists of a calmodulin binding peptide that binds specifically to calcium, a TEV protease cleavage site and Protein A that binds to IgG with high affinity. The two different purification steps increase specificity and thus reduce false positives.

However, TAP-MS only detects strong interactions that can withstand the two purification steps, while transient or weak interactions are missed. This problem could be solved using a protein cross-linking strategy [241, 242], which relies on the formation of covalent bonds between interacting proteins in cells, regardless of whether the interaction is strong, weak or transient [243-245]. A number of protein cross-linkers have been introduced, such as BS3 [246], [d_{12}]DSS and [d_6]DSG [247]. In addition, formaldehyde has been identified as a powerful cross-linking reagent, as it can enter the cell through the intact membrane, and form covalent bonds

between interacting proteins inside the cell [248, 249]. With the help of these cross-linkers, it is feasible to use TAP-MS for the comprehensive study of all types of protein interactions in cells.

1.2.7 Phosphoproteomics

Cellular functions often result in changes of the PTMs on proteins, which alter the protein-ligand and protein-protein interactions. These PTMs include phosphorylation, glycosylation, sulfation, methylation, acylation, ubiquitylation, acetylation [250]. Phosphorylation is the most extensively studied PTM and has been recognized as essential for the regulation of protein function and protein-ligand/protein-protein interactions [251, 252] (for a recent review, see Ref. [253, 254]). Glycosylation is another important PTM which regulates cell-cell recognition and communication that has drawn increasing attention in proteomics [255, 256]. Sulfation [257], methylation [258] and others have also been targeted for studying cellular functions. Here, phosphoproteomics techniques that identify phosphorylation events for the purpose of clarifying the mechanisms of cell signal transduction were discussed.

Phosphorylation occurs on tyrosine, serine and threonine of eukaryotic proteins, and is reversibly regulated by protein kinases and phosphatases. Phosphorylation often presents an activating or deactivating switch of protein activity that dynamically controls the signaling propagation in cellular networks [259], and interference of the balance of this process often leads to diseases [260]. However, drugs could be designed to activate or deactivate certain protein kinases [261] or phosphatases to regain the balance under disease conditions. For instance, imatinib, a tyrosine kinase inhibitor, has been designed for treating chronic myelogenous leukemia, gastrointestinal stromal tumors and other cancers [262]. Combined with quantitative analysis, phosphopeptide enrichment strategies can be used to clarify the mechanisms of

phosphorylation-induced changes in protein function and cell signaling transduction [186, 191, 263].

Phosphoproteins represent a small, difficult to detect portion of proteins in a whole cell lysate, thus they need to be enriched for efficient measurement in an LC-MS/MS system. The phosphopeptide/phosphoprotein enrichment step is the major difference from standard proteomics techniques, with the most successful enrichment methods to date being either antibody or affinity based.

Phosphorylation Site Specific Antibodies Immunoprecipitation using phosphotyrosine-specific antibodies followed by MS-based protein identification is a well-established strategy for the differential analysis and identification of novel activated signaling proteins in growth-factor stimulated or unstimulated cells [190, 264]. This process can also be applied to investigate the effects of drug treatment. In addition, phosphotyrosine-specific antibodies have been successfully used to globally enrich thousands of tyrosine phosphorylated peptides in cancer cells [265, 266]. Moreover, phosphoserine- and phosphothreonine antibodies are also available for monitoring phosphorylation events and discovering novel phosphosites [267].

Immobilized Metal Affinity Chromatography (IMAC) IMAC is based on the high affinity of phosphates to Fe^{3+} or Ga^{3+} that is immobilized onto porous column packing material [268, 269]. This method is most efficient in an acidic environment (pH 2-3.5 range), with nonspecific binding of nonphosphorylated peptides possible outside this pH range or when loading excessive amounts of peptide samples. Strongly acidic peptides rich in glutamic and aspartic acid also have high affinity to IMAC beads; however, these acidic groups can be methylated before IMAC enrichment, significantly increasing the selectivity of IMAC for phosphopeptides [270]. IMAC

has been successfully used in large-scale phosphoproteomics from various species [186, 270-272]. Moreover, IMAC is also useful for intact phosphoprotein enrichment [273].

Titanium Dioxide (TiO_2) Enrichment TiO_2 enrichment is a more recently developed method in large-scale phosphopeptide enrichment that features even higher affinity and selectivity than IMAC [274, 275]. TiO_2 spheres as a column packing material have replaced the silica-based supports in IMAC because of their high chemical stability and anion-exchange properties. Similar to IMAC, acidic peptides rich in glutamic and aspartic acid are also likely to be collected using TiO_2 enrichment. This problem was solved by Jørgensen and coworkers when they introduced excess 2,5-dihydroxy benzoic acid (DHB) as a competitive binder to outcompete these acidic peptides, while phosphopeptides are retained [274]. Although excess DHB greatly improves the selectivity of TiO_2 enrichment, the amount of DHB needs to be optimized from system to system, as too much DHB will result in introduction of chemical noise and poor reproducibility.

Strong Cation Exchange (SCX) SCX can also be used as a pre-separation step for phosphopeptides to exploit the difference in their solution charge states at low pH; each of the negatively charged phosphate groups reduces the net charge state by one. Therefore, phosphopeptides can be enriched in early SCX fractions by their decreased charge state. Gygi and coworkers have identified more than 2000 phosphopeptides in these early SCX factions using LC-MS/MS [276]. Coupled with IMAC or TiO_2, SCX has shown to be a powerful pre-fractionation tool in large-scale phosphoproteomics studies [186, 188, 277].

Peptide Fragmentation in Phosphoproteomics Another interesting aspect of analyzing phosphopeptides is the fragmentation step in the MS/MS workflow. Increasing attention has been given to ECD and ETD for their unique fragmentation patterns, which yield more extensive

and even backbone cleavages than CID, with PTMs (particularly phosphorylation) remaining retained on the peptide/protein fragments [169, 278-280]. However, because the efficiency of ECD and ETD is proportional to charge state, only highly charged peptides can be efficiently analyzed. The optimal strategy is to combine the data from identical samples using both CID (for singly and doubly charged peptides) and ETD (for multiply charged peptides) [281].

1.2.8 Computational tools

As the use of high performance mass spectrometers has become the norm, tens of thousands of proteins can be identified and quantified in a single experiment, and therefore computational approaches have emerged to aid in the analysis of complex proteomic data. These computational approaches are crucial not only for accurate protein identification, quantification, and the determination of PTMs, but also for the conversion of complex proteomic data into sophisticated computer models of cellular protein networks, and for the comparison of these protein networks under multiple conditions, e.g. disease versus normal. Later in this thesis, a computational tool was developed to study protein-protein interaction networks using the archived datasets in a proteomics database. Here, two computer tools that can visualize and interpret proteomic data into protein networks are discussed.

Ingenuity Pathway Analysis (IPA) IPA software (www.ingenuity.com) has drawn increasing attention in its ability to identify drug targets on a signaling pathway, provide up-to-date clinical status of drugs that target the pathway, and interpret large proteomic datasets into protein interaction networks. The IPA software allows users to upload proteomic data in a variety of ways and formats, and to compare the changes of protein abundance and protein organization

among different samples. Interpretation of these large models and their reduction to a small set of significant changes then helps to clarify the mechanism of drug action.

VisANT VisANT (http://visant.bu.edu) can be used for visualizing and analyzing biological interaction networks between genes and proteins [282]. VisANT also supports known/predicted metabolic pathway analysis by querying either co-expressed components of a pathway or physical interactions of the components. In addition, VisANT 3.5 enables the application of gene ontology (GO) in network analysis, particularly in finding over-represented GO terms in a given sub-network and expression-enriched GO modules in different experimental conditions [283].

1.3 Platelets and proteomic research

Platelets are a challenging system to study at the molecular level. Since platelets are anucleate cells, the lack of DNA prevents any genetic manipulations, for instance, transfection. Platelets contain low levels of mRNA and are capable of synthesizing proteins; however, protein synthesis in platelets is minimal and its biological relevance is still unclear [284]. In addition, platelets cannot be cultured in great abundance and isolated platelets can only be stored for a limited time, normally 5-7 days. Due to the small size, the use of microscopic techniques to study protein distribution in platelets requires high resolution and thus it can be difficult to perform. Moreover, although numerous studies have used mice to study platelet functions *in vivo*, mouse platelets may not be a perfect representation of human platelets, as for example mouse platelets express the PAR3 thrombin receptor instead of PAR1. Moreover, unlike human platelets, mouse platelets do not aggregate in response to LPA [96, 97].

Due to these unique features of platelets, proteomics has emerged as an ideal approach to study human platelet function at the protein or peptide level [285-288]. Approximately 4,000

proteins have been identified in human platelets [289-292]. Protein compositions have been characterized in microparticles [293, 294] and the soluble protein fraction derived from activated platelets [112, 295]. Proteins that are stored in platelet α-granules [113, 296] and dense granules [297] were also identified. Enrichment strategies were employed in combination with LC-MS/MS to analyze different sub-proteomes of platelets. Membrane protein composition of human platelets was studied by proteomic approaches [298-300]. Phosphoprotemics analysis was performed for resting platelets [301] and agonist-stimulated platelets [302, 303]. Similarly, glycoproteomics analysis was also applied to study human platelets [304, 305]. Moreover, comparative proteomics approaches were employed to characterize protein changes involved in platelet activation [306-310], platelet storage [311-314], platelet shedding [315], platelets in elderly populations [316] and various diseases [296, 314, 317-331].

1.4 Research hypotheses and aims

Platelet activation and platelet-monocyte aggregate (PMA) formation plays an important role in the development of atherosclerosis. Platelets can be activated by normal hemostatic stimuli such as thrombin, as well as by atherosclerotic plaque-released factors such as LPA. In response to both, platelet aggregation occurs via integrin αIIbβ3. In addition, the process of platelet activation is mediated by multiple small GTPases. Activated platelets in turn recruit monocytes to the atherosclerotic lesions and facilitate plaque formation. Activated platelets also form PMAs circulating in blood, which are established early markers for CVDs.

The overarching hypothesis of this thesis was that by characterizing protein-protein interactions and signaling pathways in platelets and PMAs in detail, it is possible to identify

potential markers and targets that would contribute to the development of intervention strategies for CVDs.

This hypothesis resulted in the following specific aims:

In the first aim, we wanted to study protein-protein interaction networks in platelet aggregation using bioinformatics; to achieve this, a novel computational tool had to be developed that could use archived datasets in a proteomics database (Chapter 2).

In the second aim, we decided to investigate activation levels of several small GTPases and signaling pathways in platelet activation in parallel; to achieve this, a novel targeted proteomics-based tool needed to be developed to quantify activity level changes of multiple small GTPase isoforms from a single sample aliquot (Chapter 3).

In the third and final aim, we sought to identify key signaling pathways and regulators involved in PMA formation; to achieve this, a quantitative phosphoproteomics strategy had to be adapted and optimized for a two-cell system in order to study the global phosphorylation events in monocytes incubated with activated platelets (Chapter 4).

Chapter 2 Development of *in silico* protein interaction analysis and application on platelet aggregation

2.1 Introduction

The ability to generate data in proteomics experiments far outstrips the ability to analyze it [332]. Indeed, as large scale proteomics on high performance mass spectrometers has become the norm [333], and experiments frequently analyze hundreds of thousands of peptides from thousands of proteins, data processing and analysis has become a significant challenge [334]. As a result, an enormous amount of data has been submitted to public databases, only a small portion of which has been studied beyond confirming the presence or absence of a group of proteins. It is likely that the large amount of data in public repositories derived from a diverse set of experiments contains useful information that is not accessible from a single proteomics experiment. For instance, by extracting the datasets that are the most likely to contain information on protein-protein interactions for a protein of interest, one should be able to identify the proteins that are frequently observed, which are either known/unknown interaction partners or non-specifically binding proteins. Using this approach, one could then generate new hypotheses for novel protein-protein interactions, i.e. perform an *in silico* protein interaction analysis.

To test this idea, the Global Proteome Machine Database (GPMDB) [335] was used, which is the largest curated and publicly available data repository for proteomics information derived from tandem mass spectrometry. As of October 2010, there are >150,000 datasets contained in the GPMDB with the identification of >26,000,000 proteins and >200,000,000 peptides. Each dataset or "model" in the GPMDB is a mass spectrometry-based proteomic experiment, which is

essentially an estimation of proteins contained in a sample, based on the MS/MS information provided, using the X!Tandem algorithm [336-338]. Each dataset contains a list of the estimated proteins with the identities of the sequenced peptides and proteins, as well as their confidence (log(e) value), intensity (log(I) value), sequence coverage and information about any relevant homologues.

In order to perform an *in silico* protein interaction analysis using the *Homo sapiens* datasets in the GPMDB, a well-known biological model was selected and a general method was developed that allows the extraction of the most appropriate datasets and their relevant features. Subsequently, this method was applied to other biological models to demonstrate its general value in identifying candidate interaction partners, and proteins that share similar functions in a protein network.

2.2 Method development

2.2.1 *In silico* protein interaction analysis

In order to develop a general method for *in silico* protein interaction analysis using the GPMDB, an adequate model protein was needed with known interaction partners and large number of identifications archived in the GPMDB. Human HIST4H4, a member of the histone H4 protein family, was chosen, because the histone octamer, which consists of various isoforms in the histone H2A, H2B, H3 and H4 protein families [339], is a well-defined complex; and HIST4H4 was positively identified in the highest number (2199) of datasets among all the histone proteins in the GPMDB as of April 21st, 2010.

Among the 2199 datasets which sequenced HIST4H4, some of them were identical, due to researchers periodically submitting the same raw data to the GPMDB multiple times. In order to eliminate these repetitive datasets, a filter was developed where datasets with all of the following three criteria were removed (Figure 2.1, step 1): the same dataset size (number of proteins identified in a dataset), the same sequence coverage for the protein of interest (HIST4H4 in this case) and the same protein identification score (log(e) value) for the protein of interest. 1981 out

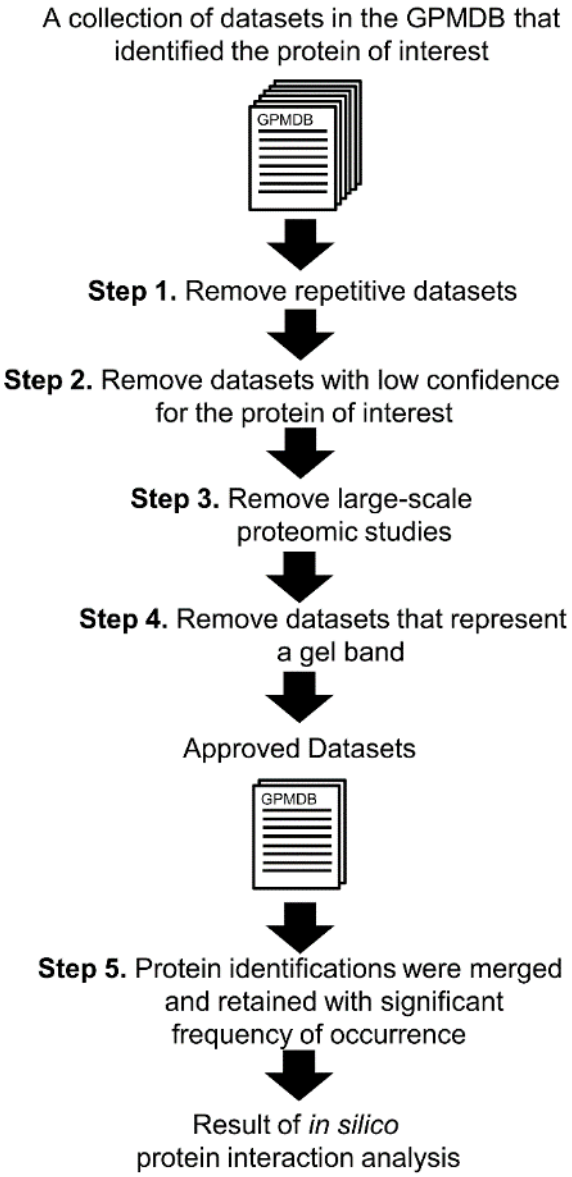

Figure 2.1 General workflow of in silico protein interaction analysis.

of the 2199 datasets remained after removing datasets identified as being repetitive. These 1981 datasets were considered unique datasets.

Next, datasets were sorted and filtered based on the confidence of identification for HIST4H4 (Figure 2.1, step 2), which consists of two parts: sequence coverage and protein identification score. As used here, sequence coverage is the number of identified amino acids of the protein of interest, and protein identification score is the log(e) value of the protein of interest, based on the expectation values of identified peptides [251]. The goal of this filter is to minimize false positives or spurious identifications by sequencing at least two small peptides or a single large one with high confidence for the protein of interest. The correlation of sequence coverage and protein identification score for HIST4H4 in the remaining 1981 datasets is shown in Figure 2.2A. Sequence coverage reached a maximum of 87 amino acids (AA) for HIST4H4 (103AA), due to the fact that some regions of HIST4H4 produce peptides upon trypsin digestion that are very small (e.g. ^{37}RRLARR^{41}), and are therefore unlikely to be observed using standard mass spectrometry techniques. Notably, HIST4H4 was not identified with a sequence coverage of 16 or 17AA (Figure 2.2B), which is due to the fact that among the most observed peptides from HIST4H4, no peptides were sequenced within this range, and the minimum number of amino acids identified from two peptides (^{47}ISGLIYEETR^{56} and ^{61}VFLENVIR^{68}) was 18AA. Therefore, sequence coverage ≥18AA for HIST4H4 could only be achieved with confident identification of at least a single 18AA peptide or two smaller peptides. A sequence coverage cutoff of ≥18AA was therefore applied, leaving 1370 out of the 1981 datasets remaining. Interestingly, while 93.5% of the identifications of HIST4H4 with sequence coverage≥18AA have log(e)≤-10 (top right quadrant, Figure 1a), only 7.0% of the HIST4H4 with lower sequence coverage were identified with log(e)≤-10 (bottom right quadrant, Figure 2.2A). This indicates that log(e)≤-10

can be used as an additional confidence cutoff to eliminate the datasets containing HIST4H4 with many amino acids sequenced but poor identification score (Figure 2.2B). Thus, sequence coverage ≥18AA and protein identification score log(e)≤-10 were considered to provide high confidence for HIST4H4 (top top right quadrant, Figure 2.2B)

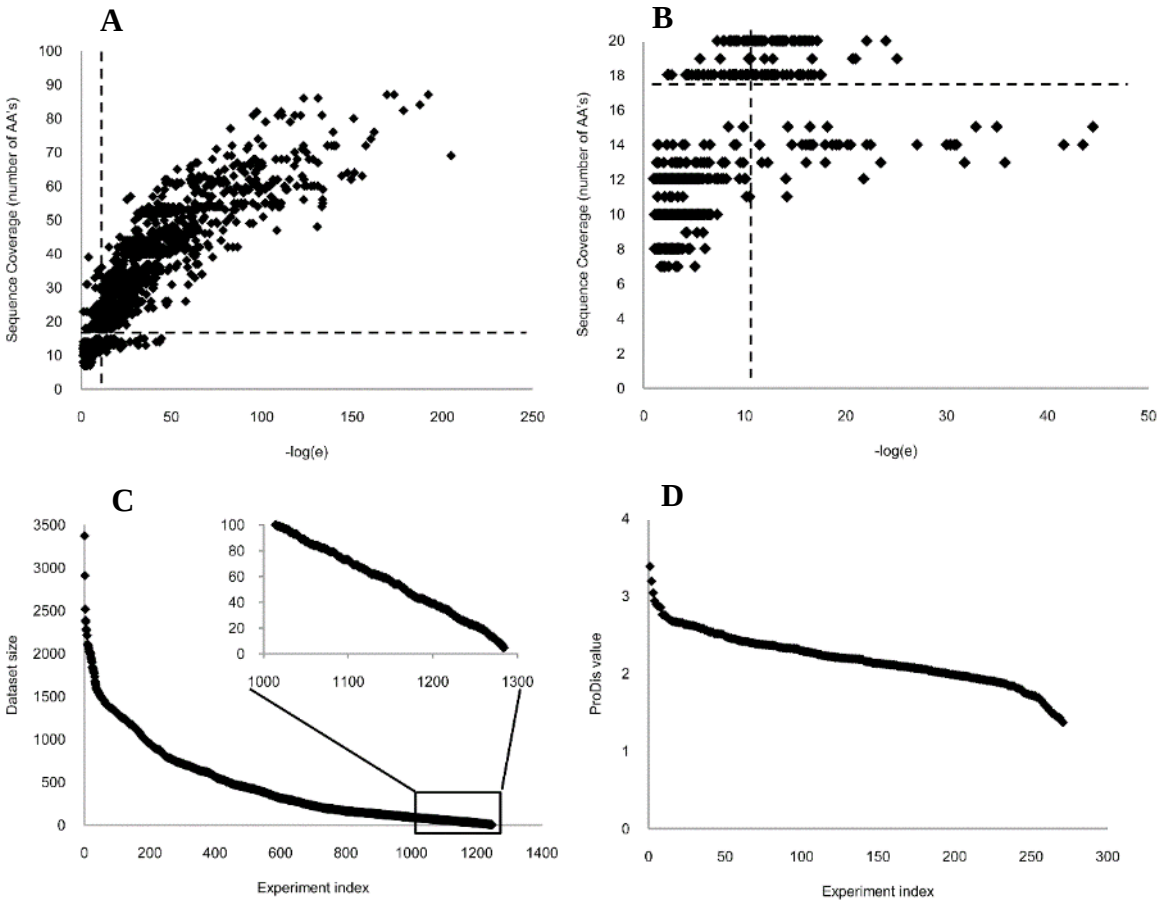

Figure 2.2 Datasets filtered based on the confidence of identification for HIST4H4. (A) The correlation of -log(e) with sequence coverage for HIST4H4 in the 2336 datasets. (**B**) Enlarged area for sequence coverage from 0 to 20AA. (**C**) The distribution of dataset size for the 1395 datasets remaining after the confidence filter. (**D**) The distribution of ProDis scores for the 271 datasets.

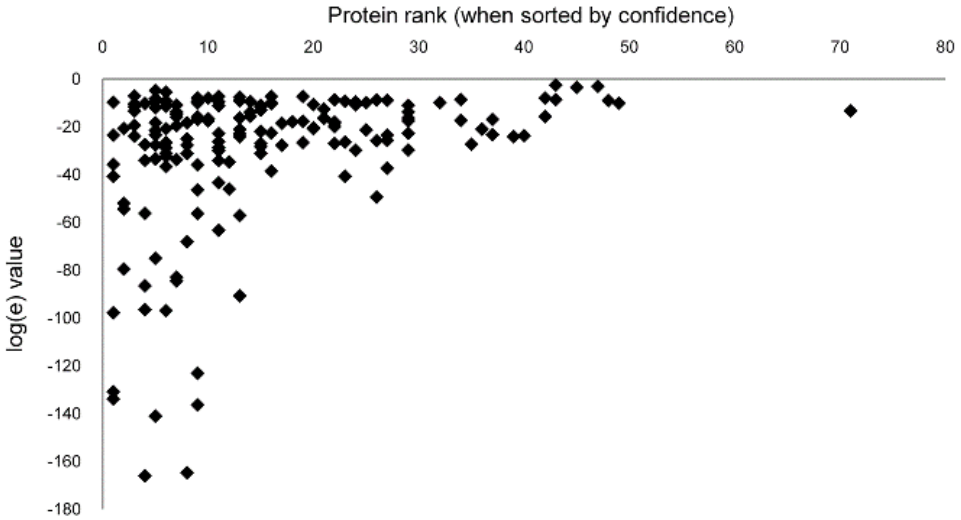

Figure 2.3 The correlation of protein rank vs confidence log(e) value.

As a result, 1284 out of the 1981 datasets were selected and extracted from the GPMDB, each being unique and containing HIST4H4 with high confidence. In general, a lower log(e) value correlates with HIST4H4 having a higher rank (when sorted by confidence); however, HIST4H4 was the top ranked protein in only a fraction of the datasets (Figure 2.3).

Among these 1284 datasets, any type of proteomic experiment may be represented, e.g. global proteomics studies, samples from enrichment of specific organelles, or phosphopeptides, co-immunoprecipitation (co-IP), or a single gel band from any such experiment. Due to the fact that researchers do not usually provide the description of how the samples were generated when submitting their data to the GPMDB, information about the exact type of each experiment is not available. Large-scale proteomics experiments, where up to 3500 proteins were identified alongside HIST4H4 (Figure 2.2C), aim to identify the highest number of proteins and therefore may have insufficient specificity to provide information about functional links. In contrast, 100 to 300 proteins can be identified in a high-throughput co-IP/MS experiment [340], and less than

100 proteins are normally identified by a standard co-IP experiment. These experiments with small number of protein identifications are the ones which are most likely to provide information on protein-protein interactions. Therefore, a dataset size filter was introduced (Figure 2.1, step 3), size being defined as the number of proteins identified in a dataset. The distribution of dataset size for the 1284 datasets is shown in Figure 2.2C. A dataset size cutoff of ≤100 proteins was used to test effects of the remaining criteria. The effect of increasing dataset size on the final result of the analysis is discussed later in this section. 271 datasets remained with dataset size ≤100 proteins.

Moreover, proteins identified from the analysis of a single gel band do not necessarily have functional links, as they may simply be co-incident as the result of a gel fractionation from a larger sample. In order to eliminate these type of datasets, a protein distribution (ProDis) filter was introduced (Figure 2.1, step 4), which is defined as a threshold in the geometric standard deviation of molecular weights (MW) of identified proteins in a given dataset (equation 1).

$$\text{ProDis} = \exp\left(\sqrt{\frac{\sum_{i=1}^{n}(\ln A_i - \ln \mu_g)}{n}}\right) \qquad \text{(equation 1)}$$

Where the geometric mean of a set of protein MW's (A_1, A_2, ..., A_n) is denoted as μ_g. ProDis describes the spread of the molecular weights of the identified proteins in a predicted one-dimensional SDS-PAGE gel, which can be visualized by the gel display feature in the GPMDB (Figure 2.4), where one can see that as the ProDis decreases, the molecular weight spread of the identified proteins becomes more focused. The distribution of ProDis for the 271 remaining datasets is shown in Figure 2.2D. Low ProDis values represent experiments which likely result from the analysis of a single gel band, whereas experiments with a high ProDis are more likely to be the result of an experiment without MW-based protein level fractionation steps. Upon manual

inspection, a ProDis of >2 was determined to be a reasonable protein distribution cutoff, as all datasets with ProDis>2 confidently identified proteins with widely varying molecular weights, whereas with decreasing ProDis, datasets were increasingly likely to contain a tightly focused grouping of identified proteins' molecular weights. As a result of applying a ProDis cutoff of > 2, 195 datasets remained.

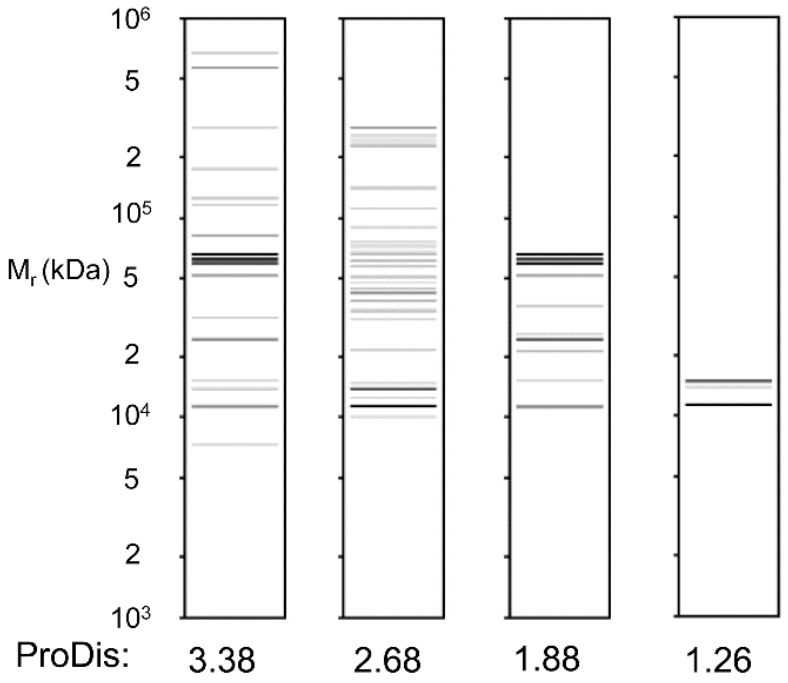

Figure 2.4 Gel display feature in the GPMDB showing protein distribution (ProDis).

These 195 datasets were unique and likely to provide information on protein-protein interactions with high confidence for HIST4H4, and therefore were considered approved datasets for *in silico* protein interaction analysis. From these approved datasets, protein identifications with the same HGNC ID were merged. Via their unique HGNC name, 2832 proteins were identified in the final result (Figure 2.5A); however, 97.4% of these proteins were observed in fewer than 20 datasets, or only about 10% of the total number of approved datasets.

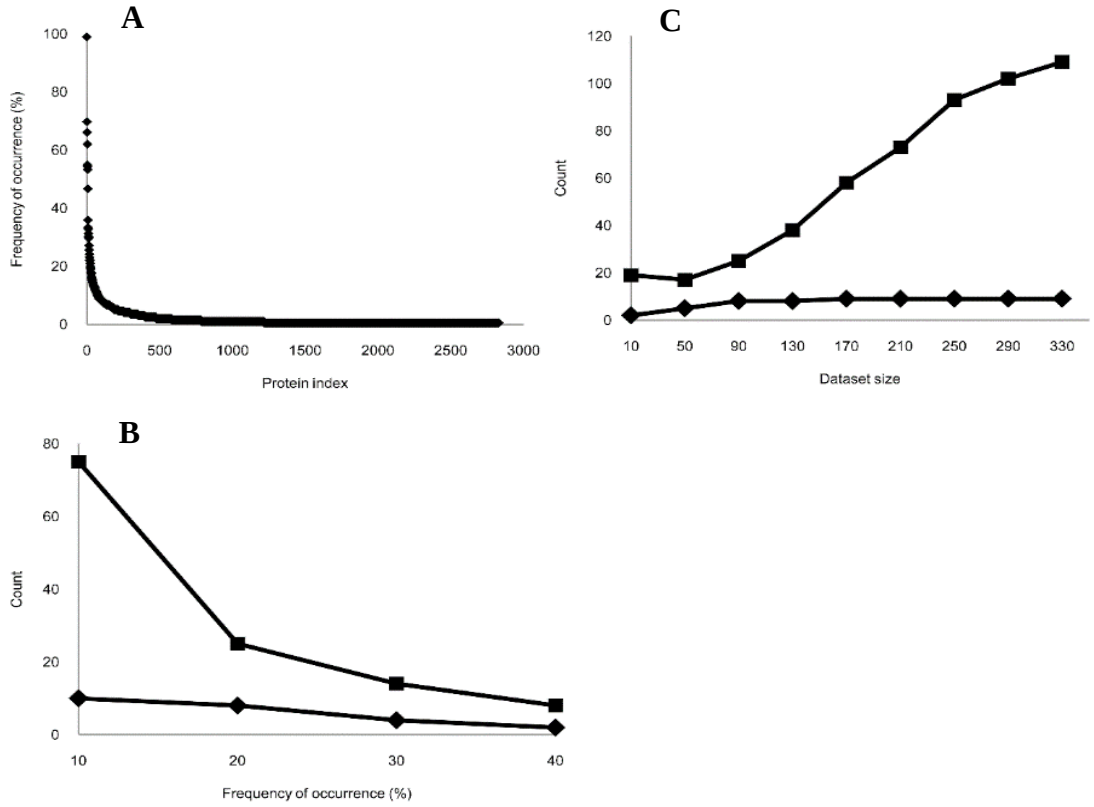

Figure 2.5 Datasets filtered by frequency of occurrence. (A) The distribution of frequency of occurrence for 2832 proteins identified in HIST4H4 analysis. **(B)** The distribution of number of histone proteins identified (♦) and number of all the proteins identified (■) in the *in silico* HIST4H4 interaction analysis using different frequency of occurrence cutoffs. **(C)** The distribution of number of histone proteins identified (♦) and number of all the proteins identified (■) in the *in silico* HIST4H4 interaction analysis using different dataset sizes.

Therefore, frequency of occurrence, which is defined as the number of observations of a protein divided by the total number of approved datasets, was introduced as a measure of the co-occurrence of the identified proteins with the protein of interest (Figure 2.1, step 5). The effect of frequency of occurrence cutoffs between 10% and 40% was tested on the proteins identified in the analysis (Figure 2.5B). Demanding a high frequency of occurrence resulted in a small number of protein identifications. With frequency of occurrence ≥40%, only two histone proteins were observed (Figure 2.5B). However, using frequency of occurrence ≥30%, the four histone proteins HIST4H4, H2AFJ, H2BFS and H3F3B were observed, i.e. one member of each of the histone H2A, H2B, H3 and H4 families, indicating the identification of a complete histone

octamer [339]. With frequency of occurrence ≥20%, eight histone proteins were observed, including additional proteins from the histone H1 protein family, a family of linker proteins, indicating that proteins that are more loosely associated with HIST4H4 were observed with a lower frequency of occurrence. Indeed, three different isoforms of histone deacetylase, HDAC2, HDAC1 and HDAC7, were identified with frequency of occurrence of 10.6%, 3% and 0.8% respectively. However, when using a lower frequency of occurrence cutoff, the number of additional proteins included in the final result increases (Figure 2.5B), raising the likelihood of a non-specific result.

By default, proteins with an identification score of log(e)≤-1 were merged in this analysis. An additional protein confidence cutoff (log(e) value) can be applied, however, when merging the protein identifications before ranking by frequencies of occurrence. Introduction of this additional step can ensure high confidence for these proteins in the final results; however, it could also result in the loss of important interaction partners. For instance, when a log(e)≤-3 confidence filter was applied, H3F3B was not identified in the final result for HIST4H4. This is due to the fact that 40 out of 136 amino acids of H3F3B are unlikely to be identified using mass spectrometry, with other regions only sequenced sporadically, resulting in 49 out of 70 observations of H3F3B having a confidence of log(e)>-3. Thus, the frequency of occurrence for H3F3B dropped from 35.9% to 10.8% in the HIST4H4 analysis when using more stringent confidence cutoff, which was then eliminated by the frequency of occurrence ≥20% cutoff.

After the frequency of occurrence cutoff is applied, the final result of an *in silico* protein interaction analysis is obtained. With the frequency of occurrence cutoff fixed at $f \geq 20\%$, the effect of increasing the dataset size from ≤10 to ≤330 proteins, on the final result was tested (Figure 2.5C). After the dataset size filter reached ≤50 proteins, the complete histone octamer

was observed, suggesting ≤50 proteins is the minimum cutoff for dataset size for this protein and filter settings without losing known strongly interaction partners. As dataset size increases to ≤90 proteins, additional proteins from the histone H1 family were observed, indicating proteins that are more loosely associated with HIST4H4 were observed with larger dataset size cutoff. As dataset size increases from ≤170 to ≤330 proteins, the number of histone proteins identified remained the same (Figure 2.5C); however, the total number of proteins identified in the final result increases continually (Figure 2.5C).

When dataset size ≤100 proteins and frequency of occurrence ≥20% were chosen, 195 datasets were approved with 25 proteins observed, eight of which belonged to the histone families in the final result (Table 2.1).

Table 2.1 The 25 proteins identified for HIST4H4 using *in silico* protein interaction analysis with dataset size ≤100 proteins and frequency of occurrence ≥20%.

f(%)	Accession	Description
100.0	HIST4H4	Histone cluster 4, H4
69.7	sp|TRYP_PIG|	Trypsin precursor
66.2	ACTG1	Actin, gamma 1
62.1	KRT1	Keratin 1
54.9	KRT9	Keratin 9
54.4	KRT2	Keratin 2
53.3	KRT10	Keratin 10
46.7	H2AFJ	H2A histone family, member J
35.9	H3F3B	H3 histone, family 3B (H3.3B)
33.3	sp|ALBU_BOVIN|	Serum albumin; BSA
32.8	H2BFS	Histone H2B type F-S
31.3	KRT14	Keratin 14
30.3	KRT5	Keratin 5
29.7	GAPDH	Glyceraldehyde-3-phosphate dehydrogenase
29.7	HIST1H1C	Histone H1.2 (Histone H1d)
27.2	HIST1H2BB	Histone cluster 1, H2bb
25.6	H2AFV	Histone H2A.V
25.6	HNRNPC	Heterogeneous nuclear ribonucleoproteins C1/C2
24.1	VIM	Vimentin
23.1	NPM1P21	Nucleolar phosphoprotein B23, numatrin
22.1	EEF1A2	Eukaryotic translation elongation factor 1 alpha 2
22.1	HNRNPA2B1	Heterogeneous nuclear ribonucleoproteins A2/B1
22.1	Ighg1	Immunoglobulin heavy constant gamma 1
21.0	HIST1H1B	Histone cluster 1, H1b
20.0	DCD	Dermcidin

2.2.2 Reverse *in silico* protein interaction analysis

"Reverse" *in silico* protein interaction analyses were also performed, which are analogous to reverse co-IP experiments, targeting H2AFJ, HIST1H2BB and H3F3B, which were identified in the aforementioned HIST4H4 analysis, representing the histone H2A, H2B and H3 protein families. Using the same thresholds at each cutoff as was used for the HIST4H4 analysis, 27, 37 and 73 proteins were identified for H2AFJ, HIST1H2BB and H3F3B analyses, respectively (Appendix B-D). The identified proteins in all four analyses presented a large degree of similarity (Figure 2.6). The large number of proteins specifically identified for H3F3B were a result of the fact that only nine datasets were approved for H3F3B, and thus proteins that were observed more than twice among all nine datasets were retained in the final result. The limited number of datasets was due to the low protein confidence with which H3F3B was commonly identified (as described earlier). Seventeen proteins were identified in all four analyses (Table 2.2), including seven proteins from the histone family, indicating observation of the complete histone octamer. Other shared proteins were either abundant cytoskeletal proteins or common contaminants that were introduced by sample preparation of mass spectrometry experiments; i.e. keratins, trypsin and serum albumin.

Table 2.2 The 17 proteins identified in all H2AFJ, HIST1H2BB, H3F3B and HIST4H4 in silico protein interaction analysis.

H2AFJ	HIST1H2B	H3F3	HIST4H4		
f(%)	*f*(%)	*f*(%)	*f*(%)	Accession	Description
61.6	48.8	44.4	66.2	ACTG1	Actin, gamma 1
100.0	34.9	77.8	46.7	H2AFJ	Histone H2A.J
24.7	27.9	44.4	25.6	H2AFV	Histone H2A.V
32.9	32.6	100.0	35.9	H3F3B	H3 histone, family 3B
23.3	20.9	33.3	21.0	HIST1H1B	Histone cluster 1, H1b
32.9	25.6	22.2	29.7	HIST1H1C	Histone H1.2
35.6	100.0	66.7	27.2	HIST1H2BB	Histone cluster 1,
68.5	72.1	88.9	100.0	HIST4H4	Histone cluster 4, H4
30.1	37.2	33.3	24.1	VIM	Vimentin
71.2	76.7	77.8	62.1	KRT1	Keratin 1
53.4	69.8	77.8	53.3	KRT10	Keratin 10
20.5	58.1	44.4	31.3	KRT14	Keratin 14
50.7	65.1	66.7	54.4	KRT2	Keratin 2
26.0	51.2	22.2	30.3	KRT5	Keratin 5
50.7	69.8	77.8	54.9	KRT9	Keratin 9
27.4	39.5	33.3	33.3	sp|ALBU_BOVI	Serum albumin;BSA
74.0	88.4	88.9	69.7	sp|TRYP_PIG|	Trypsin precursor

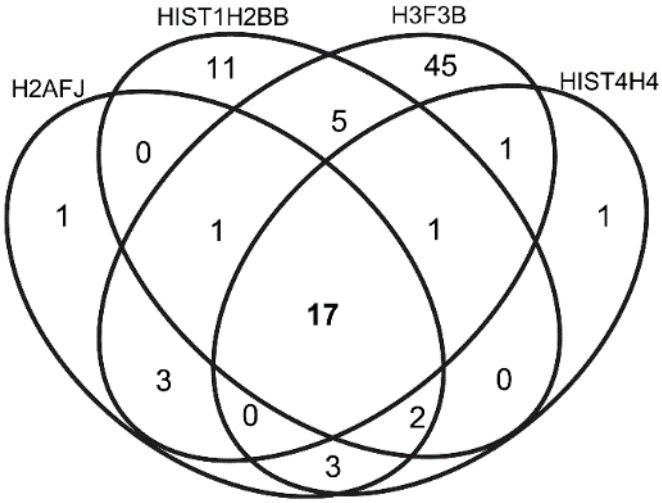

Figure 2.6 Venn diagram showing the overlap of the number of proteins identified among H2AFJ, HIST1H2BB, H3F3B and HIST4H4 analyses.

2.3 Applications

2.3.1 26S proteasome subunits

The *in silico* protein interaction analysis was applied to the proteasome, a much larger and more intricate protein complex than the histone octamer. The 26S proteasome is made up by a 20S core particle and a 19S regulatory complex at one or both ends of the core particle [341]. The 20S core particle consists of four stacked ring structures, with each of the outer two rings composed of seven distinct α subunits, and each of the inner two rings composed of seven distinct β subunits. The α subunits also associate with the base complex, six ATPase subunits and two non-ATPase subunits, in the 19S regulatory complex.

The *in silico* protein interaction analysis was first performed targeting human PSMA1, the α1 subunit in the 20S core particle, using the same thresholds at each cutoff as was used for the HIST4H4 analysis (sequence coverage ≥18AA and log(e)≤-10 for PSMA1, dataset size≤100 proteins and ProDis≥2). Only six datasets were approved and no other proteasome subunit was identified in the final result (Appendix E). When a dataset size cutoff of ≤350 proteins was used while the other thresholds remained the same, 22 datasets for PSMA1 were approved and all of the other six α subunits were identified with frequency of occurrence ≥20% (Table 2.3, column 1). Using these new thresholds, additional analyses were performed for the other six α subunits and investigated the frequencies of occurrence for each of the 26S proteasome subunits (Table 2.3). All of the seven α subunits were identified with frequency of occurrence ≥20% in all seven analyses, while all of the seven β subunits were identified with frequency of occurrence ≥15%. Also, all of the eight subunits in the base complex, i.e. PSMC1, PSMC2, PSMC3, PSMC4, PSMC5, PSMC6, PSMD1 and PSMD2, were identified with frequency of occurrence ≥10%.

Conversely, the other, more distant regulatory subunits were identified sporadically and with much lower frequencies of occurrence.

Table 2.3 The frequency of occurrence for each proteasome subunit in all PSMA1, PSMA2, PSMA3, PSMA4, PSMA5, PSMA6 and PSMA7 analyses.

PSMA1	PSMA2	PSMA3	PSMA4	PSMA5	PSMA6	PSMA7		
f(%)	*f*(%)	*f*(%)	*f*(%)	*f*(%)	*f*(%)	*f*(%)	Accession	Description
100.0	60.0	71.4	37.6	63.2	26.7	37.0	PSMA1	Proteasome 20S subunit, alpha type, 1
45.4	100.0	71.4	56.4	52.6	33.3	51.8	PSMA2	Proteasome 20S subunit, alpha type, 2
22.7	60.0	100.0	31.3	57.9	33.3	40.7	PSMA3	Proteasome 20S subunit, alpha type, 3
27.3	53.3	50.0	100.0	36.8	23.4	33.3	PSMA4	Proteasome 20S subunit, alpha type, 4
36.4	46.7	78.6	31.3	100.0	40.0	66.7	PSMA5	Proteasome 20S subunit, alpha type, 5
45.5	46.7	64.3	37.5	63.2	100.0	63.0	PSMA6	Proteasome 20S subunit, alpha type, 6
27.2	60.0	85.7	50.1	68.5	26.7	100.0	PSMA7	Proteasome 20S subunit, alpha type, 7
22.7	60.0	71.4	37.5	42.1	30.0	33.3	PSMB1	Proteasome 20S subunit, beta type, 1
27.3	66.7	35.7	37.6	31.6	16.7	22.2	PSMB2	Proteasome 20S subunit, beta type, 2
31.8	73.3	57.1	62.5	47.4	26.7	55.6	PSMB3	Proteasome 20S subunit, beta type, 3
27.3	40.0	57.1	31.3	36.8	20.0	40.7	PSMB4	Proteasome 20S subunit, beta type, 4
27.3	33.3	42.9	50.1	31.6	20.0	22.2	PSMB5	Proteasome 20S subunit, beta type, 5
27.3	46.7	50.0	25.0	42.1	26.7	25.9	PSMB6	Proteasome 20S subunit, beta type, 6
18.2	20.0	42.9	31.3	26.3	16.7	29.6	PSMB7	Proteasome 20S subunit, beta type, 7
13.6	26.7	28.6	18.8	21.1	16.7	14.8	PSMC1	Proteasome 19S regulatory subunit, ATPase, 1
18.1	26.7	28.6	31.3	21.1	10.0	14.8	PSMC2	Proteasome 19S regulatory subunit, ATPase, 2
18.2	13.3	14.3	18.8	15.8	16.7	11.1	PSMC3	Proteasome 19S regulatory subunit, ATPase, 3
13.6	20.0	21.4	18.8	15.8	10.0	14.8	PSMC4	Proteasome 19S regulatory subunit, ATPase, 4
13.6	26.7	28.6	25.0	21.1	10.0	18.5	PSMC5	Proteasome 19S regulatory subunit, ATPase, 5
13.6	33.4	28.6	25.1	21.1	10.0	18.5	PSMC6	Proteasome 19S regulatory subunit, ATPase, 6
13.6	26.7	28.6	18.8	21.1	20.0	14.8	PSMD1	Proteasome 19S regulatory subunit, non-ATPase,
18.2	46.7	28.6	31.3	31.6	23.3	18.5	PSMD2	Proteasome 19S regulatory subunit, non-ATPase,
9.1	13.3	14.3	12.5	10.5	3.3	-	PSMD3	Proteasome 19S regulatory subunit, non-ATPase,
4.5	-	-	6.3	5.3	3.3	-	PSMD4	Proteasome 19S regulatory subunit, non-ATPase,
18.2	20.0	21.4	18.8	15.8	6.7	11.1	PSMD5	Proteasome 19S regulatory subunit, non-ATPase,
-	6.7	-	-	-	6.7	-	PSMD6	Proteasome 19S regulatory subunit, non-ATPase,
4.5	6.7	-	-	-	-	-	PSMD7	Proteasome 19S regulatory subunit, non-ATPase,
13.6	13.3	14.3	12.5	10.5	6.7	7.4	PSMD8	Proteasome 19S regulatory subunit, non-ATPase,
4.5	6.7	7.1	6.3	5.3	13.3	3.7	PSMD9	Proteasome 19S regulatory subunit, non-ATPase,
9.1	13.3	14.3	12.5	10.5	3.3	7.4	PSMD10	Proteasome 19S regulatory subunit, non-ATPase,
9.0	20.0	28.5	18.8	15.8	30.0	11.1	PSMD11	Proteasome 19S regulatory subunit, non-ATPase,
13.6	20.0	14.3	12.5	15.8	16.6	7.4	PSMD12	Proteasome 19S regulatory subunit, non-ATPase,
4.5	-	-	6.3	5.3	3.3	-	PSMD13	Proteasome 19S regulatory subunit, non-ATPase,
4.5	6.7	7.1	6.3	5.3	3.3	3.7	PSMD14	Proteasome 19S regulatory subunit, non-ATPase,

Using frequency of occurrence ≥15% for all seven analyses, 88 proteins were identified in the overlap among all seven analyses after removal of common contaminants, including all seven α and seven β subunits (Appendix F). STRING 8.2 [342], which provides the most comprehensive view of protein-proteins interactions, was used to visualize functional links among these 88 proteins (Figure 2.7a). Proteasome activator subunits 1 and 2, PA28 α and β were identified, as well as ubiquitin and a large number of adaptor proteins, including various members of chaperonin containing TCP1 complex and different isoforms of 14-3-3 proteins and heat shock proteins. When a frequency of occurrence cutoff of ≥10% was used, 192 proteins were identified in the overlap of all seven analyses after removal of common contaminants (Figure 2.7b), where all the subunits in the base complex as well as the 20S core particle were observed. Additional isoforms of ubiquitin proteins and chaperones were also identified using lower frequency of occurrence cutoff.

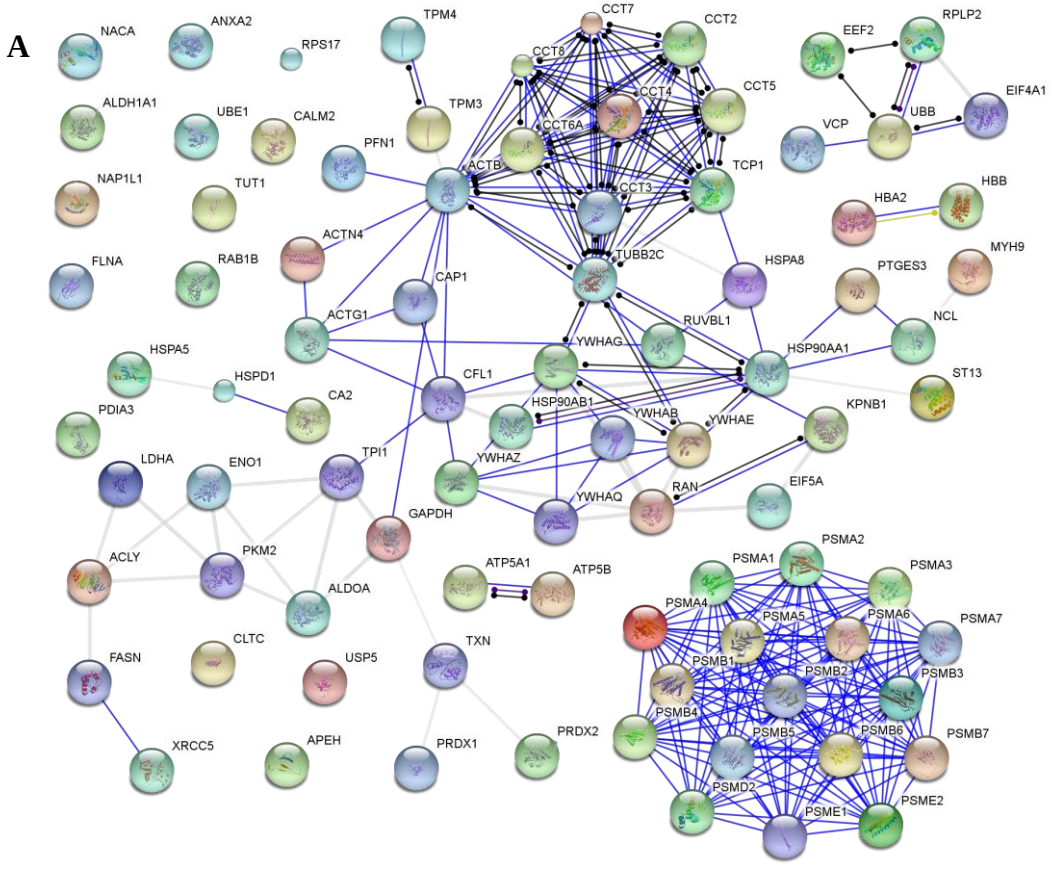

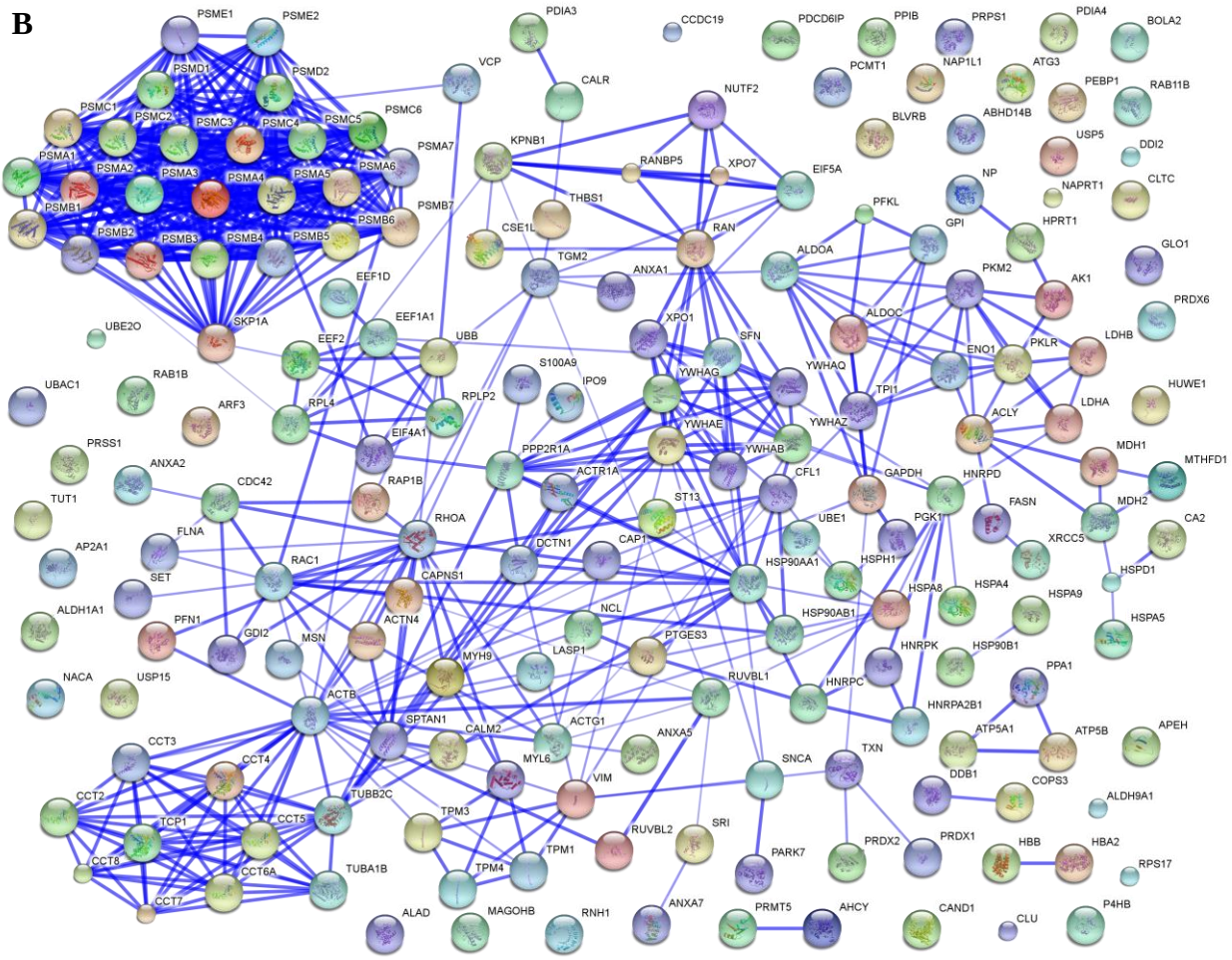

Figure 2.7 Protein interaction network for the shared proteins by PSMA1, PSMA2, PSMA3, PSMA4, PSMA5, PSMA6 and PSMA7 *in silico* protein interaction analyses using frequency of occurrence cutoff of (A) 15% and (B) 10%. STRING 8.2 was used to visualize functional links among these proteins based on the active prediction methods "Experiments" and "Databases", where stronger associations are represented by thicker lines.

2.3.2 Integrin αIIbβ3 receptor

The *in silico* protein interaction analysis was further applied to the human integrin αIIbβ3 receptor, key signaling molecules in mediating platelet activation and aggregation [343]. The distribution of dataset size for both integrin αIIb (Figure 2.8A) and integrin β3 (Figure 2.8B) indicates a cutoff for dataset size at ≤110 proteins when the threshold of other cutoffs was fixed at: sequence coverage ≥18AA, identification confidence log(e)≤-10, and ProDis≥2. When these thresholds were applied, 150 and 111 datasets were approved for integrin αIIb and integrin β3, respectively. 37 and 41 proteins were identified in the integrin αIIb and integrin β3 interaction analyses respectively, using frequency of occurrence ≥20% (Table 2.4, column 1&2). These

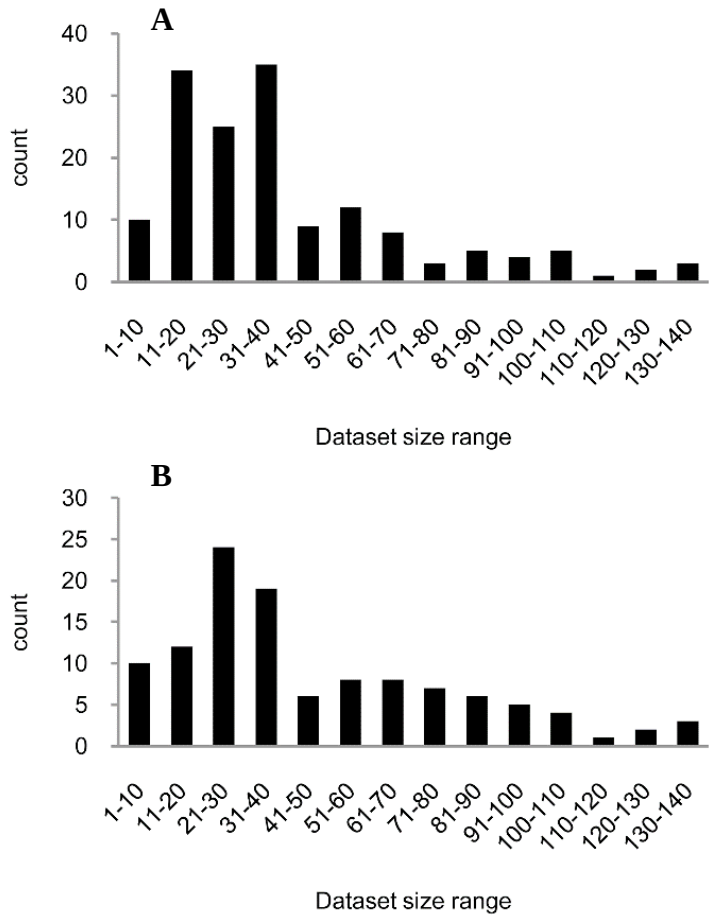

Figure 2.8 Distribution of number of (A) integrin αIIb and (B) integrin β3 at different dataset size ranges.

protein lists presented considerable similarity, and interestingly, talin1, kindlin-3 (FERMT3) and Rap1b were identified in both analyses. The direct binding of talin1 to the integrin β3 tail was shown to be a crucial step that triggers integrin αIIbβ3 activation [344-346]. The loss of talin1 results in severe bleeding, due to the binding of platelet integrins to ligands, with platelet aggregation becoming compromised. Similarly, a recent study showed that the same phenotype occurred in kindlin-3 deficient platelets despite a normal amount of talin1 [347]. This suggests that both talin1 and kindlin-3 are required to mediate integrin activation, however, the mechanism of this regulation remains unknown [348]. In addition, Rap1b, a small GTPase, was also shown to be essential for normal platelet function [349], and to induce the formation of the integrin activation complex which in turn activates platelets [350]. Other common proteins identified in both analyses include fibrinogen, coagulation factor XIII, vinculin and other abundant cytoskeletal proteins (Table 2.4, column 1&2).

Due to their known interaction with integrin αIIbβ3 complex, additional *in silico* protein interaction analysis were performed targeting talin1, kindlin-3 and Rap1b, using the same threshold at each cutoff as was used for integrin αIIb and integrin β3 analyses. Thirty three, 50 and 72 proteins were identified for talin1, kindlin-3 and Rap1b, respectively (Appendix G-I). Twenty six proteins, besides keratin 1 and trypsin, were identified in all five analyses (Table 2.4, column 3), including all five of these proteins. The functional links of these 26 proteins were visualized using STRING 8.2 (Figure 2.9).

Table 2.4 The 37 and 41 proteins identified for integrin αIIb and integrin β3 *in silico* protein interaction analyses (column 1&2), respectively; the 28 proteins shared by talin1, kindlin-3, integrin αIIb, integrin β3 and Rap1b *in silico* protein interaction analyses (column 3).

Integrin α2b		Integrin β3		Five proteins	
f(%)	Accession	*f*(%)	Accession	Accession	Description
36.7	ACTB	40.5	ACTB	ACTB	Actin, cytoplasmic 1
54.7	ACTG1	56.8	ACTG1	ACTG1	Actin, cytoplasmic 2
50.0	ACTN1	50.4	ACTN1	ACTN1	Alpha-actinin-1
24.7	CFL1	26.1	CFL1	CFL1	Cofilin-1
52.0	F13A1	47.7	F13A1	F13A1	Coagulation factor XIII A chain Precursor
55.3	FERMT3	56.7	FERMT3	FERMT3	Fermitin family homolog 3
27.3	FGA	32.4	FGA	FGA	Fibrinogen alpha chain Precursor
30.0	FGG	34.2	FGG	FGG	Fibrinogen gamma chain Precursor
84.7	FLNA	84.6	FLNA	FLNA	Filamin-A
36.7	GAPDH	38.7	GAPDH	GAPDH	Glyceraldehyde-3-phosphate dehydrogenase
41.3	GP1BA	35.1	GP1BA	GP1BA	Platelet glycoprotein Ib alpha chain precursor
29.4	GSN	37.8	GSN	GSN	Gelsolin Precursor
100.0	ITGA2B	70.3	ITGA2B	ITGA2B	Integrin alpha-IIb Precursor
60.7	ITGB3	100.0	ITGB3	ITGB3	Integrin beta-3 Precursor
32.0	KRT1	38.7	KRT1	KRT1	Keratin 1
24.0	KRT10	29.7	KRT10	-	Keratin 10
24.7	KRT9	30.6	KRT9	-	Keratin 9
22.7	LDHB	27.0	LDHB	-	L-lactate dehydrogenase B chain
32.7	LIMS1	35.1	LIMS1	LIMS1	LIM and senescent cell antigen-like-containing domain
39.3	MMRN1	39.6	MMRN1	MMRN1	Multimerin-1 precursor
70.7	MYH9	61.3	MYH9	MYH9	Myosin-9
32.0	PKM2	36.9	PKM2	PKM2	Pyruvate kinase isozymes M1/M2
28.0	PLEK	24.3	PLEK	PLEK	Pleckstrin
30.0	RAP1B	28.8	RAP1B	RAP1B	Ras-related protein Rap-1b Precursor
56.0	sp|TRYP_PI	62.2	sp|TRYP_PI	sp|TRYP_PI	Trypsin precursor
20.0	TAGLN2	30.6	TAGLN2	TAGLN2	Transgelin-2
79.3	THBS1	77.5	THBS1	THBS1	Thrombospondin-1 Precursor
76.0	TLN1	72.9	TLN1	TLN1	Talin-1
27.3	TUBA4A	22.5	TUBA4A	TUBA4A	Tubulin alpha-4A chain
31.3	TUBB1	38.7	TUBB1	TUBB1	Tubulin beta-1 chain
27.3	VCL	33.3	VCL	-	Vinculin (Metavinculin)
22.6	ZYX	20.7	ZYX	ZYX	Zyxin
21.3	PFN1	-	-	-	Profilin 1
26.0	PPBP	-	-	-	Pro-platelet basic protein
20.0	STOM	-	-	-	Stomatin
23.3	TPM4	-	-	-	Tropomyosin 4
20.0	VWF	-	-	-	von Willebrand factor
-	-	27.9	ACTN4	-	Actinin, alpha 4
-	-	20.7	CCDC19	-	Tubulin beta chain
-	-	26.1	HBB	-	Hemoglobin, beta
-	-	20.7	MYL12A	-	Myosin, light chain 12A, regulatory, non-sarcomeric
-	-	26.1	MYL6	-	Myosin, light chain 6, alkali, smooth muscle and non-
-	-	20.7	RSU1	-	Ras suppressor protein 1
-	-	22.5	TUBA1B	-	Tubulin, alpha 1b
-	-	25.2	WDR1	-	WD repeat domain 1
-	-	20.7	YWHAZ	-	14-3-3 protein zeta/delta

A core network involved in platelet activation and aggregation was identified that consists of integrin αIIb, integrin β3, talin1, FGA, FGG and Rap1b. However, the functional link of kindlin-3 to integrin αIIbβ3 was not shown, which may be due to the fact that the recent finding of the binding of kindlin-3 to integrin β3 has yet to be archived in the STRING database. Other proteins identified in the analysis were mainly abundant cytoskeletal proteins.

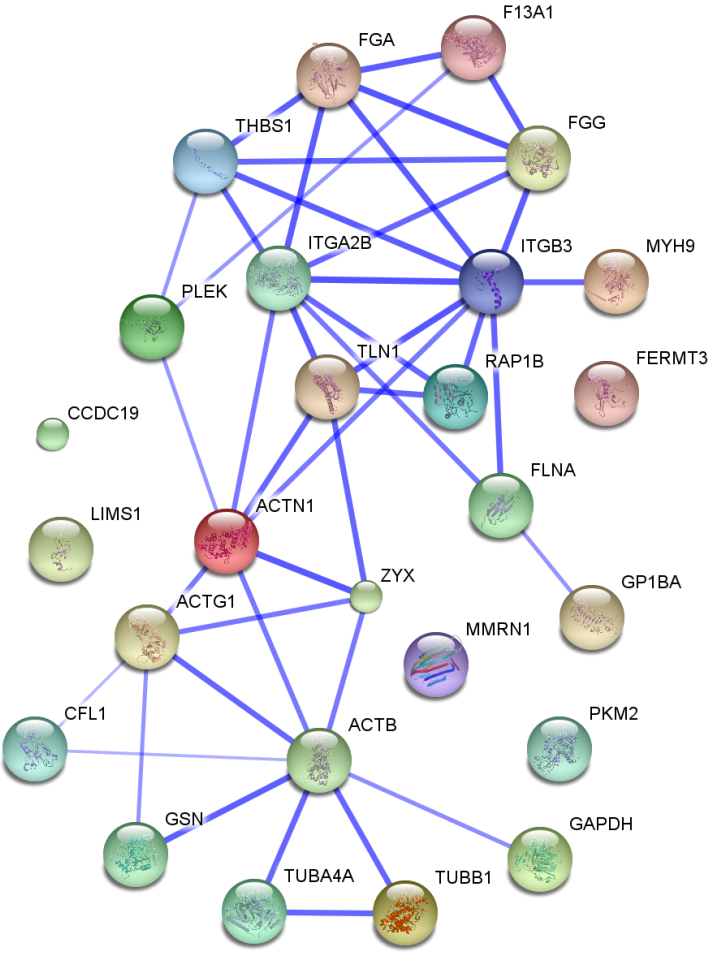

Figure 2.9 Protein interaction network for the 26 proteins shared by talin1, kindlin-3, Rap1b, integrin αIIb and β3 *in silico* protein interaction analyses. STRING 8.2 was used to visualize functional links among these proteins based on the active prediction methods "Experiments" and "Databases", where stronger associations are represented by thicker lines.

2.3.3 Identification of background proteins by comparative analysis

Co-IP experiments are known to contain proteins that do not bind the bait protein in a specific manner. Instead, they are due to non-specific binding to beads, bait, interacting proteins or contaminants. These background proteins are typically identified by comparing co-IP results of proteins that show distinct features. Similarly, if two proteins do not have functional links, then the shared proteins identified from these two proteins' *in silico* protein interaction analyses are expected to be background proteins. HIST4H4 is mainly localized in the nucleus and integrin αIIb is expressed specifically in platelets which lack a nucleus, and thus HIST4H4 and integrin αIIb cannot be functionally-linked. Indeed, no approved datasets were shared by these two human proteins (sequence coverage≥18AA and log(e)≤-10 for HIST4H4, dataset size≤100 proteins and ProDis≥2). Seven proteins were observed in both analyses (Table 2.5), including common contaminants resulting from sample preparation of a mass spectrometry experiment, i.e. keratins and trypsin, and abundant proteins, i.e. actin and GAPDH.

Table 2.5 The seven proteins identified in both integrin αIIb and HIST4H4 analyses, which are expected to be background proteins.

Accession	Description
KRT1	Keratin 1
KRT10	Keratin 10
KRT2	Keratin 2
KRT9	Keratin 9
sp|TRYP_PIG|	Trypsin precursor
ACTG1	Actin, gamma 1
GAPDH	Glyceraldehyde-3-phosphate

2.4 Validation

Without statistical or experimental validation, an independent assessment of the predicted interactions may not be possible. To address this concern, a formaldehyde-supported co-IP experiment targeting integrin β1 was performed in order to study its interaction partners (detailed method described elsewhere [351]), and used the resulting list of proteins as a biochemical comparison for our in silico interaction analysis. Integrin β1 complexes were precipitated from activated human platelets and 11 proteins, other than integrin β1, were identified consistently (Appendix J). An *in silico* protein interaction analysis was then performed targeting integrin β1 (sequence coverage≥18AA and log(e)≤-10 for integrin β1, dataset size≤50 proteins, ProDis≥2 and frequency of occurrence≥10%), where 18 proteins were identified after removal of common contaminants (Appendix K). Nine proteins were identified with both methods, only vinculin and Tu translation elongation factor were identified by the biochemical approach but not identified using *in silico* protein interaction analysis. Furthermore, integrin β1 interaction partners were identified using the STRING database [342], which is the most comprehensive resource of protein-protein interactions as it incorporates information from other databases such as BioGRID [352], HPRD [353], IntAct [354], MINT [355] and KEGG [356]. By selecting the active prediction methods "Experiments" and "Databases", only those interactions for which experimental evidence exists were included. Twenty eight human integrin β1 interaction partners were obtained from the STRING database, when a confidence score cutoff of at least 0.950 was used (Appendix L). This cutoff was chosen because a significant gap in the confidence score was observed (from 0.957 to 0.917). These 28 proteins as well as all adaptor proteins and integrin α subunits known to interact with integrin β1 from literature [357, 358] were also compared with the results of the formaldehyde-supported co-IP experiment and *in silico* protein interaction

analysis (Figure 2.10). Four proteins were identified using all of the methods: integrin α6, integrin α2, talin1 and filamin. Integrin α4 and integrin α5 were identified using all approaches except the co-IP method. In addition, myosin, actin and kindlin-3, which are known interaction partners of integrin β1, were identified using the *in silico* protein interaction analysis, but not the STRING database. BioGRID was also used to identify integrin β1 interaction partners. With three key interaction partners, integrin α2, integrin α4 and integrin α5, missing in this database, this dataset was not used for the comparison (Appendix M).

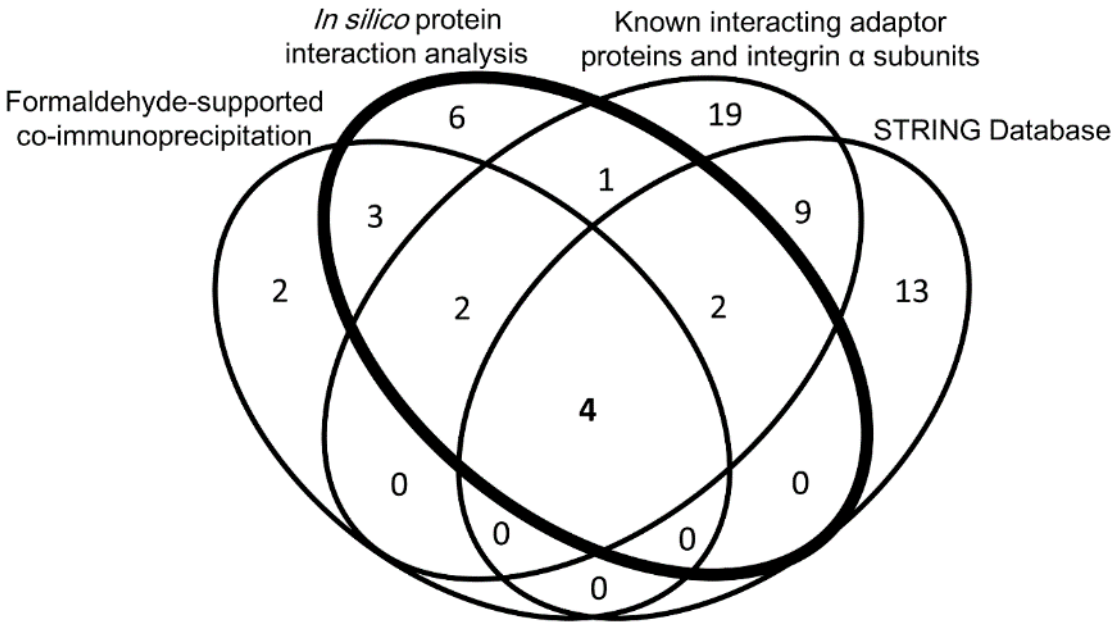

Figure 2.10 Venn diagram showing the overlap between the proteins interacting with integrin β1 that were identified via formaldehyde-supported co-immunoprecipitation, *in silico* protein interaction analysis (in bold), the literature or the STRING database.

2.5 Discussion

A general method for *in silico* protein interaction analysis using the GPMDB was developed (Scheme 1). This method begins with searching for a protein of interest in the GPMDB, which can be identified by either its HGNC name or a particular Ensembl accession number. If the search is performed using the HGNC name, the datasets for all Ensembl accession numbers which apply to that HGNC name will be collected. In addition, this collection of datasets only includes positive identifications for the specific isoforms of the protein of interest (at least one unique peptide being sequenced that confirms the presence of the specific protein of interest), whereas datasets that identified the protein of interest as a possible homologue are not collected. The same criteria are used when merging protein identifications from the approved datasets (Scheme 1, step 5): all Ensembl accession numbers that apply to a particular HGNC name are merged and used to calculate its frequency of occurrence, and only the positive identifications are selected for this calculation.

This collection of datasets is then sorted and filtered based on four experimental variables (Scheme 1, step 1-4): repetitive datasets, confidence for the protein of interest, dataset size and protein distribution. These four filters are independent of each other, and thus no particular order is required for their application. Also, the thresholds for each filter are user definable based on the characteristics of the protein of interest and the desired size and protein distribution of the datasets.

The repetitive dataset filter is based on the three following criteria: dataset size, sequence coverage amount and protein identification score for the protein of interest. Datasets with all three of the experimental values identical are treated as the exact same datasets and all but one are removed. Slight variation of just one of these three values between any two datasets was not

observed among the 195 approved datasets for HIST4H4 (sequence coverage ≥18AA and log(e)≤-10 for HIST4H4, dataset size≤100 proteins and ProDis≥2).

The confidence filter is based on both sequence coverage and log(e) value for the protein of interest. When a sequence coverage≥18AA filter was applied to the HIST4H4, about 30% of the datasets were removed. Subsequently, the application of log(e)≤-10 only removed 6.5% of the remaining datasets, suggesting sequence coverage≥18AA is a high confidence cutoff similar to log(e)≤-10. Therefore, sequence coverage≥18AA and log(e)≤-10 are also used for other analyses, including other histone proteins, the proteasome α subunits, integrin αIIb and integrin β3. Although a low confidence cutoff can be applied to include more datasets for generation of the final result, it increases the possibility of false identifications of the protein target. Typically, the top protein rank (when sorted by confidence) is achieved for the bait protein in a co-IP experiment. Our analyses have shown that this is true in only a subset of the approved datasets, suggesting that the majority of the datasets used in this analysis did not target HIST4H4 as bait.

Due to the fact that the submission of datasets to the GPMDB does not require information on the experimental conditions used to create the data and virtually all types of proteomic studies are stored in the GPMDB, the dataset size filter was introduced in order to extract small datasets that may provide information on protein-protein interaction. These small datasets can be generated not only from co-IP experiments, but also from affinity-purification MS, enrichment of an organelle, phospho- or glycoproteins etc. Therefore, sampling across these different types of experiments allows identification of proteins which commonly co-occur, i.e. direct/indirect interaction partners, proteins that are functionally linked, and common contaminants from sample preparation of a MS experiment. The method still works with high dataset size cutoff, but spurious coincident identifications will be more prevalent.

The protein distribution filter is based on the ProDis value of a given dataset, which is shown to be a valid tool to eliminate datasets resulting from analysis of a single gel band. Although a low ProDis cutoff can be applied, doing so increased the chance of datasets containing a tightly-focused group of molecular weights in their identified proteins.

The remaining datasets after the four filters are considered approved datasets for the protein of interest. The 195 approved datasets for HIST4H4 were only 8.9% of the 2199 datasets in the GPMDB that positively identified HIST4H4. Therefore, the large number of datasets contained in the GPMDB is crucial.

Subsequently, protein identifications from these approved datasets are merged (Scheme 1, step 5). An additional protein confidence cutoff (log(e) value) can be applied before ranking by frequencies of occurrence to ensure high confidence for the proteins in the final results. However, care must be taken because true interaction partners that are commonly identified with low confidence could be eliminated using this additional cutoff. Therefore, this additional protein confidence cutoff was not used in this study.

The frequency of occurrence cutoff directly controls the number of protein identifications in the final result. More loosely-associated or transient interaction partners of the protein of interest could potentially be be identified using lower frequency of occurrence cutoff; however, the low frequency of occurrence setting necessary to obtain these interacting proteins in the final result would likely increase the identification of false positives and background proteins.

The reverse analyses targeting H2AFJ, HIST1H2BB and H3F3B identified 17 proteins in all four analyses, including seven proteins from the histone family. This indicated the observation of the complete histone octamer, and confirmed the result from the HIST4H4 analysis. These

results suggest that reverse analyses can be used to evaluate the result from the original protein interaction analysis.

When applying this method to the analysis of proteasome subunits, the frequencies of occurrence for each proteasome subunit in the seven analyses for the α subunits indicate that the α subunits associate with each other with high affinity, while the interactions become increasingly weak from the β subunits to the base subunits, and to the regulatory subunits. Interestingly, the proteasome activator subunits 1 and 2, PA28 α and β, which stimulate proteasome to degrade small peptides [359], were also identified. In addition, the observation of ubiquitin may be due to the fact that it targets and covalently binds to substrates leading to degradation through the ubiquitin-proteasome pathway [359]. Also, a large number of adaptor proteins including proteins from the TCP1 complex were identified, which may facilitate the process of protein degradation.

Application of this method to the analysis of the integrin αIIbβ3 receptor identified known interaction partners, talin1, kindlin-3 and Rap1b in separate analysis for both molecules. Proteins that are involved in platelet activation and aggregation were also identified, including fibrinogen that binds to activated integrin αIIbβ3 to facilitate platelet aggregation [360, 361]; coagulation factor XIII, which when activated by thrombin, cross-links fibrin to form an insoluble clot [362]; vinculin, a membrane cytoskeletal protein, that binds to talin and actin to facilitate platelet spreading and movement [363, 364]. In all five analyses for integrin αIIb, integrin β3 talin1, kindlin-3 and Rap1b, a core protein network that plays an essential role in platelet activation and aggregation was identified, as well as other proteins that may be part of a larger protein interaction network required for platelet activation and aggregation. Although some of these proteins were not shown to interact with any other proteins using the catalogued interactions in

the STRING database, the role of these proteins in platelet activation and aggregation could be evaluated in subsequent targeted proteomics experiments. The fact that no such functional connection to kindlin-3 is drawn, despite its known involvement in this process, indicates that our method is capable of identifying links that are not yet present in public interaction databases. Taken together, these results suggest that *in silico* protein interaction analysis can be used to study stable protein complexes as well as more transient and lower affinity interactions, which is reflected in the differences in the corresponding frequency and the dataset size filters that need to be chosen.

In silico protein interaction analysis can be considered as a "virtual IP". A co-IP experiment targets the protein of interest using a highly specific antibody, whereas a virtual IP utilizes high identification specificity to target the protein of interest. Moreover, defined dataset size and frequency of occurrence cutoffs were used to control the number of proteins identified in the virtual IP, which is analogous to the washing steps in a co-IP experiment. A lower dataset size cutoff and/or higher frequency of occurrence cutoff in a virtual IP analysis, is similar to more stringent washing steps being employed in a co-IP experiment, where fewer proteins would be identified, but those which remained would be more abundant and/or have stronger interactions with the target protein. Most importantly, the results for both methods consist of true interaction partners, as well as non-specifically binding and contaminating proteins. Therefore, although these two approaches use quite distinct experimental methods, the concepts and the information that is obtained are comparable.

Additional evidence for this conclusion comes from the validation of the *in silico* protein interaction analysis, by the formaldehyde-supported co-IP experiment targeting integrin β1. Nine proteins were identified by both methods, and an additional nine proteins only by the *in silico*

approach, which may be due to the fact that the co-IP experiment was performed on platelets and under one specific experimental condition; in contrast, *in silico* protein interaction analysis compiles data from various cell types and experimental conditions. Furthermore, when comparing these results to the 28 top-scoring interaction partners in the STRING database, or to known interacting adaptor proteins and integrin α subunits in the literature, 28 known interaction partners were not identified in either the co-IP or the *in silico* protein interaction analysis. This may be explained by the fact that specific experimental conditions are required for the identification of these interactions. For example, the interaction between integrin-linked kinase (ILK) and integrin β1 was determined *in vitro* using the yeast two-hybrid method [365], yet this interaction may not occur in platelets, or may not be captured by proteomic studies. In addition, Melusin is also a known interaction partner; however, only a fragment of Melusin was shown to interact with integrin β1, while the full-length Melusin did not [366]. Moreover, 22 known interaction partners of integrin β1 were not found in the STRING database, while key interaction partners of integrin β1 were missing from BioGRID, which suggests that databases may not include all the protein-protein interaction information from literature. In contrast, three of these were identified using the *in silico* approach, indicating that additional known and novel interaction partners may be identified using *in silico* protein interaction analysis. This suggests that each of these approaches generates distinct but overlapping results, i.e. that the *in silico* analysis complements co-IP experiments and information stored in the protein-protein interaction databases, and expands the repertoire of available tools.

In silico protein interaction analysis has several advantages: 1) the large number of datasets archived in the GPMDB makes this approach unbiased, because inherent biases and systematic errors in an analysis are averaged out, providing a natural control for various false positives, non-

specific interactions and impurities that plague single experiment analysis; 2) these datasets were collected under many different experimental conditions in many different laboratories, therefore various functional links occurring under many biological conditions are extracted and incorporated in the analysis; 3) the number of datasets in the GPMDB is consistently increasing, which would enable *in silico* protein interaction analysis to be used on more and more proteins everyday; 4) data in GPMDB is publicly available, which makes *in silico* protein interaction analysis available at no cost; and 5) the *in silico* protein interaction analysis is available at http://gpmdb.thegpm.org/thegpm-cgi/pvip.pl, and analyses can be completed within minutes.

When users perform analyses online, trying various values for dataset size is suggested, while setting the other parameters as default. If the number of identified proteins or approved datasets is too low/high, then increasing/decreasing the value for dataset size may help. Also, changing the value for frequency of occurrence directly affects the number of proteins identified in the result. Higher identification confidence setting for other proteins may slightly decrease the number of proteins identified and lower the possibility of false identifications. In addition, changing the sequence coverage and identification confidence for the protein of interest is not recommended, unless the protein of interest is difficult to identify with high confidence as in the case of H3F3B (described in the method development section). Finally, lowering the ProDis value is not recommended, only if the number of datasets remaining is too small, as lowering the ProDis value greatly increases the number of datasets.

In conclusion, a general method for *in silico* protein interaction analysis using publicly available data in the GPMDB was developed, which is shown to be a novel and solid tool for identifying known/candidate protein interactions and proteins that share similar functions in a

protein network. Therefore, *in silico* protein interaction analysis can be used as a hypothesis generator for the study of protein-protein interactions and mapping of protein networks.

Chapter 3 Development of quantitative multiplexed small GTPase activity assay using targeted proteomics and application in the context of agonist-induced platelet activation

3.1 Introduction

Small GTPases are a superfamily of structurally and functionally conserved monomeric GTP-binding proteins, and they are ubiquitous molecular switches in eukaryotes [367-369]. This superfamily consists of five subfamilies, i.e. Ras, Rho, Arf, Rab and Ran, which are all key signaling molecules involved in a diverse range of biological functions, including cell cycle progression, cytoskeleton reorganization, cell adhesion, migration, and apoptosis [370-375]. Small GTPases have similar sizes with molecular weights of 20 - 40 kDa [367], and share a high degree of sequence homology but have distinct functions [376]. Small GTPases cycle between GTP-bound active and GDP-bound inactive forms, regulated by GEFs (guanine nucleotide-exchange factor), GAPs (GTPase-activating proteins), and GDIs (guanine nucleotide dissociation inhibitors) [377]. The active small GTPases will bind to downstream effector proteins to carry out critical cellular and physiological functions. Deregulation of the activity level of small GTPases can lead to various types of diseases, including cancer [378-380]. In addition, different small GTPase isoforms can function in concert, with activation of each necessary for a particular cellular function [381].

Current approaches to study small GTPase activity utilize the GTPase-binding domain of individual downstream effector proteins to pull down specific active small GTPases. However,

binding domains are generally non-specific and co-purify multiple small GTPases and their isoforms [382]. Precipitated active small GTPases are then detected by immunoassays, such as Western blot analysis [383]. This results in several limitations: only one small GTPase at a time is evaluated, and therefore measuring activity level of multiple small GTPases in a single sample is not possible; high quality antibodies required for detection are not available for all GTPases, and the available ones may show cross reactivity and therefore do not distinguish individual small GTPase isoforms; antibodies are generally associated with high costs, and in some cases varying quality due to batch production [384]; and finally, highly accurate quantification is difficult to achieve. Unlike other signaling events, e.g. protein phosphorylation, which is routinely studied on a large scale using phosphoproteomics [188], investigating small GTPase activation systematically is hampered by these limitations of Western blotting.

Targeted proteomics techniques, i.e. selected/multiple reaction monitoring (SRM/MRM), have the potential to overcome the limitations of current approaches. They have emerged as a powerful tool to study a pre-defined set of proteins from cells in differentially perturbed states [385-387]. And targeted proteomics was selected as the Method of the Year 2012 by Nature Methods [388]. Non-targeted "shot-gun" proteomics aims to sequence as many peptides as possible from a complex mixture, has limited reproducibility in identifying low abundant peptides, and is generally biased towards highly abundant species [389]. In contrast, the targeted MRM approach takes advantage of the high selectivity of triple quadrupole (QQQ) mass spectrometers, which are capable of isolating precursor and product ions of proteotypic peptides unique to a pre-defined set of proteins and therefore efficiently eliminate contaminating highly abundant proteins and achieve high accuracy quantification. Careful selection of proteotypic peptides unique to a particular protein allows one to distinguish protein isoforms that are difficult to detect using immune-based

assays. In addition, MRM assays can be used to quantify hundreds of analytes in a single LC-MRM-MS run [386]. These features make MRM an ideal method for the analysis of small GTPases.

In this study, an assay called quantitative multiplexed small GTPase activity assay was developed. To demonstrate that this MRM assay can be employed to monitor differential activation of small GTPase isoforms in biological systems, platelets were used as a model because multiple small GTPases are involved in the process of agonist-stimulated platelet activation and aggregation, induced for instance by thrombin, collagen and ADP [133, 390]. Lysophosphatidic acid (LPA), which accumulates in atherosclerotic plaques, is another platelet agonist and a possible regulator of acute thrombosis and platelet function in atherogenesis [78]. Signaling pathways involved in LPA-stimulated platelets are not well known. Therefore, the newly developed MRM-based assay was applied to platelets stimulated with LPA, thrombin and ADP to better understand the effects of LPA on the activity of small GTPase isoforms in human platelets. More generally, this work demonstrated the successful use of MRM assay to quantify activity levels of multiple small GTPase isoforms in a single sample, and revealed co-activation of these proteins in response to agonists over time and differential activation in response to inhibitor treatment. This widely applicable approach is anticipated to be used to study signaling pathways and inhibitor screening in many other human cell lines or tissues.

In addition, in this chapter, P-selectin translocation, which is one of the hallmarks of platelet activation is also investigated using flow cytometry. In resting platelets, P-selectins are stored as integral proteins on the membrane of α-granules. Upon platelet activation, P-selectins are translocated to the surface membrane on platelets by fusion of the α-granule membrane and platelet plasma membrane. Thrombin or collage-induced platelet activation requires the activation of Rac and Rho small GTPases as well as calcium influx, as discussed in Section

1.1.2. LPA-induced platelet secretion was not well characterized, but similar pathways might be involved.

Therefore, the goal of this chapter is to develop a quantitative multiplexed small GTPase activity assay using MRM and apply this assay to study platelet activation induced by thrombin, ADP and LPA. In addition, to characterize how LPA stimulates platelets compared to thrombin and ADP in terms of small GTPase involvement and P-selectin translocation.

3.2 Methods

3.2.1 Platelet isolation and stimulation

Ethical approval for platelet isolation from whole blood from healthy blood donors was obtained from the Clinical Research Ethics Board at the University of British Columbia (H12-00757) and written consent was granted by the blood donors. After discarding the first 4 mL, blood was drawn into vacutainer blood collection tubes containing citrate-dextrose (ACD solution A, BD Biosciences, Mississauga, ON, Canada). Platelet-rich plasma was isolated from whole blood following initial centrifugation at 150 relative centrifugal force (rcf) at room temperature for 15 min. To minimize contamination from other blood cells, only the top two thirds of the platelet-rich plasma was collected and centrifuged at 720 rcf at room temperature for 10 min in the presence of a half volume of ACD. Subsequently, the platelet pellet was carefully washed with CGSA buffer (10 mM trisodium citrate, 30 mM dextrose and 1 unit / ml apyrase (Sigma, Oakville, ON, Canada)) to remove plasma proteins and then centrifuged at 720 rcf at room temperature for 10 min. The platelet wash step was repeated and platelets were resuspended in Krebs-Ringer buffer (4 mM KCl , 107 mM NaCl, 20 mM $NaHCO_3$, 2 mM Na_2SO_4, 19 mM tri-sodium citrate, 0.5% (wt/vol) glucose in H_2O, pH 6.1). Platelet counts were

determined by hemocytometer and adjusted to physiological concentration (300 x 10^9/L) using HEPES buffer (10 mM HEPES, 137 mM NaCl, 2.9 mM KCl, 12mM $NaHCO_3$, pH 7.4), and supplemented with $CaCl_2$ to a final concentration of 2.5 mM. Platelets were rested at room temperature for 30 min before stimulation.

To stimulate platelets, 0.2 unit / ml thrombin (Sigma, Oakville, ON, Canada), 100 μM ADP (Sigma, Oakville, ON, Canada), 0.19 mg / ml collagen (Bio/Data Corporation, Horsham, PA, USA) or 20 μM LPA (alkyl-LPA 16:0, Avanti Polar Lipids, Alabaster, AL, USA) was added to 0.5 ml of platelets at physiological concentration at 37 °C for different time points. After stimulation, platelets were immediately lysed by adding 2X lysis buffer (2% NP-40, 100 mM Tris•HCl, pH 7.4, 400 mM NaCl, 5 mM $MgCl_2$, 20% glycerol, with protease inhibitor cocktail (2 tablets / 10 mL, Roche, Basel, Switzerland)). As a positive control, lysate from resting platelets was incubated immediately after addition of 0.1 mM GTPγs at 30 °C for 15 min. For inhibitor studies, 2 unit / ml apyrase was added to platelets and incubated for 1 min before stimulation. Incubation with 25 μM LY294002 (Sigma, Oakville, ON, Canada) or 100 nM wortmannin (Santa Cruz, Dallas, TX, USA) was performed for 15 min.

3.2.2 Expression of effector binding domains

Four binding domains, GST-Raf1-RBD (Ras binding domain, Addgene plasmid 13338 [391]), GST-Rhotekin-RBD (Rho binding domain, Addgene plasmid 15247 [392]), GST-PAK1-PBD (Pak1 binding domain, Addgene plasmid 12217) and GST-RalGDS-RBD (Rap binding domain, a kind gift from Dr. Michael Gold at the University of British Columbia), were used for precipitation of active small GTPases.

For all four binding domain expressions, bacteria containing binding domain plasmid were inoculated into 100 ml Lysogeny broth (LB) plus 100 μg / ml ampicillin. After overnight incubation and shaking at 37 ^{o}C, the bacteria culture was diluted into 1 L LB plus ampicillin. Incubation and shaking at 37 ^{o}C was continued until OD_{600} reaches 0.8. Binding domain expression was then induced by adding IPTG to a final concentration at 0.1 mM, incubation and shaking at 26 ^{o}C for 4 hrs. For GST-Rhotekin-RBD, due to the low binding activity when expression is performed at 26 ^{o}C, IPTG was added to a final concentration at 0.5 mM, incubation and shaking at 37 ^{o}C for 2 hrs. After IPTG-induced binding domain expression, the bacteria were collected by centrifugation at 4,000 rcf at 4 ^{o}C for 10 min. Supernatant was removed and the bacteria pellet was lysed on ice for 30 min with 10 ml lysis buffer (1% NP-40, 50 mM Tris-HCl, pH 7.4, 150 mM NaCl, 5 mM $MgCl_2$, 1 mM DTT, 1 mg / ml lysozyme with protease inhibitor cocktail (1 tablet / 10 mL, Roche, Basel, Switzerland)). The bacteria suspension was then sonicated six times, 15 sec each at 14 W with 1 min interruption between sonications. They lysate was clarified by centrifugation at 30,000 rcf at 4 ^{o}C for 45 min. The supernatant was supplemented with 10% glycerol and stored at -80 ^{o}C in aliquots. For GST-Rhotekin-RBD, a purification step was required to retain activity before storage. The bacteria lysate containing GST-Rhotekin-RBD binding domain was incubated with pre-washed glutathione resin for 45 min at 4 ^{o}C. The resin was washed three times with 1X lysis buffer (1% NP-40, 50 mM Tris-HCl, 200 mM NaCl, 2.5 mM $MgCl_2$, 10% glycerol, with protease inhibitor cocktail (1 tablet / 10 mL, Roche, Basel, Switzerland)) and resuspended in the same buffer and stored at -80 ^{o}C in aliquots. To ensure that sufficient amount of purified binding domains was used for each pull down, the amount of binding domain from 20 μl of resin suspension was quantified by comparing with BSA standards (2.5, 5, 10 and 20 μg) on a 12% SDS gel.

3.2.3 Precipitation of active small GTPases

An excess amount of individual binding domain (> 20 μg) was added to 20 μl glutathione resin and incubated for 45 min at 4 °C. For GST-Rhotekin-RBD, this purification step was performed before storage. Equal amounts of resin that contained the four different binding domains were mixed and washed three times with 1X lysis buffer (1% NP-40, 50 mM Tris•HCl, 200 mM NaCl, 2.5 mM $MgCl_2$, 10% glycerol, with protease inhibitor cocktail (1 tablet / 10 mL, Roche, Basel, Switzerland)). The resin was incubated with platelet lysates at 4 °C for 45 min. After the incubation, the resin was washed three times with the same 1X lysis buffer. To preserve the activity of small GTPases, all steps were carried out at 4 °C and without delay in between steps. Small GTPases were eluted by adding 2X SDS sample buffer to the beads, incubating at room temperature for 2 min, and boiling at 99 °C for 5 min.

3.2.4 Western blotting

Cell lysate was clarified by centrifugation at 16,000 rcf for 10 min at 4 ℃, and supernatant was collected, from which protein concentration was determined using BCA assay (Pierce, Rockford, IL, USA). The sample was electrophoresed by SDS-PAGE on a 12% gel in running buffer (192 mM glycine, 25 mM Trizma base, 0.1% SDS in dH_2O, pH 8.3). The gel was equilibrated in transfer buffer (39 mM glycine, 48 mM Trizma base, 0.037% SDS, 20% methanol in dH_2O, pH 8.3). Proteins were transferred to a methanol activated Immobilon-P Transfer Membrane (polyvinylidene fluoride (PVDF), Millipore, Billerica, MA, USA) in the transfer buffer solution. The membrane was then incubated in blocking solution (5 % milk powder dissolved in PBST (8 g NaCl, 0.2 g KCl, 144 g Na_2HPO_4, 0.24 g KH_2PO_4, 2 ml of Tween-20 dissolved in 800 ml of dH2O) for 1 h at room temperature on a shaking platform. The

membrane was washed three times with PBST and incubated with a primary antibody at a concentration of 1:10,000 overnight at 4 ℃ in PBST supplemented with 3% BSA. After the incubation, the membrane was washed three times with PBST and incubated with an Alexa Fluor 680 secondary antibody at a concentration of 1:10,000 in the blocking solution. Following three washes in PBS, protein level was detected using an Odyssey infrared imaging system (LI-COR Biosciences, Lincoln, NE, USA).

For detection of small GTPases, rabbit polyclonal anti-Rap1 (Pierce, Rockford, IL, USA), rabbit polyclonal anti-Rho (Pierce, Rockford, IL, USA), mouse monoclonal anti-Cdc42 (Pierce, Rockford, IL, USA), and mouse monoclonal anti-Ras (Pierce, Rockford, IL, USA) were used, followed by Alexa Fluor 680 goat anti-rabbit or anti-mouse IgG (H+L) (Molecular Probes, Eugene, OR, USA).

3.2.5 In-gel trypsin digestion and addition of internal standards

Samples were separated on a 12% acrylamide gel and visualized using Coomassie blue staining. The protein bands from the 15-25kDa region of the gel were excised. In-gel digestion was performed essentially as described previously [393]. The gel pieces were reduced in 10 mM dithiothreitol at 56 ^{o}C for 30 min, followed by alkylation with 55 mM iodoacetamide at room temperature for 45 min. Trypsin digestion was performed in 50 mM NH_4HCO_3 at 37 ^{o}C for at least 16 hours. Then, peptides were extracted from the gel pieces by adding extraction buffer (1:2 (vol / vol) 5% formic acid / acetonitrile) and heavy isotope-labeled peptides (see below) were spiked in. Samples were then desalted by stage-tip, and resuspended in 0.5% acetic acid prior to analysis by mass spectrometry.

3.2.6 Proteotypic peptides for MRM quantification

Heavy isotope-labeled form of proteotypic peptides, i.e. arginine ($^{13}C_6$; $^{15}N_4$) and lysine ($^{13}C_6$; $^{15}N_2$) at C-terminus, were obtained as custom synthesized PEPOtec SRM crude peptide from Thermo Pierce (Rockford, IL, USA).

3.2.7 Sequence alignment for small GTPase isoforms

Sequence alignment was generated using default setting of the Clustal Omega [394].

3.2.8 LC-MRM-MS analysis

An Agilent triple quadruple 6460 (Agilent, Santa Clara, CA, USA) with the ChipCube nanospray ion source coupled with an Agilent 1200 nanoflow HPLC was used for MRM analysis. For peptide optimization and MRM sample analysis, 43 mm and 150 mm 75 μm ID C18 chips were used, respectively. Solvent A (3% acetonitrile + 0.1% formic acid) and solvent B (90% acetonitrile + 0.1% formic acid) were employed. For the MRM assay, 5% to 35% of solvent B over 22 min at a flow rate of 0.3 μl / min was applied. Resolution of both MS1 and MS2 was set to 'unit', and dwell time of each transition was set to 20 ms. Transition peak identification and quantification was performed using Skyline (2.5.0.5675) [395].

3.2.9 LC-MS/MS analysis

Protein identification was performed using a nano LC-MS/MS system. Peptide mixtures were separated on a PicoTip column (o.d. = 360, I.d. = 75, tip = 15 ± 1 μm) from New Objective (Woburn, MA, USA) packed with reverse-phase C18 material (15 cm, C18 magic, 100 Å, 3 μm,

Michrom Bioresources, Auburn, CA, USA). Solvent A (0.5% acetic acid) and solvent B (80% acetonitrile + 0.5% acetic acid) were employed. A linear gradient of 6% to 80% solvent B over 30 min at a flow rate of 0.6 µl / min was applied via an Agilent 1100 nano HPLC pump (Agilent, Santa Clara, CA, USA). Data-dependent MS and MS/MS spectra were acquired on an LTQ-FTICR mass spectrometer (Thermo Fisher Scientific, San Jose, CA, USA). Proteins were identified by searching the MS and MS/MS spectra using X!Tandem CYCLONE (2012.10.01.1). Raw data is accessible at gpmdb.thegpm.org with GPMDB model numbers.

3.2.10 Flow cytometry analysis

Physiological concentration of platelets activated with the different agonists in the presence of absence of inhibitors (as detailed in the figure legends) were subjected to staining with 5 µl of PE conjugated mouse anti-human CD62P (eBioscience, San Diego, CA, USA) to monitor P-selectin levels on platelet surface.

3.2.11 Statistical analysis

Differences in small GTPase activation level were analyzed using GraphPad Prism version 6.01. Paired t tests were used to determine if a treatment had a significant effect compared to control, which was normalized to 100%. One-way ANOVA with Dunnett's test was used to determine if multiple inhibitors had significant inhibitory effects compared to control, which was normalized to 100%. A two tailed p value < 0.05 was considered statistically significant.

3.3 Results

3.3.1 General workflow

A general workflow for the MRM-based quantitative multiplexed profiling of active small GTPase isoforms was developed, as shown in Figure 3.1. Equal amounts of glutathione resin that have four different individual effector binding domains bound to it are mixed, washed and incubated with cell lysates to precipitate active small GTPases. The resin is then washed, and bound proteins are eluted by incubating and boiling with SDS sample buffer. Subsequently, proteins are separated on a 12% SDS gel, and the 15 - 25 kDa region that contains the targeted small GTPases is excised and subjected to in-gel trypsin digestion. Finally, after sample cleaning, the peptide mixture is analyzed by a QQQ mass spectrometer using the MRM assay targeting the small GTPase isoforms.

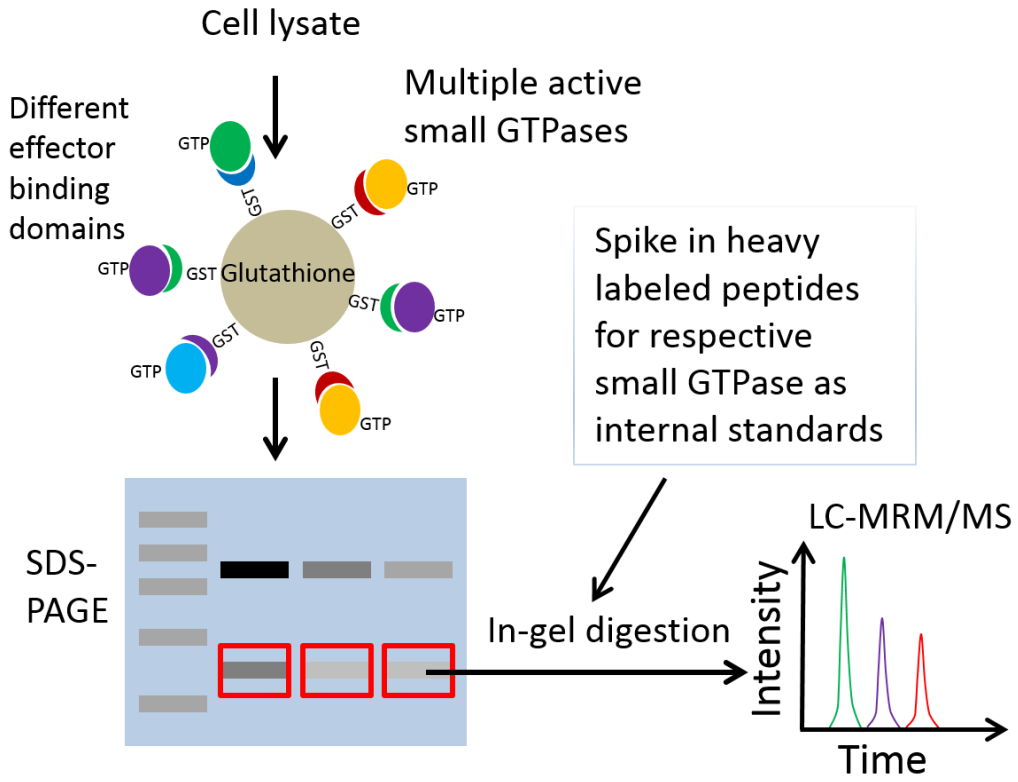

Figure 3.1 General workflow for quantitative multiplexed profiling of small GTPase isoforms using targeted proteomics.

3.3.2 Development of active small GTPase pull-down assay

3.3.2.1 Validation of effector binding domains

Four different effector binding domains which are known to bind active small GTPases were selected: GST-Raf1-RBD for Ras isoforms, GST-PAK1-PBD for Rac isoforms and Cdc42, GST-RalGDS-RBD for Rap isoforms, and GST-Rhotekin-RBD for Rho isoforms. These four binding domains were individually validated by Western blotting. Active Ras, Cdc42, Rap1 and RhoA was precipitated from platelets treated with GTPγs as positive control using GST-Raf1-RBD, GST-PAK1-PBD, GST-RalGDS-RBD, and GST-Rhotekin-RBD, respectively (Figure 3.2). In contrast, the active small GTPases could not be precipitated from platelets treated with GDP as negative control, confirming that each of these four binding domains only precipitates active, but not inactive, small GTPases. The small GTPase isoforms that were precipitated by the binding domains were further evaluated using non-targeted mass spectrometry. Active Rac1, Rac2 and

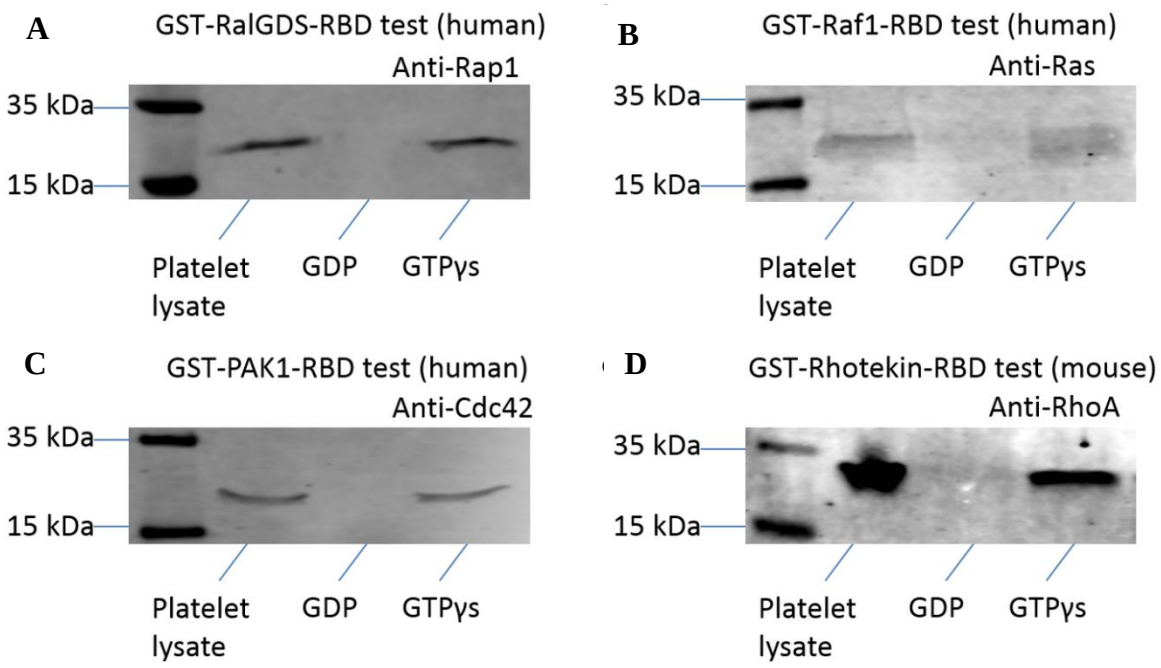

Figure 3.2 Validation of activity of effector binding domains using Western blotting. (**A**) Active Rap1 pull down by GST-RalGDS-RBD, (**B**) active Ras pull down by GST-Raf1-RBD, (**C**) active Cdc42 pull down by GST-PAK1-PBD, and (**D**) active Rho pull down by GST-Rhotekin-RBD. Roughly 10 µg lysate was used as the control. For the GTPγs and GDP were used as positive and negative controls, respectively.

Cdc42 (by GST-PAK1-PBD), Rap1A, Rap1B and Rap2B (by GST-RalGDS-RBD), RhoA and RhoC (by GST-Rhotekin-RBD), and NRas/HRas and KRas (by GST-Raf1-RBD) in human platelets (Table 3.1).

Table 3.1 Different small GTPase isoforms can be precipitated by effector binding domains in human platelets. Platelet lysate (500μg) was treated with GTPγs to activate small GTPases, which were then precipitated by an effector binding domain bound to glutathione beads. The bound small GTPases were then eluted and run on a 12% SDS-PAGE, where the 15-25 kDa region was excised and in-gel digested. Digested samples were analyzed by FT-ICR mass spectrometer. Raw data is accessible at gpmdb.thegpm.org with GPMDB model numbers.

Effector binding Domain	GPMDB model number	Small GTPase
GST-RalGDS-RBD	GPM32100040475	Rap1B
		Rap1A
		Rap2B
GST-PAK1-PBD	GPM32100041580	Cdc42
		Rac2
		Rac1
GST-Rhotekin-RBD	GPM32100041662	RhoA
		RhoC
GST-Raf1-RBD	GPM32100041659	NRas/HRas
	GPM32100041581	KRas

3.3.3 Development of MRM assays

3.3.3.1 Selection of proteotypic peptides

To build the MRM assay, stringent criteria [396, 397] were initially used for the selection of proteotypic peptides. This resulted in zero candidates for Rap1A, Rap1B and Rac1, and only one to two candidates for the other small GTPases. This is likely due to their small size and high sequence similarity, which is shown in (Figure 3.3). Therefore, a series of relaxed criteria to

identify candidate proteotypic peptides for each small GTPase were applied: the proteotypic peptides had to be unique to the small GTPase isoform, have a peptide length of 8-25 amino acids, contain a maximum of one chemically-induced modification for cysteine and/or methionine, be fully tryptic with a maximum of one missed cleavage, and have been observed at least once in the global proteome machine database (GPMDB). Observation in the GPMDB was used as a reference for peptide intensity as described in our previous study [398]. Using these criteria, two to six candidate proteotypic peptides were identified for each small GTPase isoform (Table 3.2).

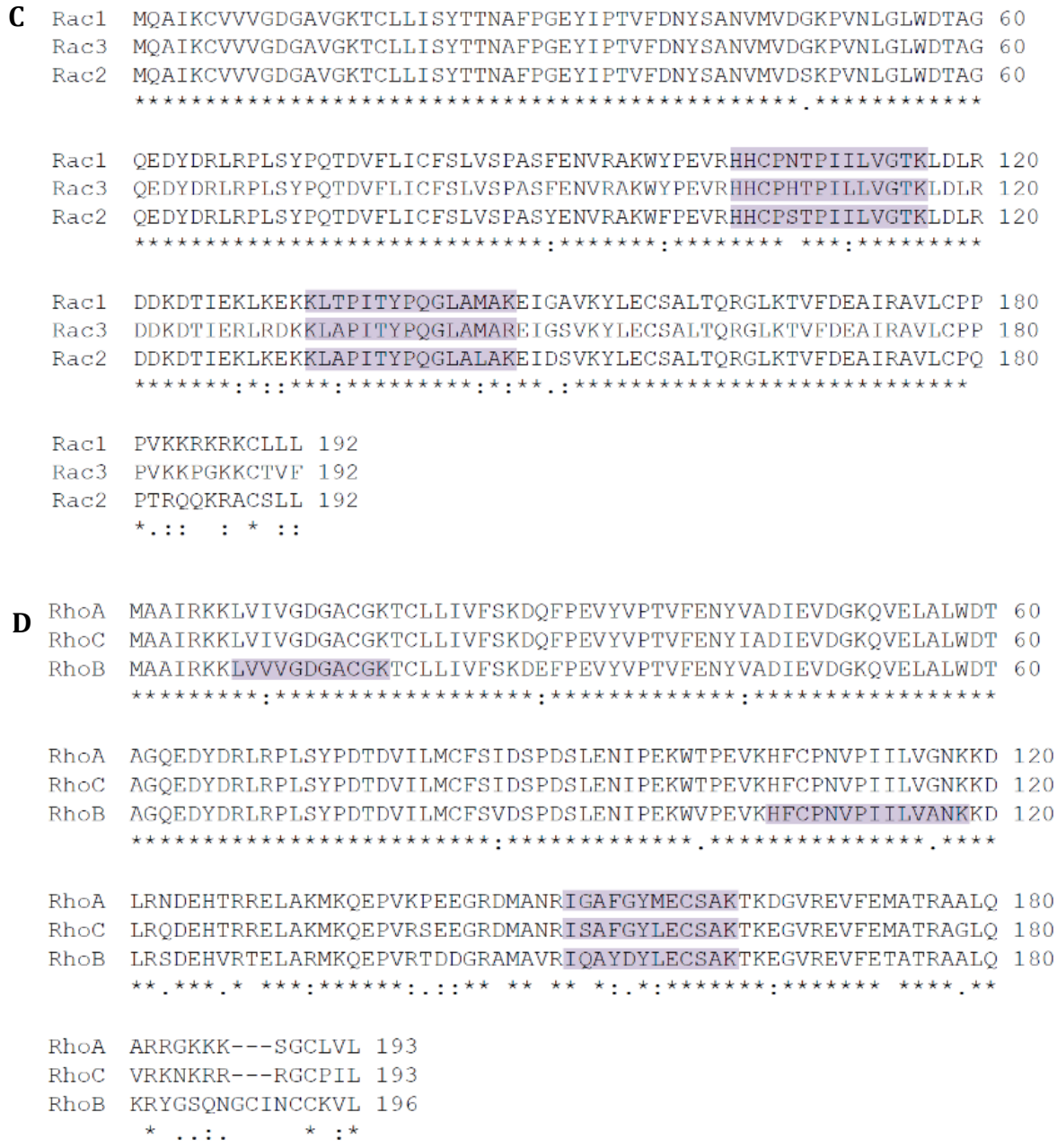

Figure 3.3 Sequence alignment for (A) Rap1, (B) Ras, (C) Rac and (D) Rho small GTPase isoforms reveals high similarity. Candidate proteotypic peptides are highlighted in purple.

Table 3.2 Candidate proteotypic peptides for small GTPase isoforms. These peptides passed the following filters: unique to small GTPase isoform, peptide length of 8-25 amino acids, maximum one chemically-induced modification for cysteine and/or methionine, tryptic peptide with maximum one miss cleavage, and minimum one observation in the GPMDB. * represents the peptides that were synthesized and further tested. # denotes number of GPMDB observations as of May 31, 2011. Cys, cysteine; Met, methionine; ESS, empirical suitability score from peptide atlas.

Small GTPase	Candidate proteotypic peptides	Length	Modification	Miss cleavage	GPMDB observations			ESS
					z=1	z=2	z=3	
NRas	SFADINLYR*	9	—	No	—	226	—	0.47
	TGEGFLCVFAINNSK*	15	Cys	No	—	84	—	0.39
HRas	SFEDIHQYR*	9	—	No	106	5444	45	0.39
	SYGIPYIETSAK*	12	—	No	343	1286	—	0.38
KRas	SFEDIHHYR*	9	—	No	41	223	3	0.45
	DSEDVPMVLVGNK*	13	Met	No	—	75	—	0.35
	VKDSEDVPMVLVGNK*	15	Met	Yes	—	193	122	0.28
	TRQGVDDAFYTLVR	14	—	Yes	—	6	11	0.23
RhoA	DQFPEVYVPTVFENYVADIEVDGK*	24	—	No	—	3000	1867	0.65
	IGAFGYMECSAK*	12	Cys, Met	No	11	1648	—	0.55
	MKQEPVKPEEGR	12	Met	Yes	14	457	612	0.32
	DGVREVFEMATR	12	Met	Yes	—	9	160	0.24
RhoB	IQAYDYLECSAK*	12	Cys	No	—	144	—	0.69
	HFCPNVPIILVANK*	14	Cys	No	—	23	75	0.44
	LVVVGDGACGK	11	Cys	No	1	35	—	0.36
	HFCPNVPIILVANKK	15	Cys	Yes	—	23	75	0.25
	KLVVVGDGACGK	12	Cys	Yes	—	1	1	0.23
RhoC	DQFPEVYVPTVFENYIADIEVDGK*	24	—	No	—	1714	962	0.50
	ISAFGYLECSAK*	12	Cys	No	7	2776	24	0.46
	EGVREVFEMATR	12	Met	Yes	—	24	236	0.23
Rap1A	DTEDVPMILVGNK*	13	Met	No	—	546	40	0.38
	VKDTEDVPMILVGNK*	15	Met	Yes	—	677	727	0.30
Rap1B	DTDDVPMILVGNK*	13	Met	No	—	1701	131	0.46
	VKDTDDVPMILVGNK*	15	Met	Yes	47	3140	3363	0.38
Rac1	HHCPNTPIILVGTK*	14	Cys	No	231	1141	1447	0.67
	LTPITYPQGLAMAK*	14	Met	No	86	2713	257	0.61
	KLTPITYPQGLAMAK*	15	Met	Yes	62	1567	1289	0.40
	EIGAVKYLECSALTQR	16	Cys	Yes	—	26	1	0.23
Rac2	LAPITYPQGLALAK*	14	—	No	16	2004	316	0.76
	HHCPSTPIILVGTK*	14	Cys	No	38	383	539	0.55
	AVLCPQPTR	9	Cys	No	22	302	—	0.51
	KLAPITYPQGLALAK	15	—	Yes	6	592	559	0.38
	EIDSVKYLECSALTQR	16	Cys	Yes	—	17	43	0.22
Rap2B	ASVDELFAEIVR*	12	—	No	15	793	42	0.81

Small GTPase	Candidate proteotypic peptides	Length	Modifi-cation	Miss cleavage	GPMDB observations			ESS
					z=1	z=2	z=3	
	SALTVQFVTGSFIEK*	15	—	No	—	145	15	0.52
	ALAEEWSCPFMETSAK	16	Cys, Met	No	—	136	—	0.52
	VDLEGEREVSYGEGK	15	—	Yes	—	15	33	0.30
	NKASVDELFAEIVR	14	—	Yes	—	45	38	0.25
	VPMILVGNKVDLEGER	16	Met	Yes	—	3	13	0.23
Cdc42	TPFLLVGTQIDLR*	13	—	No	12	11505	255	0.64
	WVPEITHHCPK*	11	Cys	No	122	1578	253	0.46
	TCLLISYTTNK*	11	Cys	No	30	1287	—	0.43
	DDPSTIEK	8	—	No	3	290	—	0.37

Based on the empirical suitability score from Peptide Atlas, the top two to three candidate proteotypic peptides were custom synthesized with heavy isotope-labeled C-terminal lysine or arginine. Signal intensity, i.e. total peak area, for each of these candidate peptides was tested using the QQQ mass spectrometer, and peptides showing solubility issues (3 peptides) or multiple interfering peaks (2 peptides) were eliminated. Furthermore, the longer proteotypic peptides containing a missed cleavage for KRas, Rap1A and Rap1B were selected, because their signal intensity was 2.5, 8 and 40 times higher than their shorter counterparts, respectively. Proteotypic peptides with different charge states (+2 and +3) based on the observations in the GPMDB were tested, the charge state with higher signal intensity was selected. In this way, 12 proteotypic peptides with the highest signal intensity for each of the 12 small GTPase isoforms were selected (Table 3.3).

Table 3.3 MRM parameters of proteotypic peptides for small GTPase isoforms. Mass to charge ratios listed are for unlabeled forms of the peptides. C*, cysteine carbamidomethylation (+57.021); M*, methionine oxidation (+15.995).

Small GTPase	Proteotypic peptide sequence	Precursor charge state	Q1 m/z	Q3 m/z	Fragmentor voltage (V)	Collision energy (V)	Product ion type
NRas	SFADINLYR	+2	549.783	565.309	200	18	y4+
			549.783	793.420	200	15	y6+
			549.783	864.457	200	13	y7+
HRas	SYGIPYIETSAK	+2	664.840	454.740	220	18	y8++
			664.840	908.472	220	19	y8+
			664.840	1078.578	220	15	y10+
KRas	VKDSEDVPMVLVGNK	+3	543.955	417.246	120	12	y4+
			543.955	429.249	120	9	y8++
			543.955	857.491	120	12	y8+
KRas	VKDSEDVPM*VLVGNK	+3	549.287	417.246	120	14	y4+
			549.287	437.251	120	12	y8++
			549.287	873.496	120	15	y8+
RhoA	IGAFGYMEC*SAK	+2	667.299	725.296	200	18	y6+
			667.299	888.359	200	19	y7+
			667.299	945.380	200	18	y8+
RhoA	IGAFGYM*EC*SAK	+2	667.299	554.725	200	19	y9++
			667.299	741.291	200	23	y6+
			667.299	961.375	200	20	y8+
RhoB	IQAYDYLEC*SAK	+2	675.296	993.444	220	21	y8+
			675.296	1156.507	220	20	y9+
			675.296	1227.544	220	18	y10+
RhoC	ISAFGYLEC*SAK	+2	673.326	707.339	180	18	y6+
			673.326	927.424	180	18	y8+
			673.326	1074.492	180	18	y9+
Rap1A	VKDTEDVPMILVGNK	+3	553.299	417.246	165	10	y4+
			553.299	436.257	165	10	y8++
			553.299	871.507	165	11	y8+
Rap1A	VKDTEDVPM*ILVGNK	+3	558.631	417.246	165	14	y4+
			558.631	444.255	165	10	y8++
			558.631	887.502	165	14	y8+
Rap1B	VKDTDDVPMILVGNK	+3	548.627	417.246	140	11	y4+
			548.627	436.257	140	9	y8++
			548.627	530.330	140	10	y5+
Rap1B	VKDTDDVPM*ILVGNK	+3	553.959	417.246	140	11	y4+
			553.959	444.255	140	10	y8++
			553.959	895.516	140	10	y8+
Rap2B	ASVDELFAEIVR	+2	674.859	587.351	240	10	y5+
			674.859	734.420	240	19	y6+
			674.859	847.504	240	19	y7+
Rac1	LTPITYPQGLAMAK	+2	752.416	645.350	220	10	y12++
			752.416	815.444	220	26	y8+
			752.416	1079.555	220	23	y10+
Rac1	LTPITYPQGLAM*AK	+2	760.413	653.347	220	10	y12++
			760.413	831.439	220	23	y8+
			760.413	1095.550	220	24	y10+
Rac2	LAPITYPQGLALAK	+2	728.432	636.372	220	14	y12++
			728.432	797.488	220	23	y8+
			728.432	1061.599	220	23	y10+
Cdc42	TC*LLISYTTNK	+2	657.342	713.346	240	18	y6+
			657.342	826.431	240	21	y7+
			657.342	939.515	240	21	y8+

3.3.3.2 Selection and optimization of MRM transitions

For each of the 12 proteotypic peptides, the response of the top six transitions predicted by the Skyline software [395] were monitored to identify the three transitions that had the highest signal intensity using the QQQ mass spectrometer (Figure 3.4A). The sensitivity of the assay was further improved by optimizing the fragmentor voltage for each precursor ion, and the collision

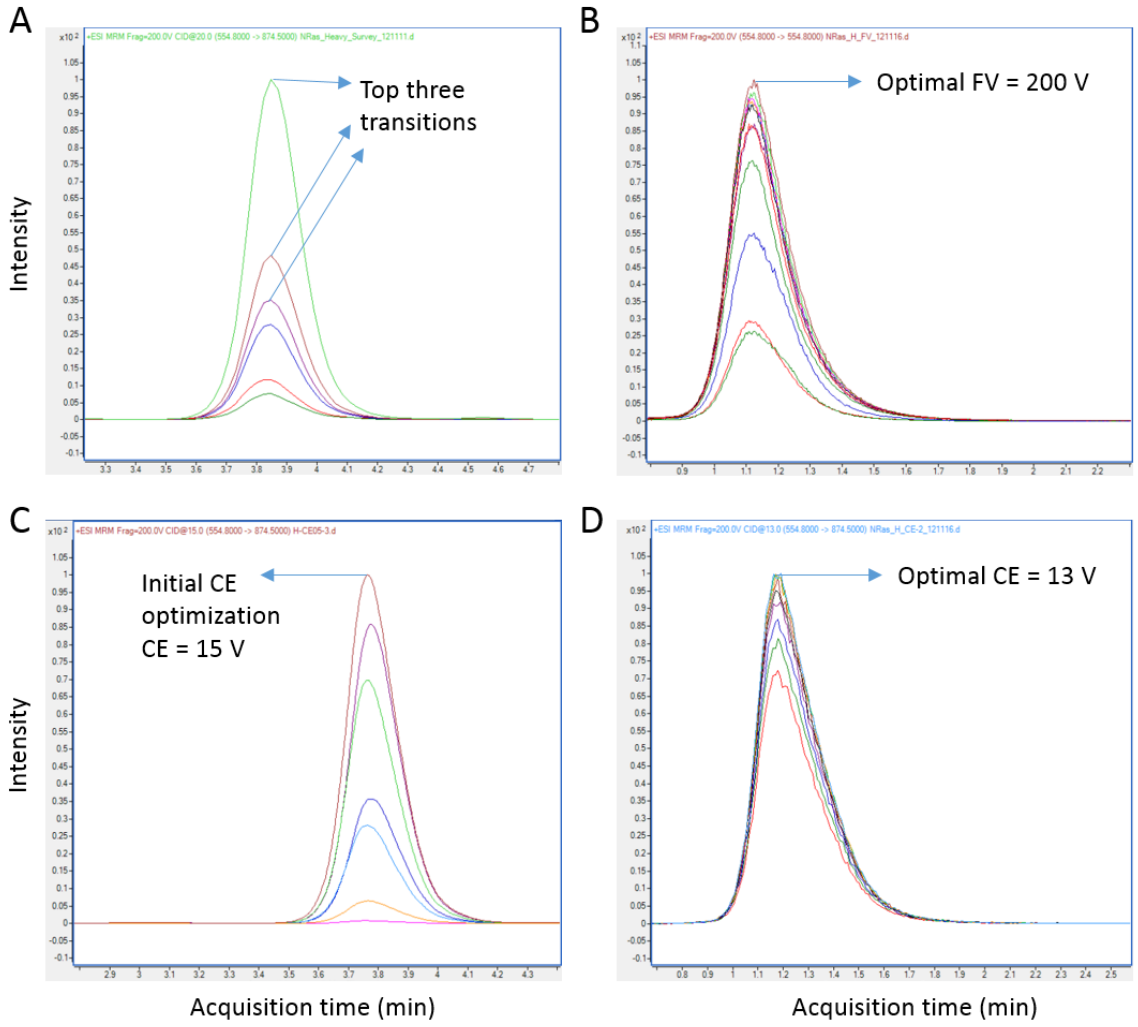

Figure 3.4 Top transition selection and peptide optimization using triple quadrupole mass spectrometry. NRas proteotypic peptide SFADINLYR with heavy labeled arginine ($^{13}C_6$; $^{15}N_4$) was used as an example. (**A**) Top three transitions were selected based on intensity; (**B**) Optimal FV for precursor ion 554.7867 m / z was achieved at 200 V (FV range = 60 to 280 V with 20 V increment tested); (**C**) Initial CE optimization for transition 554.7867 – 874.4657 m / z CE = 15 V (CE range = 5 to 35 V with 5 V increment tested); (**D**) Optimal CE was achieved at 13 V for the same transition (CE range = 11 to 19 V with 1 V increment tested). FV, fragmentor voltage; CE, collision energy.

energy for each transition (Figure 3.4B-D). Amongst chemically-induced modifications, cysteine carbamidomethylation is generally complete; conversely, methionine oxidation, which generally occurs during sample preparation, is often incomplete. Therefore, if a selected proteotypic peptide contained methionine, transitions for both native and oxidized methionine forms of the peptides were optimized. Altogether, the final MRM assay targeted 17 peptide forms: 12 native peptides for the 12 small GTPase isoforms plus the oxidized form of five peptides containing methionine for KRas, RhoA, Rap1A, Rap1B and Rac1. The corresponding top proteotypic peptide and optimized MRM parameters for each small GTPase are shown in Table 3.3.

3.3.4 Validation of MRM assays

3.3.4.1 Validation of MRM assay using Western blotting

Active Rap1B in platelets treated with different agonists were precipitated by GST-RalGDS-RBD and evaluated using the MRM assay or Western blotting (Figure 3.5). The three transitions for Rap1B showed consistent quantification results in all conditions with coefficient of variation (CV) < 5%. Activity level changes of Rap1B were quantified by the MRM assay, showing a 1 : 54.9 : 22.6 : 22.2 : 1.5 ratio for unstimulated: positive control (GTPγS): thrombin-treated: collagen-treated: LPA-treated platelet samples. A similar trend using Western blotting was observed; however, due to oversaturated signals in the positive control, thrombin- and collagen-treated samples, reliable quantification was not possible.

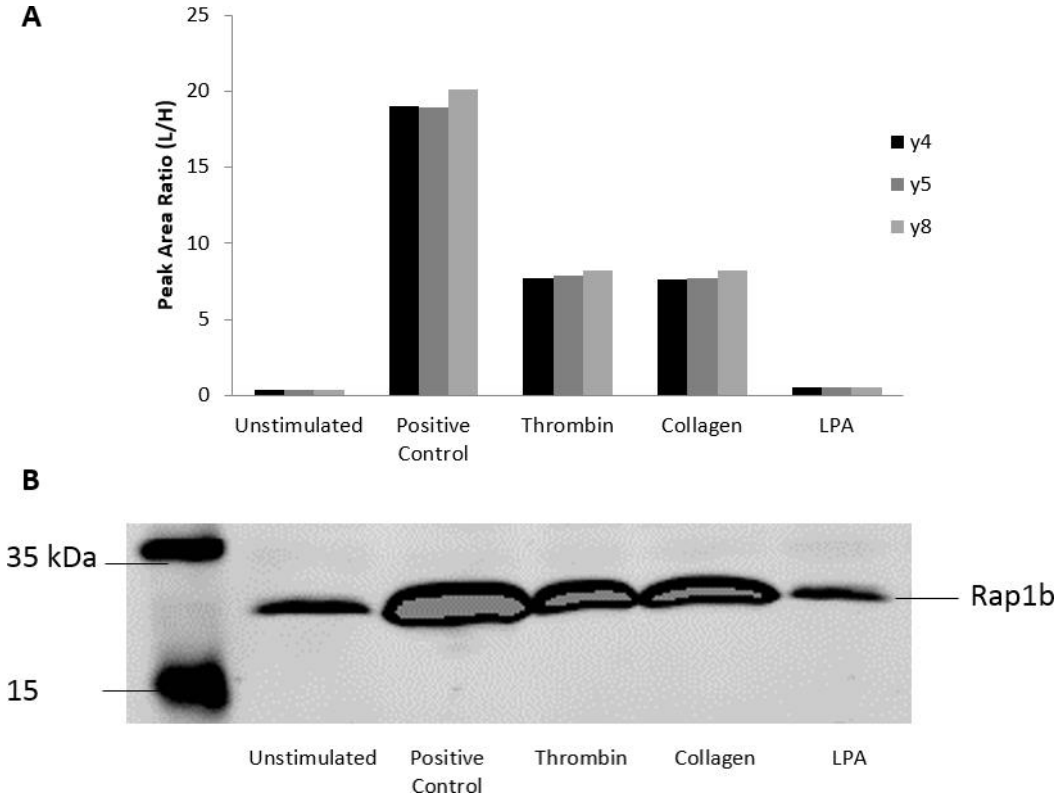

Figure 3.5 Validation of MRM assay using Western blotting. Active Rap1B pull down experiments were performed using GST-RalGDS-RBD in platelets stimulated with positive control (GTPγs), 1 U/ml thrombin, 0.19 mg/ml collagen or 20 μM LPA for 10 min, and analyzed by (**A)** MRM assay and (**B)** Western blotting. Three transitions, i.e. y4, y5 and y8, for Rap1B were used for quantification. The coefficient of variation for the three transitions at each condition were less than 5%.

3.3.4.2 Sensitivity of the MRM assays

The sensitivity of the MRM assay and Western blotting was compared in a dilution series, where active Rap1b was precipitated from GTPγs-treated platelet lysate at 1, 5, 25 and 125 times dilution. The eluted sample was split in half and analyzed by both methods. Although weak signal was still observable at 5 times dilution, no signal was identified at 25 or 125 times dilution using Western blotting. In contrast, quantifiable signal from Rap1b in platelets was observed at all dilutions using the MRM assay.

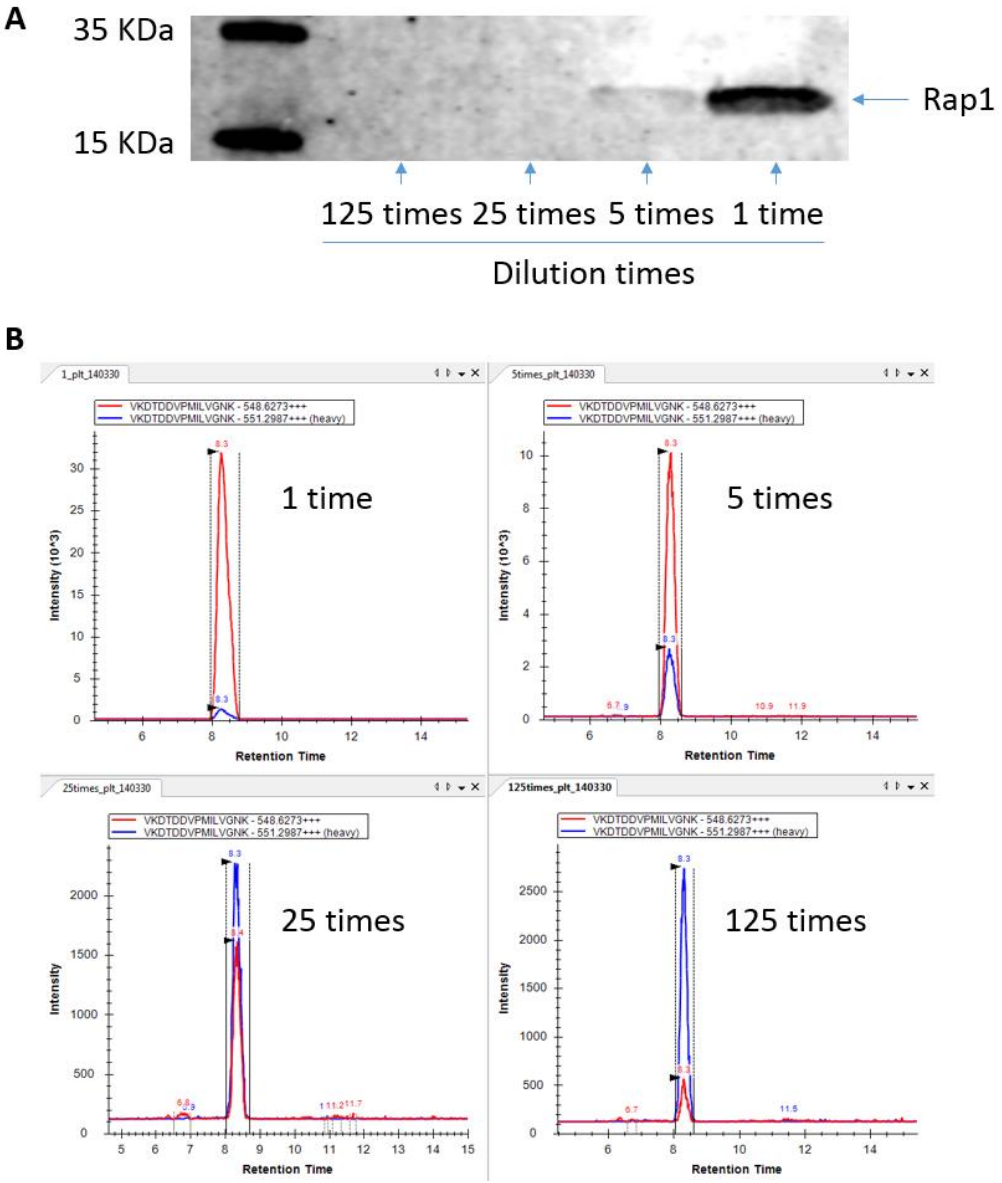

Figure 3.6 Comparison of the sensitivity of the MRM assay and Western blotting from active Rap1b pull down in platelets diluted 1, 5, 25 and 125 times. (**A**) Weak band was observed at 5 time dilution with no signal observed at 25 or 125 dilutions using Western blotting. (**B**) Quantifiable signal from Rap1b in platelets (red) was observed at all dilutions using the MRM assay. Heavy isotopically labeled Rap1 peptide was shown in blue.

3.3.4.3 Validation of reproducibility of multiplexed MRM assays

The multiplexed MRM assay was applied to platelet lysates treated with GTPγs. Technique variation was evaluated for the whole workflow, i.e. multiplexed active small GTPase pull down followed by in-gel digestion and MRM analysis were performed in parallel from identical

biological samples. Ten out of the 12 targeted small GTPases (the exceptions being RhoB and HRas) were quantified. All of the quantitative measurements had a CV < 20%, and nine of them had a CV < 15% in five technical replicates (Table 3.4).

Table 3.4 Technical repeats of activity levels of small GTPases in platelets treated with GTPγs. Platelet lysates were treated with GTPγs for 15 min, then the cells were then lysed, and the multiplex active small GTPase pull down assay was applied. All 13 quantitative measurements had a CV < 20%, and 11 of these had a CV < 15%. Avg, average; Std, standard deviation; CV, coefficient of variation, C*, cysteine carbamidomethylation; M*, methionine oxidation (n = 5).

Small GTPase	Proteotypic peptide sequence	Light/Heavy peak area ratio		
		Avg	Std	CV%
NRas	SFADINLYR	0.244	0.029	11.8
HRas	SYGIPYIETSAK	-	-	-
KRas	VKDSEDVPMVLVGNK	0.533	0.075	14.1
KRas	VKDSEDVPM*VLVGNK	-	-	-
RhoA	IGAFGYMEC*SAK	0.244	0.037	14.9
RhoA	IGAFGYM*EC*SAK	-	-	-
RhoB	IQAYDYLEC*SAK	-	-	-
RhoC	ISAFGYLEC*SAK	0.058	0.011	18.2
Rap1A	VKDTEDVPMILVGNK	1.686	0.214	12.7
Rap1A	VKDTEDVPM*ILVGNK	0.772	0.084	10.8
Rap1B	VKDTDDVPMILVGNK	76.483	6.186	8.1
Rap1B	VKDTDDVPM*ILVGNK	21.102	3.279	15.5
Rap2B	ASVDELFAEIVR	0.501	0.028	5.5
Rac1	LTPITYPQGLAMAK	0.046	0.006	13.3
Rac1	LTPITYPQGLAM*AK	-	-	-
Rac2	LAPITYPQGLALAK	0.142	0.012	8.7
Cdc42	TC*LLISYTTNK	1.094	0.075	6.8

The multiplexed MRM assay was further validated in platelets stimulated with thrombin. The activity level of all ten quantified small GTPases showed significant increase ($p < 0.05$, paired t test) in response to thrombin treatment (Figure 3.7). All quantitative measurements for thrombin-treated samples had a CV < 20%, and nine of them had a CV < 15% in three technical replicates (Table 3.5).

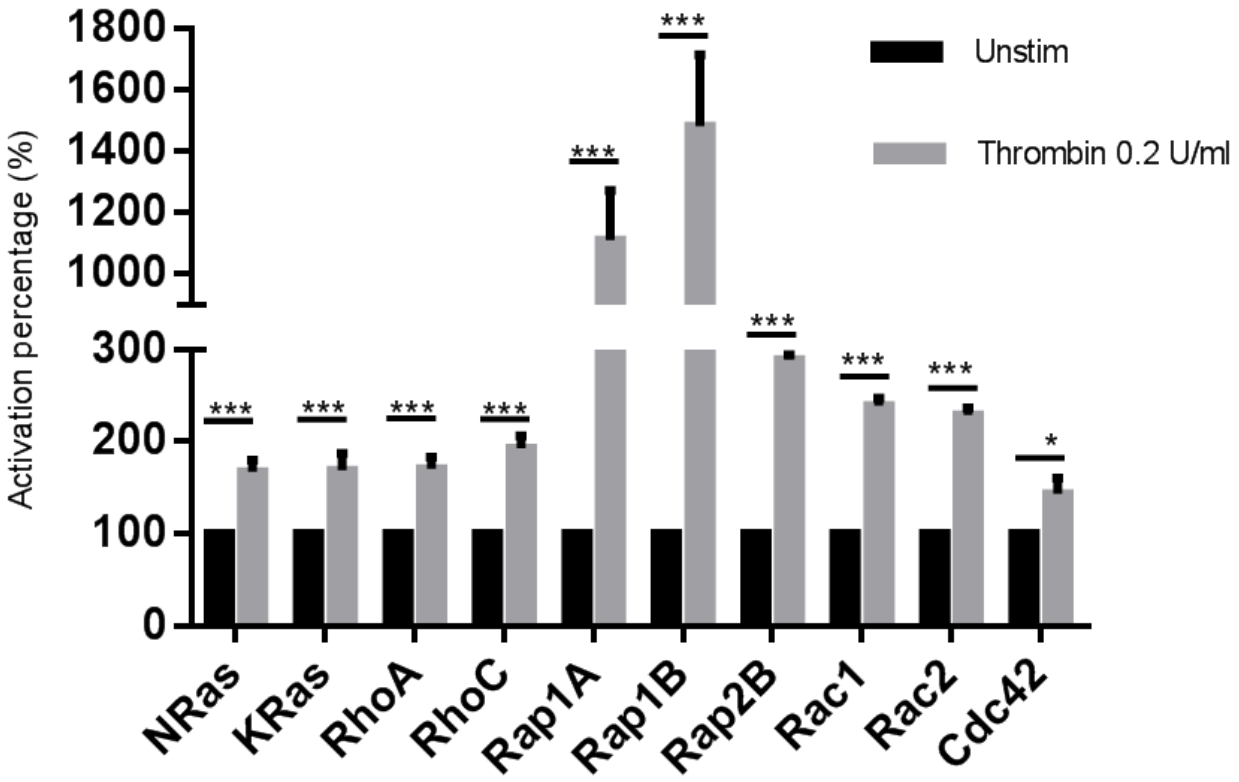

Figure 3.7 Technical repeats of activity levels of small GTPases in platelets treated with thrombin. Platelets were stimulated with 0.2 U/mL thrombin for 1 min, the cells were then lysed, and the multiplex active small GTPase pull down assay was applied. Activation levels of platelets are reported relative to the unstimulated platelets (average of three measurements) which was normalized to 100%. Results are expressed as mean ± SD, asterisk (*) indicates significance (paired t tests, *p<0.05, ***p<0.001; n = 3).

Table 3.5 Technical repeats of activity levels of small GTPases in platelets treated with thrombin. Platelets were stimulated with 0.2 U/mL thrombin for 1 min, the cells were then lysed, and the multiplex active small GTPase pull down assay was applied. Activation levels of platelets are reported relative to the unstimulated platelets (average of three measurements) which was normalized to 100%. All the quantitative measurements for thrombin-treated samples had a CV < 20%, and 90% (9/10) had a CV < 15%. Std, standard deviation; CV, coefficient of variation (n = 3).

Small GTPase	Control (%)	Thrombin (%)	Std	CV%
NRas	100.0	167.2	12.4	7.4
KRas	100.0	169.1	18.0	10.6
RhoA	100.0	170.6	12.3	7.2
RhoC	100.0	192.9	13.2	6.8
Rap1A	100.0	1110.0	163.0	14.7
Rap1B	100.0	1481.6	231.6	15.6
Rap2B	100.0	289.1	5.5	1.9
Rac1	100.0	239.5	8.0	3.4
Rac2	100.0	228.9	7.7	3.4
Cdc42	100.0	143.6	16.5	11.5

3.3.5 Applications

3.3.5.1 Relative expression level of multiple small GTPases in three different cell types

The applicability of this MRM assay to examine the relative expression levels of the 12 small GTPase isoforms across three different cell types, i.e. platelets, THP-1 (human monocytic cell line) and HUVEC (human primary endothelial cell), was evaluated. 100 μg lysate from these three cell types were directly separated on a 12% gel without active small GTPase precipitation. Peak area ratios of light/heavy proteotypic peptides with all three transitions of each light peptide co-eluting with the heavy isotope-labeled counterpart were used as a proxy for the expression level of the corresponding small GTPase (Table 3.6). Ten small GTPases (all except for HRas

Table 3.6 Relative expression level of multiple small GTPase isoforms in three different cells. 100 μg of platelet, THP-1 cell and HUVEC lysates were separated on a 12% gel, and 15-25 kDa regions were in gel digested. Peak areas ratios of light/heavy proteotypic peptides were used as a proxy for the relative expression level of the corresponding small GTPase. Relative expression level of small GTPases in HUVEC or THP-1 are reported relative to the platelets (except for RhoB and HRas) which was normalized to 100%. C*, cysteine carbamidomethylation; M*, methionine oxidation.

Small GTPase	Proteotypic peptide sequence	Relative expression level (%)		
		Platelet	THP-1	HUVEC
NRas	SFADINLYR	100.0	253.7	214.0
HRas	SYGIPYIETSAK	-	-	100.0
KRas	VKDSEDVPMVLVGNK	100.0	85.6	142.3
KRas	VKDSEDVPM*VLVGNK	-	-	-
RhoA	IGAFGYMEC*SAK	100.0	147.8	103.0
RhoA	IGAFGYM*EC*SAK	100.0	90.0	101.8
RhoB	IQAYDYLEC*SAK	-	-	100.0
RhoC	ISAFGYLEC*SAK	100.0	38.1	228.1
Rap1A	VKDTEDVPMILVGNK	100.0	129.4	64.0
Rap1A	VKDTEDVPM*ILVGNK	100.0	-	-
Rap1B	VKDTDDVPMILVGNK	100.0	5.6	6.1
Rap1B	VKDTDDVPM*ILVGNK	100.0	-	-
Rap2B	ASVDELFAEIVR	100.0	22.3	57.3
Rac1	LTPITYPQGLAMAK	100.0	49.6	94.9
Rac1	LTPITYPQGLAM*AK	100.0	41.7	104.7
Rac2	LAPITYPQGLALAK	100.0	157.3	25.6
Cdc42	TC*LLISYTTNK	100.0	69.8	70.5

and RhoB) were identified for platelet and THP-1 cells, and all 12 small GTPases were found in HUVEC cells.

3.3.5.2 Time-resolved activation profiles of multiple small GTPases

In order to compare the effect of LPA stimulation on small GTPases in platelet activation to known agonists, the multiplexed MRM assay was employed to study the activation profiles of the 12 small GTPases in platelets stimulated with thrombin, ADP, or LPA at different time points. Activation profiles of ten small GTPases were obtained in three independent biological replicates of different donors (Figure 3.8). Stimulation of platelets with thrombin resulted in fast activation of all small GTPases except KRas. The highest activation level was observed within the first two minutes, after which it gradually decreased.

When compared to GTPγs-treated platelets as a reference for normalization of the individual GTPase activation levels, i.e. 100%, resting platelets showed a low level of activation for Rap1A and Rap1B of 6.4 ± 2.2% and 2.5 ± 0.5%, respectively. Conversely, 9.3 and 17.4 fold activation increase after 1 min thrombin activation was observed for Rap1A (59.3 ± 3.0%) and Rap1B (43.5 ± 9.0%), respectively. Similar activation profiles were obtained for Rap1A and Rap1B from both methionine oxidized and native forms (Figure 3.9). Peptides containing an oxidized methionine eluted slightly earlier and showed 4 times less signal intensity than their counterparts in native form.

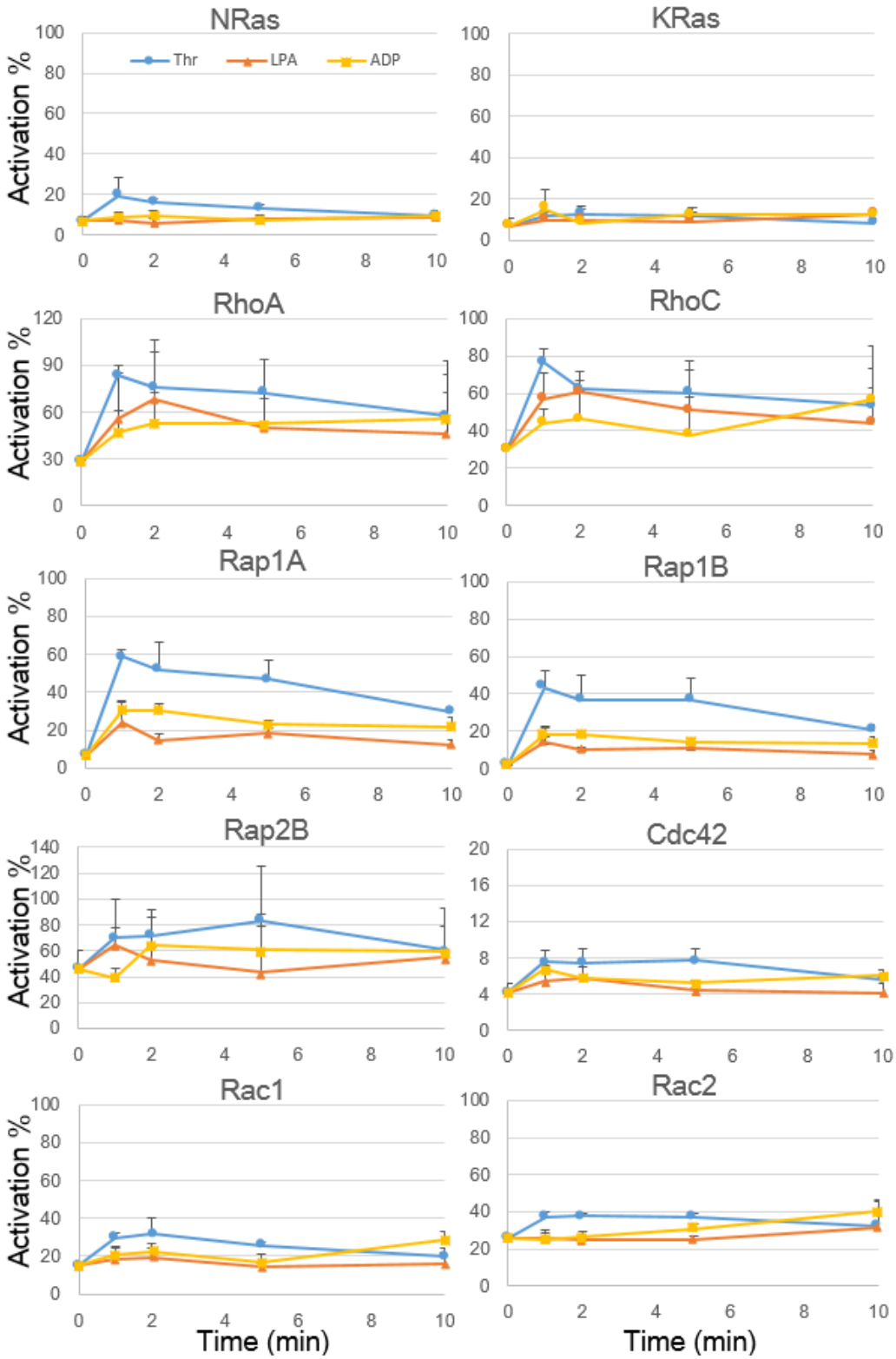

Figure 3.8 Time-resolved activation profiles of nine small GTPases in platelets stimulated with different agonists. Platelets were stimulated with 0.2 U/mL thrombin (Thr), 100 µM ADP, or 20 µM LPA at pre-defined time points. The cells were then lysed, and the multiplexed active small GTPase pull down assay was applied. Activation levels of platelets are reported relative to the positive control (treatment of platelets with GTPγs) which was normalized to 100% (n=3).

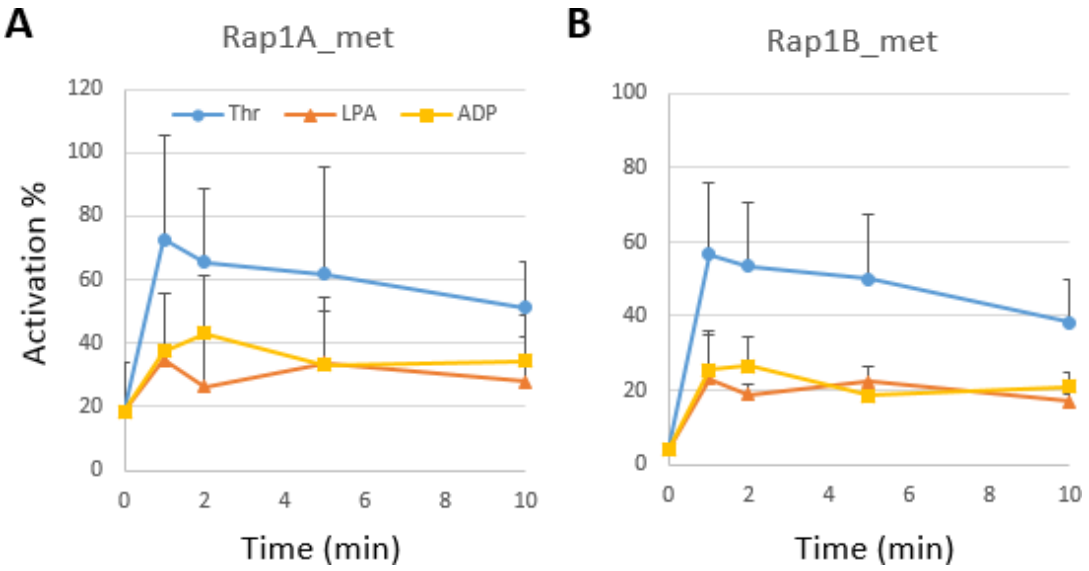

Figure 3.9 Time-resolved activation profiles of (A) Rap1A and (B) Rap1B (proteotypic peptides with methionine oxidation) in platelets stimulated with different agonists. Platelets were stimulated with 0.2 U/mL thrombin (Thr), 100 µM ADP, or 20 µM LPA at pre-defined time points, the cells were then lysed, and the multiplexed active small GTPase pull down assay was applied. Activation levels of platelets are reported relative to the positive control (treatment of platelets with GTPγs) which was normalized to 100%. (n=3).

3.3.5.3 Activity level of small GTPases in response to inhibitor treatment

The MRM assay was applied to study the effects of inhibitor treatment on small GTPase activities following thrombin- and LPA-induced platelet activation. Specifically, the ADP scavenger, apyrase, was used as well as LY294002 and wortmannin, two inhibitors of PI3 Kinase. Activation levels of most small GTPases remained unaffected by the inhibitor treatment following activation with either thrombin or LPA. However, the activity levels of Rap1A and Rap1B upon pre-treatment with each of the three inhibitors, and NRas and Cdc42 upon pre-treatment with apyrase showed statistically significant decrease ($p < 0.05$, one-way ANOVA) in LPA but not thrombin-treated platelets in three independent biological replicates (Figure 3.10).

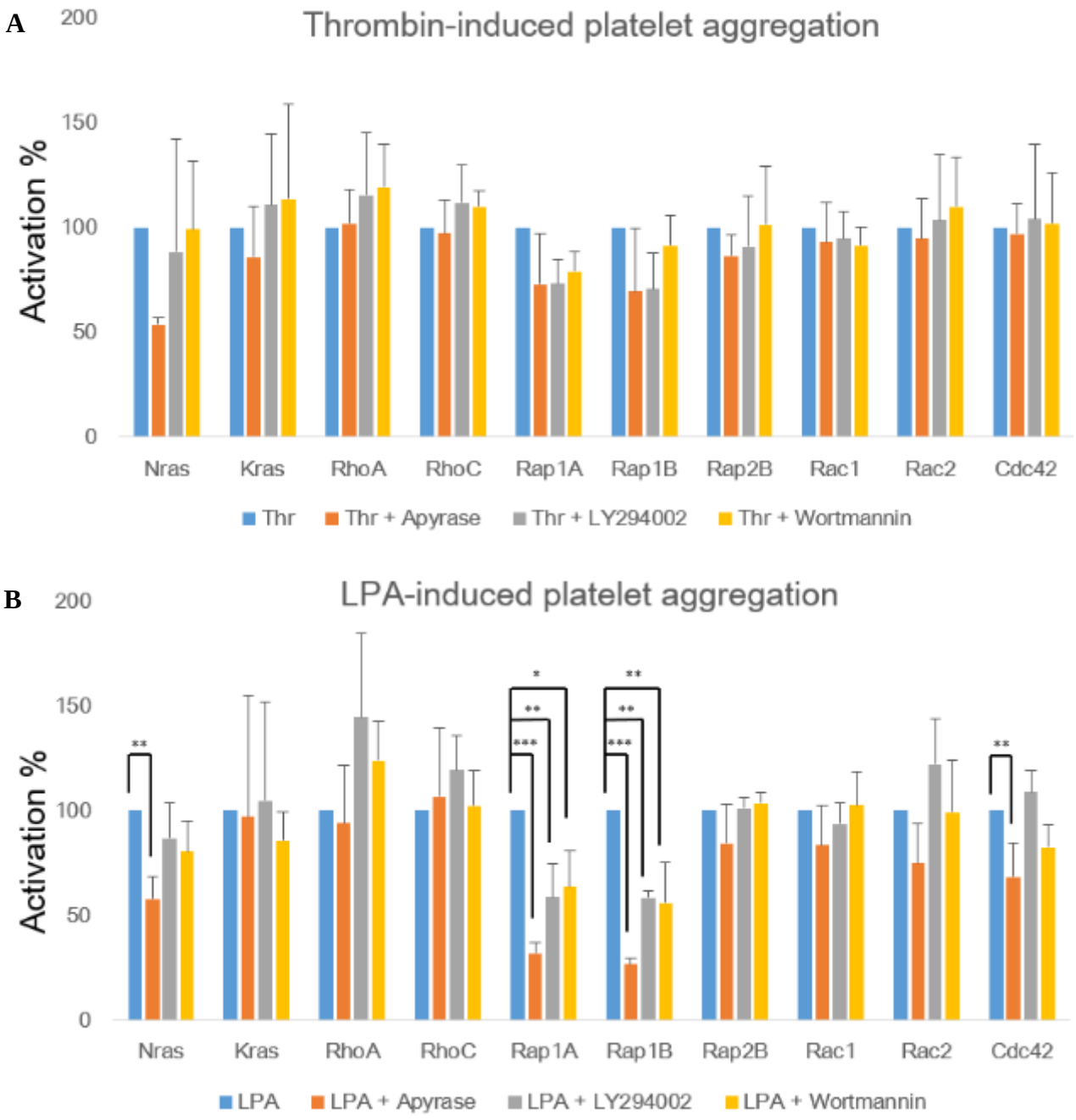

Figure 3.10 Treatment with ADP scavenger apyrase, or PI3K inhibitor LY294002 and wortmannin significantly reduced activation of Rap1A and Rap1B in LPA treated platelets. Platelets were stimulated with (**A**) 0.2 U/ml thrombin or (**B**) 20 µM LPA in the presence or absence of inhibitors for 1 min (2 U/ml apyrase), or 15min (25 µM LY294002 or 100 nM wortmannin). Activation levels of small GTPases in platelets are reported relative to the control (no inhibitor treatment) which was normalized to 100%. Results are expressed as mean ± s.d., asterisk (*) indicates significance (one-way ANOVA with Dunnett's test, *p<0.05, **p<0.01, ***p<0.001; n = 3).

3.3.6 P-selectin levels in platelet activation

In order to further understand the role of PI3K-Rap1, Rho-ROCK, Rac, ADP and calcium in platelet activation, the effect of apyrase and inhibitors for PI3K, Rac and ROCK as well as a calcium chelator was tested on P-selectin surface expression levels in platelet activation induced by thrombin or LPA. No significant changes in P-selectin levels after either thrombin- or LPA-induced platelet activation in presence of apyrase or PI3K inhibitors (LY294002 and wortmannin) were observed in three biological replicates (Figure 3.11). However, treatment with Rac inhibitor NSC23766 or the calcium chelator BAPTA-AM showed significant decrease in P-selectin levels in both thrombin- and LPA-induced platelet activation in three biological replicates (Figure 3.12). Interestingly, treatment with the ROCK inhibitor Y27632 resulted in a significant decrease in P-selectin levels in thrombin- but not LPA-induced platelet activation (Figure 3.12).

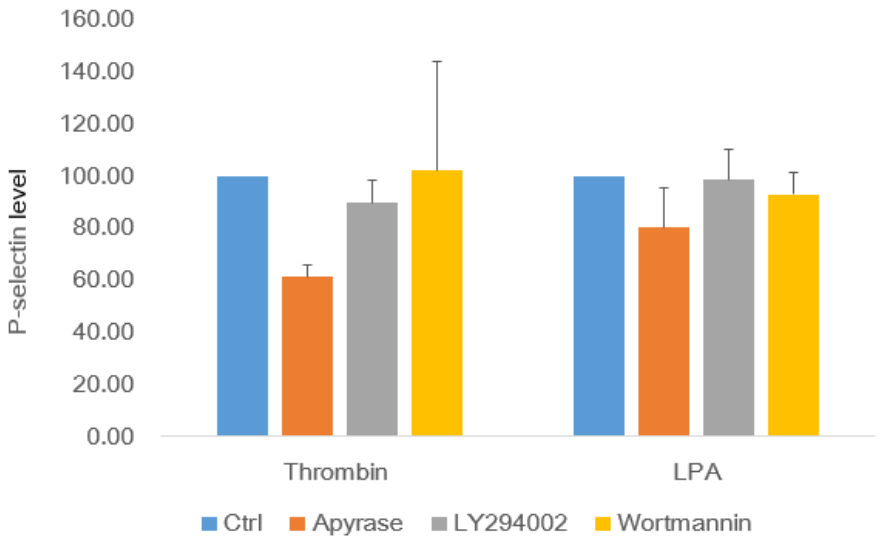

Figure 3.11 Effect of apyrase and PI3K inhibitors on P-selectin level in thrombin- or LPA-treated platelets. Platelets were stimulated with 0.2 U/ml thrombin or 20 μM LPA in the presence or absence of inhibitors for 1 min (2 U/ml apyrase), or 15min (25 μM LY294002 or 100 nM wortmannin). P-selectin level was not significant changed by any of the three inhibitors in either thrombin or LPA treated platelets. P-selectin levels in platelets are reported relative to the control (no inhibitor treatment) which was normalized to 100%. Results are expressed as mean ± s.d. (one-way ANOVA with Dunnett's test; n = 3).

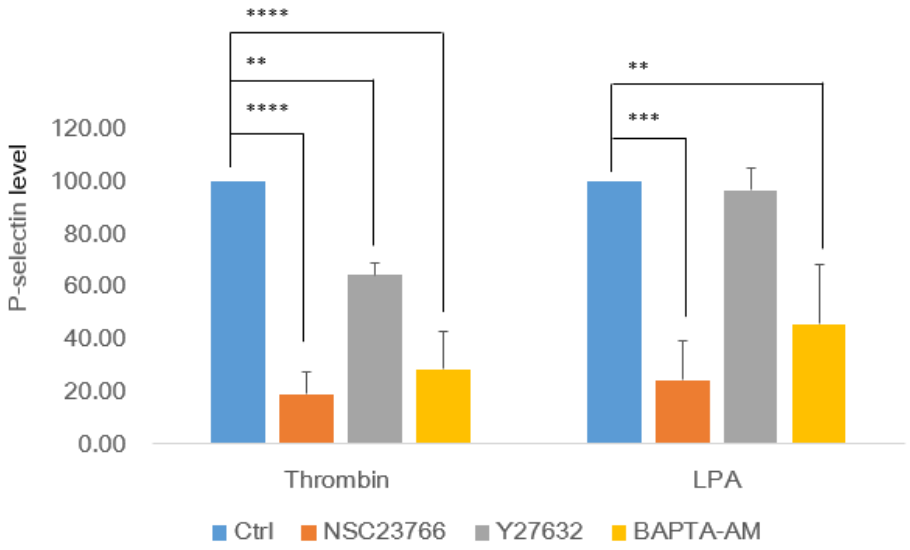

Figure 3.12 Effect of Rac and ROCK inhibitors and calcium chelator on P-selectin levels in thrombin- or LPA-treated platelets. Platelets were stimulated with 0.2 U/ml thrombin or 20 μM LPA in the presence or absence of 150 μM NSC23766, 20 μM Y27632 or 50 μM BAPTA-AM for 15min. P-selectin level was significantly decreased by Y27632 in thrombin- but not LPA treated platelets, it was also significantly decreased by NSC23766 or BAPTA-AM in both thrombin and LPA treated platelets. P-selectin levels in platelets are reported relative to the control (no inhibitor treatment) which was normalized to 100%. Results are expressed as mean ± s.d., asterisk (*) indicates significance (one-way ANOVA with Dunnett's test, *$p<0.05$, **$p<0.01$, ***$p<0.001$, ****$p<0.0001$; n = 3).

3.4 Discussion

This study presents a novel approach that will open up new avenues in cell signaling research: for the first time, the activity levels of multiple small GTPases can be quantified in parallel and from a single sample aliquot. To achieve this, quantitative targeted proteomics has been employed, because of its inherent ability to multiplex, distinguish and quantify different isoforms with high reproducibility. Indeed, MRM-based assays provide several advantages over Western blot assays. Firstly, multiplexing in Western blot is generally achieved by analyzing multiple sample aliquots in parallel using different antibodies. Therefore, information of multiple small GTPases from a single aliquot is not attainable this way. In contrast, multiple proteins can be

monitored from a single aliquot using targeted proteomics. By employing four of the best characterized binding domains, we were able to precipitate up to 12 active small GTPases, and analyze them simultaneously. The MRM assay is scalable, and could be further expanded if additional well-characterized binding domains were developed and added to precipitate other small GTPase subfamilies. Alternatively, additional proteotypic peptides could be developed to include additional small GTPase isoforms or disease-relevant splice variants of the existing small GTPases, e.g. Rac1B, a Rac1 splice variant, which is involved in lung cancer progression [399]. Non-human protein could also be targeted, which would require replacing the proteotypic peptides if the human binding domains show cross-reactivity but the proteotypic peptide sequences were not conserved, or the binding domains and peptides otherwise. Sequence-conserved species such as mouse and rat can already be targeted by the existing MRM assay, demonstrating its versatility.

Secondly, resolving isoform-specific information by Western blotting requires development of high quality antibodies. In contrast, differentiation of closely related isoforms is readily accomplished in MRM assays using unique proteotypic peptides for each small GTPase isoform. Due to the high sequence homology of small GTPases, only a limited number of candidate peptides could be identified even when using relaxed selection criteria. Only one proteotypic peptide was selected and used for quantification of each small GTPase, yet this did not hamper the overall performance. Peptides with and without methionine oxidation were monitored, and similar profiles were achieved for both forms (Figure 3.9), demonstrating the ability of MRM assays to also monitor protein modifications.

Thirdly, quantification is an indirect measurement in Western blots, where signals are produced by a secondary antibody. Moreover, the dynamic range of film-based or digital

imaging-based methods is generally limited to two orders of magnitude. Conversely, targeted proteomics directly measure peptides digested from target proteins with a dynamic range of 4–5 orders of magnitude [400]. Indeed, reliable quantification was observed with this assay, even though the selected proteotypic peptides did not necessarily meet all of the criteria of ideal candidates. CVs similar to those achieved here (< 20%) were reported also for other MRM studies [401], attesting to the remarkable excellent overall performance of our MRM assay. Relative quantification was used in this study because activation level changes of small GTPases compared to a control were the intended biological readout. Absolute quantification at peptide or protein levels was not necessary, and would be difficult to achieve in this case, because any sample loss that occurs prior to the addition of a standard, e.g. during cell lysis and protein digestion, would still not be addressed.

In order to demonstrate the ability of the MRM assay to provide novel insights into biological processes, a suitable system was needed. We chose to study human platelets and their response to different agonists over time or inhibitor treatment, because the process of agonist-stimulated platelet activation and aggregation is known to involve multiple small GTPases. Regulation of activity level of ten small GTPases could indeed be monitored simultaneously. All 12 small GTPase isoforms were identified in HUVEC cells; whereas ten small GTPases were found in platelets, the absence of HRas and RhoB from platelets is consistent with a recent non-targeted global platelet proteome analysis [290], demonstrating that the MRM assay accurately mirrors the corresponding cellular proteome. The activation profiles of all ten small GTPases in thrombin-induced platelet activation follow the same trend: highest activation level was observed within the first two minutes, after which it gradually decreased. This confirms the assay's ability to provide time-resolved activation profiles, and implies that all of these small GTPases act in

concert to mediate platelet activation. In addition, activity levels of all ten small GTPases in LPA- and ADP-induced platelet activation showed similar profiles, indicating that similar pathways were activated by these agonists. This suggests that LPA acts on platelets by employing the secondary agonist ADP that is released from platelet granules upon LPA stimulation, which is in agreement with the observation of ADP receptor antagonists inhibiting LPA-induced platelet aggregation [402].

Next, the MRM assay was applied to thrombin- and LPA-induced platelet activation in presence or absence of PI3K inhibitors as well as an ADP scavenger apyrase. Activity level of eight out of ten small GTPases remained unchanged in both thrombin- and LPA-induced platelet activation in response to PI3K inhibitor treatment, only Rap1A and Rap1B showed significant decrease in LPA- but not thrombin-induced platelet activation. This indicates that only Rap1 small GTPases are downstream of PI3K and the other small GTPases are independent of this pathway. Moreover, the activity of Rap2B was not affected by PI3K inhibitor treatment, whereas Rap1A and Rap1B showed significant decreased activity upon treatment, illustrating that isoform-specific regulation can be monitored by the MRM assay. It is worth noting that these two Rap1 isoforms cannot be distinguished by commonly used anti-Rap1 antibodies, highlighting the novel biological insight that can be gained with this MRM assay. These results together indicate that targeting the PI3K-Rap1 pathway could potentially be a useful antiplatelet strategy in cardiovascular disease [403].

In response to the same set of inhibitors, i.e. PI3K inhibitors (wortmannin and LY294002) and apyrase, P-selectin translocation levels remained unchanged in platelet activation induced by LPA or thrombin. This suggests that the PI3K pathway is not required for P-selectin translocation, and distinct pathway(s) are involved in platelet secretion (P-selectin translocation)

and platelet aggregation. Furthermore, treatment of either the small GTPase Rac inhibitor or calcium chelator significantly reduced thrombin- and LPA-induced P-selectin translocation, suggesting that Rac activation or calcium production might potentially be targeted for reduction of P-selectin translocation induced by LPA. Interestingly, unlike thrombin, the same process induced by LPA was not affected by ROCK inhibitor treatment. Evidence from other studies indicated that LPA-induced platelet shape change was mediated by $G_{12/13}$-Rho pathway [22, 93]. This implies that LPA-induced P-selectin translocation is independent of platelet shape change as well as the Rho – ROCK pathway, which is required for thrombin-induced P-selectin translocation [102].

In summary, our results confirm that monitoring the activity levels of multiple small GTPase isoforms provides access to a unique layer of cellular signaling that could not be systematically investigated until now. This is reminiscent of protein phosphorylation, where the introduction of high-throughput proteomics methods resulted in novel insights into the coordination of cellular responses. Indeed, mass spectrometric phosphotyrosine profiling using phosphotyrosine-specific antibodies is used successfully to study signaling networks [272, 404] and inhibitor treatments [405]. Likewise, we anticipate that this multiplexed MRM assay targeting active small GTPases, which are ubiquitously expressed in a wide range of cells and organisms, will also be applicable to a large number of biological systems and questions.

Chapter 4 Global phosphorylation events in monocytes incubated with activated platelets using phosphoproteomics

4.1 Introduction

Platelet activation and aggregation is the main process in thrombosis, and current evidence suggests that platelet activation is also involved in inflammation, i.e. activated platelets bind to and activate leukocytes, and form platelet-leukocyte aggregates, which constitutes a functional link between thrombosis and inflammation [406]. Among the different types of leukocytes, monocytes were shown to be preferred by platelets in the formation of aggregates in CVDs [16, 407]. Indeed, circulating platelet-monocyte aggregates (PMAs) in blood have been established as an early marker of acute cardiovascular events, e.g. stroke [15], stable coronary artery disease [16] and hypertension [17]. Therefore, understanding how signaling events are regulated in monocytes in response to exposure to activated platelets may help in developing intervention strategies for CVDs.

As discussed in section 1.1.4, the formation of PMAs induces inflammatory cascades in monocytes, i.e. synthesis of IL-1β, IL-8 and MCP-1 [408, 409], as well as expression of COX-2 [410] and tissue factors [411]. In addition to direct binding to monocytes, platelets release soluble factors, i.e. RANTES and PF4, that amplify the recruitment of monocytes to the endothelium and accelerate atherosclerosis [146]. Moreover, a recent study showed that phospho-Akt in primary monocytes was elevated after incubation with activated platelets, suggesting that the PI3K pathway was involved in this process [412]. However, signaling events in monocytes in response to incubation with activated platelets are largely uncharacterized.

Phosphoproteomics techniques enable the systematic investigation of protein phosphorylation, which is essential for cellular signaling events [188]. Therefore, quantitative phosphoproteomics was employed to study global phosphorylation events in monocytes incubated with activated platelets. As discussed in section 1.2.7, phosphoproteins represent a small, difficult to detect portion of proteins in a whole cell lysate, thus a combination of different enrichment strategies is commonly used for efficient analysis by mass spectrometry. Here, a fractionation strategy (strong cation exchange) coupled with phosphopeptide enrichment (TiO_2 and IMAC) was chosen and subsequently optimized. Furthermore, in order to quantify the phosphorylation changes in monocytes and eliminate overlapping platelet peptides that could affect quantification, a metabolic labeling strategy, i.e. stable isotope labeling by amino acids in cell culture (SILAC) [185], was employed. A triple SILAC system was established with THP-1 cells used as a model for primary monocytes [413], i.e. THP-1 cells were cultured with medium- or heavy-labeled amino acids (medium and heavy SILAC channels), with platelets having unlabeled amino acids as "light" SILAC channel. Phosphorylation changes from the medium and heavy SILAC channels can therefore be quantified independent of the light SILAC channel. Using this method, global phosphorylation events in THP-1 cells in response co-incubation with thrombin- or LPA-activated platelets were quantified, and regulated phosphoproteins and signaling pathways were then identified.

4.2 Methods

4.2.1 Cell culture

The human monocytic cell line THP-1 (American Type Culture Collection, Rockville, MD) was maintained in Roswell Park Memorial Institute (RPMI) 1640 medium (Invitrogen, Frederick, MD), supplemented with 10 % fetal bovine serum (FBS; Invitrogen Corporation, Carlsbad, CA) and 100 units/ml of penicillin/streptomycin. For SILAC labeling, THP-1 cells were maintained in lysine, arginine and glutamine depleted RPMI 1640 (Caisson Labs, North Logan, UT) supplemented with 10 % dialyzed FBS (Invitrogen Corporation, Carlsbad, CA), 100 units / ml of penicillin/streptomycin, 100 units / ml of L-glutamine and either medium labeled, 0.075 mg / ml $^{2}D_{4}$-L-lysine and 0.044 mg / ml $^{13}C_{6}$-L-arginine or heavy labeled 0.077 mg / ml $^{13}C_{6}$,$^{15}N_{2}$-L-lysine and 0.045 mg / ml $^{13}C_{6}$,$^{15}N_{4}$-L-arginine (Cambridge Isotope Labs, Andover, MA, USA). Cells were grown for at least five doublings to allow full incorporation of labeled amino acids.

4.2.2 Platelet isolation and stimulation

Ethical approval for platelet isolation from whole blood from healthy blood donors was obtained from the Clinical Research Ethics Board at the University of British Columbia (H12-00757), and written consent was granted by the blood donors. After discarding the first 4 mL, blood was drawn into vacutainer blood collection tubes containing citrate-dextrose (ACD solution A, BD Biosciences, Mississauga, ON, Canada). Platelet-rich plasma was isolated from whole blood following initial centrifugation at 150 relative centrifugal force (rcf) at room temperature for 15 min. To minimize contamination from other blood cells, only the top two thirds of the platelet-rich plasma was collected and centrifuged at 720 rcf at room temperature

for 10 min in the presence of a half volume of ACD. Subsequently, the platelet pellet was carefully washed with CGSA buffer (10 mM trisodium citrate, 30 mM dextrose and 1 unit / ml apyrase) to remove plasma proteins and then centrifuged at 720 rcf at room temperature for 10 min. The platelet wash step was repeated and platelets were resuspended in Krebs-Ringer buffer (4 mM KCl, 107 mM NaCl, 20 mM $NaHCO_3$, 2 mM Na_2SO_4, 19 mM tri-sodium citrate, 0.5% (wt/vol) glucose in H2O, pH 6.1). Platelet counts were determined by using a hemocytometer and adjusted to physiological concentration (300 x 10^9/L) using HEPES buffer (10 mM HEPES, 137 mM NaCl, 2.9 mM KCl, 12mM $NaHCO_3$, pH 7.4) or RPMI 1640 medium. Platelets were rested at room temperature for 30 min before stimulation.

4.2.3 Cell lysis (option 1)

Cell lysis was performed essentially as described [414]. Briefly, after treatment, cells were centrifuged at 450 rcf for 3 min at room temperature, the supernatant was removed, and the pellet was washed with ice-cold PBS. For SILAC experiments, cells with different SILAC labeling were counted and mixed at 1:1 ratio, and centrifuged at 450 rcf for 3 min, the supernatant was removed and the pellet was resuspended separately in lysis buffer (1% NP-40, 0.1% sodium deoxycholate, 150 mM NaCl, 1 mM EDTA, 50 mM Tris (pH 7.5), phosphatase inhibitors (1 mM sodium orthovanadate, 5 mM sodium fluorate, 5 mM β-glycerolphosphate), and protease inhibitor cocktail (1 tablet / 10 mL, Roche, Basel, Switzerland)). Lysates were clarified at 4 ℃ for 10 min at 16,000 g, proteins from supernatant were precipitated over one hour by ice-cold acetone, pelleted by centrifugation for 2 min at 2,000 g, and re-dissolved in 8 M urea containing 1% N-octylglucoside and phosphatase inhibitors. Cell lysis was performed using this condition unless otherwise stated.

4.2.4 Cell lysis (option 2)

After treatment, cells were centrifuged at 450 g for 3 min at room temperature, the supernatant was removed and the pellet was washed with ice-cold PBS. For SILAC experiments, medium and heavy SILAC labeled THP-1 cells were counted and mixed at 1:1 ratio. The SILAC cell mixture was centrifuged at 450 rcf for 3 min, the supernatant was removed and the pellet was resuspended in lysis buffer (1% Na deoxycholate in 50 mM NH_4HCO_3) and immediately placed in a heating block at 99°C for 10min. Benzonase (1:10,000) and a final concentration of 1.5 mM $MgCl_2$ was added to the lysate and the sample was incubated at room temperature for 30 min to degrade DNA.

4.2.5 In-solution trypsin digestion

BCA assay was performed for cell lysate samples at 10 times dilution to determine protein concentration. A total of 4 mg protein sample was used. Then, proteins from cell lysates were reduced by addition of dithiothreitol to a final concentration of 5 mM in 50 mM ammonium bicarbonate solution for 30 min at 37 ℃ and alkylated with 14 mM iodoacetamide in 50 mM ammonium bicarbonate solution for 30 min in the dark at room temperature. 5 mM dithiothreitol was added to quench the alkylation for 15 min at room temperature. The sample was digested by Lys-C (1:160 Lys-C: protein) at room temperature for 4 hours prior to trypsin digestion (1:100 trypsin: protein) with 1 mM $CaCl_2$ overnight at 37 ℃.

4.2.6 Peptide desalting

After protein digestion, formic acid was added to the peptide solutions to reach pH < 2.5 and the solution was centrifuged at 16,000 rcf for 10 min. The supernatant was desalted on a 200 mg

SepPak cartridge. The cartridge was first conditioned twice with 3 mL ACN, followed by 3 mL 50% acetonitrile (ACN) 50% acetic acid (AcOH) and then 3 mL 0.5% AcOH. Subsequently, samples were loaded onto the cartridge slowly, and washed twice with 1 mL 0.5% AcOH, and finally eluted slowly twice with 1 mL 50% ACN/0.5% AcOH. ACN from the eluted peptide solution was removed by centrifugation at 35 ℃ for 30 min. The remaining sample was frozen in liquid N_2, and lyophilized overnight at -50 ℃. The samples were stored at -80 ℃ until further analysis.

4.2.7 Strong cation exchange

Desalted peptide sample was dissolved in SCX buffer A (30% ACN, 5 mM KH_2PO_4, pH 2.7). The SCX fractionation was performed using an Ettan MDLC system (GE healthcare, Little Chalfont, Bucks, UK) coupled with a ZORBAX 300-SCX column (4.6 mm ID × 150 mm (5 μm), Agilent, Santa Clara, CA, USA). Peptides were separated based on a linear gradient from 0% to 13% buffer B (30% ACN, 5mM KH_2PO_4, 350mM KCl, pH 2.7) for 20 min and 100% buffer B for 5 min. Twenty-six 300 μL fractions were collected and UV-Vis absorption at 280 nm were measured on a NanoDrop spectrophotometer (Thermo Fisher Scientific, San Jose, CA, USA). Twelve early fractions based on the peptide concentration were collected, and ACN was removed by centrifugation at 35 ℃ for 30 min. Then the samples were desalted with 50 μl 50% C18 beads (J.T. Baker, Phillipsburg, NJ, USA). The C18 beads in methanol was loaded onto a 200 μl pipet tip, methanol was removed by centrifugation at 400 g, and conditioned with 250-300μL sample buffer (1% TFA, 5% ACN). The pooled SCX fractions were then loaded onto C18 tips by centrifugation at 100 rcf for 20 min, washed with 200 μL sample buffer at 400 g, and eluted twice with 50 μL TiO_2 buffer B (80% ACN/0.1% TFA) at 50 rcf for 15 min.

4.2.8 Phosphopeptide enrichment

TiO_2 beads (10:1 w/w, sample to protein, GL Sciences, Peterborough, ON, Canada) were prepared in TiO_2 buffer B and loaded onto a 200 µL pipet tip packed with C8 membrane (3M Empore, St. Paul, MN, USA). TiO_2 tips were washed with 20 µL TiO_2 buffer B at 200 rcf for 2 min and then with 20 µL TiO_2 Buffer C (70% ACN, 0.1% TFA, 29.2% (300mg/mL) lactic acid) at 250 rcf for 2 min. Samples eluted following the protocol from section 4.2.6 in 100 µL TiO_2 buffer B were diluted with 100 µL TiO_2 buffer D (41.5% ACN, 0.1% TFA, 58.4% lactic acid) to reach TiO_2 buffer C conditions, i.e. 70% ACN, 0.1% TFA, 29.2% (300mg/mL) lactic acid.

The diluted samples was slowly loaded to the washed TiO_2 tip at 100 rcf over 30 min. Non-phosphopeptides were washed away with 20 µL TiO_2 Buffer C at 250 rcf for 5 min and then with 20 µL TiO_2 Buffer B at 250 rcf for 5 min. The phosphopeptides were eluted stepwise with 20 µL 5% NH_4OH, 20 µl 0.5% pyrrolidine and 3µl TiO_2 buffer B at 50 rcf for 10 min into 10 µL 50% TFA to ensure that pH was below 2.5.

For IMAC enrichment, IMAC beads (Sigma, Oakville, ON, Canada) were washed twice with IMAC loading buffer (50% ACN, 0.1% TFA). Peptides were incubated with IMAC beads for 30 min at room temperature with vigorous shaking. After incubation, IMAC beads were loaded onto 200 µL pipet tip packed with C8 membrane, and washed with 20 µL IMAC loading buffer twice. The phosphopeptides were eluted with 50 µL 5% NH_4OH. For SIMAC enrichment, IMAC sample loading and washing flow-through was collected and subjected to TiO_2 enrichment.

After elution of phosphopeptides, samples were desalted on homemade StageTips [415].

4.2.9 LC-MS/MS analysis

Peptides were analzyed using a nano LC-MS/MS system, either with a LTQ-FT-ICR (Thermo

Fisher Scientific, San Jose, CA, USA) or a LTQ-Orbitrap Velos mass spectrometer (Thermo Fisher Scientific, San Jose, CA, USA). For the LTQ-FT-ICR instrument, peptide mixtures were separated on a PicoTip column (o.d. = 360, I.d. = 75, tip = 15 ± 1 µm) from New Objective (Woburn, MA, USA) packed with reverse-phase C18 material (15 cm, C18 magic, 100 Å, 3 µm, Michrom Bioresources, Auburn, CA, USA). Solvent A (0.5% acetic acid) and solvent B (80% acetonitrile + 0.5% acetic acid) were used. A linear gradient of 6% to 80% solvent B over 30 min at a flow rate of 0.6 µl / min was applied via an Agilent 1100 nano HPLC pump (Agilent, Santa Clara, CA, USA). Data-dependent MS and MS/MS spectra were acquired.

For the LTQ-Orbitrap Velos instrument, an Agilent 1290 nano HPLC pump (Agilent, Santa Clara, CA, USA) was employed. Peptide mixtures were separated on a PicoTip column (o.d. = 360, I.d. = 75, tip = 15 ± 1 µm) from New Objective (Woburn, MA, USA) packed with reverse-phase C18 material (15 cm, C18 magic, 100 Å, 3 µm, Michrom Bioresources, Auburn, CA, USA). Data-dependent MS and MS/MS spectra were acquired.

4.2.10 Mass spectrometry data analysis

Proteins were identified by searching the MS and MS/MS spectra using X!Tandem CYCLONE. Raw data is accessible at gpmdb.thegpm.org with GPMDB model numbers. For quantitative proteomics, proteins were identified by searching the MS and MS/MS spectra using MaxQuant (version 1.5.0.0) [416], database search was performed by Andromeda [417] against UniProt/Swiss-Prot (16/5/2014, subset human). Search parameters included two missed cleavages by trypsin, fixed carbamidylmethyl modification on cysteine, and variable modifications, i.e. methionine oxidation, protein N-terminal acetylation, $^{2}D_{4}$-L-lysine, $^{13}C_{6}$-L-arginine, $^{13}C_{6}$,$^{15}N_{2}$-L-lysine and $^{13}C_{6}$,$^{15}N_{4}$-L-arginine, as well as phosphorylation of serine,

threonine, and tyrosine. The peptide mass tolerance was 4.5 ppm and the MS/MS tolerance was 0.5 Da. False discovery rate was set to 1% at peptide and at protein levels. Phosphorylation site localization probabilities were defined as class I ($p > 0.75$), class II ($0.75 > p > 0.5$), or class III ($p < 0.5$) based on PTM scoring [188]. Gene Ontology enrichment analysis was performed with the DAVID functional annotation tool [418]. Ingenuity Pathway Analysis (Ingenuity® Systems, www.ingenuity.com) for phosphoproteomics in THP-1 cells was performed using the following filters: data sources: all; confidence: experimentally observed and high (predicted); species: human; and tissues and cells lines: primary monocytes and leukemia cell lines.

4.2.11 Platelet-monocyte aggregate formation

Platelets were activated in the presence of 2.5 mM GPRP peptide (Millipore, Billerica, MA, USA) to prevent aggregation, then activated or resting platelets were added to 200 µl of 1 X 10^6/ml THP-1 cells at a ratio of 10 : 1 for platelets : THP-1. The cells were then incubated at 37 ° for 10 min on a rotator.

For phosphoproteomics analysis, activated platelets were added to heavy SILAC labeled THP-1 cells using the same conditions. After incubation, the same number of medium and heavy SILAC labeled THP-1 cells were centrifuged separately at 450 rcf for 10 min, and washed with ice cold PBS. The cells were centrifuged separately at 450 rcf for 10 min again, lysed, and the lysates were combined using the lysis buffer described in section 4.2.3.

4.2.12 Adhesion assay

96-well microtiter plates (Corning Costar, Cambridge, MA, USA) were coated by incubation with fibronectin (10 µg / ml in PBS, Millipore, Billerica, MA, USA) overnight at 4 ℃. After

incubation, the wells were washed with PBS and then blocked with 2% BSA at room temperature for 1 h just before use. THP-1 cells treated with or without resting or activated platelets, as described in section 4.2.11, were labeled with calcein-AM (Life Technologies, Carlsbad, CA, USA) at a final concentration of 10 µl per one million cells. The cells were then incubated in the fibronectin-coated plate at 37 ℃ for 30 min. After incubation, non-adherent cells were removed by washing twice with PBS. Adhesion was quantified with a Fluoroskan Ascent plate reader (Labsystems, Waltham, MA, USA). Nine measurements at excitation wavelength of 485 nm and emission wavelength of 527 nm for each sample were recorded. The adhesion ratio was calculated as fluorescence from adherent cells divided by total fluorescence from cells originally added.

4.2.13 Flow cytometry analysis

For platelet-monocyte aggregate formation, 5 µl of FITC-conjugated mouse anti-human CD41a (BD Biosciences, Mississauga, ON, Canada) was added to the cells, and incubated for 20 minutes at room temperature in the dark. 1.8 ml of FACS buffer (1×PBS, 0.5% BSA) was added to each sample, and samples were analyzed on LSR II flow cytometer (BD Biosciences, Mississauga, ON, Canada). Platelet-monocyte aggregate formation was quantified based on CD41a positive events on monocytes. All platelet stimulation experiments were performed within 3 hours after blood collection.

4.2.14 Western blotting

Western blotting was performed as described in section 3.4.2. Anti-phospho-Akt (Ser473) (193H12) rabbit monoclonal antibody (Cell Signaling, Danvers, MA, USA) at a concentration of

1:1,000 overnight at 4 ℃ in PBST supplemented with 3% BSA was used. Subsequently, the membrane was incubated with Alexa Fluor 680 goat anti-rabbit IgG (H+L) (Molecular Probes, Eugene, OR, USA) at a concentration of 1:10,000 in the blocking solution. Protein level was detected using an Odyssey infrared imaging system (LI-COR Biosciences, Lincoln, NE, USA). For actin as loading control, after analysis for phospho-Akt, the membrane was stripped with a buffer containing 62.5 mM Tris HCl (pH 6.8), 2% SDS (wt / vol), and 100 mM β-mercaptoethanol. Membrane was re-blocked in the blocking solution for 1 h at room temperature on a shaking platform, and re-probed with monoclonal anti-β-actin mouse antibody (Sigma, Oakville, ON, Canada) at a concentration of 1:2,000 overnight at 4 ℃ in PBST supplemented with 3% BSA. Subsequently, the membrane was incubated with Alexa Fluor 680 goat anti-mouse IgG (H+L) (Molecular Probes, Eugene, OR, USA) at a concentration of 1:10,000 in the blocking solution and analyzed on the Odyssey infrared imaging system.

4.3 Results

4.3.1 Optimization of the phosphopeptide enrichment method

4.3.1.1 Sample loading using different relative centrifugal forces

In order to test the effect of the relative centrifugal force (rcf) during sample loading on the coverage of phosphopeptides, TiO_2 phosphopeptide enrichment from tryptic digest of normal THP-1 cells was performed with different rcfs. THP-1 cells were lysed using lysis condition#2, protein concentration was determined by BCA assay, and 2 mg of protein of the THP-1 lysate was in-solution digested, desalted and split into two samples of equal volume. TiO_2 beads were conditioned and packed into pipet tips. Subsequently, both samples were loaded onto the TiO_2 tips by using a centrifuge with 500 or 100 rcf. Phosphopeptides were then eluted, desalted and

analyzed using mass spectrometry. As a result, 340 and 494 phosphopeptides were identified using 500 or 100 rcf, respectively (Table 4.1). In addition, 597 and 913 phosphorylation sites were identified using 500 or 100 rcf, respectively. These results represent 45% more phosphopeptides and 53% more phosphorylation sites identified using the lower speed at 100 rcf, while maintaining similar phosphopeptide enrichment ratio. Therefore, the lower sample loading speed was used for all other phosphopeptide enrichment studies.

Table 4.1 Comparison of different relative centrifugal force (rcf) during sample loading for phosphopeptide enrichment.

Sample loading rcf	GPM#	#Phosphopeptides	#Peptides	Enrichment ratio	#Phosphosites
500	GPM32100034548	340	382	89.0%	597
100	GPM32100034549	494	609	81.1%	913

4.3.1.2 Strong cation exchange coupled with TiO_2

The effect of using strong cation exchange fractionation (SCX) in addition to TiO_2 phosphopeptide enrichment was tested. Phosphopeptide enrichment was performed essentially as described in section 4.3.1.1, with the exception of 4 mg of protein from THP-1 lysate being split into two samples with equal volume for phosphopeptide enrichment with or without SCX fractionation. Twenty five fractions were collected immediately after sample injection, adjacent fractions were combined to obtain a total of 13 samples (Figure 4.1). Phosphopeptides in each of these samples were enriched separately and analyzed using mass spectrometry. After combining the results of all fractions, 1305 phosphopeptides and 1616 phosphorylation sites were identified (Table 4.2). In contrast, without SCX fractionation, 565 phosphopeptides and 637 phosphorylation sites were identified. Using SCX fractionation resulted in 130% more identified phosphopeptides and 154% more phosphorylation sites.

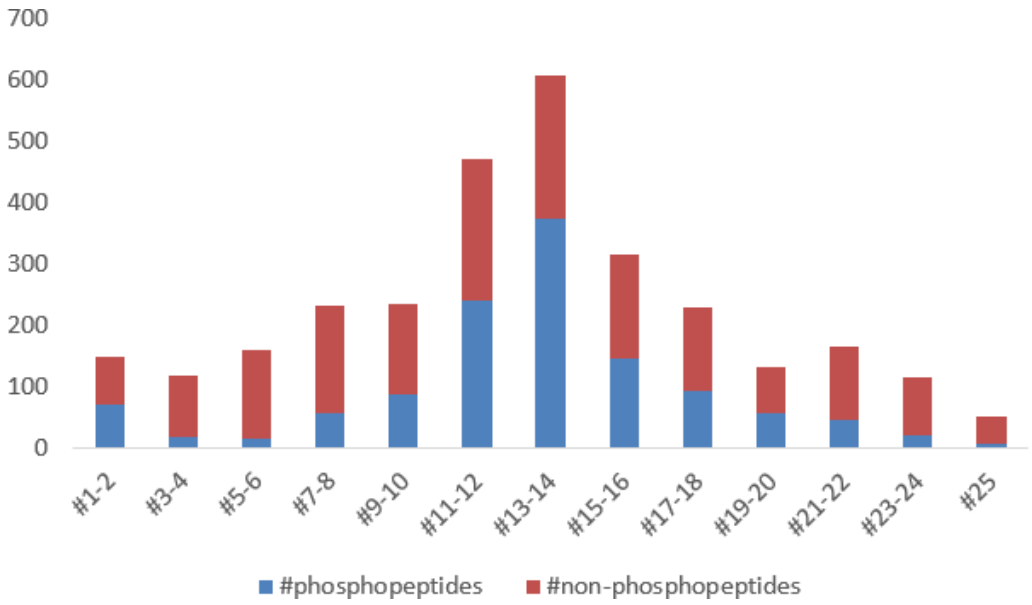

Figure 4.1 Distribution of phosphopeptides and non-phosphopeptides using strong cation exchange followed by TiO_2 phosphopeptide enrichment. Adjacent fractions were combined to obtain a total of 13 samples.

Table 4.2 Comparison of TiO_2 phosphopeptide enrichment with or without strong cation exchange fractionation.

Sample	GPM#	#Phosphopeptides	#Peptides	Enrichment ratio	#Phosphosites
TiO_2	GPM32100034823	565	766	73.8%	637
SCX-TiO_2	GPM32100034837	1305	3063	42.6%	1616

4.3.1.3 Sequential elution from IMAC and TiO_2

In order to test the difference of IMAC and TiO_2 in phosphopeptide enrichment performance and to determine whether the two approaches are complementary, sequential elution from IMAC

SIMAC	GPM#	#Phosphopeptides	#Peptides	Enrichment ratio	#Phosphosites
IMAC	GPM00300008794	872	1010	86.3%	1372
TiO_2	GPM00300008797	1644	2244	73.3%	1727

and TiO_2 (SIMAC) [419] was employed and tested. Sample preparation prior to phosphopeptide enrichment was performed the same as in section 4.3.1.1, with the exception of using 2 mg of protein from THP-1 lysate for phosphopeptide enrichment. Using SIMAC, phosphopeptides were enriched first by IMAC beads, and flow throughs from IMAC sample loading and washing steps were collected and used for subsequent TiO_2 phosphopeptide enrichment. Phosphopeptides from IMAC and TiO_2 enrichment were eluted separately, desalted and analyzed using mass spectrometry. IMAC enrichment resulted in the identification of 872 phosphopeptides and 1372 phosphorylation sites, whereas 1644 phosphopeptides and 1727 phosphorylation sites were identified using TiO_2 enrichment (Table 4.3). Compared to IMAC enrichment, 89% more phosphopeptides and 26% more phosphorylation sites were identified using TiO_2. Of all the phosphopeptides, only 180 were identified using both methods (Figure 4.2A), and more than 50% of phosphopeptides identified using IMAC were multiply phosphorylated, whereas TiO2 enriched more than 90% mono-phosphorylated peptides (Figure 4.2B), indicating phosphopeptide enrichment coverage obtained by using these two reagents was largely complementary. Due to the quality issues from different batches of IMAC beads, only TiO_2 beads were used for subsequent quantitative phosphoproteomics studies.

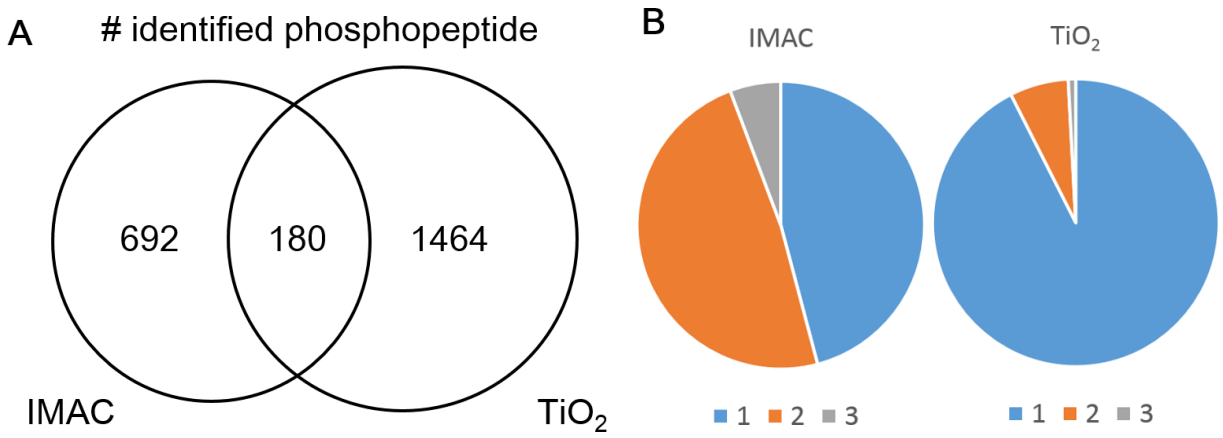

Figure 4.2 Phosphopeptide enrichment by IMAC and TiO_2 are complementary. A. venn diagram showing the shared the phosphopeptides identified by IMAC and TiO2. **B.** The distribution of the peptides with one, two or three phosphorytion sites in IMAC and TiO2 enrichment.

4.3.1.4 Orbitrap Velos vs FT-ICR

To test the effect of using different mass spectrometers on the identification of phosphopeptides, samples following phosphopeptide enrichment were analyzed using the Orbitrap Velos or the FT-ICR instruments (both Thermo Scientific). Phosphopeptide enrichment was performed the same as section 4.3.1.1, with the exception of using 2 mg of protein from THP-1 lysate for phosphopeptide enrichment. Prior to mass spectrometry analysis, the sample was split in half and analyzed by either of the two mass spectrometers. Using FT-ICR, 631 phosphopeptides and 674 phosphorylation sites were identified. In contrast, 2030 phosphopeptides and 2171 phosphorylation sites were identified using the Orbitrap Velos (Table 4.4).

Table 4.4 Comparison of the number of phosphopeptides analyzed using FT-ICR and Orbitrap Velos.

Instrument	GPM#	#Phosphopeptides	#Peptides	Enrichment ratio	#Phosphosites
FT-ICR	GPM32100049185	631	967	65.3%	674
Orbitrap Velos	GPM32100049430	2030	2716	74.7%	2171

4.3.1.5 Cell lysis conditions

In order to test the effect of cell lysis conditions on the recovery of protein phosphorylation, two commonly used lysis conditions were compared: lysis condition#1 represented a mild condition using 1% NP40 and 0.1% sodium deoxycholate with phosphatase and protease inhibitors; whereas lysis condition#2 applied harsh conditions with 1% sodium deoxycholate without inhibitors and immediate heating at 99°C for 10 minutes. THP-1 cells were incubated with resting platelets, or thrombin- or LPA-activated platelets for 10 or 30 minutes and lysed using either lysis condition#1 or #2. The proteins in the cell lysates were separated using 12% SDS-PAGE, and Western blotting was used to detect phosphorylated Akt. Although the actin loading control only showed slightly lower amounts of starting material using lysis condition#2, phosphor-Akt levels were greatly reduced (Figure 4.3). Therefore, lysis condition#1 was used for quantitative phosphoproteomics analysis.

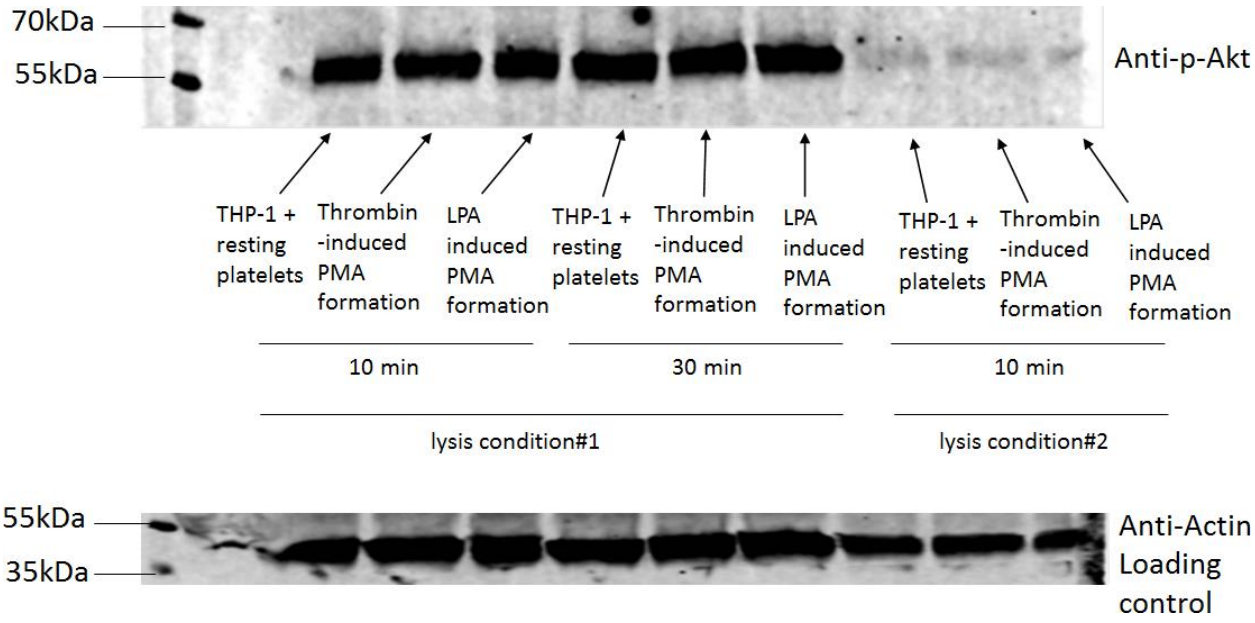

Figure 4.3 Comparison of phosphorylation levels of Akt resulted from two different lysis conditions using Western blotting. Lysis condition#1, mild condition using 1% NP40 and 0.1% sodium deoxycholate with phosphatase and protease inhibitors. Lysis condition#2, harsh condition with 1% sodium deoxycholate without inhibitors and immediate heating at 99 ℃ for 10 minutes. Akt phosphorylation level was greatly reduced using lysis condition#2. PMA, platelet-monocyte aggreagte.

4.3.2 Platelet-monocyte aggregate formation

Before applying the optimized phosphopeptide enrichment method to a proteomic study of the signaling pathways involved in platelet-monocyte aggregate (PMA) formation, conditions for thrombin- and LPA-induced PMA formation were evaluated. Platelets were activated by thrombin or LPA in presence of 2.5 mM GPRP, which binds to fibrinogen to prevent platelet aggregation [412]. Activated platelets were then incubated with THP-1 cells for 10 minutes, and FITC-CD41a antibody (integrin αIIb, platelet marker) was added and incubated with the cells prior to analysis by flow cytometry. Platelets and THP-1 cells were separated by their size using forward and side scatter (Figure 4.4A), then PMA formation was evaluated based on the CD41a positive events on THP-1 cells (Figure 4.4B). Using this method, a statistically significant increase (paired t test, $p<0.05$) for both thrombin- and LPA-induced PMA formation was observed (Figure 4.5).

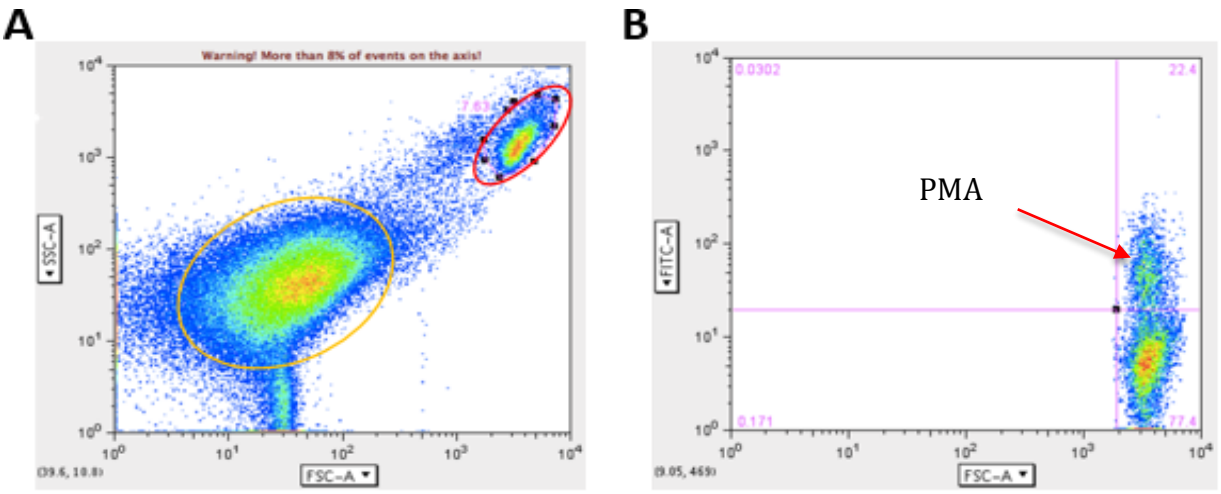

Figure 4.4 Platelet-monocyte aggregate (PMA) formation analyzed by flow cytometry. Activated platelets were incubated with THP-1 and labeled with CD41a-FITC antibody. (**A**) Platelets and THP-1 cells (including PMA) were separated by size, i.e. orange circle represents platelet population, and red circle represents THP-1 and PMA populations. (**B**) PMA percentage was identified based on CD41a positive events on THP-1 cells, i.e. 22.4%.

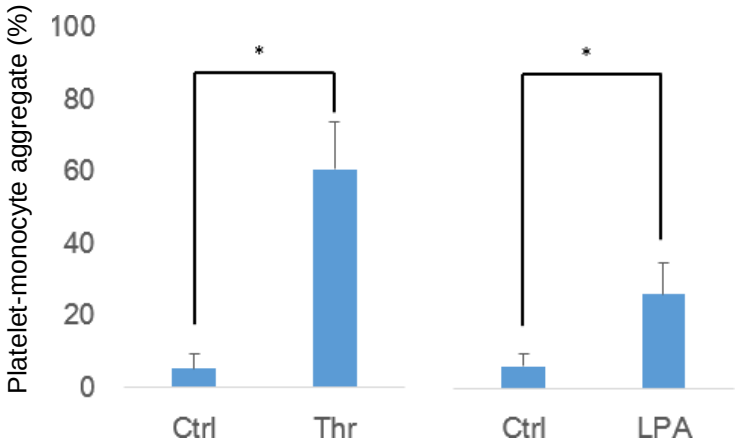

Figure 4.5 Platelet-monocyte aggregate formation induced by thrombin or LPA. Platelets were stimulated with 1 U / ml thrombin (Thr) or 20 μM LPA for 10 min in presence of 2.5 mM GPRP. Subsequently, activated platelets were incubated with THP-1 cells at 10 : 1 ratio for 10 min. Platelet-monocyte aggregate level were identified based on CD41a positive events on THP-1 cells using flow cytometry. Results are expressed as mean ± s.d., asterisk (*) indicates significance (paired t test, *$p<0.05$; n = 3 - 4).

4.3.3 Phosphoproteomics analysis of platelet-monocyte aggregate formation

4.3.3.1 Workflow for quantitative phosphoproteomics

To study the global phosphorylation events in monocytes in response to binding to platelets, a triple SILAC system was employed (Figure 4.6). THP-1 cells were used as a model for monocytes, and were medium or heavy SILAC labeled with platelets having unlabeled amino acids as the "light" SILAC channel. Only the peptides from the medium and heavy SILAC channel were quantified, eliminating overlap from platelet peptides that could affect quantification by SILAC.

The workflow for studying the triple SILAC system using phosphoproteomics was as follows: platelets were stimulated with thrombin or LPA for 10 min in presence of 2.5 mM GPRP. Subsequently, activated platelets were incubated with heavy SILAC labeled THP-1 cells at 10 : 1 ratio for 10 min. After incubation, platelets with heavy SILAC labeled THP-1 cells were combined with medium SILAC labeled THP-1 cells that had not been exposed to platelets, and subjected to cell lysis, trypsin digestion, phosphopeptide enrichment and mass spectrometry analysis.

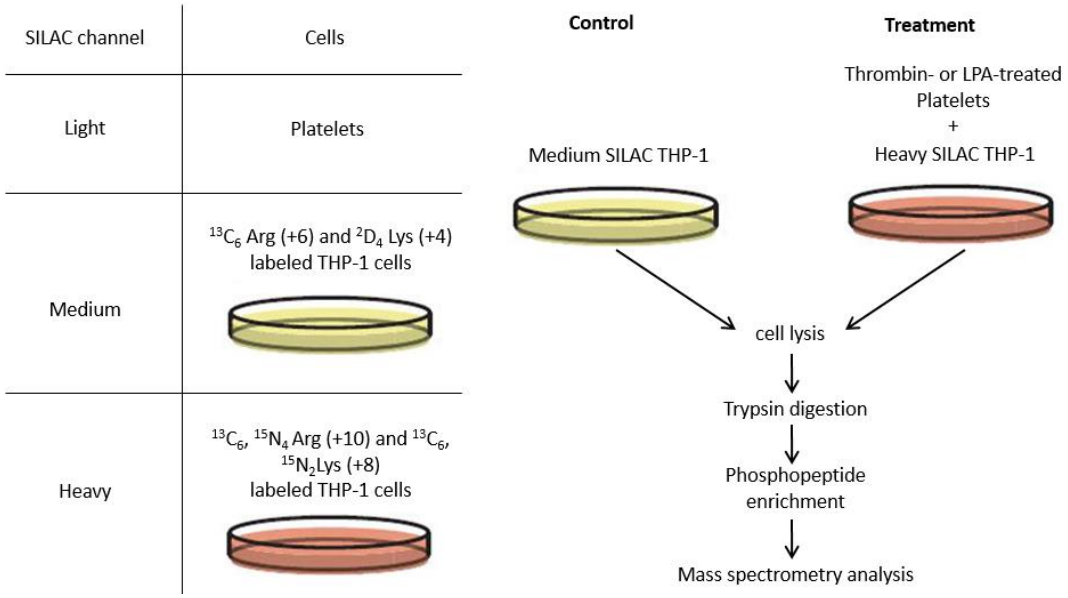

Figure 4.6 Workflow for studying global phosphorylation changes in THP-1 cells in response to binding with platelets using phosphoproteomics. Platelets are stimulated with thrombin or LPA for 10 min in presence of 2.5 mM GPRP. Subsequently, activated platelets are incubated with heavy SILAC labeled THP-1 cells at 10 : 1 ratio for 10 min. After incubation, platelets with heavy SILAC labeled THP-1 cells are combined with medium SILAC labeled THP-1 cells, and subject to cell lysis, trypsin digestion, phosphopeptide enrichment and mass spectrometry analysis.

Phosphopeptide enrichment was achieved using optimized conditions, i.e. combined SILAC cells were lysed using lysis condition#1, followed by Lys-Cc and trypsin double digestion, peptides were fractionated by SCX, and subjected to TiO2 phosphopeptide enrichment and analysis on the Orbitrap mass spectrometer (Figure 4.7). In order to eliminate variation in the amount of medium and heavy labeled starting material, a fraction of the peptide mixture was analyzed directly by the Orbitrap without phosphopeptide enrichment, and the average heavy to medium ratio from this fraction was used to normalize samples after phosphopeptide enrichment.

Furthermore, in order to ensure that full incorporation of medium and heavy labeled lysine and arginine was achieved for THP-1 cells, a SILAC incorporation test was performed by analyzing aliquots taken in 2-3 day intervals. After day 11 of culturing THP-1 cells in SILAC medium, the percentage of peptides containing medium labeled lysine and/or arginine reached a plateau at around 94% (Figure 4.8). Therefore, THP-1 cells were cultured in SILAC media for at least two weeks before they were used for the quantitative phosphoproteomics.

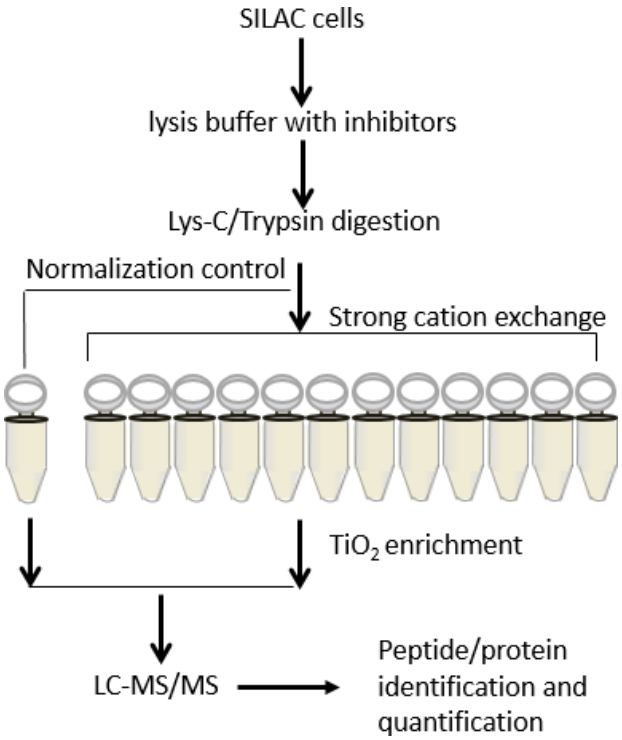

Figure 4.7 Workflow for phosphopeptide enrichment. Combined SILAC cells were lysed in presence of phosphatase and protease inhibitors, followed by Lys-c and trypsin double digestion. A fraction of the peptide mixture was used as a normalization control, which was analyzed directly using an Orbitrap mass spectrometer without phosphopeptide enrichment. The rest of the peptides were fractionated by strong cation exchange, followed by TiO_2 phosphopeptide enrichment and analyzed by the Orbitrap.

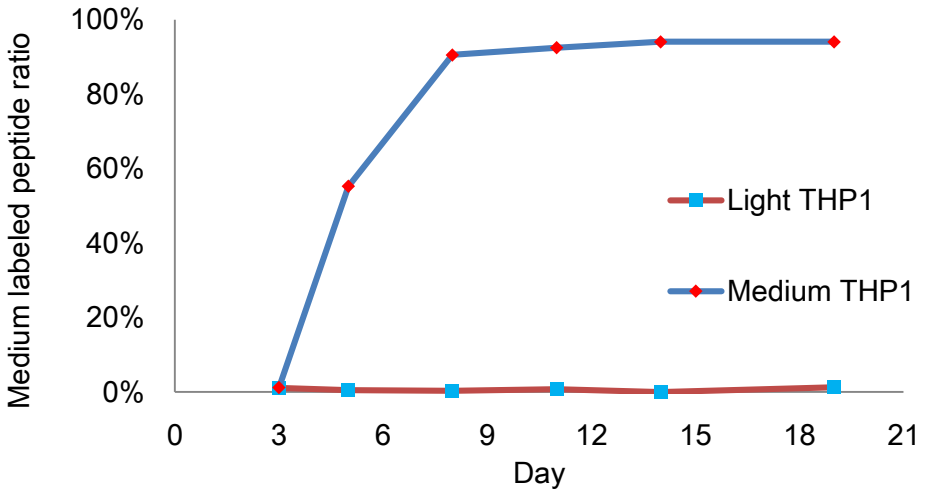

Figure 4.8 SILAC incorporation test for THP-1 cells. After day 11 of culturing THP-1 cells in SILAC medium, the percentage of medium labeled lysine (+4) and arginine (+6) reached a plateau at around 94%. Whereas the percentage of medium labeled lysine (+4) and arginine (+6) remained below 1% in THP-1 cells cultured in SILAC medium supplemented with normal lysine and arginine.

4.3.3.2 Bioinformatics analysis of all identified and quantified phosphorylation events

Using the workflow described in section 4.3.3.1, 2,945 unique phosphopeptides from 1,540 proteins were identified in thrombin-induced PMA formation in at least one of three biological replicates, and similarly 2,227 unique phosphopeptides from 1,231 proteins were identified in LPA-induced PMA formation in at least one of three biological replicates (false discovery rate < 1% at the peptide and at the protein level). Of all the phosphorylation sites identified, the distribution of phosphorylated serine, threonine and tyrosine residues was 87.5% : 11.2% : 1.3% and 85.7% : 12.9% : 1.4% in thrombin- and LPA-induced PMA formation, respectively (Table 4.5). In addition, more than 65% of all identified phosphorylation sites had Class I ($p > 0.75$) localization probability based on the PTM scoring reported by MaxQuant (Table 4.5). Phosphorylation sites with Class II ($0.75 > p > 0.5$) or Class III ($p < 0.5$) localization probability were considered ambiguous.

Peptide quantification was obtained for 78.7% and 79.7% of all identified phosphopeptides in thrombin- and LPA-induced PMA formation, respectively. Only the phosphopeptides that were quantified in at least two biological replicates were analyzed further. In order to identify the signaling pathways in THP-1 cells involved in these two conditions, proteins corresponding to all quantified phosphopeptides were analyzed using Ingenuity Pathway Analysis. Top canonical pathways these proteins were associated with included ERK/MAPK signaling, insulin receptor signaling, Fcγ receptor-mediated phagocytosis, nitric oxide signaling and leukocyte

Table 4.5 Distribution of phosphorylated serine, threonine and tyrosine, and localization probability among all identified phosphorylation sites. Class I ($p > 0.75$), class II ($0.75 > p > 0.5$), class III ($p < 0.5$).

	Ser	Thr	Tyr	Class I	Class II	Class III
Thrombin-induced PMA formation	2576 87.5%	330 11.2%	39 1.3%	1912	505	529
LPA-induced PMA formation	1908 85.7%	288 12.9%	31 1.4%	1530	345	352

extravasation signaling (p<0.01), all of these were shared by both thrombin- and LPA-induced PMA formation (Table 4.6). In addition, RhoA signaling and signaling for Rho family GTPases (p<0.01) were identified in thrombin-induced PMA formation; in contrast, canonical pathways such as DNA methylation and transcriptional repression signaling, PI3K/Akt signaling, and protein kinase A signaling (p<0.01) were only identified in LPA-induced PMA formation.

Furthermore, the 426 quantified phosphopeptides corresponding to 202 phosphoproteins that were shared by both thrombin- and LPA-induced PMA formation were used to further compare the two conditions by Ingenuity Pathway Analysis (Figure 4.9). Top canonical pathways in THP-1 cells that were shared by both conditions included ERK/MAPK signaling, insulin receptor signaling, Fcγ receptor-mediated phagocytosis, nitric oxide signaling and leukocyte extravasation signaling, Rac signaling and PI3K/Akt signaling (p<0.01) (Table 4.7).

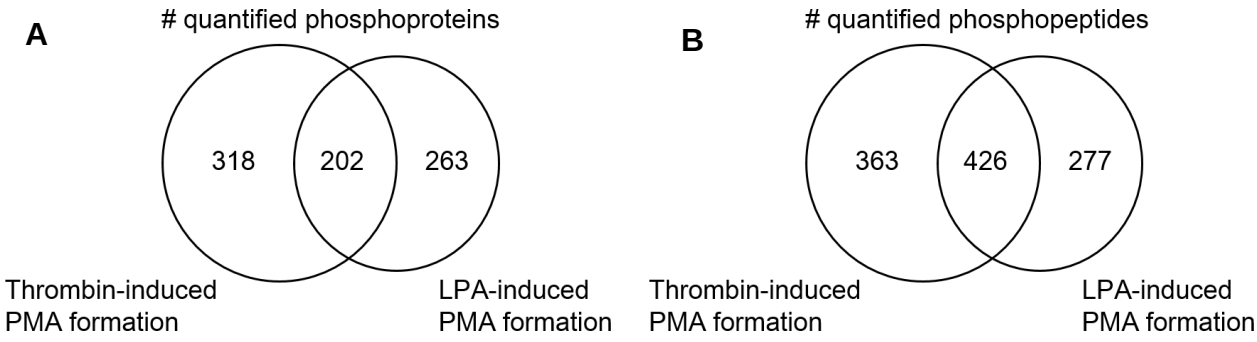

Figure 4.9 Number of quantified (A) phosphopeptides and (B) phosphoproteins shared in thrombin- and LPA-induced platelet-monocyte aggregate (PMA) formation.

Table 4.6 Most highly enriched canonical pathways in thrombin- and LPA-induced platelet monocyte aggregate (PMA) formation. Analysis was performed using Ingenuity Pathway Analysis, only pathways with $p < 0.01$ were shown.

Ingenuity Canonical Pathways	p value	
	Thrombin	LPA
ERK/MAPK Signaling	4.8978E-06	0.0002
Insulin Receptor Signaling	0.0003	0.0004
Fcγ Receptor-mediated Phagocytosis in Macrophages and Monocytes	0.0009	9.1201E-05
Nitric Oxide Signaling in the Cardiovascular System	0.0012	0.0024
FLT3 Signaling in Hematopoietic Progenitor Cells	0.0022	0.0011
GNRH Signaling	0.0026	0.0004
Melatonin Signaling	0.0028	0.0016
Leukocyte Extravasation Signaling	0.0035	0.0005
Role of NFAT in Cardiac Hypertrophy	0.0037	0.0044
PPARα/RXRα Activation	0.0051	0.0023
B Cell Receptor Signaling	0.0058	0.0025
Fc Epsilon RI Signaling	0.0059	0.0095
Corticotropin Releasing Hormone Signaling	0.0063	0.0009
Synaptic Long Term Potentiation	0.0063	0.0033
Phospholipase C Signaling	0.0085	0.0014
AMPK Signaling	0.0098	-
Renin-Angiotensin Signaling	0.0050	-
RhoA Signaling	0.0020	-
Signaling by Rho Family GTPases	0.0081	-
Biotin-carboxyl Carrier Protein Assembly	-	0.0091
Cholecystokinin/Gastrin-mediated Signaling	-	0.0028
DNA Methylation and Transcriptional Repression Signaling	-	0.0060
Estrogen Receptor Signaling	-	0.0054
FAK Signaling	-	0.0083
GDP-glucose Biosynthesis	-	0.0091
Glioma Signaling	-	0.0062
Glucose and Glucose-1-phosphate Degradation	-	0.0091
Gα12/13 Signaling	-	0.0095
HGF Signaling	-	0.0011
Molecular Mechanisms of Cancer	-	0.0074
Natural Killer Cell Signaling	-	0.0083
Neuregulin Signaling	-	0.0034
PI3K/AKT Signaling	-	0.0041
PPAR Signaling	-	0.0024
Prostate Cancer Signaling	-	0.0091
Protein Kinase A Signaling	-	0.0093
PTEN Signaling	-	0.0085
RAR Activation	-	0.0068
Role of IL-17F in Allergic Inflammatory Airway Diseases	-	0.0093
Sertoli Cell-Sertoli Cell Junction Signaling	-	0.0060
Thrombopoietin Signaling	-	0.0039

Table 4.7 Most highly enriched canonical pathways using shared quantified phosphoproteins in thrombin- and LPA-induced platelet monocyte aggregate (PMA) formation. Analysis was performed using Ingenuity Pathway analysis, only pathways with $p < 0.01$ were shown.

Ingenuity Canonical Pathways	p value
ERK/MAPK Signaling	4.3652E-05
Fcγ Receptor-mediated Phagocytosis in Macrophages and Monocytes	0.0001
Insulin Receptor Signaling	0.0001
Leukocyte Extravasation Signaling	0.0002
FLT3 Signaling in Hematopoietic Progenitor Cells	0.0010
Rac Signaling	0.0010
Neuregulin Signaling	0.0022
PI3K/AKT Signaling	0.0029
Hypoxia Signaling in the Cardiovascular System	0.0038
Fc Epsilon RI Signaling	0.0048
Synaptic Long Term Potentiation	0.0050
Nitric Oxide Signaling in the Cardiovascular System	0.0087
PPAR Signaling	0.0087
Prostate Cancer Signaling	0.0091

4.3.3.3 Bioinformatics analysis of all regulated phosphorylation events

After normalizing the ratio changes of the phosphopeptides based on the ratios obtained in the normalization control sample, the average ratios of all phosphopeptides were determined. Average SILAC ratio increased by 3.8% and 5.3% for thrombin- and LPA-induced PMA formation, respectively (Figure 4.10). Only those phosphopeptides with a magnitude of 1.46- and

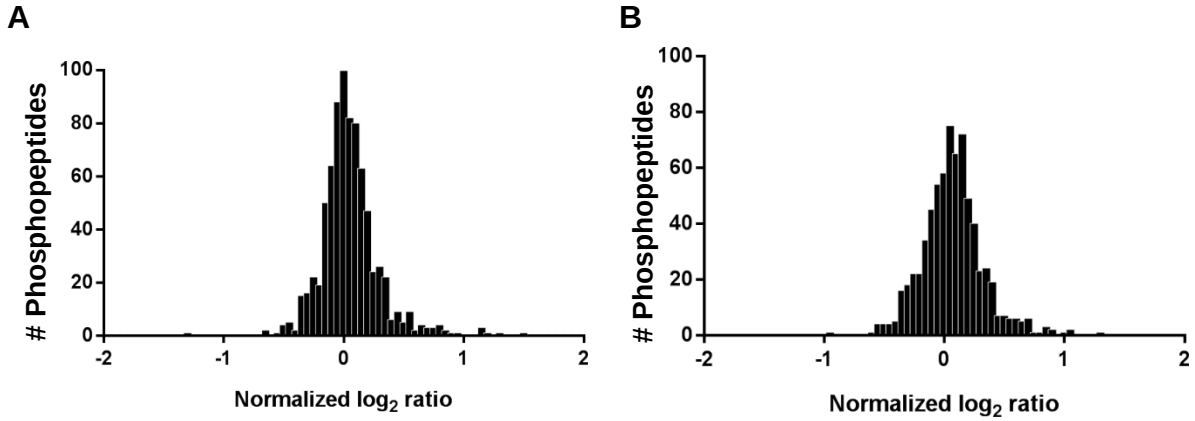

Figure 4.10 Histograms of log_2-transformed SILAC ratios for all quantified phosphopeptides in (A) thrombin- and (B) LPA-induced PMA formation. The SILAC ratios were normalized based on the average ratio in the normalization control sample.

1.5-fold change (either up or down) were considered regulated, representing 95% confidence interval cutoff for thrombin- and LPA-induced PMA formation, respectively. Using these cutoffs, 42 phosphopeptides (corresponding to 35 phosphoproteins) and 30 phosphopeptides (corresponding to 25 phosphoproteins) were found to be regulated in thrombin- and LPA-induced PMA formation, respectively (Figure 4.11). Of all the regulated phosphorylation sites, the ratio of serine, threonine and tyrosine was 90.3%: 8.1%: 1.6%, which was similar to the distribution of all the identified phosphorylation sites in these samples.

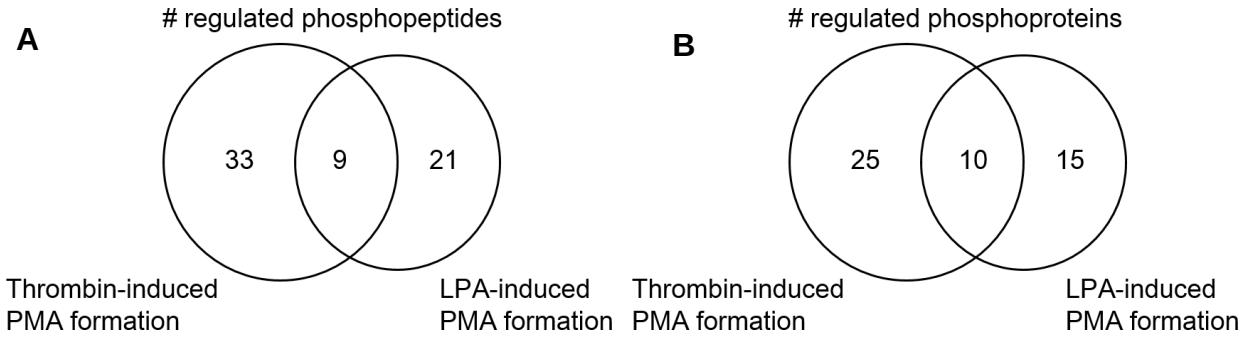

Figure 4.11 Number of regulated (A) phosphopeptides and (B) phosphoproteins shared in thrombin- and LPA-induced platelet-monocyte aggregate (PMA) formation.

In order to identify the key biological processes that were impacted by thrombin- and LPA-induced PMA formation only, the regulated phosphoproteins were analyzed using DAVID functional annotation tool. Here, DAVID functional annotation tool was used to identify regulated biological processess. In contrast, Ingenuity Pathway Analysis was employed earlier to map canonical pathways. As a result, leukocyte activation and leukocyte-mediated immunity were involved in thrombin-induced PMA formation; in contrast, only RNA-related processes were found in LPA-induced PMA formation (Table 4.8).

A number of the regulated phosphoproteins were manually selected because they were known to be involved in leukocyte activation, cytoskeleton organization and small GTPase activation

(Table 4.9). These included regulators for different small GTPases, i.e. guanine nucleotide exchange factor for Rac1 (ARHGEF6 [420]), Rab35 (DENND1A [421]), Rho and Rac (DOCK5 [422]), as well as GTPase-activating protein for Rab (TBC1D5 [423]), Rap1 and Rap2 (SIPA1 [424]), Rho (MYO9B [425]) and Rab3 (RAB3GAP1 [426]). In addition, phosphorylation of mediators for cytoskeleton reorganization, i.e. stathmin [427], formin-binding protein 1 [428], formin-like protein 1 [429], CapZ-interacting protein [430] and unconventional myosin-IXb [425], were also regulated. Moreover, phosphorylation events were also regulated on proteins mediating leukocyte function, which included Rap1-integrin-mediated adhesion (RIAM [431]), migration (STK10 [432]), cytokine production (MAP3K7 / Transforming growth factor-beta-activated kinase 1 [433]) and leukocyte activation (PRAM1 [434], L-plastin [435] and LSP1 [436]). Unfortunately, phosphor-Akt levels could not be assessed because no phosphopeptides from Akt were identified in either thrombin- or LPA-PMA formation.

Table 4.8 Most highly enriched Gene ontology (GO) terms in thrombin- and LPA-induced platelet monocyte aggregate (PMA) formation. Gene enrichment analysis was performed using DAVID functional annotation tool, only terms with $p < 0.01$ were shown.

Thrombin-induced PMA formation	p value
regulation of leukocyte activation	0.00756
regulation of cell activation	0.00873
regulation of leukocyte mediated immunity	0.00965

LPA-induced PMA formation	p value
nucleic acid transport	0.00073
establishment of RNA localization	0.00073
RNA transport	0.00073
RNA localization	0.00080
nucleobase, nucleoside, nucleotide and nucleic acid transport	0.00114

Table 4.9 Regulated phosphorylation sites that were involved in thrombin- and LPA-induced Platelet-monocyte aggregate (PMA) formation. Ratios are expressed as average fold change ± s.d., * denotes ambiguous phosphorylation sites, i.e. with class II or III localization probability. Phosphorylation sites were not considered regulated, i.e. changes less than 1.5 fold, were shown in grey.

Uniprot ID	Gene name	Protein name	Function	Thrombin-induced PMA formation		LPA-induced PMA formation	
				Phosphosite	Ratio	Phosphosite	Ratio
Leukocyte activation							
Q96QH2	PRAM1	PML-RARA-regulated adapter molecule 1	May be involved in integrin signaling in neutrophils	Ser48	2.33 ± 0.28		
						Ser484	1.75 ± 0.14
O14617	AP3D1	AP-3 complex subunit delta-1	Facilitate budding of vesicles from the Golgi membrane	Ser658	2.23 ± 0.56	Ser658	1.85 ± 0.48
Q0VD83	APOBR	Apolipoprotein B receptor	Macrophage receptor, could be involved in foam cell formation	Ser175	1.84 ± 0.29	Ser175	1.65 ± 0.42
O94804	STK10	Serine/threonine-protein kinase 10	Regulate lymphocyte migration	Ser454	1.61 ± 0.59	Ser454	1.12 ± 0.06
O43318	MAP3K7	Mitogen-activated protein kinase kinase kinase 7	Mediate various cytokines including interleukin-1	Ser389	1.51 ± 0.34	Ser389	1.38 ± 0.23
P41162	ETV3	ETS translocation variant 3	Contribute to growth arrest during terminal macrophage differentiation	Ser245, Ser250	1.26 ± 0.12	Ser245, Ser250	1.78 ± 0.05
P13796	LCP1	Plastin-2	Actin-binding protein. Plays a role in the activation of T-cells			Ser5	1.85 ± 0.43
Q7Z5R6	RIAM	Rap1-GTP-interacting adapter molecule	Mediate Rap1-induced adhesion.	Ser526	1.66 ± 0.02		
O75995	SASH3	SAM and SH3 domain-containing protein 3	May function as a signaling adapter protein in lymphocytes	Ser38	1.54 ± 0.20		
Q16539	MAPK14	Mitogen-activated protein kinase 14	Essential component of the MAPK pathway	Tyr182	1.46 ± 0.09		
P33241	LSP1	Lymphocyte-specific protein 1	May mediate neutrophil activation and chemotaxis	Ser204	0.42 ± 0.00		
Cytoskeleton organization							
P16949	STMN1	Stathmin	Regulation of the microtubule filament system	Ser25	2.42 ± 0.61	Ser25	2.11 ± 0.98
				Ser16	1.70 ± 0.43	Ser16	1.33 ± 0.22
Q13884	SNTB1	Beta-1-syntrophin	May link various receptors to the actin cytoskeleton	Ser225	2.53 ± 0.27	Ser225	2.06 ± 0.70
				Ser87	1.67 ± 0.08	Ser87	1.01 ± 0.05
O95466	FMNL1	Formin-like protein 1	Regulate cell morphology and cytoskeletal organization	Ser184	0.67 ± 0.09	Ser184	0.67 ± 0.38
Q6JBY9	RCSD1	CapZ-interacting protein	Remodel actin filament assembly	Ser83	0.99 ± 0.04	Ser83	0.51 ± 0.11
Q13459	MYO9B	Unconventional myosin-IXb	Remodel actin cytoskeleton and Rho activity			Ser1405	0.66 ± 0.09
Q96RU3	FNBP1	Formin-binding protein 1	Coordinate membrane tubulation	Ser497	1.75 ± 0.06		
Q9NXR1	NDE1	Nuclear distribution protein nudE homolog 1	Centrosome duplication and formation	Ser306	1.58 ± 0.18		
Small GTPase activity							
Q15042	RAB3GAP1	Rab3 GTPase-activating protein catalytic subunit	Regulate Rab3 activity	Ser537	1.88 ± 0.29	Ser537	1.81 ± 0.56
Q9H7D0	DOCK5	Dedicator of cytokinesis protein 5	Regulate Rho and Rac activity	Ser1789	1.99 ± 0.02	Ser1789	2.46 ± 1.22
Q13370	PDE3B	cGMP-inhibited 3',5'-cyclic phosphodiesterase B	Regulate cAMP binding of RAPGEF3	Ser442	1.72 ± 0.04	Ser442	1.57 ± 0.42
Q8TEH3	DENND1A	DENN domain-containing protein 1A	Regulate Rab35 activity	Ser520	1.63 ± 0.30	Ser520	1.40 ± 0.01
Q92609	TBC1D5	TBC1 domain family member 5	Regulate Rab activity	Ser44	1.57 ± 0.15	Ser44	1.14 ± 0.04
Q96FS4	SIPA1	Signal-induced proliferation-associated protein 1	Regulate Rap1 and Rap2 activity	Ser839*	1.71 ± 0.00	Ser839	1.22 ± 0.37
				Ser837*	1.81 ± 0.17		
Q15052	ARHGEF6	Rho guanine nucleotide exchange factor 6	Regulate Rac1 activity	Ser684	1.94 ± 0.11	Ser684	1.21 ± 0.18
Q7Z6P3	RAB44	Ras-related protein Rab-44	Small GTPase involves is protein transport	Ser263	1.51 ± 0.07	Ser263	1.11 ± 0.08

Uniprot ID	Gene name	Protein name	Function	Thrombin-induced PMA formation		LPA-induced PMA formation	
				Phosphosite	Ratio	Phosphosite	Ratio
RNA processing							
Q09161	NCBP1	Nuclear cap-binding protein subunit 1	Involve in translation regulation	Ser22	1.50 ± 0.15	Ser22	1.63 ± 0.52
Q9UKV3	ACIN1	Apoptotic chromatin condensation inducer in the nucleus	Regulate RNA transcription	Ser710	1.81 ± 0.04	Ser710	1.37 ± 0.41
Q13263	TRIM28	Transcription intermediary factor 1-beta	Regulate RNA transcription	Thr541	1.82 ± 0.18	Thr541	1.44 ± 0.69
O94913	PCF11	Pre-mRNA cleavage complex 2 protein Pcf11	Involve in mRNA processing	Ser494	1.07 ± 0.03	Ser494	1.51 ± 0.07
Q9UKL3	CASP8AP2	CASP8-associated protein 2	Regulate Transcription	Ser875	1.08 ± 0.16	Ser875	1.64 ± 0.23
Q9UQ35	SRRM2	Serine/arginine repetitive matrix protein 2	Involve in mRNA processing			Ser2102	1.59 ± 0.14
						Thr2104	1.51 ± 0.15
P51003	PAPOLA	Poly(A) polymerase alpha	Involve in mRNA processing			Ser24	1.61 ± 0.21
Q7Z5L9	IRF2BP2	Interferon regulatory factor 2-binding protein 2	Regulate Transcription			Ser240	1.65 ± 0.29
Q96T58	SPEN	Msx2-interacting protein	Regulate Transcription			Ser1222	1.51 ± 0.09
Q9NVR2	INTS10	Integrator complex subunit 10	Regulate RNA transcription	Ser231	1.48 ± 0.10		
Q04637	EIF4G1	Eukaryotic translation initiation factor 4 gamma 1	Recognition of the mRNA cap	Ser1231	1.51 ± 0.00		
Others							
P12270	TPR	Nucleoprotein TPR	Trafficking across the nuclear envelope	Ser2155	1.80 ± 0.48	Ser2155	1.51 ± 0.46
Q53EL6	PDCD4	Programmed cell death protein 4	Inhibit translation initiation	Ser457	1.39 ± 0.18	Ser457	1.53 ± 0.10
Q4G0F5	VPS26B	Vacuolar protein sorting-associated protein 26B	Protein transport	Ser302*	1.59 ± 0.31	Ser302	1.23 ± 0.10
				Ser304*	1.57 ± 0.35	Ser304	1.15 ± 0.15
Q96B97	SH3KBP1	SH3 domain-containing kinase-binding protein 1	Regulate of endocytosis and lysosomal degradation	Ser587	0.65 ± 0.13	Ser587	0.82 ± 0.29
Q9UBC2	EPS15L1	Epidermal growth factor receptor substrate 15-like 1	Regulate endocytosis	Ser229	1.51 ± 0.07	Ser229	1.27 ± 0.50
Q9NWW5	CLN6	Ceroid-lipofuscinosis neuronal protein 6	Regulate proteolysis	Ser31	1.18 ± 0.05	Ser31	1.53 ± 0.25
Q6NXT4	SLC30A6	Zinc transporter 6	Zinc-efflux transporter	Ser382*	1.54 ± 0.28		
O95249	GOSR1	Golgi SNAP receptor complex member 1	Protein transport	Ser230	1.50 ± 0.02		
Q8TEM1	NUP210	Nuclear pore membrane glycoprotein 210	Nuclear pore assembly and fusion			Ser1874	1.66 ± 0.51
Q99700	ATXN2	Ataxin-2	Involve in EGFR trafficking			Thr771	1.54 ± 0.27
O75592	MYCBP2	E3 ubiquitin-protein ligase MYCBP2	Mediate ubiquitination			Ser3467	1.63 ± 0.21
Q5UIP0	RIF1	Telomere-associated protein RIF1	Mediate cell cycle progression			Ser1421	1.98 ± 0.30
Q9HAW4	CLSPN	Claspin	Mediate cell cycle progression			Ser1289	1.55 ± 0.28
Q15418	RPS6KA1	Ribosomal protein S6 kinase alpha-1	Downstream of ERK (MAPK1/ERK2 and MAPK3/ERK1) signaling	Ser380	2.25 ± 1.11		
Q9Y6G9	DYNC1LI1	Cytoplasmic dynein 1 light intermediate chain 1	Involve in mitosis	Ser516	1.49 ± 0.28		
				Thr515*	1.48 ± 0.24		
O75410	TACC1	Transforming acidic coiled-coil-containing protein 1	Likely promote cell division	Ser276	2.90 ± 1.22		

4.3.4 Phospho-Akt in platelet-monocyte aggregation using Western blotting

Akt phosphorylation was shown to be regulated in primary monocytes in response to co-incubation with activated platelets [412]. Since no phosphopeptides from Akt were identified in our thrombin- or LPA-PMA formation analyses, Western blotting was performed to investigate the phospho-Akt level changes in THP-1 cells in response to co-incubation with activated platelets. Platelets were stimulated with thrombin or LPA for 10 min in presence of 2.5 mM GPRP. Subsequently, activated platelets were incubated with THP-1 cells at 10 : 1 ratio for 10 min. After incubation, the cells were lysed using lysis condition#1, and the proteins from the cell lysates were separated using 12% SDS-PAGE and anti-phospho-Akt antibody was used to detect the phosphorylation level on Akt using Western blotting. This showed that treatment with resting or activated platelets did not result in an increase in phospho-Akt level (Figure 4.12).

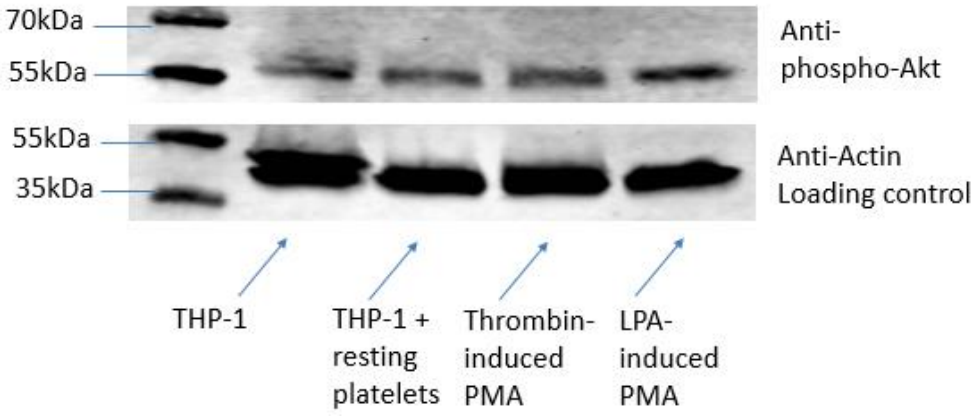

Figure 4.12 Phospho-Akt level changes in THP-1 cells in response to co-incubation with resting or activated platelets using Western blotting. PMA, platelet-monocyte aggregate.

4.3.5 Functional validation of platelet-monocyte aggregation

Phosphoproteomics analysis revealed that in response to co-incubation with activated platelets, phosphoproteins that were involved in leukocyte activation and adhesion were regulated in THP-1 cells. In order to validate this result, adhesion of THP-1 cells to fibronectin in response to co-incubation with activated platelets was tested. PMA formation was performed as described in section 4.3.4, then a calcein-AM dye was added to the cells and the mixtures were incubated on a fibronectin-coated plate. After incubation, non-adherent cells were removed and the adhesion ratio was calculated as fluorescence from adherent cells divided by total fluorescence from cells originally added. This demonstrated that incubation with resting platelets did not result in a significant increase in adhesion capability of THP-1 cells compared to THP-1 alone, whereas both thrombin- and LPA-induced PMA formation significantly increased adhesion of THP-1 cells to fibronectin (one-way ANOVA with Dunnett's test, $P<0.05$) in three biological replicates (Figure 4.13).

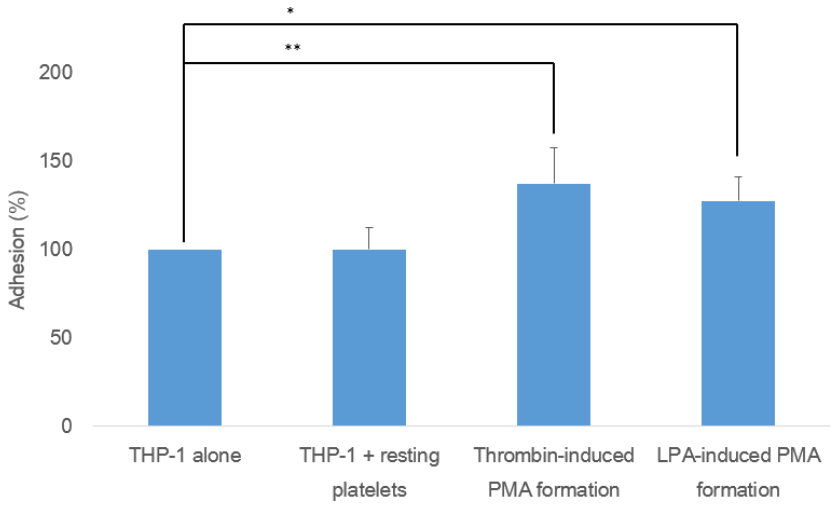

Figure 4.13 Both thrombin- and LPA-induced platelet-monocyte aggregate (PMA) formation significantly increased THP-1 cells adhesion to fibronectin. Adhesion (%) in THP-1 cells are reported relative to the control (THP-1 cells alone) which was normalized to 100%. Results are expressed as mean ± s.d., asterisk (*) indicates significance (one-way ANOVA with Dunnett's test, **p<0.01, *p<0.05; n = 3).

4.4 Discussion

Global phosphorylation events in THP-1 cells incubated with activated platelet were studied using the optimized phosphopeptide enrichment method, which is the first time signaling changes in such a two-cell system were systematically investigated. This was achieved by using the triple SILAC strategy. In order to distinguish proteins originated from platelets and monocytes, proteins from these two types of cells need to be differentially labeled before mixing. Therefore, chemical labeling, e.g. iTRAQ [196] or dimethyl labeling [437], on protein or peptide level after cell lysis is not feasible in this system; and the triple SILAC system served this purpose well, where platelet peptides from the light SILAC channel was effectively removed from interfering with quantification in medium- and heavy-labeled THP-1 cells.

Using this system, the results from the quantitative phosphoproteomics revealed key biological processes, i.e. leukocyte activation, cytoskeleton organization and small GTPase activation in THP-1 cells exposed to activated platelets. Moreover, a number of potential key phosphoproteins were identified, including RIAM, which mediates Rap1-induced adhesion [431]; SKT10 (LOK), which regulates lymphocyte migration [432]; MAP3K7, which is shown to mediate IL-1 production [433]; L-plastin, which plays a role T-cell activation [435] and LSP1, which may mediate neutrophil chemotaxis [436]. The function of these proteins was not well-defined in THP-1 cells, but they might also be involved in similar processes, and may be functionally relevant in the process of PMA formation. Moreover, in addition to the phosphoproteins that control cytoskeleton organziation, mediators for a variety of small GTPses, i.e. Rap, Rho, Rac, and Rab, were regulated, suggesting that multiple small GTPases were employed to regulate cytoskeleton organization, protein transport and/or integrin-mediated adhesion. This was validated using the adhesion assay, where both thrombin and LPA-induced PMA formation

significantly increased adhesion of THP-1 cells to fibronectin. These results provided a functional link between the phosphorylation signaling events and phenotypic changes in THP-1 cells in response to exposure to activated platelets.

A previous study in our lab showed that microparticles released from activated platelets also contained integrin receptors [438]. Binding of microparticles to THP-1 cells cannot be distinguished from intact platelets using the experimental set up in this study. Therefore PMA formation here refers to both intact platelet-monocyte binding and platelet microparticle-monocyte binding. In addition, platelet releasate, i.e. the soluble proteins and factors released by activated platelets, might also play a role in mediating THP-1 activation. As a result, protein phosphorylation events in THP-1 cells were regulated by a combination of these interactions. Moreover, an incubation time of ten minutes was chosen to allow PMA to form, using which both thrombin- and LPA-activated platelets incubated with THP-1 cells showed significant increase in PMA formation. The same condition was thus used for quantitative phosphoproteomics analysis to identify signaling pathways and key regulators. Earlier time points could be used to gain a further understanding of the initial signaling events and obtain a dynamic regulation profile of protein phosphorylation events. Akt phosphorylation level in THP-1 cells was not increased in response to exposure to activated platelets. In contrast, Akt phosphorylation level significantly increased in primary monocytes treated with thrombin-activated platelets [412]. Therefore, although THP-1 cells are considered a good model system for monocytes [439], differences exist between the cell line and primary cells and the results may need to be validated using primary cells.

Chapter 5 Conclusion and future work

The research presented in this thesis focuses on the characterization of protein-protein interaction and signaling pathways in platelets and in platelet-monocyte aggregate (PMA) formation to identify potential markers and signaling pathways, which would contribute to the development of intervention strategies for CVDs.

To achieve this, two novel proteomics tools have been developed: *in silico* protein interaction analysis (Chapter 2) and a quantitative multiplexed small GTPase activity assay (Chapter 3). The former tool is bioinformatics-based, and utilizes a series of filters to select those from the large number of proteomics datasets archived in the GPMDB that resemble a co-IP experiment targeting a protein of interest. Therefore, this tool can be considered as a "virtual IP", which was shown to be a valid and solid approach for identifying known and candidate protein interactions and proteins that share similar functions in a protein network. The latter tool is based on targeted proteomics: up to 12 active small GTPase isoforms can be precipitated simultaneously, and a MRM assay targeting these isoforms is used to quantify the relative activity changes. This approach has several advantages over Western blotting, the currently used detection method: multiplexing within a single sample, reliable quantification, and the ability to distinguish isoforms without the need to develop high quality antibodies. This approach is the first time a solution is presented to study activity of multiple small GTPases in parallel.

Using *in silico* protein interaction analysis, a core network involved in platelet aggregation has been identified that consists of integrin αIIb, integrin β3, talin1, fibrinogen alpha and gamma chain, Rap1b and many cytoskeletal proteins (Chapter 2), which represents a general view of the process in platelets in response to various agonists. This network expands our knowledge on the

protein interactions that occur during platelet aggregation, and these interacting partners could potentially be markers for platelet aggregation.

Using the quantitative multiplexed small GTPase activity assay, small GTPase activity changes in platelet activation induced by thrombin, ADP and LPA have been evaluated (Chapter 3). In addition, using PI3K inhibitors, only the activation levels of the small GTPases Rap1A and Rap1B are reduced without affecting other small GTPase isoforms in LPA-induced platelet activation. These results show that different small GTPases are involved in distinct pathways, and PI3K-Rap1 pathway is mainly involved in the process of LPA-induced platelet aggregation. Moreover, flow cytometry analysis has revealed that the small GTPase Rac and calcium are key regulators for LPA-induced platelet secretion, whereas PI3 kinase or the small GTPase Rho are not involved in this process.

In Chapter 4, quantitative phosphoproteomics for the first time has provided a systematic view of signaling changes in monocytes in response to incubation with activated platelets using a triple SILAC system, this has uncovered several key biological processes, including leukocyte activation, cytoskeleton organization and regulation of small GTPase activity. Functional validation has shown both thrombin and LPA activated platelets to induce the formation of platelet-monocyte aggregates, both of which significantly increase the adhesion of THP-1 cells to fibronectin.

Based on the findings in this thesis, a mechanism of how LPA induces platelet activation can be proposed (Figure 5.1), in which LPA binds to an unknown receptor on platelets, which triggers Rac and calcium-dependent P-selectin translocation and Rho – ROCK dependent platelet shape change. These lead to platelet secretion, including the release of the second wave agonist

ADP and coagulation factors. ADP in turn activates $P2Y_1$ and $P2Y_{12}$, which results in activation of the PI3K – Rap1b pathways. Activation of these pathways then leads to platelet aggregation.

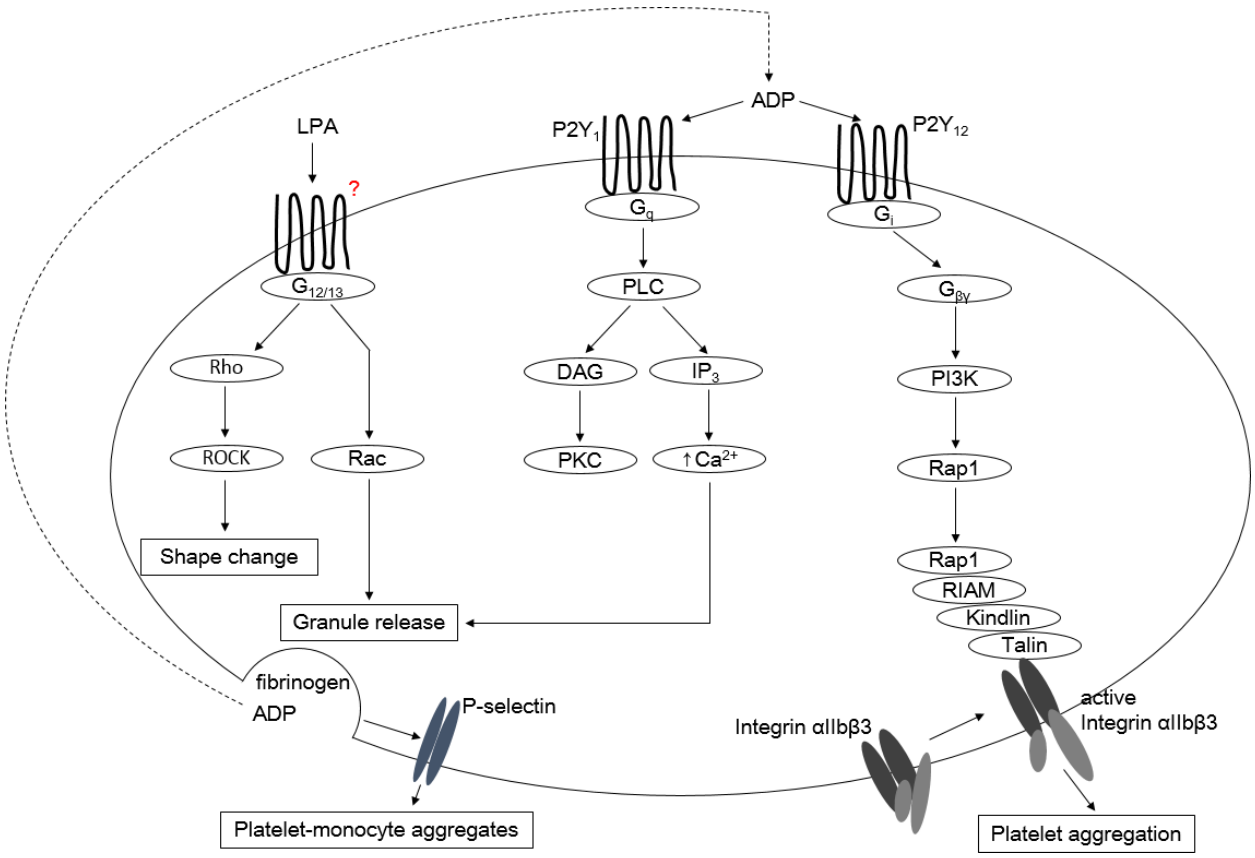

Figure 5.1 Proposed mechanism for LPA-induced platelet activation. LPA binds to an unknown receptor on platelets, which triggers Rac and calcium dependent platelet secretion, i.e. release of second wave agonist ADP, coagulation factor fibrinogen, and translocation of P-selectin. ADP in turn activates $P2Y_1$ and $P2Y_{12}$, which resulted in activation of NRas - MAPK as well as PI3K – Rap1b pathways. Both of these pathways contribute to platelet aggregation. ADP, Adenosine diphosphate; DAG, diacylglycerol; GDP, guanosine diphosphate; GTP, guanosine triphosphate; IP_3, Inositol triphosphate; $P2Y_1$, purinergic receptor $P2Y_1$; $P2Y_{12}$, purinergic receptor $P2Y_{12}$; PI3K, phosphoinositide 3-kinase; PKC, protein kinase C; PLC, phospholipase C; RIAM, Rap1-interacting adaptor molecule; ROCK, Rho-associated protein kinase. This illustration does not exclude additional receptors or pathways involved in platelet functions.

The work described in this thesis also contributes to the area of platelet-mediated CVDs, and the design of better intervention strategies. Platelet secretion and aggregation are two major events following agonist-stimulated platelet activation. Platelet aggregation has been a major process that is targeted when developing antiplatelet strategies [18], e.g. antagonists for integrin αIIbβ3. However, lack of integrin β3 has been shown to promote atherosclerosis in mice [440] and patients with Glanzmann thrombasthenia [441], suggesting that lack of platelet aggregation might not prevent the development of atherosclerosis. On the other hand, the increase of P-selectin levels on the platelet surface during platelet secretion promotes PMA formation, which might play an important role in the development of atherosclerosis. Interaction with activated platelets causes monocytes to become activated and more adhesive, which promotes the development of the atherosclerotic plaque. Therefore, antiplatelet therapies that target P-selectin/PSGL-1 binding, or pathways leading to P-selectin translocation in platelets, such as small GTPase Rac activation and calcium influx, might potentially be a better therapeutic option.

The results presented in this thesis on the signaling pathways in platelets and monocytes in the context of CVDs, as well as the use of the newly developed proteomics tools, open new avenues of research. Regarding the functional studies on platelets, a number of pathways that are involved in LPA-induced platelet activation have now been determined. However, the exact receptor(s) responsible for LPA binding to platelets are still not identified, partly due to the lack of potent inhibitors for individual suspected LPA receptors. Quantitative phosphoproteomics techniques that have been used in Chapter 4 to study PMA signaling can be modified and applied to also investigate the initial phosphorylation events in LPA-induced platelet activation, including the receptor level. To quantify the phosphorylation changes, proteins or peptides from platelets will need to be chemically labeled with strategies such as iTRAQ [196] or dimethyl

labeling [437], because platelets have little metabolic activity that is necessary for SILAC labeling.

Similarly, the quantitative multiplexed small GTPase activity assay developed and used to study platelet activation in Chapter 3 can be employed to investigate small GTPase activity changes in THP-1 cells incubated with activated platelets. The experimental design would be modified to use unlabeled platelets, medium SILAC labeled THP-1 cells and heavy isotope-labeled peptide internal standards. Since the results of our phosphoproteomics study suggest regulation of the activity levels of multiple small GTPases in THP-1 cells incubated with activated platelets, employing the targeted proteomics assay would not only validate the phosphoproteomics study, but also reveal how these small GTPase isoforms are regulated. Due to the fact that small GTPases in platelets would interfere with the ones in THP-1 cells in the two-cell system, such a study is not possible using traditional methods, such as Western blotting.

Moreover, the quantitative multiplexed small GTPase activity assay could be further expanded by employing additional well-characterized binding domains for other small GTPase isoforms, e.g. Arf, Ral and Rab. The throughput of this method could also be further improved by integrating in-solution digestion into the workflow. To achieve this, issues with sample loss when removing SDS, and contamination by binding domains and polymers would first need to be addressed. Furthermore, this method would also benefit from the development of more sensitive mass spectrometers, because more conditions could be monitored while consuming less material. Likewise, the number of the phosphopeptides and phosphorylation sites using the quantitative phosphoproteomics strategy could be increased with better instruments, and more time points and/or conditions such as inhibitor treatment could be monitored to gain a dynamic regulation profile of phosphorylation events. Using less material is an advantage in platelet

research, since other platelet preparation approaches could then be employed, e.g. gel-filtration of platelets [442], which would eliminate contaminating blood cells more effectively, but result in a lower platelet recovery rate.

Finally, our studies have used platelets obtained from healthy donors. Employing these approaches to platelets from patients with a particular CVD at different stages will reveal differences caused by the disease, and may help identify processes that could play a role in the development of CVDs.

In summary, the research in this thesis has furthered our understanding of platelet function in the context of cardiovascular disease, which might serve as a basis for designing more targeted approaches for antiplatelet therapies. In addition, the proteomics tools we have developed and validated now enable the exploration of new avenues of research, as demonstrated by their successful application to study biological systems.

Bibliography

1. *Global status report on noncommunicable disaeses 2010*, in *Geneva, World Health Organization*. 2011.
2. *Global atlas on cardiovascular disease prevention and control*, in *Geneva, World Health Organization*. 2011.
3. Mathers, C.D. and Loncar, D., *Projections of global mortality and burden of disease from 2002 to 2030.* PLoS Med, 2006. **3**(11): p. e442.
4. Ross, R., *The pathogenesis of atherosclerosis: a perspective for the 1990s.* Nature, 1993. **362**(6423): p. 801-809.
5. Hansson, G.K. and Hermansson, A., *The immune system in atherosclerosis.* Nat Immunol, 2011. **12**(3): p. 204-212.
6. Libby, P., Ridker, P.M., and Hansson, G.K., *Progress and challenges in translating the biology of atherosclerosis.* Nature, 2011. **473**(7347): p. 317-325.
7. McGill, H.C., McMahan, C.A., and Gidding, S.S., *Preventing Heart Disease in the 21st Century Implications of the Pathobiological Determinants of Atherosclerosis in Youth (PDAY) Study.* Circulation, 2008. **117**(9): p. 1216-1227.
8. Weber, C. and Noels, H., *Atherosclerosis: current pathogenesis and therapeutic options.* Nat Med, 2011. **17**(11): p. 1410-1422.
9. Davì, G. and Patrono, C., *Platelet activation and atherothrombosis.* N Engl J Med, 2007. **357**(24): p. 2482-2494.
10. Totani, L. and Evangelista, V., *Platelet–leukocyte interactions in cardiovascular disease and beyond.* Arterioscler Thromb Vasc Biol, 2010. **30**(12): p. 2357-2361.
11. Zarbock, A., Polanowska-Grabowska, R.K., and Ley, K., *Platelet-neutrophil-interactions: linking hemostasis and inflammation.* Blood Rev, 2007. **21**(2): p. 99-111.
12. Li, N., *Platelet–lymphocyte cross-talk.* J Leukoc Biol, 2008. **83**(5): p. 1069-1078.
13. Woollard, K.J. and Geissmann, F., *Monocytes in atherosclerosis: subsets and functions.* Nat Rev Cardiol, 2010. **7**(2): p. 77-86.
14. van Gils, J.M., Zwaginga, J.J., and Hordijk, P.L., *Molecular and functional interactions among monocytes, platelets, and endothelial cells and their relevance for cardiovascular diseases.* J Leukoc Biol, 2009. **85**(2): p. 195-204.
15. McCabe, D.J., Harrison, P., Mackie, I.J., Sidhu, P.S., Purdy, G., Lawrie, A.S., Watt, H., Brown, M.M., and Machin, S.J., *Platelet degranulation and monocyte–platelet complex formation are increased in the acute and convalescent phases after ischaemic stroke or transient ischaemic attack.* Br J Haematol, 2004. **125**(6): p. 777-787.
16. Furman, M.I., Benoit, S.E., Barnard, M.R., Valeri, C.R., Borbone, M.L., Becker, R.C., Hechtman, H.B., and Michelson, A.D., *Increased platelet reactivity and circulating monocyte-platelet aggregates in patients with stable coronary artery disease.* J Am Coll Cardiol, 1998. **31**(2): p. 352-358.
17. Nomura, S., Kanazawa, S., and Fukuhara, S., *Effects of efonidipine on platelet and monocyte activation markers in hypertensive patients with and without type 2 diabetes mellitus.* J Hum Hypertens, 2002. **16**(8): p. 539-547.

18. Michelson, A.D., *Antiplatelet therapies for the treatment of cardiovascular disease.* Nat Rev Drug Discov, 2010. **9**(2): p. 154-169.
19. Siess, W., *Athero-and thrombogenic actions of lysophosphatidic acid and sphingosine-1-phosphate.* Biochim Biophys Acta, 2002. **1582**(1-3): p. 204-215.
20. Siess, W., Zangl, K.J., Essler, M., Bauer, M., Brandl, R., Corrinth, C., Bittman, R., Tigyi, G., and Aepfelbacher, M., *Lysophosphatidic acid mediates the rapid activation of platelets and endothelial cells by mildly oxidized low density lipoprotein and accumulates in human atherosclerotic lesions.* Proc Natl Acad Sci U S A, 1999. **96**(12): p. 6931-6936.
21. Zhou, Z., Subramanian, P., Sevilmis, G., Globke, B., Soehnlein, O., Karshovska, E., Megens, R., Heyll, K., Chun, J., Saulnier-Blache, J.S., Reinholz, M., van Zandvoort, M., Weber, C., and Schober, A., *Lipoprotein-derived lysophosphatidic acid promotes atherosclerosis by releasing CXCL1 from the endothelium.* Cell Metab, 2011. **13**(5): p. 592-600.
22. Haserück, N., Erl, W., Pandey, D., Tigyi, G., Ohlmann, P., Ravanat, C., Gachet, C., and Siess, W., *The plaque lipid lysophosphatidic acid stimulates platelet activation and platelet-monocyte aggregate formation in whole blood: involvement of P2Y1 and P2Y12 receptors.* Blood, 2004. **103**(7): p. 2585-2592.
23. Moolenaar, W.H., *Lysophosphatidic acid, a multifunctional phospholipid messenger.* J Biol Chem, 1995. **270**(22): p. 12949-12952.
24. Goetzl, E.J. and An, S., *Diversity of cellular receptors and functions for the lysophospholipid growth factors lysophosphatidic acid and sphingosine 1-phosphate.* FASEB J, 1998. **12**(15): p. 1589-1598.
25. Michelson, A.D., *Platelets.* Academic Press, 2013. **3rd edition**.
26. Italiano, J.E. and Shivdasani, R.A., *Megakaryocytes and beyond: the birth of platelets.* J Thromb Haemost., 2003. **1**(6): p. 1174-1182.
27. Healy, A.M., Pickard, M.D., Pradhan, A.D., Wang, Y., Chen, Z., Croce, K., Sakuma, M., Shi, C., Zago, A.C., and Garasic, J., *Platelet expression profiling and clinical validation of myeloid-related protein-14 as a novel determinant of cardiovascular events.* Circulation, 2006. **113**(19): p. 2278-2284.
28. Leeksma, C.H.W. and Cohen, J.A., *Determination of the life of human blood platelets using labelled diisopropylfluorophosphonate.* Nature, 1955. **175**: p. 552-553.
29. Semple, J.W., Italiano, J.E., and Freedman, J., *Platelets and the immune continuum.* Nat Rev Immunol, 2011. **11**(4): p. 264-274.
30. Ross, R., *Atherosclerosis—an inflammatory disease.* N Engl J Med. , 1999. **340**(2): p. 115-126.
31. Langer, H.F. and Gawaz, M., *Platelet-vessel wall interactions in atherosclerotic disease.* Thromb Haemost., 2008. **99**(3): p. 480-486.
32. Davì, G. and Patrono, C., *Platelet activation and atherothrombosis.* N Engl J Med. , 2007. **357**(24): p. 2482-2494.
33. Lindemann, S., Tolley, N.D., Dixon, D.A., McIntyre, T.M., Prescott, S.M., Zimmerman, G.A., and Weyrich, A.S., *Activated platelets mediate inflammatory signaling by regulated interleukin 1β synthesis.* J Cell Biol., 2001. **154**(3): p. 485-490.
34. Jin, R.C., Voetsch, B., and Loscalzo, J., *Endogenous mechanisms of inhibition of platelet function.* Microcirculation, 2005. **12**(3): p. 247-258.

35. Radomski, M.W., Palmer, R.M.J., and Moncada, S., *Endogenous nitric oxide inhibits human platelet adhesion to vascular endothelium.* Lancet., 1987. **330**(8567): p. 1057-1058.
36. Tateson, J.E., Moncada, S., and Vane, J.R., *Effects of prostacyclin (PGX) on cyclic AMP concentrations in human platelets.* Prostaglandins, 1977. **13**(3): p. 389-397.
37. Marcus, A.J., Safier, L.B., Hajjar, K.A., Ullman, H.L., Islam, N., Broekman, M.J., and Eiroa, A.M., *Inhibition of platelet function by an aspirin-insensitive endothelial cell ADPase. Thromboregulation by endothelial cells.* J Clin Invest. , 1991. **88**(5): p. 1690-1696.
38. Ikeda, Y., Handa, M., Kawano, K., Kamata, T., Murata, M., Araki, Y., Anbo, H., Kawai, Y., Watanabe, K., and Itagaki, I., *The role of von Willebrand factor and fibrinogen in platelet aggregation under varying shear stress.* J Clin Invest., 1991. **87**(4): p. 1234-1240.
39. Kroll, M.H., Harris, T.S., Moake, J.L., Handin, R.I., and Schafer, A.I., *von Willebrand factor binding to platelet GpIb initiates signals for platelet activation.* J Clin Invest., 1991. **88**(5): p. 1568-1573.
40. Nieswandt, B. and Watson, S.P., *Platelet-collagen interaction: is GPVI the central receptor?* Blood, 2003. **102**(2): p. 449-461.
41. Offermanns, S., *Activation of platelet function through G protein–coupled receptors.* Circ Res., 2006. **99**(12): p. 1293-1304.
42. Offermanns, S., Toombs, C.F., Hu, Y.H., and Simon, M.I., *Defective platelet activation in G alpha(q)-deficient mice.* Nature, 1997. **389**(6647): p. 183-186.
43. Shattil, S.J. and Brass, L.F., *Induction of the fibrinogen receptor on human platelets by intracellular mediators.* J Biol Chem, 1987. **262**(3): p. 992-1000.
44. Walker, T.R. and Watson, S.P., *Synergy between Ca2+ and protein kinase C is the major factor in determining the level of secretion from human platelets.* Biochem J, 1993. **289**(Pt 1): p. 277-282.
45. D.E., C. and J., N.E., *G protein beta gamma subunits.* Annu Rev Pharmacol Toxicol, 1997. **37**: p. 167-203.
46. Cantley, L.C., *The phosphoinositide 3-kinase pathway.* Science, 2002. **296**(5573): p. 1655-1657.
47. Hart, M.J., Jiang, X., Kozasa, T., Roscoe, W., Singer, W.D., Gilman, A.G., Sternweis, P.C., and Bollag, G., *Direct stimulation of the guanine nucleotide exchange activity of p115 RhoGEF by Galpha13.* Science, 1998. **280**(5372): p. 2112-2114.
48. Fukuhara, S., Chikumi, H., and Gutkind, J.S., *RGS-containing RhoGEFs: the missing link between transforming G proteins and Rho?* Oncogene, 2001. **20**(13): p. 1661-1668.
49. Cattaneo, M., Canciani, M.T., Lecchi, A., Kinlough-Rathbone, R.L., Packham, M.A., Mannucci, P.M., and Mustard, J.F., *Released adenosine diphosphate stabilizes thrombin-induced human platelet aggregates.* Blood, 1990. **75**(5): p. 1081-1086.
50. Cattaneo, M., Akkawat, B., Kinlough-Rathbone, R.L., Packham, M.A., Cimminiello, C., and Mannucci, P.M., *Ticlopidine facilitates the deaggregation of human platelets aggregated by thrombin.* Thromb Haemost, 1994. **71**(1): p. 91-94.
51. Trumel, C., Payrastre, B., Plantavid, M., Hechler, B., Viala, C., Presek, P., Martinson, E.A., Cazenave, J.-P., Chap, H., and Gachet, C., *A key role of adenosine diphosphate in the irreversible platelet aggregation induced by the PAR1-activating peptide through the late activation of phosphoinositide 3-kinase.* Blood, 1999. **94**(12): p. 4156-4165.

52. Léon, C., Hechler, B., Vial, C., Leray, C., Cazenave, J.P., and Gachet, C., *The P2Y1 receptor is an ADP receptor antagonized by ATP and expressed in platelets and megakaryoblastic cells.* FEBS Lett, 1997. **403**(1): p. 26-30.
53. Daniel, J.L., Dangelmaier, C., Jin, J., Ashby, B., Smith, J.B., and Kunapuli, S.P., *Molecular basis for ADP-induced platelet activation I. Evidence for three distinct ADP receptors on human platelets.* J Biol Chem, 1998. **273**(4): p. 2024-2029.
54. Jin, J., Daniel, J.L., and Kunapuli, S.P., *Molecular basis for ADP-induced platelet activation II. The P2Y1 receptor mediates ADP-induced intracellular calcium mobilization and shape change in platelets.* J Biol Chem, 1998. **273**(4): p. 2030-2034.
55. Hollopeter, G., Jantzen, H.-M., Vincent, D., Li, G., England, L., Ramakrishnan, V., Yang, R.-B., Nurden, P., Nurden, A., Julius, D., and Conley, P.B., *Identification of the platelet ADP receptor targeted by antithrombotic drugs.* Nature, 2001. **409**(6817): p. 202-207.
56. Soulet, C., Hechler, B., GRATACAP, M.P., Plantavid, M., Offermanns, S., Gachet, C., and Payrastre, B., *A differential role of the platelet ADP receptors P2Y1 and P2Y12 in Rac activation.* J Thromb Haemost, 2005. **3**(10): p. 2296-2306.
57. Savi, P., Zachayus, J.-L., Delesque-Touchard, N., Labouret, C., Hervé, C., Uzabiaga, M.-F., Pereillo, J.-M., Culouscou, J.-M., Bono, F., Ferrara, P., and Herbert, J.M., *The active metabolite of Clopidogrel disrupts P2Y12 receptor oligomers and partitions them out of lipid rafts.* Proc Natl Acad Sci U S A, 2006. **103**(29): p. 11069-11074.
58. Ohlmann, P., Laugwitz, K., Nurnberg, B., Spicher, K., Schultz, G., Cazenave, J., and Gachet, C., *The human platelet ADP receptor activates Gi2 proteins.* Biochem J, 1995. **312**(Pt 3): p. 775-779.
59. Gratacap, M.-P., Hérault, J.-P., Viala, C., Ragab, A., Savi, P., Herbert, J.-M., Chap, H., Plantavid, M., and Payrastre, B., *FcγRIIA requires a Gi-dependent pathway for an efficient stimulation of phosphoinositide 3-kinase, calcium mobilization, and platelet aggregation.* Blood, 2000. **96**(10): p. 3439-3446.
60. Hirsch, E., Bosco, O., Tropel, P., Laffargue, M., Calvez, R., Altruda, F., WYMANN, M., and Montrucchio, G., *Resistance to thromboembolism in PI3Kγ-deficient mice.* FASEB J, 2001. **15**(11): p. 2019-2021.
61. Canobbio, I., Stefanini, L., Cipolla, L., Ciraolo, E., Gruppi, C., Balduini, C., Hirsch, E., and Torti, M., *Genetic evidence for a predominant role of PI3Kbeta catalytic activity in ITAM- and integrin-mediated signaling in platelets.* Blood, 2009. **114**(10): p. 2193-2196.
62. Jantzen, H.M., Milstone, D.S., Gousset, L., Conley, P.B., and Mortensen, R.M., *Impaired activation of murine platelets lacking G alpha(i2).* J Clin Invest, 2001. **108**(3): p. 477-483.
63. Kauffenstein, G., Bergmeier, W., Eckly, A., Ohlmann, P., Leon, C., Cazenave, J., Nieswandt, B., and Gachet, C., *The P2Y(12) receptor induces platelet aggregation through weak activation of the alpha(IIb)beta(3) integrin--a phosphoinositide 3-kinase-dependent mechanism.* FEBS Lett, 2001. **505**(2): p. 281-290.
64. Kamae, T., Shiraga, M., Kashiwagi, H., Kato, H., Tadokoro, S., Kurata, Y., Tomiyama, Y., and Kanakura, Y., *Critical role of ADP interaction with P2Y12 receptor in the maintenance of alpha(IIb)beta3 activation: association with Rap1B activation.* J Thromb Haemost, 2006. **4**(6): p. 1379-1387.
65. Dorsam, R.T. and Kunapuli, S.P., *Central role of the P2Y12 receptor in platelet activation.* J Clin Invest, 2004. **113**(3): p. 340-345.

66. Mann, K.G., Butenas, S., and Brummel, K., *The dynamics of thrombin formation.* Arterioscler Thromb Vasc Biol, 2003. **23**(1): p. 17-25.
67. Heemskerk, J.W., Bevers, E.M., and Lindhout, T., *Platelet activation and blood coagulation.* Thromb Haemost, 2002. **88**(2): p. 186-194.
68. Coughlin, S.R., *Thrombin signalling and protease-activated receptors.* Nature, 2000. **407**(6801): p. 258-264.
69. Kahn, M.L., Zheng, Y.-W., Huang, W., Bigornia, V., Zeng, D., Moff, S., Farese, R.V., Tam, C., and Coughlin, S.R., *A dual thrombin receptor system for platelet activation.* Nature, 1998. **394**(6694): p. 690-694.
70. Vu, T.-K.H., Hung, D.T., Wheaton, V.I., and Coughlin, S.R., *Molecular cloning of a functional thrombin receptor reveals a novel proteolytic mechanism of receptor activation.* Cell, 1991. **64**(6): p. 1057-1068.
71. Coughlin, S.R., *Protease‐activated receptors in hemostasis, thrombosis and vascular biology.* J Thromb Haemost, 2005. **3**(8): p. 1800-1814.
72. Russo, A., Soh, U.J., and Trejo, J., *Proteases display biased agonism at protease-activated receptors: location matters!* Mol Interv, 2009. **9**(2): p. 87-96.
73. Covic, L., Gresser, A.L., and Kuliopulos, A., *Biphasic kinetics of activation and signaling for PAR1 and PAR4 thrombin receptors in platelets.* Biochemistry, 2000. **39**(18): p. 5458-5467.
74. Klages, B., Brandt, U., Simon, M.I., Schultz, G., and Offermanns, S., *Activation of G12/G13 results in shape change and Rho/Rho-kinase–mediated myosin light chain phosphorylation in mouse platelets.* J Cell Biol, 1999. **144**(4): p. 745-754.
75. Wu, C.C., Wu, S.Y., Liao, C.Y., Teng, C.M., Wu, Y.C., and Kuo, S.C., *The roles and mechanisms of PAR4 and P2Y12/phosphatidylinositol 3‐kinase pathway in maintaining thrombin‐induced platelet aggregation.* Br J Pharmacol, 2010. **161**(3): p. 643-658.
76. Covic, L., Singh, C., Smith, H., and Kuliopulos, A., *Role of the PAR4 thrombin receptor in stabilizing platelet-platelet aggregates as revealed by a patient with Hermansky-Pudlak syndrome.* Thromb Haemost, 2002. **87**(4): p. 722-727.
77. Rother, E., Brandl, R., Baker, D.L., Goyal, P., Gebhard, H., Tigyi, G., and Siess, W., *Subtype-selective antagonists of lysophosphatidic acid receptors inhibit platelet activation triggered by the lipid core of atherosclerotic plaques.* Circulation, 2003. **108**(6): p. 741-747.
78. Smyth, S.S., Cheng, H.-Y., Miriyala, S., Panchatcharam, M., and Morris, A.J., *Roles of lysophosphatidic acid in cardiovascular physiology and disease.* Biochim Biophys Acta, 2008. **1781**(9): p. 563-570.
79. Eichholtz, T., Jalink, K., Fahrenfort, I., and Moolenaar, W.H., *The bioactive phospholipid lysophosphatidic acid is released from activated platelets.* Biochem J, 1993. **291**(Pt 3): p. 677-680.
80. Simon, M.-F., Chap, H., and Douste-Blazy, L., *Human platelet aggregation induced by 1-alkyl-lysophosphatidic acid and its analogs: a new group of phospholipid mediators?* Biochem Biophys Res Commun, 1982. **108**(4): p. 1743-1750.
81. Tokumura, A., Sinomiya, J., Kishimoto, S., Tanaka, T., Kogure, K., Sugiura, T., Satouchi, K., Waku, K., and Fukuzawa, K., *Human platelets respond differentially to*

lysophosphatidic acids having a highly unsaturated fatty acyl group and alkyl ether-linked lysophosphatidic acids. Biochem J, 2002. **365**(Pt 3): p. 617-628.
82. Choi, J.W., Herr, D.R., Noguchi, K., Yung, Y.C., Lee, C.-W., Mutoh, T., Lin, M.-E., Teo, S.T., Park, K.E., Mosley, A.N., and Chun, J., *LPA receptors: subtypes and biological actions.* Annu Rev Pharmacol Toxicol, 2010. **50**: p. 157-186.
83. Kihara, Y., Maceyka, M., Spiegel, S., and Chun, J., *Lysophospholipid receptor nomenclature review: IUPHAR Review 8.* Br J Pharmacol, 2014. **Epub ahead of print**.
84. Chun, J., Hla, T., Lynch, K.R., Spiegel, S., and Moolenaar, W.H., *International union of basic and clinical pharmacology. LXXVIII. Lysophospholipid receptor nomenclature.* Pharmacol Rev, 2010. **62**(4): p. 579-587.
85. Ishii, S., Noguchi, K., and Yanagida, K., *Non-Edg family lysophosphatidic acid (LPA) receptors.* Prostaglandins Other Lipid Mediat, 2009. **89**(3-4): p. 57-65.
86. Tabata, K.-i., Baba, K., Shiraishi, A., Ito, M., and Fujita, N., *The orphan GPCR GPR87 was deorphanized and shown to be a lysophosphatidic acid receptor.* Biochem Biophys Res Commun, 2007. **363**(3): p. 861-866.
87. Murakami, M., Shiraishi, A., Tabata, K., and Fujita, N., *Identification of the orphan GPCR, P2Y(10) receptor as the sphingosine-1-phosphate and lysophosphatidic acid receptor.* Biochem Biophys Res Commun, 2008. **371**(4): p. 707-712.
88. Oka, S., Ota, R., Shima, M., Yamashita, A., and Sugiura, T., *GPR35 is a novel lysophosphatidic acid receptor.* Biochem Biophys Res Commun, 2010. **395**(2): p. 232-237.
89. McIntyre, T.M., Pontsler, A.V., Silva, A.R., Hilaire, A.S., Xu, Y., Hinshaw, J.C., Zimmerman, G.A., Hama, K., Aoki, J., Arai, H., and Prestwich, G.D., *Identification of an intracellular receptor for lysophosphatidic acid (LPA): LPA is a transcellular PPARγ agonist.* Proc Natl Acad Sci U S A, 2003. **100**(1): p. 131-136.
90. Khandoga, A., Khandoga, A., Fujiwara, Y., Goyal, P., Pandey, D., Tsukahara, R., Bolen, A., Guo, H., Wilke, N., Liu, J., Valentine, W.J., Durgam, G.G., Miller, D.D., Jiang, G., Prestwich, G.D., Tigyi, G., and Siess, W., *Lysophosphatidic acid-induced platelet shape change revealed through LPA1-5 receptor-selective probes and albumin.* Platelets, 2008. **19**(6): p. 415-427.
91. Hooks, S.B., Santos, W.L., Im, D.-S., Heise, C.E., Macdonald, T.L., and Lynch, K.R., *Lysophosphatidic acid-induced mitogenesis is regulated by lipid phosphate phosphatases and is Edg-receptor independent.* J Biol Chem, 2001. **276**(7): p. 4611-4621.
92. Gueguen, G., Gaigé, B., Grévy, J.-M., Rogalle, P., Bellan, J., Wilson, M., Klaébé, A., Pont, F., Simon, M.-F., and Chap, H., *Structure-activity analysis of the effects of lysophosphatidic acid on platelet aggregation.* Biochemistry, 1999. **38**(26): p. 8440-8450.
93. Retzer, M. and Essler, M., *Lysophosphatidic acid-induced platelet shape change proceeds via Rho/Rho kinase-mediated myosin light-chain and moesin phosphorylation.* Cell Signal, 2000. **12**(9-10): p. 645-648.
94. Pamuklar, Z., Lee, J.S., Cheng, H.-Y., Panchatcharam, M., Steinhubl, S., Morris, A.J., Charnigo, R., and Smyth, S.S., *Individual heterogeneity in platelet response to lysophosphatidic acid: evidence for a novel inhibitory pathway.* Arterioscler Thromb Vasc Biol, 2008. **28**(3): p. 555-561.

95. Schumacher, K., Classen, H., and Späth, M., *Platelet aggregation evoked in vitro and in vivo by phosphatidic acids and lysoderivatives: identity with substances in aged serum (DAS).* Thromb Haemost, 1979. **42**(2): p. 631-640.
96. Tokumura, A., Fukuzawa, K., Isobe, J., and Tsukatani, H., *Lysophosphatidic acid-induced aggregation of human and feline platelets: structure-activity relationship.* Biochem Biophys Res Commun, 1981. **99**(2): p. 391-398.
97. Pamuklar, Z., Federico, L., Liu, S., Umezu-Goto, M., Dong, A., Panchatcharam, M., Fulerson, Z., Berdyshev, E., Natarajan, V., Fang, X., van Meeteren, L.A., Moolenaar, W.H., Mills, G.B., Morris, A.J., and Smyth, S.S., *Autotaxin/lysopholipase D and lysophosphatidic acid regulate murine hemostasis and thrombosis.* J Biol Chem, 2009. **284**(11): p. 7385-7394.
98. Escolar, G. and White, J.G., *The platelet open canalicular system: a final common pathway.* Blood cells, 1991. **17**(3): p. 467-485.
99. Frojmovic, M., Wong, T., and White, J.G., *Platelet plasma membrane is equally distributed between surface and osmotically-evaginable surface-connecting membrane, independent of size, subpopulation or species.* Nouv Rev Fr Hematol, 1992. **34**(1): p. 99-110.
100. Flaumenhaft, R., Dilks, J.R., Rozenvayn, N., Monahan-Earley, R.A., Feng, D., and Dvorak, A.M., *The actin cytoskeleton differentially regulates platelet α-granule and dense-granule secretion.* Blood, 2005. **105**(10): p. 3879-3887.
101. Woronowicz, K., Dilks, J.R., Rozenvayn, N., Dowal, L., Blair, P.S., Peters, C.G., Woronowicz, L., and Flaumenhaft, R., *The platelet actin cytoskeleton associates with SNAREs and participates in alpha-granule secretion.* Biochemistry, 2010. **49**(21): p. 4533-4542.
102. Suzuki, Y., Yamamoto, M., Wada, H., Ito, M., Nakano, T., Sasaki, Y., Narumiya, S., Shiku, H., and Nishikawa, M., *Agonist-induced regulation of myosin phosphatase activity in human platelets through activation of Rho-kinase.* Blood, 1999. **93**(10): p. 3408-3417.
103. Watanabe, Y., Ito, M., Kataoka, Y., Wada, H., Koyama, M., Feng, J., Shiku, H., and Nishikawa, M., *Protein kinase C–catalyzed phosphorylation of an inhibitory phosphoprotein of myosin phosphatase is involved in human platelet secretion.* Blood, 2001. **97**(12): p. 3798-3805.
104. Nishikawa, M., Tanaka, T., and Hidaka, H., *Ca2+-calmodulin-dependent phosphorylation and platelet secretion.* Nature, 1980. **287**(5785): p. 863-865.
105. Paul, B.Z., Daniel, J.L., and Kunapuli, S.P., *Platelet shape change is mediated by both calcium-dependent and-independent signaling pathways Role of p160 Rho-associated coiled-coil-containing protein kinase in platelet shape change.* J Biol Chem, 1999. **274**(40): p. 28293-28300.
106. Riondino, S., Gazzaniga, P.P., and Pulcinelli, F.M., *Convulxin induces platelet shape change through myosin light chain kinase and Rho kinase.* Eur J Biochem, 2002. **269**(23): p. 5878-5884.
107. Akbar, H., Kim, J., Funk, K., Cancelas, J., Shang, X., Chen, L., Johnson, J., Williams, D., and Zheng, Y., *Genetic and pharmacologic evidence that Rac1 GTPase is involved in regulation of platelet secretion and aggregation.* J Thromb Haemost, 2007. **5**(8): p. 1747-1755.

108. Dwivedi, S., Pandey, D., Khandoga, A.L., Brandl, R., and Siess, W., *Rac1-mediated signaling plays a central role in secretion-dependent platelet aggregation in human blood stimulated by atherosclerotic plaque.* J Transl Med, 2010. **8**: p. 128.
109. Gilio, K., Harper, M.T., Cosemans, J.M., Konopatskaya, O., Munnix, I.C., Prinzen, L., Leitges, M., Liu, Q., Molkentin, J.D., Heemskerk, J.W., and Poole, A.W., *Functional divergence of platelet protein kinase C (PKC) isoforms in thrombus formation on collagen.* J Biol Chem, 2010. **285**(30): p. 23410-23419.
110. Nagy, B.J., Bhavaraju, K., Getz, T., Bynagari, Y., Kim, S., and Kunapuli, S., *Impaired activation of platelets lacking protein kinase C-theta isoform.* Blood, 2009. **113**(11): p. 2557-2567.
111. R, C., T, G., Jr, N.B., K, B., Y, M., S, B.Y., S, M., K, N., and P., K.S., *Protein kinase C[delta] differentially regulates platelet functional responses.* Arterioscler Thromb Vasc Biol, 2009. **29**(5): p. 699-705.
112. Coppinger, J.A., Cagney, G., Toomey, S., Kislinger, T., Belton, O., McRedmond, J.P., Cahill, D.J., Emili, A., Fitzgerald, D.J., and Maguire, P.B., *Characterization of the proteins released from activated platelets leads to localization of novel platelet proteins in human atherosclerotic lesions.* Blood, 2004. **103**(6): p. 2096-2104.
113. Maynard, D.M., Heijnen, H.F., Horne, M.K., White, J.G., and Gahl, W.A., *Proteomic analysis of platelet α-granules using mass spectrometry.* J Thromb Haemost, 2007. **5**(9): p. 1945-1955.
114. Berger, G., Masse, J.M., and Cramer, E.M., *Alpha-granule membrane mirrors the platelet plasma membrane and contains the glycoproteins Ib, IX, and V.* Blood, 1996. **87**(4): p. 1385-1395.
115. Smyth, S.S., Reis, E.D., Zhang, W., Fallon, J.T., Gordon, R.E., and Coller, B.S., *Beta(3)-integrin-deficient mice but not P-selectin-deficient mice develop intimal hyperplasia after vascular injury: correlation with leukocyte recruitment to adherent platelets 1 hour after injury.* Circulation, 2001. **103**(20): p. 2501-2507.
116. Fernandes, L.S., Conde, I.D., Wayne Smith, C., Kansas, G.S., Snapp, K.R., Bennet, N., Ballantyne, C., McIntire, L.V., O'Brian Smith, E., Klem, J.A., Mathew, S., Frangogiannis, N., Turner, N.A., Maresh, K.J., and Kleiman, N.S., *Platelet-monocyte complex formation: effect of blocking PSGL-1 alone, and in combination with alphaIIbbeta3 and alphaMbeta2, in coronary stenting.* Thromb Res, 2003. **111**(3): p. 171-177.
117. Holmsen, H. and Weiss, H.J., *Secretable storage pools in platelets.* Annu Rev Med, 1979. **30**(1): p. 119-134.
118. Benveniste, J., Henson, P.M., and Cochrane, C.G., *Leukocyte-dependent histamine release from rabbit platelets. The role of IgE, basophils, and a platelet-activating factor.* J Exp Med, 1972. **136**(6): p. 1356-1377.
119. Maurer-Spurej, E. and Devine, D.V., *Platelet aggregation is not initiated by platelet shape change.* Lab Invest, 2001. **81**(11): p. 1517-1525.
120. Savage, B., Cattaneo, M., and Ruggeri, Z.M., *Mechanisms of platelet aggregation.* Curr Opin Hematol, 2001. **8**(5): p. 270-276.
121. Coller, B.S., Peerschke, E.I., Scudder, L.E., and Sullivan, C., *A murine monoclonal antibody that completely blocks the binding of fibrinogen to platelets produces a thrombasthenic-like state in normal platelets and binds to glycoproteins IIb and/or IIIa.* J Clin Invest, 1983. **72**(1): p. 325-338.

122. Bhatt, D.L. and Topol, E.J., *Current role of platelet glycoprotein IIb/IIIa inhibitors in acute coronary syndromes.* JAMA, 2000. **284**(12): p. 1549-1558.
123. Lischke, S. and Schneider, D.J., *Recent developments in the use of antiplatelet agents to prevent cardiovascular events.* Future Cardiol, 2011. **7**(3): p. 403-413.
124. Niiya, K., Hodson, E., Bader, R., Byers-Ward, V., Koziol, J.A., Plow, E.F., and Ruggeri, Z.M., *Increased surface expression of the membrane glycoprotein IIb/IIIa complex induced by platelet activation. Relationship to the binding of fibrinogen and platelet aggregation.* Blood, 1987. **70**(2): p. 475-483.
125. Wagner, C.L., Mascelli, M.A., Neblock, D.S., Weisman, H.F., Coller, B.S., and Jordan, R.E., *Analysis of GPIIb/IIIa receptor number by quantification of 7E3 binding to human platelets.* Blood, 1996. **88**(3): p. 907-914.
126. Woods, V.L., Wolff, L.E., and Keller, D.M., *Resting platelets contain a substantial centrally located pool of glycoprotein IIb-IIIa complex which may be accessible to some but not other extracellular proteins.* J Biol Chem, 1986. **261**(32): p. 15242-15251.
127. Wencel-Drake, J.D., Plow, E.F., Kunicki, T.J., Woods, V.L., Keller, D.M., and Ginsberg, M.H., *Localization of internal pools of membrane glycoproteins involved in platelet adhesive responses.* Am J Pathol, 1986. **124**(2): p. 324-334.
128. Kawasaki, H., Springett, G.M., Toki, S., Canales, J.J., Harlan, P., Blumenstiel, J.P., Chen, E.J., Bany, I.A., Mochizuki, N., Ashbacher, A., Matsuda, M., Housman, D.E., and Graybiel, A.M., *A Rap guanine nucleotide exchange factor enriched highly in the basal ganglia.* Proc Natl Acad Sci U S A, 1998. **95**(22): p. 13278-13283.
129. Stefanini, L., Roden, R.C., and Bergmeier, W., *CalDAG-GEFI is at the nexus of calcium-dependent platelet activation.* Blood, 2009. **114**(12): p. 2506-2514.
130. Crittenden, J.R., Bergmeier, W., Zhang, Y., Piffath, C.L., Liang, Y., Wagner, D.D., Housman, D.E., and Graybiel, A.M., *CalDAG-GEFI integrates signaling for platelet aggregation and thrombus formation.* Nat Med, 2004. **10**(9): p. 982-986.
131. Chrzanowska-Wodnicka, M., Smyth, S.S., Schoenwaelder, S.M., Fischer, T.H., and White, G.C.n., *Rap1b is required for normal platelet function and hemostasis in mice.* J Clin Invest, 2005. **115**(3): p. 680-687.
132. Chen, J., De, S., Damron, D.S., Chen, W.S., Hay, N., and Byzova, T.V., *Impaired platelet responses to thrombin and collagen in AKT-1–deficient mice.* Blood, 2004. **104**(6): p. 1703-1710.
133. Woulfe, D., Jiang, H., Mortensen, R., Yang, J., and Brass, L.F., *Activation of Rap1B by Gi family members in platelets.* J Biol Chem, 2002. **277**(26): p. 23382-23390.
134. Lee, H.-S., Lim, C.J., Puzon-McLaughlin, W., Shattil, S.J., and Ginsberg, M.H., *RIAM activates integrins by linking talin to ras GTPase membrane-targeting sequences.* J Biol Chem, 2009. **284**(8): p. 5119-5127.
135. Ma, Y.-Q., Yang, J., Pesho, M.M., Vinogradova, O., Qin, J., and Plow, E.F., *Regulation of integrin αIIbβ3 activation by distinct regions of its cytoplasmic tails.* Biochemistry, 2006. **45**(21): p. 6656-6662.
136. Moser, M., Nieswandt, B., Ussar, S., Pozgajova, M., and Fässler, R., *Kindlin-3 is essential for integrin activation and platelet aggregation.* Nat Med, 2008. **14**(3): p. 325-330.
137. Shattil, S.J., Kim, C., and Ginsberg, M.H., *The final steps of integrin activation: the end game.* Nat Rev Mol Cell Biol, 2010. **11**(4): p. 288-300.
138. Moser, M., Legate, K.R., Zent, R., and Fässler, R., *The tail of integrins, talin, and kindlins.* Science, 2009. **324**(5929): p. 895-899.

139. MA, Y.Q., Qin, J., and Plow, E.F., *Platelet integrin alpha(IIb)beta(3): activation mechanisms.* J Thromb Haemost, 2007. **5**(7): p. 1345-1352.
140. Liu, S., Calderwood, D.A., and Ginsberg, M.H., *Integrin cytoplasmic domain-binding proteins.* J Cell Sci, 2000. **113**(Pt 20): p. 3563-3571.
141. Ahn, K.C., Jun, A.J., Pawar, P., Jadhav, S., Napier, S., McCarty, O.J., and Konstantopoulos, K., *Preferential binding of platelets to monocytes over neutrophils under flow.* Biochem Biophys Res Commun, 2005. **329**(1): p. 345-355.
142. Michelson, A.D., Barnard, M.R., Krueger, L.A., Valeri, C.R., and Furman, M.I., *Circulating monocyte-platelet aggregates are a more sensitive marker of in vivo platelet activation than platelet surface P-selectin studies in baboons, human coronary intervention, and human acute myocardial infarction.* Circulation, 2001. **104**(13): p. 1533-1537.
143. McEver, R.P. and Martin, M.N., *A monoclonal antibody to a membrane glycoprotein binds only to activated platelets.* J Biol Chem, 1984. **259**(15): p. 9799-9804.
144. Coller, B.S., Peerschke, E.I., Scudder, L.E., and Sullivan, C.A., *Studies with a murine monoclonal antibody that abolishes ristocetin-induced binding of von Willebrand factor to platelets: additional evidence in support of GPIb as a platelet receptor for von Willebrand factor.* Blood, 1983. **61**(1): p. 99-110.
145. da Costa Martins, P.A., van Gils, J.M., Mol, A., Hordijk, P.L., and Zwaginga, J.J., *Platelet binding to monocytes increases the adhesive properties of monocytes by up-regulating the expression and functionality of β1 and β2 integrins.* J Leukoc Biol, 2006. **79**(3): p. 499-507.
146. Huo, Y., Schober, A., Forlow, S.B., Smith, D.F., Hyman, M.C., Jung, S., Littman, D.R., Weber, C., and Ley, K., *Circulating activated platelets exacerbate atherosclerosis in mice deficient in apolipoprotein E.* Nat Med, 2003. **9**(1): p. 61-67.
147. Blann, A.D., Lip, G.Y., Beevers, D.G., and McCollum, C.N., *Soluble P-selectin in atherosclerosis: a comparison with endothelial cell and platelet markers.* Thromb Haemost, 1997. **77**(6): p. 1077-1080.
148. Ruf, A. and Patscheke, H., *Flow cytometric detection of activated platelets: comparison of determining shape change, fibrinogen binding, and P-selectin expression.* Semin Thromb Hemost, 1995. **21**(2): p. 146-151.
149. Berger, G., Hartwell, D.W., and Wagner, D.D., *P-Selectin and platelet clearance.* Blood, 1998. **92**(11): p. 4446-4452.
150. Michelson, A.D., Barnard, M.R., Hechtman, H.B., MacGregor, H., Connolly, R.J., Loscalzo, J., and Valeri, C.R., *In vivo tracking of platelets: circulating degranulated platelets rapidly lose surface P-selectin but continue to circulate and function.* Proc Natl Acad Sci U S A, 1996. **93**(21): p. 11877-11882.
151. van Gils, J.M., da Costa Martins, P.A., Mol, A., Hordijk, P.L., and Zwaginga, J.J., *Transendothelial migration drives dissociation of plateletmonocyte complexes.* Thromb Haemost, 2008. **100**(2): p. 271-279.
152. Smith, J.B. and Willis, A.L., *Aspirin selectively inhibits prostaglandin production in human platelets.* Nat New Biol, 1971. **231**(25): p. 235-237.
153. Anderson, N.L. and Anderson, N.G., *Proteome and proteomics: new technologies, new concepts, and new words.* Electrophoresis, 1998. **19**(11): p. 1853-1861.
154. Blackstock, W.P. and Weir, M.P., *Proteomics: quantitative and physical mapping of cellular proteins.* Trends Biotechnol, 1999. **17**(3): p. 121-127.

155. Cravatt, B.F., Simon, G.M., and Yates, J.R.r., *The biological impact of mass-spectrometry-based proteomics.* Nature, 2007. **450**(7172): p. 991-1000.
156. Domon, B. and Aebersold, R., *Mass spectrometry and protein analysis.* Science, 2006. **312**(5771): p. 212-217.
157. Hager, J.W., *A new linear ion trap mass spectrometer.* Rapid Commun Mass Spectrom, 2002. **16**(6): p. 512-540.
158. Lange, V., Picotti, P., Domon, B., and Aebersold, R., *Selected reaction monitoring for quantitative proteomics: a tutorial.* Mol Syst Biol, 2008. **4**: p. 222.
159. Marshall, A.G., Hendrickson, C.L., and Jackson, G.S., *Fourier transform ion cyclotron resonance mass spectrometry: a primer.* Mass Spectrom Rev, 1998. **17**(1): p. 1–35.
160. Senko, M.W., Hendrickson, C.L., Emmett, M.R., Shi, S.D.H., and Marshall, A.G., *External accumulation of ions for enhanced electrospray ionization Fourier transform ion cyclotron resonance mass spectrometry.* J Am Soc Mass Spectrom, 1997. **8**(9): p. 970-976.
161. Hardman, M. and Makarov, A.A., *Interfacing the orbitrap mass analyzer to an electrospray ion source.* Anal Chem, 2003. **75**(7): p. 1699-1705.
162. Hu, Q., Noll, R.J., Li, H., Makarov, A., Hardman, M., and Graham Cooks, R., *The Orbitrap: a new mass spectrometer.* J Mass Spectrom, 2005. **40**(4): p. 430-443.
163. Aebersold, R. and Mann, M., *Mass spectrometry-based proteomics.* Nature, 2003. **422**(6928): p. 198-207.
164. Fenn, J.B., Mann, M., Meng, C.K., Wong, S.F., and Whitehouse, C.M., *Electrospray ionization for mass spectrometry of large biomolecules.* Science, 1989. **246**(4926): p. 64-71.
165. Karas, M. and Hillenkamp, F., *Laser desorption ionization of proteins with molecular masses exceeding 10,000 daltons.* Anal Chem, 1988. **60**(20): p. 2299-2301.
166. Steen, H. and Mann, M., *The ABC's (and XYZ's) of peptide sequencing.* Nat Rev Mol Cell Biol, 2004. **5**(9): p. 699-711.
167. Wells, J.M. and McLuckey, S.A., *Collision-induced dissociation (CID) of peptides and proteins.* Methods Enzymol, 2005. **402**: p. 148-185.
168. McLafferty, F.W., Horn, D.M., Breuker, K., Ge, Y., Lewis, M.A., Cerda, B., Zubarev, R.A., and Carpenter, B.K., *Electron capture dissociation of gaseous multiply charged ions by Fourier-transform ion cyclotron resonance.* J Am Soc Mass Spectrom, 2001. **12**(3): p. 245-249.
169. Syka, J.E.P., Coon, J.J., Schroeder, M.J., Shabanowitz, J., and Hunt, D.F., *Peptide and protein sequence analysis by electron transfer dissociation mass spectrometry.* Proc Natl Acad Sci U S A, 2004. **101**(26): p. 9528-9533.
170. Mikesh, L.M., Ueberheide, B., Chi, A., Coon, J.J., Syka, J.E.P., Shabanowitz, J., and Hunt, D.F., *The utility of ETD mass spectrometry in proteomic analysis.* Biochim Biophys Acta, 2006. **1764**(12): p. 1811-1822.
171. Eng, J.K., McCormack, A.L., and Yates, J.R., *An approach to correlate tandem mass spectral data of peptides with amino acid sequences in a protein database.* J Am Soc Mass Spectrom, 1994. **5**(11): p. 976-989.
172. Perkins, D.N., Pappin, D.J.C., Creasy, D.M., and Cottrell, J.S., *Probability-based protein identification by searching sequence databases using mass spectrometry data.* Electrophoresis, 1999. **20**(18): p. 3551-3567.

173. Clauser, K.R., Baker, P., and Burlingame, A.L., *Role of accurate mass measurement (+/- 10 ppm) in protein identification strategies employing MS or MS/MS and database searching.* Anal Chem, 1999. **71**(14): p. 2871-2882.
174. Craig, R. and Beavis, R.C., *TANDEM: matching proteins with tandem mass spectra.* Bioinformatics, 2004. **20**(9): p. 1466-1467.
175. Geer, L.Y., Markey, S.P., Kowalak, J.A., Wagner, L., Xu, M., Maynard, D.M., Yang, X., Shi, W., and Bryant, S.H., *Open mass spectrometry search algorithm.* J Proteome Res, 2004. **3**(5): p. 958-964.
176. Nesvizhskii, A.I., Vitek, O., and Aebersold, R., *Analysis and validation of proteomic data generated by tandem mass spectrometry.* Nat Methods, 2007. **4**(10): p. 787-797.
177. Sze, S.K., Ge, Y., Oh, H.B., and McLafferty, F.W., *Top-down mass spectrometry of a 29-kDa protein for characterization of any posttranslational modification to within one residue.* Proc Natl Acad Sci U S A, 2002. **99**(4): p. 1774-1779.
178. Han, X., Jin, M., Breuker, K., and McLafferty, F.W., *Extending top-down mass spectrometry to proteins with masses greater than 200 kilodaltons.* Science, 2006. **314**(5796): p. 109-112.
179. Chait, B.T., *Mass Spectrometry: Bottom-Up or Top-Down?* Science, 2006. **314**(5796): p. 65-66.
180. Siuti, N. and Kelleher, N.L., *Decoding protein modifications using top-down mass spectrometry.* Nat Methods, 2007. **4**(10): p. 817-821.
181. Bantscheff, M., Schirle, M., Sweetman, G., Rick, J., and Kuster, B., *Quantitative mass spectrometry in proteomics: a critical review.* Anal Bioanal Chem, 2007. **389**(4): p. 1017-1031.
182. Ong, S.E. and Mann, M., *Mass spectrometry–based proteomics turns quantitative.* Nat Chem Biol, 2005. **1**(5): p. 252-262.
183. Ishihama, Y., Oda, Y., Tabata, T., Sato, T., Nagasu, T., Rappsilber, J., and Mann, M., *Exponentially modified protein abundance index (emPAI) for estimation of absolute protein amount in proteomics by the number of sequenced peptides per protein.* Mol Cell Proteomics, 2005. **4**(9): p. 1265-1272.
184. Rappsilber, J., Ryder, U., Lamond, A.I., and Mann, M., *Large-scale proteomic analysis of the human spliceosome.* Genome Res, 2002. **12**(8): p. 1231-1245.
185. Ong, S.E., Blagoev, B., Kratchmarova, I., Kristensen, D.B., Steen, H., Pandey, A., and Mann, M., *Stable isotope labeling by amino acids in cell culture, SILAC, as a simple and accurate approach to expression proteomics.* Mol Cell Proteomics, 2002. **1**(5): p. 376-386.
186. Gruhler, A., Olsen, J.V., Mohammed, S., Mortensen, P., Faergeman, N.J., Mann, M., and Jensen, O.N., *Quantitative phosphoproteomics applied to the yeast pheromone signaling pathway.* Mol Cell Proteomics, 2005. **4**(3): p. 310-327.
187. Mann, M., *Functional and quantitative proteomics using SILAC.* Nat Rev Mol Cell Biol, 2006. **7**(12): p. 952-958.
188. Olsen, J.V., Blagoev, B., Gnad, F., Macek, B., Kumar, C., Mortensen, P., and Mann, M., *Global, in vivo, and site-specific phosphorylation dynamics in signaling networks.* Cell, 2006. **127**(3): p. 635-648.
189. Park, K.S., Mohapatra, D.P., Misonou, H., and Trimmer, J.S., *Graded regulation of the Kv2. 1 potassium channel by variable phosphorylation.* Science, 2006. **313**(5789): p. 976-979.

190. Blagoev, B., Ong, S.E., Kratchmarova, I., and Mann, M., *Temporal analysis of phosphotyrosine-dependent signaling networks by quantitative proteomics.* Nat Biotechnol, 2004. **22**(9): p. 1139-1145.
191. Hinsby, A.M., Olsen, J.V., and Mann, M., *Tyrosine phosphoproteomics of fibroblast growth factor signaling: a role for insulin receptor substrate-4.* J Biol Chem, 2004. **279**(45): p. 46438-46447.
192. Harsha, H.C., Molina, H., and Pandey, A., *Quantitative proteomics using stable isotope labeling with amino acids in cell culture.* Nat Protoc, 2008. **3**(3): p. 505-516.
193. Krüger, M., Moser, M., Ussar, S., Thievessen, I., Luber, C.A., Forner, F., Schmidt, S., Zanivan, S., F ssler, R., and Mann, M., *SILAC mouse for quantitative proteomics uncovers kindlin-3 as an essential factor for red blood cell function.* Cell, 2008. **134**(2): p. 353-364.
194. Julka, S. and Regnier, F., *Quantification in proteomics through stable isotope coding: a review.* J Proteome Res, 2004. **3**(3): p. 350-363.
195. Gygi, S.P., Rist, B., Gerber, S.A., Turecek, F., Gelb, M.H., and Aebersold, R., *Quantitative analysis of complex protein mixtures using isotope-coded affinity tags.* Nat Biotechnol, 1999. **17**(10): p. 994-999.
196. Ross, P.L., Huang, Y.N., Marchese, J.N., Williamson, B., Parker, K., Hattan, S., Khainovski, N., Pillai, S., Dey, S., Daniels, S., Purkayastha, S., Juhasz, P., Martin, S., Bartlet-Jones, M., He, F., Jacobson, A., and Pappin, D.J., *Multiplexed protein quantitation in Saccharomyces cerevisiae using amine-reactive isobaric tagging reagents.* Mol Cell Proteomics, 2004. **3**(12): p. 1154-1169.
197. Schulze, W.X. and Mann, M., *A novel proteomic screen for peptide-protein interactions.* J Biol Chem, 2004. **279**(11): p. 10756-10764.
198. Han, D.K., Eng, J., Zhou, H., and Aebersold, R., *Quantitative profiling of differentiation-induced microsomal proteins using isotope-coded affinity tags and mass spectrometry.* Nat Biotechnol, 2001. **19**(10): p. 946-951.
199. Cox, J. and Mann, M., *MaxQuant enables high peptide identification rates, individualized p.p.b.-range mass accuracies and proteome-wide protein quantification.* Nat Biotechnol, 2008. **26**(12): p. 1367-1372.
200. MacCoss, M.J., Wu, C.C., Liu, H., Sadygov, R., and Yates, J.R.r., *A correlation algorithm for the automated quantitative analysis of shotgun proteomics data.* Anal Chem, 2003. **75**(24): p. 6912-6921.
201. Keller, A., Eng, J., Zhang, N., Li, X., and Aebersold, R., *A uniform proteomics MS/MS analysis platform utilizing open XML file formats.* Mol Syst Biol, 2005. **1**: p. 2005.0017.
202. Lin, W.T., Hung, W.N., Yian, Y.H., Wu, K.P., Han, C.L., Chen, Y.R., Chen, Y.J., Sung, T.Y., and Hsu, W.L., *Multi-Q: a fully automated tool for multiplexed protein quantitation.* J Proteome Res, 2006. **5**(9): p. 2328-2338.
203. Shadforth, I.P., Dunkley, T.P.J., Lilley, K.S., and Bessant, C., *i-Tracker: For quantitative proteomics using iTRAQ.* BMC Genomics, 2005. **6**(1): p. 145.
204. Sleno, L. and Emili, A., *Proteomic methods for drug target discovery.* Curr Opin Chem Biol, 2008. **12**(1): p. 46-54.
205. Veenstra, T.D., *Proteomic approaches in drug discovery.* Drug Discov Today: Technologies, 2006. **3**(4): p. 433-440.
206. Conrads, T.P., Hood, B.L., and Veenstra, T.D., *Sampling and analytical strategies for biomarker discovery using mass spectrometry.* Biotechniques, 2006. **40**(6): p. 799-805.

207. Carrette, O., Burkhard, P.R., Sanchez, J.C., and Hochstrasser, D.F., *State-of-the-art two-dimensional gel electrophoresis: a key tool of proteomics research.* Nat Protoc, 2006. **1**(2): p. 812-823.
208. Pietrogrande, M.C., Marchetti, N., Dondi, F., and Righetti, P.G., *Decoding 2D-PAGE complex maps: Relevance to proteomics.* J Chromatogr B Analyt Technol Biomed Life Sci, 2006. **833**(1): p. 51-62.
209. Campostrini, N., Areces, L.B., Rappsilber, J., Pietrogrande, M.C., Dondi, F., Pastorino, F., Ponzoni, M., and Righetti, P.G., *Spot overlapping in two-dimensional maps: a serious problem ignored for much too long.* Proteomics, 2004. **5**(9): p. 2385-2395.
210. Pietrogrande, M.C., Marchetti, N., Tosi, A., Dondi, F., and Righetti, P.G., *Decoding two-dimensional polyacrylamide gel electrophoresis complex maps by autocovariance function: a simplified approach useful for proteomics.* Electrophoresis, 2005. **26**(14): p. 2739-2748.
211. Alban, A., David, S.O., Bjorkesten, L., Andersson, C., Sloge, E., Lewis, S., and Currie, I., *A novel experimental design for comparative two-dimensional gel analysis: two-dimensional difference gel electrophoresis incorporating a pooled internal standard.* Proteomics, 2003. **3**(1): p. 36-44.
212. Calderwood, M.A., Venkatesan, K., Xing, L., Chase, M.R., Vazquez, A., Holthaus, A.M., Ewence, A.E., Li, N., Hirozane-Kishikawa, T., Hill, D.E., Vidal, M., Kieff, E., and Johannsen, E., *Epstein–Barr virus and virus human protein interaction maps.* Proc Natl Acad Sci U S A, 2007. **104**(18): p. 7606-7611.
213. Limviphuvadh, V., Tanaka, S., Goto, S., Ueda, K., and Kanehisa, M., *The commonality of protein interaction networks determined in neurodegenerative disorders (NDDs).* Bioinformatics, 2007. **23**(16): p. 2129-2138.
214. Lim, J., Hao, T., Shaw, C., Patel, A.J., Szabó, G., Rual, J.F., Fisk, C.J., Li, N., Smolyar, A., Hill, D.E., Barabási, A.L., Vidal, M., and Zoghbi, H.Y., *A protein–protein interaction network for human inherited ataxias and disorders of Purkinje cell degeneration.* Cell, 2006. **125**(4): p. 801-814.
215. Uetz, P., Dong, Y.A., Zeretzke, C., Atzler, C., Baiker, A., Berger, B., Rajagopala, S.V., Roupelieva, M., Rose, D., Fossum, E., and Haas, J., *Herpesviral protein networks and their interaction with the human proteome.* Science, 2006. **311**(5758): p. 239-242.
216. Schadt, E.E., Friend, S.H., and Shaywitz, D.A., *A network view of disease and compound screening.* Nat Rev Drug Discov, 2009. **8**(4): p. 286-295.
217. Köcher, T. and Superti-Furga, G., *Mass spectrometry-based functional proteomics: from molecular machines to protein networks.* Nat Methods, 2007. **4**(10): p. 807-815.
218. Ideker, T. and Sharan, R., *Protein networks in disease.* Genome Res, 2008. **18**(4): p. 644-652.
219. Figeys, D., *Mapping the human protein interactome.* Cell Res, 2008. **18**(7): p. 716-724.
220. Kast, J., *Making connections for life: an in vivo map of the yeast interactome.* HFSP J, 2008. **2**(5): p. 244-250.
221. Fields, S. and Song, O., *A novel genetic system to detect protein protein interactions.* Nature, 1989. **340**(6230): p. 245-246.
222. von Mering, C., Krause, R., Snel, B., Cornell, M., Oliver, S.G., Fields, S., and Bork, P., *Comparative assessment of large-scale data sets of protein-protein interactions.* Nature, 2002. **417**(6887): p. 399-403.

223. Cai, Y.D. and Chou, K.C., *Predicting 22 protein localizations in budding yeast.* Biochem Biophys Res Commun, 2004. **323**(2): p. 425-428.
224. Chou, K.C. and Cai, Y.D., *Predicting protein localization in budding yeast.* Bioinformatics, 2005. **21**(7): p. 944-950.
225. Chou, K.C. and Shen, H.B., *Euk-mPLoc: a fusion classifier for large-scale eukaryotic protein subcellular location prediction by incorporating multiple sites.* J Proteome Res, 2007. **6**(5): p. 1728-1734.
226. Suter, B., Kittanakom, S., and Stagljar, I., *Two-hybrid technologies in proteomics research.* Curr Opin Biotechnol, 2008. **19**(4): p. 316-323.
227. Vidal, M., Brachmann, R.K., Fattaey, A., Harlow, E., and Boeke, J.D., *Reverse two-hybrid and one-hybrid systems to detect dissociation of protein-protein and DNA-protein interactions.* Proc Natl Acad Sci U S A, 1996. **93**(19): p. 10315-10320.
228. Hirst, M., Ho, C., Sabourin, L., Rudnicki, M., Penn, L., and Sadowski, I., *A two-hybrid system for transactivator bait proteins.* Proc Natl Acad Sci U S A, 2001. **98**(15): p. 8726-8731.
229. Licitra, E.J. and Liu, J.O., *A three-hybrid system for detecting small ligand–protein receptor interactions.* Proc Natl Acad Sci U S A, 1996. **93**(23): p. 12817-12821.
230. Eyckerman, S., Verhee, A., Van der Heyden, J., Lemmens, I., Van Ostade, X., Vandekerckhove, J., and Tavernier, J., *Design and application of a cytokine-receptor-based interaction trap.* Nat Cell Biol, 2001. **3**(12): p. 1114-1119.
231. Pelletier, J.N., Campbell-Valois, F.X., and Michnick, S.W., *Oligomerization domain-directed reassembly of active dihydrofolate reductase from rationally designed fragments.* Proc Natl Acad Sci U S A, 1998. **95**(21): p. 12141-12146.
232. Remy, I. and Michnick, S.W., *Clonal selection and in vivo quantitation of protein interactions with protein-fragment complementation assays.* Proc Natl Acad Sci U S A, 1999. **96**(10): p. 5394-5399.
233. Tarassov, K., Messier, V., Landry, C.R., Radinovic, S., Molina, M.M.S., Shames, I., Malitskaya, Y., Vogel, J., Bussey, H., and Michnick, S.W., *An in vivo map of the yeast protein interactome.* Science, 2008. **320**(5882): p. 1465-1470.
234. Michnick, S.W., Remy, I., Campbell-Valois, F.X., Vallée-Bélisle, A., and Pelletier, J.N., *Detection of protein-protein interactions by protein fragment complementation strategies.* Methods Enzymol, 2000. **328**: p. 208-230.
235. Galarneau, A., Primeau, M., Trudeau, L.E., and Michnick, S.W., *Beta-lactamase protein fragment complementation assays as in vivo and in vitro sensors of protein-protein interactions.* Nat Biotechnol, 2002. **20**(6): p. 619-622.
236. Wehrman, T., Kleaveland, B., Her, J.H., Balint, R.F., and Blau, H.M., *Protein–protein interactions monitored in mammalian cells via complementation of β-lactamase enzyme fragments.* Proc Natl Acad Sci U S A, 2002. **99**(6): p. 3469-3474.
237. Ghosh, I., Hamilton, A.D., and Regan, L., *Antiparallel leucine zipper-directed protein reassembly: application to the green fluorescent protein.* J Am Chem Soc, 2000. **122**(23): p. 5658-5659.
238. Michnick, S.W., Ear, P.H., Manderson, E.N., Remy, I., and Stefan, E., *Universal strategies in research and drug discovery based on protein-fragment complementation assays.* Nat Rev Drug Discov, 2007. **6**(7): p. 569-582.
239. Gingras, A.C., Gstaiger, M., Raught, B., and Aebersold, R., *Analysis of protein complexes using mass spectrometry.* Nat Rev Mol Cell Biol, 2007. **8**(8): p. 645-654.

240. Puig, O., Caspary, F., Rigaut, G., Rutz, B., Bouveret, E., Bragado-Nilsson, E., Wilm, M., and Séraphin, B., *The tandem affinity purification (TAP) method: a general procedure of protein complex purification.* Methods, 2001. **24**(3): p. 218-229.
241. Guerrero, C., Tagwerker, C., Kaiser, P., and Huang, L., *An integrated mass spectrometry-based proteomic approach: quantitative analysis of tandem affinity-purified in vivo cross-linked protein complexes (QTAX) to decipher the 26 S proteasome-interacting network.* Mol Cell Proteomics, 2006. **5**(2): p. 366-378.
242. Vasilescu, J., Guo, X., and Kast, J., *Identification of protein-protein interactions using in vivo cross-linking and mass spectrometry.* Proteomics, 2004. **4**(12): p. 3845-3854.
243. Sinz, A., *Chemical cross-linking and mass spectrometry to map three-dimensional protein structures and protein-protein interactions.* Mass Spectrom Rev, 2006. **25**(4): p. 663-682.
244. Trakselis, M.A., Alley, S.C., and Ishmaels, F.T., *Identification and mapping of protein-protein interactions by a combination of cross-linking, cleavage, and proteomics.* Bioconjug Chem, 2005. **16**(4): p. 741-750.
245. Rinner, O., Seebacher, J., Walzthoeni, T., Mueller, L., Beck, M., Schmidt, A., Mueller, M., and Aebersold, R., *Identification of cross-linked peptides from large sequence databases.* Nat Methods, 2008. **5**(4): p. 315-318.
246. Ihling, C., Schmidt, A., Kalkhof, S., Schulz, D.M., Stingl, C., Mechtler, K., Haack, M., Beck-Sickinger, A.G., Cooper, D.M., and Sinz, A., *Isotope-labeled cross-linkers and Fourier transform ion cyclotron resonance mass spectrometry for structural analysis of a protein/peptide complex.* J Am Soc Mass Spectrom, 2006. **17**(8): p. 1100-1113.
247. Seebacher, J., Mallick, P., Zhang, N., Eddes, J.S., Aebersold, R., and Gelb, M.H., *Protein cross-linking analysis using mass spectrometry, isotope-coded cross-linkers, and integrated computational data processing.* J Proteome Res, 2006. **5**(9): p. 2270-2282.
248. Schmitt-Ulms, G., Hansen, K., Liu, J., Cowdrey, C., Yang, J., DeArmond, S.J., Cohen, F.E., Prusiner, S.B., and Baldwin, M.A., *Time-controlled transcardiac perfusion cross-linking for the study of protein interactions in complex tissues.* Nat Biotechnol, 2004. **22**(6): p. 724-731.
249. Sutherland, B.W., Toews, J., and Kast, J., *Utility of formaldehyde cross-linking and mass spectrometry in the study of protein-protein interactions.* J Mass Spectrom, 2008. **43**(6): p. 699-715.
250. Jensen, O.N., *Interpreting the protein language using proteomics.* Nat Rev Mol Cell Biol, 2006. **7**(6): p. 391-403.
251. Cohen, P., *The regulation of protein function by multisite phosphorylation–a 25 year update.* Trends Biochem Sci, 2000. **25**(12): p. 596-601.
252. Pawson, T. and Scott, J.D., *Protein phosphorylation in signaling–50 years and counting.* Trends Biochem Sci, 2005. **30**(6): p. 286-290.
253. Macek, B., Mann, M., and Olsen, J.V., *Global and site-specific quantitative phosphoproteomics: principles and applications.* Annu Rev Pharmacol Toxicol, 2009. **49**: p. 199-221.
254. Collins, M.O., Yu, L., and Choudhary, J.S., *Analysis of protein phosphorylation on a proteome-scale.* Proteomics, 2007. **7**(16): p. 2751-2768.
255. Wilson, N.L., Schulz, B.L., Karlsson, N.G., and Packer, N.H., *Sequential analysis of N-and O-linked glycosylation of 2D-PAGE separated glycoproteins.* J Proteome Res, 2002. **1**(6): p. 521-529.

256. Harvey, D.J., *Proteomic analysis of glycosylation: structural determination of N-and O-linked glycans by mass spectrometry.* Expert Rev Proteomics, 2005. **2**(1): p. 87-101.
257. Abbosh, P.H., Montgomery, J.S., Starkey, J.A., Novotny, M., Zuhowski, E.G., Egorin, M.J., Moseman, A.P., Golas, A., Brannon, K.M., Balch, C., Huang, T.H., and Nephew, K.P., *Dominant-negative histone H3 lysine 27 mutant derepresses silenced tumor suppressor genes and reverses the drug-resistant phenotype in cancer cells.* Cancer Res, 2006. **66**(11): p. 5582-5591.
258. Farzan, M., Mirzabekov, T., Kolchinsky, P., Wyatt, R., Cayabyab, M., Gerard, N.P., Gerard, C., Sodroski, J., and Choe, H., *Tyrosine sulfation of the amino terminus of CCR5 facilitates HIV-1 entry.* Cell, 1999. **96**(5): p. 667-676.
259. Hunter, T., *Protein kinases and phosphatases: the yin and yang of protein phosphorylation and signaling.* Cell, 1995. **80**(2): p. 225-236.
260. Schlessinger, J., *Cell signaling by receptor tyrosine kinases.* Cell, 2000. **103**(2): p. 211-225.
261. Cohen, P., *Protein kinases—the major drug targets of the twenty-first century?* Nat Rev Drug Discov, 2002. **1**(4): p. 309-315.
262. Deininger, M.W. and Druker, B.J., *Specific targeted therapy of chronic myelogenous leukemia with imatinib.* Pharmacol Rev, 2003. **55**(3): p. 401-423.
263. Daub, H., Olsen, J.V., Bairlein, M., Gnad, F., Oppermann, F.S., K rner, R., Greff, Z., Kéri, G., Stemmann, O., and Mann, M., *Kinase-selective enrichment enables quantitative phosphoproteomics of the kinome across the cell cycle.* Mol Cell, 2008. **31**(3): p. 438-448.
264. Salomon, A.R., Ficarro, S.B., Brill, L.M., Brinker, A., Phung, Q.T., Ericson, C., Sauer, K., Brock, A., Horn, D.M., Schultz, P.G., and Peters, E.C., *Profiling of tyrosine phosphorylation pathways in human cells using mass spectrometry.* PNAS, 2003. **100**(2): p. 443-448.
265. Rush, J., Moritz, A., Lee, K.A., Guo, A., Goss, V.L., Spek, E.J., Zhang, H., Zha, X.M., Polakiewicz, R.D., and Comb, M.J., *Immunoaffinity profiling of tyrosine phosphorylation in cancer cells.* Nat. Biotechnol., 2005. **23**(1): p. 94-101.
266. Rikova, K., Guo, A., Zeng, Q., Possemato, A., Yu, J., Haack, H., Nardone, J., Lee, K., Reeves, C., Li, Y., Hu, Y., Tan, Z., Stokes, M., Sullivan, L., Mitchell, J., Wetzel, R., Macneill, J., Ren, J.M., Yuan, J., Bakalarski, C.E., Villen, J., Kornhauser, J.M., Smith, B., Li, D., Zhou, X., Gygi, S.P., Gu, T.L., Polakiewicz, R.D., Rush, J., and Comb, M.J., *Global survey of phosphotyrosine signaling identifies oncogenic kinases in lung cancer.* Cell, 2007. **131**(6): p. 1190-1203.
267. Gronborg, M., Kristiansen, T.Z., Stensballe, A., Andersen, J.S., Ohara, O., Mann, M., Jensen, O.N., and Pandey, A., *A mass spectrometry-based proteomic approach for identification of serine/threonine-phosphorylated proteins by enrichment with phospho-specific antibodies: identification of a novel protein, Frigg, as a protein kinase A substrate.* Mol Cell Proteomics, 2002. **1**(7): p. 517-527.
268. Posewitz, M.C. and Tempst, P., *Immobilized gallium (III) affinity chromatography of phosphopeptides.* Anal Chem, 1999. **71**(14): p. 2883-2892.
269. Stensballe, A., Andersen, S., and Jensen, O.N., *Characterization of phosphoproteins from electrophoretic gels by nanoscale Fe (III) affinity chromatography with off-line mass spectrometry analysis.* Proteomics, 2001. **1**(2): p. 207-222.

270. Ficarro, S.B., McCleland, M.L., Stukenberg, P.T., Burke, D.J., Ross, M.M., Shabanowitz, J., Hunt, D.F., and White, F.M., *Phosphoproteome analysis by mass spectrometry and its application to Saccharomyces cerevisiae.* Nat Biotechnol, 2002. **20**(3): p. 301-305.
271. Nuhse, T.S., Stensballe, A., Jensen, O.N., and Peck, S.C., *Large-scale analysis of in vivo phosphorylated membrane proteins by immobilized metal ion affinity chromatography and mass spectrometry.* Mol Cell Proteomics, 2003. **2**(11): p. 1234-1243.
272. Zhang, Y., Wolf-Yadlin, A., Ross, P.L., Pappin, D.J., Rush, J., Lauffenburger, D.A., and White, F.M., *Time-resolved mass spectrometry of tyrosine phosphorylation sites in the epidermal growth factor receptor signaling network reveals dynamic modules.* Mol. Cell Proteomics, 2005. **4**(9): p. 1240-1250.
273. Collins, M.O., Yu, L., Coba, M.P., Husi, H., Campuzano, I., Blackstock, W.P., Choudhary, J.S., and Grant, S.G., *Proteomic analysis of in vivo phosphorylated synaptic proteins.* J Biol Chem, 2004. **280**(7): p. 5972-5982.
274. Larsen, M.R., Thingholm, T.E., Jensen, O.N., Roepstorff, P., and Jørgensen, T.J., *Highly selective enrichment of phosphorylated peptides from peptide mixtures using titanium dioxide microcolumns.* Mol Cell Proteomics, 2005. **4**(7): p. 873-886.
275. Pinkse, M.W.H., Uitto, P.M., Hilhorst, M.J., Ooms, B., and Heck, A.J.R., *Selective isolation at the femtomole level of phosphopeptides from proteolytic digests using 2D-NanoLC-ESI-MS/MS and titanium oxide precolumns.* Anal Chem, 2004. **76**(14): p. 3935-3943.
276. Beausoleil, S.A., Jedrychowski, M., Schwartz, D., Elias, J.E., Villén, J., Li, J., Cohn, M.A., Cantley, L.C., and Gygi, S.P., *Large-scale characterization of HeLa cell nuclear phosphoproteins.* Proc Natl Acad Sci U S A, 2004. **101**(33): p. 12130-12135.
277. Villén, J., Beausoleil, S.A., Gerber, S.A., and Gygi, S.P., *Large-scale phosphorylation analysis of mouse liver.* Proc Natl Acad Sci U S A, 2007. **104**(5): p. 1488-1493.
278. Chi, A., Huttenhower, C., Geer, L.Y., Coon, J.J., Syka, J.E.P., Bai, D.L., Shabanowitz, J., Burke, D.J., Troyanskaya, O.G., and Hunt, D.F., *Analysis of phosphorylation sites on proteins from Saccharomyces cerevisiae by electron transfer dissociation (ETD) mass spectrometry.* Proc Natl Acad Sci U S A, 2007. **104**(7): p. 2193-2198.
279. Zubarev, R.A., Horn, D.M., Fridriksson, E.K., Kelleher, N.L., Kruger, N.A., Lewis, M.A., Carpenter, B.K., and McLafferty, F.W., *Electron capture dissociation for structural characterization of multiply charged protein cations.* Anal Chem, 2000. **72**(3): p. 563-573.
280. Stensballe, A., Jensen, O.N., Olsen, J.V., Haselmann, K.F., and Zubarev, R.A., *Electron capture dissociation of singly and multiply phosphorylated peptides.* Rapid Commun Mass Spectrom, 2000. **14**(19): p. 1793-1800.
281. Good, D.M., Wirtala, M., McAlister, G.C., and Coon, J.J., *Performance characteristics of electron transfer dissociation mass spectrometry.* Mol Cell Proteomics, 2007. **6**(11): p. 1942-1951.
282. Hu, Z., Mellor, J., Wu, J., Kanehisa, M., Stuart, J.M., and DeLisi, C., *Towards zoomable multidimensional maps of the cell.* Nat Biotechnol, 2007. **25**(5): p. 547-554.
283. Hu, Z., Hung, J.H., Wang, Y., Chang, Y.C., Huang, C.L., Huyck, M., and DeLisi, C., *VisANT 3.5: multi-scale network visualization, analysis and inference based on the gene ontology.* Nucleic Acids Res, 2009. **37**(Web Server issue): p. W115-121.
284. Weyrich, A.S., Schwertz, H., Kraiss, L.W., and Zimmerman, G.A., *Protein synthesis by platelets: historical and new perspectives.* J Thromb Haemost, 2009. **7**(2): p. 241-246.

285. Howes, J.-M., *Proteomic profiling of platelet signalling.* Expert Rev Proteomics, 2013. **10**(4): p. 355-364.
286. Di Michele, M., Van Geet, C., and Freson, K., *Recent advances in platelet proteomics.* Expert Rev Proteomics, 2012. **9**(4): p. 451-466.
287. Senis, Y. and García, Á., *Platelet proteomics: state of the art and future perspective*, in *Platelets and Megakaryocytes*. 2012, Springer. p. 367-399.
288. Wright, B., Stanley, R.G., Kaiser, W.J., and Gibbins, J.M., *The integration of proteomics and systems approaches to map regulatory mechanisms underpinning platelet function.* Proteomics Clin Appl, 2013. **7**(1-2): p. 144-154.
289. O'Neill, E.E., Brock, C.J., von Kriegsheim, A.F., Pearce, A.C., Dwek, R.A., Watson, S.P., and Hebestreit, H.F., *Towards complete analysis of the platelet proteome.* Proteomics, 2002. **2**(3): p. 288-305.
290. Burkhart, J.M., Vaudel, M., Gambaryan, S., Radau, S., Walter, U., Martens, L., Geiger, J., Sickmann, A., and Zahedi, R.P., *The first comprehensive and quantitative analysis of human platelet protein composition allows the comparative analysis of structural and functional pathways.* Blood, 2012. **120**(15): p. e73-82.
291. García, A., Prabhakar, S., Brock, C.J., Pearce, A.C., Dwek, R.A., Watson, S.P., Hebestreit, H.F., and Zitzmann, N., *Extensive analysis of the human platelet proteome by two‐dimensional gel electrophoresis and mass spectrometry.* Proteomics, 2004. **4**(3): p. 656-668.
292. Marcus, K., Immler, D., Sternberger, J., and Meyer, H.E., *Identification of platelet proteins separated by two‐dimensional gel electrophoresis and analyzed by matrix assisted laser desorption/ionization‐time of flight‐mass spectrometry and detection of tyrosine‐phosphorylated proteins.* Electrophoresis, 2000. **21**(13): p. 2622-2636.
293. Garcia, B.A., Smalley, D.M., Cho, H., Shabanowitz, J., Ley, K., and Hunt, D.F., *The platelet microparticle proteome.* J Proteome Res, 2005. **4**(5): p. 1516-1521.
294. Dean, W.L., Lee, M.J., Cummins, T.D., Schultz, D.J., and Powell, D.W., *Proteomic and functional characterisation of platelet microparticle size classes.* Thromb Haemost, 2009. **102**(4): p. 711-718.
295. Piersma, S.R., Broxterman, H.J., Kapci, M., de Haas, R.R., Hoekman, K., Verheul, H.M., and Jiménez, C.R., *Proteomics of the TRAP-induced platelet releasate.* J Proteomics, 2009. **72**(1): p. 91-109.
296. Maynard, D.M., Heijnen, H.F., Gahl, W.A., and GUNAY‐AYGUN, M., *The α‐granule proteome: novel proteins in normal and ghost granules in gray platelet syndrome.* J Thromb Haemost, 2010. **8**(8): p. 1786-1796.
297. Hernández-Ruiz, L., Valverde, F., Jimenez-Nuñez, M.D., Ocaña, E., Sáez-Benito, A., Rodríguez-Martorell, J., Bohórquez, J.-C., Serrano, A., and Ruiz, F.A., *Organellar proteomics of human platelet dense granules reveals that 14-3-3ζ is a granule protein related to atherosclerosis.* J Proteome Res, 2007. **6**(11): p. 4449-4457.
298. Moebius, J., Zahedi, R.P., Lewandrowski, U., Berger, C., Walter, U., and Sickmann, A., *The human platelet membrane proteome reveals several new potential membrane proteins.* Mol Cell Proteomics, 2005. **4**(11): p. 1754-1761.
299. Lewandrowski, U., Wortelkamp, S., Lohrig, K., Zahedi, R.P., Wolters, D.A., Walter, U., and Sickmann, A., *Platelet membrane proteomics: a novel repository for functional research.* Blood, 2009. **114**(1): p. e10-19.

300. Kaiser, W.J., Holbrook, L.-M., Tucker, K.L., Stanley, R.G., and Gibbins, J.M., *A functional proteomic method for the enrichment of peripheral membrane proteins reveals the collagen binding protein Hsp47 is exposed on the surface of activated human platelets.* J Proteome Res, 2009. **8**(6): p. 2903-2914.
301. Zahedi, R.P., Lewandrowski, U., Wiesner, J., Wortelkamp, S., Moebius, J., Schütz, C., Walter, U., Gambaryan, S., and Sickmann, A., *Phosphoproteome of resting human platelets.* J Proteome Res, 2007. **7**(2): p. 526-534.
302. García, Á., Senis, Y.A., Antrobus, R., Hughes, C.E., Dwek, R.A., Watson, S.P., and Zitzmann, N., *A global proteomics approach identifies novel phosphorylated signaling proteins in GPVI ‐ activated platelets: Involvement of G6f, a novel platelet Grb2 ‐ binding membrane adapter.* Proteomics, 2006. **6**(19): p. 5332-5343.
303. Maguire, P.B., Wynne, K.J., Harney, D.F., O'Donoghue, N.M., Stephens, G., and Fitzgerald, D.J., *Identification of the phosphotyrosine proteome from thrombin activated platelets.* Proteomics, 2002. **2**(6): p. 642-648.
304. Lewandrowski, U., Moebius, J., Walter, U., and Sickmann, A., *Elucidation of N-glycosylation sites on human platelet proteins a glycoproteomic approach.* Mol Cell Proteomics, 2006. **5**(2): p. 226-233.
305. Lewandrowski, U., Zahedi, R.P., Moebius, J., Walter, U., and Sickmann, A., *Enhanced N-glycosylation site analysis of sialoglycopeptides by strong cation exchange prefractionation applied to platelet plasma membranes.* Mol Cell Proteomics, 2007. **6**(11): p. 1933-1941.
306. García, A., Prabhakar, S., Hughan, S., Anderson, T.W., Brock, C.J., Pearce, A.C., Dwek, R.A., Watson, S.P., Hebestreit, H.F., and Zitzmann, N., *Differential proteome analysis of TRAP-activated platelets: involvement of DOK-2 and phosphorylation of RGS proteins.* Blood, 2004. **103**(6): p. 2088-2095.
307. Senis, Y., Antrobus, R., Severin, S., Parguina, A., Rosa, I., Zitzmann, N., Watson, S., and García, A., *Proteomic analysis of integrin alphaIIbbeta3 outside-in signaling reveals Src-kinase-independent phosphorylation of Dok-1 and Dok-3 leading to SHIP-1 interactions.* J Thromb Haemost, 2009. **7**(10): p. 1718-1726.
308. Schulz, C., Leuschen, N.V., Fröhlich, T., Lorenz, M., Pfeiler, S., Gleissner, C.A., Kremmer, E., Kessler, M., Khandoga, A.G., Engelmann, B., Ley, K., Massberg, S., and Arnold, G.J., *Identification of novel downstream targets of platelet glycoprotein VI activation by differential proteome analysis: implications for thrombus formation.* Blood, 2010. **115**(20): p. 4102-4110.
309. Coppinger, J.A., O'Connor, R., Wynne, K., Flanagan, M., Sullivan, M., Maguire, P.B., Fitzgerald, D.J., and Cagney, G., *Moderation of the platelet releasate response by aspirin.* Blood, 2007. **109**(11): p. 4786-4792.
310. Tucker, K.L., Kaiser, W.J., Bergeron, A.L., Hu, H., Dong, J.f., Tan, T.H., and Gibbins, J.M., *Proteomic analysis of resting and thrombin ‐ stimulated platelets reveals the translocation and functional relevance of HIP ‐ 55 in platelets.* Proteomics, 2009. **9**(18): p. 4340-4354.
311. Thon, J.N., Schubert, P., Duguay, M., Serrano, K., Lin, S., Kast, J., and Devine, D.V., *Comprehensive proteomic analysis of protein changes during platelet storage requires complementary proteomic approaches.* Transfusion, 2008. **48**(3): p. 425-435.

312. Thiele, T., Steil, L., Gebhard, S., Scharf, C., Hammer, E., Brigulla, M., Lubenow, N., Clemetson, K.J., Völker, U., and Greinacher, A., *Profiling of alterations in platelet proteins during storage of platelet concentrates.* Transfusion, 2007. **47**(7): p. 1221-1233.
313. Glenister, K.M., Payne, K.A., and Sparrow, R.L., *Proteomic analysis of supernatant from pooled buffy‐coat platelet concentrates throughout 7‐day storage.* Transfusion, 2008. **48**(1): p. 99-107.
314. Springer, D.L., Miller, J.H., Spinelli, S.L., Pasa-Tolic, L., Purvine, S.O., Daly, D.S., Zangar, R.C., Jin, S., Blumberg, N., Francis, C.W., Taubman, M.B., Casey, A.E., Wittlin, S.D., and Phipps, R.P., *Platelet proteome changes associated with diabetes and during platelet storage for transfusion.* J Proteome Res, 2009. **8**(5): p. 2261-2272.
315. Fong, K.P., Barry, C., Tran, A.N., Traxler, E.A., Wannemacher, K.M., Tang, H.-Y., Speicher, K.D., Blair, I.A., Speicher, D.W., Grosser, T., and Brass, L.F., *Deciphering the human platelet sheddome.* Blood, 2011. **117**(1): p. e15-e26.
316. Winkler, W., Zellner, M., Diestinger, M., Babeluk, R., Marchetti, M., Goll, A., Zehetmayer, S., Bauer, P., Rappold, E., Miller, I., Roth, E., Allmaier, G., and Oehler, R., *Biological variation of the platelet proteome in the elderly population and its implication for biomarker research.* Mol Cell Proteomics, 2008. **7**(1): p. 193-203.
317. Fröbel, J., Cadeddu, R.-P., Hartwig, S., Bruns, I., Wilk, C.M., Kündgen, A., Fischer, J.C., Schroeder, T., Steidl, U.G., Germing, U., Lehr, S., Haas, R., and Czibere, A., *Platelet proteome analysis reveals integrin-dependent aggregation defects in patients with myelodysplastic syndromes.* Mol Cell Proteomics, 2013. **12**(5): p. 1272-1280.
318. Banfi, C., Brioschi, M., Marenzi, G., De Metrio, M., Camera, M., Mussoni, L., and Tremoli, E., *Proteome of platelets in patients with coronary artery disease.* Exp Hematol, 2010. **38**(5): p. 341-350.
319. Parguina, A.F., Grigorian-Shamajian, L., Agra, R.M., Teijeira-Fernandez, E., Rosa, I., Alonso, J., Vinuela-Roldan, J.E., Seoane, A., Gonzalez-Juanatey, J.R., and García, Á., *Proteins involved in platelet signaling are differentially regulated in acute coronary syndrome: a proteomic study.* PLoS One, 2010. **5**(10): p. e13404.
320. Zellner, M., Baureder, M., Rappold, E., Bugert, P., Kotzailias, N., Babeluk, R., Baumgartner, R., Attems, J., Gerner, C., Jellinger, K., Roth, E., Oehler, R., and Umlauf, E., *Comparative platelet proteome analysis reveals an increase of monoamine oxidase-B protein expression in Alzheimer's disease but not in non-demented Parkinson's disease patients.* J Proteomics, 2012. **75**(7): p. 2080-2092.
321. Pieroni, L., Finamore, F., Ronci, M., Mattoscio, D., Marzano, V., Mortera, S.L., Quattrucci, S., Federici, G., Romano, M., and Urbani, A., *Proteomics investigation of human platelets in healthy donors and cystic fibrosis patients by shotgun nUPLC-MSE and 2DE: a comparative study.* Mol Biosyst, 2011. **7**(3): p. 630-639.
322. Arias-Salgado, E.G., Larrucea, S., Butta, N., Fernández, D., García-Muñoz, S., Parrilla, R., and Ayuso, M.S., *Variations in platelet protein associated with arterial thrombosis.* Thromb Res, 2008. **122**(5): p. 640-647.
323. López‐Farré, A.J., Zamorano‐Leon, J.J., Azcona, L., Modrego, J., Mateos‐Cáceres, P.J., González‐Armengol, J., Villarroel, P., Moreno‐Herrero, R., Rodríguez‐Sierra, P., Segura, A., Tamargo, J., and Macaya, C., *Proteomic changes related to "bewildered"*

circulating platelets in the acute coronary syndrome. Proteomics, 2011. **11**(16): p. 3335-3348.
324. Parguiña, A.F., Grigorian-Shamagian, L., Agra, R.M., López-Otero, D., Rosa, I., Alonso, J., Teijeira-Fernández, E., González-Juanatey, J.R., and García, Á., *Variations in Platelet Proteins Associated With ST-Elevation Myocardial Infarction Novel Clues on Pathways Underlying Platelet Activation in Acute Coronary Syndromes.* Arterioscler Thromb Vasc Biol, 2011. **31**(12): p. 2957-2964.
325. Mateos-Caceres, P.J., Macaya, C., Azcona, L., Modrego, J., Mahillo, E., Bernardo, E., Fernandez-Ortiz, A., and López-Farré, A.J., *Different expression of proteins in platelets from aspirin-resistant and aspirin-sensitive patients.* Thromb Haemost, 2010. **103**(1): p. 160-170.
326. Volpi, E., Giusti, L., Ciregia, F., Da Valle, Y., Giannaccini, G., Berti, S., Clerico, A., and Lucacchini, A., *Platelet proteome and clopidogrel response in patients with stable angina undergoing percutaneous coronary intervention.* Clin Biochem, 2012. **45**(10-11): p. 758-765.
327. Sacristán, D., Marques, M., Zamorano‐León, J.J., Luque, M., Armengol, J., del Castillo, J., Martín, J., Delpón, E., Ramos‐Mozo, P., de Prada, T.P., Tamargo, J., Barrientos, A., Macaya, C., and López-Farré, A., *Modifications by Olmesartan medoxomil treatment of the platelet protein profile of moderate hypertensive patients.* Proteomics Clin Appl, 2008. **2**(9): p. 1300-1312.
328. Walkowiak, B., Kaminska, M., Okrój, W., Tanski, W., Sobol, A., Zbróg, Z., and Przybyszewska-Doros, I., *The blood platelet proteome is changed in UREMIC patients.* Platelets, 2007. **18**(5): p. 386-388.
329. Maurer-Spurej, E., Kahr, W.H., Carter, C.J., Pittendreigh, C., Cameron, M., and Cyr, T.D., *The value of proteomics for the diagnosis of a platelet-related bleeding disorder.* Platelets, 2008. **19**(5): p. 342-351.
330. Di Michele, M., Thys, C., Waelkens, E., Overbergh, L., D'Hertog, W., Mathieu, C., De Vos, R., Peerlinck, K., Van Geet, C., and Freson, K., *An integrated proteomics and genomics analysis to unravel a heterogeneous platelet secretion defect.* J Proteomics, 2011. **74**(6): p. 902-913.
331. Mattoscio, D., Evangelista, V., De Cristofaro, R., Recchiuti, A., Pandolfi, A., Di Silvestre, S., Manarini, S., Martelli, N., Rocca, B., Petrucci, G., Angelini, D.F., Battistini, L., Robuffo, I., Pensabene, T., Pieroni, L., Furnari, M.L., Pardo, F., Quattrucci, S., Lancellotti, S., Davì, G., and Romano, M., *Cystic fibrosis transmembrane conductance regulator (CFTR) expression in human platelets: impact on mediators and mechanisms of the inflammatory response.* FASEB J, 2010. **24**(10): p. 3970-3980.
332. Patterson, S.D., *Data analysis--the Achilles heel of proteomics.* Nat Biotechnol, 2003. **21**(3): p. 221-222.
333. Domon, B. and Aebersold, R., *Mass spectrometry and protein analysis.* Science, 2006. **312**(5771): p. 212-217.
334. Nesvizhskii, A.I., Vitek, O., and Aebersold, R., *Analysis and validation of proteomic data generated by tandem mass spectrometry.* Nat Methods, 2007. **4**(10): p. 787-797.
335. Craig, R., Cortens, J.P., and Beavis, R.C., *Open source system for analyzing, validating, and storing protein identification data.* J Proteome Res, 2004. **3**(6): p. 1234-1242.

336. Fenyö, D. and Beavis, R.C., *A method for assessing the statistical significance of mass spectrometry-based protein identifications using general scoring schemes.* Anal Chem, 2003. **75**(4): p. 768-774.
337. Craig, R. and Beavis, R.C., *TANDEM: matching proteins with tandem mass spectra.* Bioinformatics, 2004. **20**(9): p. 1466-1467.
338. Craig, R. and Beavis, R.C., *A method for reducing the time required to match protein sequences with tandem mass spectra.* Rapid Commun Mass Spectrom, 2003. **17**(20): p. 2310-2316.
339. Luger, K., Mäder, A.W., Richmond, R.K., Sargent, D.F., and Richmond, T.J., *Crystal structure of the nucleosome core particle at 2.8 A resolution.* Nature, 1997. **389**(6648): p. 251-260.
340. Malovannaya, A., Li, Y., Bulynko, Y., Jung, S.Y., Wang, Y., Lanz, R.B., O'Malley, B.W., and Qin, J., *Streamlined analysis schema for high-throughput identification of endogenous protein complexes.* Proc Natl Acad Sci U S A, 2010. **107**(6): p. 2431-2436.
341. Voges, D., Zwickl, P., and Baumeister, W., *The 26S proteasome: a molecular machine designed for controlled proteolysis.* Annu Rev Biochem, 1999. **68**: p. 1015-1068.
342. Jensen, L.J., Kuhn, M., Stark, M., Chaffron, S., Creevey, C., Muller, J., Doerks, T., Julien, P., Roth, A., Simonovic, M., Bork, P., and von Mering, C., *STRING 8--a global view on proteins and their functional interactions in 630 organisms.* Nucleic Acids Res, 2009. **37**(Database issue): p. D412-416.
343. Bennett, J.S., *Structure and function of the platelet integrin alphaIIbbeta3.* J Clin Invest, 2005. **115**(12): p. 3363-3369.
344. Tadokoro, S., Shattil, S.J., Eto, K., Tai, V., Liddington, R.C., de Pereda, J.M., Ginsberg, M.H., and Calderwood, D.A., *Talin binding to integrin beta tails: a final common step in integrin activation.* Science, 2003. **302**(5642): p. 103-106.
345. Nieswandt, B., Moser, M., Pleines, I., Varga-Szabo, D., Monkley, S., Critchley, D., and Fässler, R., *Loss of talin1 in platelets abrogates integrin activation, platelet aggregation, and thrombus formation in vitro and in vivo.* J Exp Med, 2007. **204**(13): p. 3113-3118.
346. Petrich, B.G., Marchese, P., Ruggeri, Z.M., Spiess, S., Weichert, R.A., Ye, F., Tiedt, R., Skoda, R.C., Monkley, S.J., Critchley, D.R., and Ginsberg, M.H., *Talin is required for integrin-mediated platelet function in hemostasis and thrombosis.* J Exp Med, 2007. **204**(13): p. 3103-3011.
347. Moser, M., Nieswandt, B., Ussar, S., Pozgajova, M., and Fässler, R., *Kindlin-3 is essential for integrin activation and platelet aggregation.* Nat Med, 2008. **14**(3): p. 325-330.
348. Moser, M., Legate, K.R., Zent, R., and Fässler, R., *The tail of integrins, talin, and kindlins.* Science, 2009. **324**(5929): p. 895-899.
349. Chrzanowska-Wodnicka, M., Smyth, S.S., Schoenwaelder, S.M., Fischer, T.H., and White, G.C.n., *Rap1b is required for normal platelet function and hemostasis in mice.* J Clin Invest, 2005. **115**(3): p. 680-687.
350. Han, J., Lim, C.J., Watanabe, N., Soriani, A., Ratnikov, B., Calderwood, D.A., Puzon-McLaughlin, W., Lafuente, E.M., Boussiotis, V.A., Shattil, S.J., and Ginsberg, M.H., *Reconstructing and deconstructing agonist-induced activation of integrin alphaIIbbeta3.* Curr Biol, 2006. **16**(18): p. 1796-1806.
351. Klockenbusch, C. and Kast, J., *Optimization of formaldehyde cross-linking for protein interaction analysis of non-tagged integrin β1.* J Biomed Biotechnol, 2010. **2010: 927585**.

352. Breitkreutz, B.J., Stark, C., Reguly, T., Boucher, L., Breitkreutz, A., Livstone, M., Oughtred, R., Lackner, D.H., J, B., Wood, V., Dolinski, K., and Tyers, M., *The BioGRID interaction database: 2008 update.* Nucleic Acids Res, 2007. **36**(Database issue): p. D637-640.
353. Mishra, G.R., Suresh, M., Kumaran, K., Kannabiran, N., Suresh, S., Bala, P., Shivakumar, K., Anuradha, N., Reddy, R., Raghavan, T.M., Menon, S., Hanumanthu, G., Gupta, M., Upendran, S., Gupta, S., Mahesh, M., Jacob, B., Mathew, P., Chatterjee, P., Arun, K.S., Sharma, S., Chandrika, K.N., Deshpande, N., Palvankar, K., Raghavnath, R., Krishnakanth, R., Karathia, H., Rekha, B., Nayak, R., Vishnupriya, G., Kumar, H.G., Nagini, M., Kumar, G.S., Jose, R., Deepthi, P., Mohan, S.S., Gandhi, T.K., Harsha, H.C., Deshpande, K.S., Sarker, M., Prasad, T.S., and Pandey, A., *Human protein reference database—2006 update.* Nucleic Acids Res, 2006. **34**(Database issue): p. D411-414.
354. Kerrien, S., Alam-Faruque, Y., Aranda, B., Bancarz, I., Bridge, A., Derow, C., Dimmer, E., Feuermann, M., Friedrichsen, A., Huntley, R., Kohler, C., Khadake, J., Leroy, C., Liban, A., Lieftink, C., Montecchi-Palazzi, L., Orchard, S., Risse, J., Robbe, K., Roechert, B., Thorneycroft, D., Zhang, Y., Apweiler, R., and Hermjakob, H., *IntAct—open source resource for molecular interaction data.* Nucleic Acids Res, 2006. **35**(Database issue): p. D561-565.
355. Chatr-aryamontri, A., Ceol, A., Palazzi, L.M., Nardelli, G., Schneider, M.V., Castagnoli, L., and Cesareni, G., *MINT: the Molecular INTeraction database.* Nucleic Acids Res, 2007. **35**(Database issue): p. D572-574.
356. Kanehisa, M., Araki, M., Goto, S., Hattori, M., Hirakawa, M., Itoh, M., Katayama, T., Kawashima, S., Okuda, S., Tokimatsu, T., and Yamanishi, Y., *KEGG for linking genomes to life and the environment.* Nucleic Acids Res, 2008. **36**(Database issue): p. D480-484.
357. Legate, K.R. and Fässler, R., *Mechanisms that regulate adaptor binding to beta-integrin cytoplasmic tails.* J Cell Sci, 2009. **122**(Pt 2): p. 187-198.
358. Hynes, R.O., *Integrins: bidirectional, allosteric signaling machines.* Cell, 2002. **110**(6): p. 673-687.
359. DeMartino, G.N. and Slaughter, C.A., *The proteasome, a novel protease regulated by multiple mechanisms.* J Biol Chem, 1999. **274**(32): p. 22123-22126.
360. Buensuceso, C.S., Obergfell, A., Soriani, A., Eto, K., Kiosses, W.B., Arias-Salgado, E.G., Kawakami, T., and Shattil, S.J., *Regulation of outside-in signaling in platelets by integrin-associated protein kinase C beta.* J Biol Chem, 2005. **280**(1): p. 644-653.
361. Obergfell, A., Eto, K., Mocsai, A., Buensuceso, C., Moores, S.L., Brugge, J.S., Lowell, C.A., and Shattil, S.J., *Coordinate interactions of Csk, Src, and Syk kinases with [alpha]IIb[beta]3 initiate integrin signaling to the cytoskeleton.* J Cell Biol, 2002. **157**(2): p. 265-275.
362. Brummel, K.E., Paradis, S.G., Butenas, S., and Mann, K.G., *Thrombin functions during tissue factor-induced blood coagulation.* Blood, 2002. **100**(1): p. 148-152.
363. Critchley, D.R., *Cytoskeletal proteins talin and vinculin in integrin-mediated adhesion.* Biochem Soc Trans, 2004. **32**(Pt 5): p. 831-836.
364. Hagmann, J. and Burger, M.M., *Phosphorylation of vinculin in human platelets spreading on a solid surface.* J Cell Biochem, 1992. **50**(3): p. 237-244.
365. Hannigan, G.E., Leung-Hagesteijn, C., Fitz-Gibbon, L., Coppolino, M.G., Radeva, G., Filmus, J., Bell, J.C., and Dedhar, S., *Regulation of cell adhesion and anchorage-*

dependent growth by a new 1-integrin-linked protein kinase. Nature, 1996. **379**(6560): p. 91-96.
366. Brancaccio, M., Guazzone, S., Menini, N., Sibona, E., Hirsch, E., De Andrea, M., Rocchi, M., Altruda, F., Tarone, G., and Silengo, L., *Melusin is a new muscle-specific interactor for beta1 integrin cytoplasmic domain.* J Biol Chem, 1999. **274**(41): p. 29282-29288.
367. Takai, Y., Sasaki, T., and Matozaki, T., *Small GTP-binding proteins.* Physiol Rev, 2001. **81**(1): p. 153-208.
368. Bourne, H.R., Sanders, D.A., and McCormick, F., *The GTPase superfamily: conserved structure and molecular mechanism.* Nature, 1991. **349**(6305): p. 117-127.
369. Wennerberg, K., Rossman, K.L., and Der, C.J., *The Ras superfamily at a glance.* J Cell Sci, 2005. **118**(Pt 5): p. 843-846.
370. Jaffe, A.B. and Hall, A., *Rho GTPases: biochemistry and biology.* Annu Rev Cell Dev Biol, 2005. **21**: p. 247-269.
371. Stenmark, H., *Rab GTPases as coordinators of vesicle traffic.* Nat Rev Mol Cell Biol, 2009. **10**(8): p. 513-525.
372. Kinbara, K., Goldfinger, L.E., Hansen, M., Chou, F.-L., and Ginsberg, M.H., *Ras GTPases: integrins' friends or foes?* Nat Rev Mol Cell Biol, 2003. **4**(10): p. 767-778.
373. Bos, J.L., *Linking Rap to cell adhesion.* Curr Opin Cell Biol, 2005. **17**(2): p. 123-128.
374. Ridley, A.J., Schwartz, M.A., Burridge, K., Firtel, R.A., Ginsberg, M.H., Borisy, G., Parsons, J.T., and Horwitz, A.R., *Cell migration: integrating signals from front to back.* Science, 2003. **302**(5651): p. 1704-1709.
375. Mitin, N., Rossman, K.L., and Der, C.J., *Signaling interplay in Ras superfamily function.* Curr Biol, 2005. **15**(14): p. R563-574.
376. Castellano, E. and Santos, E., *Functional specificity of ras isoforms: so similar but so different.* Genes Cancer, 2011. **2**(3): p. 216-231.
377. Cherfils, J. and Zeghouf, M., *Regulation of Small GTPases by GEFs, GAPs, and GDIs.* Physiol Rev, 2013. **93**(1): p. 269-309.
378. Stites, E.C. and Ravichandran, K.S., *A systems perspective of Ras signaling in cancer.* Clin Cancer Res, 2009. **15**(5): p. 1510-1513.
379. Sahai, E. and Marshall, C.J., *RHO–GTPases and cancer.* Nat Rev Cancer, 2002. **2**(2): p. 133-142.
380. Vega, F.M. and Ridley, A.J., *Rho GTPases in cancer cell biology.* FEBS Lett, 2008. **582**(14): p. 2093-2101.
381. Iden, S. and Collard, J.G., *Crosstalk between small GTPases and polarity proteins in cell polarization.* Nat Rev Mol Cell Biol, 2008. **9**(11): p. 846-859.
382. Reeder, M.K., Serebriiskii, I.G., Golemis, E.A., and Chernoff, J., *Analysis of small GTPase signaling pathways using p21-activated kinase mutants that selectively couple to Cdc42.* Journal of Biological Chemistry, 2001. **276**(44): p. 40606-40613.
383. Knaus, U.G., Bamberg, A., and Bokoch, G.M., *Rac and Rap GTPase activation assays.* Methods Mol Biol, 2007. **412**: p. 59-67.
384. Uhlén, M. and Hober, S., *Generation and validation of affinity reagents on a proteome‐wide level.* J Mol Recognit, 2009. **22**(2): p. 57-64.
385. Gillette, M.A. and Carr, S.A., *Quantitative analysis of peptides and proteins in biomedicine by targeted mass spectrometry.* Nat Methods, 2013. **10**(1): p. 28-34.

386. Picotti, P. and Aebersold, R., *Selected reaction monitoring-based proteomics: workflows, potential, pitfalls and future directions.* Nat Methods, 2012. **9**(6): p. 555-566.
387. Lange, V., Picotti, P., Domon, B., and Aebersold, R., *Selected reaction monitoring for quantitative proteomics: a tutorial.* Molecular systems biology, 2008. **4**(1).
388. Gillette, M.A. and Carr, S.A., *Quantitative analysis of peptides and proteins in biomedicine by targeted mass spectrometry.* Nature methods, 2013. **10**(1): p. 28-34.
389. Domon, B. and Aebersold, R., *Options and considerations when selecting a quantitative proteomics strategy.* Nat Biotechnol, 2010. **28**(7): p. 710-721.
390. Aslan, J.E. and McCarty, O.J., *Rho GTPases in platelet function.* J Thromb Haemost, 2013. **11**(1): p. 35-46.
391. Brtva, T.R., Drugan, J.K., Ghosh, S., Terrell, R.S., Campbell-Burk, S., Bell, R.M., and Der, C.J., *Two distinct Raf domains mediate interaction with Ras.* J Biol Chem, 1995. **270**(17): p. 9809-9812.
392. Ren, X.D., Kiosses, W.B., and Schwartz, M.A., *Regulation of the small GTP-binding protein Rho by cell adhesion and the cytoskeleton.* Embo J, 1999. **18**(3): p. 578-585.
393. Shevchenko, A., Tomas, H., Havlis, J., Olsen, J.V., and Mann, M., *In-gel digestion for mass spectrometric characterization of proteins and proteomes.* Nat Protoc, 2006. **1**(6): p. 2856-2860.
394. McWilliam, H., Li, W., Uludag, M., Squizzato, S., Park, Y.M., Buso, N., Cowley, A.P., and Lopez, R., *Analysis tool web services from the EMBL-EBI.* Nucleic Acids Res, 2013. **41**(Web Server issue): p. W597-600.
395. MacLean, B., Tomazela, D.M., Shulman, N., Chambers, M., Finney, G.L., Frewen, B., Kern, R., Tabb, D.L., Liebler, D.C., and MacCoss, M.J., *Skyline: an open source document editor for creating and analyzing targeted proteomics experiments.* Bioinformatics, 2010. **26**(7): p. 966-968.
396. Zhao, Y. and Brasier, A.R., *Applications of selected reaction monitoring (SRM)-mass spectrometry (MS) for quantitative measurement of signaling pathways.* Methods, 2013. **61**(3): p. 313-322.
397. Lange, V., Picotti, P., Domon, B., and Aebersold, R., *Selected reaction monitoring for quantitative proteomics: a tutorial.* Mol Syst Biol, 2008. **4**(1): p. 222.
398. Walsh, G.M., Lin, S., Evans, D.M., Khosrovi-Eghbal, A., Beavis, R.C., and Kast, J., *Implementation of a data repository-driven approach for targeted proteomics experiments by multiple reaction monitoring.* J Proteomics, 2009. **72**(5): p. 838-852.
399. Stallings-Mann, M.L., Waldmann, J., Zhang, Y., Miller, E., Gauthier, M.L., Visscher, D.W., Downey, G.P., Radisky, E.S., Fields, A.P., and Radisky, D.C., *Matrix metalloproteinase induction of Rac1b, a key effector of lung cancer progression.* Sci. Transl. Med. , 2012. **4**(142): p. 142ra95.
400. Picotti, P. and Aebersold, R., *Selected reaction monitoring-based proteomics: workflows, potential, pitfalls and future directions.* Nat. Methods., 2012. **9**(6): p. 555-566.
401. Zhao, Y., Tian, B., Edeh, C.B., and Brasier, A.R., *Quantitation of the dynamic profiles of the innate immune response using multiplex selected reaction monitoring-mass spectrometry.* Mol. Cell Proteomics. , 2013. **12**(6): p. 1513-1529.
402. Haserück, N., Erl, W., Pandey, D., Tigyi, G., Ohlmann, P., Ravanat, C., Gachet, C., and Siess, W., *The plaque lipid lysophosphatidic acid stimulates platelet activation and platelet-monocyte aggregate formation in whole blood: involvement of P2Y1 and P2Y12 receptors.* Blood, 2004. **103**(7): p. 2585-2592.

403. Michelson, A.D., *Antiplatelet therapies for the treatment of cardiovascular disease.* Nat. Rev. Drug Discov., 2010. **9**(2): p. 154-169.
404. Rush, J., Moritz, A., Lee, K.A., Guo, A., Goss, V.L., Spek, E.J., Zhang, H., Zha, X.-M., Polakiewicz, R.D., and Comb, M.J., *Immunoaffinity profiling of tyrosine phosphorylation in cancer cells.* Nat. Biotechnol., 2005. **23**(1): p. 94-101.
405. Salomon, A.R., Ficarro, S.B., Brill, L.M., Brinker, A., Phung, Q.T., Ericson, C., Sauer, K., Brock, A., Horn, D.M., Schultz, P.G., and Peters, E.C., *Profiling of tyrosine phosphorylation pathways in human cells using mass spectrometry.* Proc Natl Acad Sci U S A., 2003. **100**(2): p. 443-448.
406. Cerletti, C., Tamburrelli, C., Izzi, B., Gianfagna, F., and de Gaetano, G., *Platelet-leukocyte interactions in thrombosis.* Thromb Res, 2012. **129**(3): p. 263-266.
407. Rinder, C.S., Bonan, J.L., Rinder, H.M., Mathew, J., Hines, R., and Smith, B.R., *Cardiopulmonary bypass induces leukocyte-platelet adhesion.* Blood, 1992. **79**(5): p. 1201-1205.
408. Neumann, F.-J., Marx, N., Gawaz, M., Brand, K., Ott, I., Rokitta, C., Sticherling, C., Meinl, C., May, A., and Schömig, A., *Induction of cytokine expression in leukocytes by binding of thrombin-stimulated platelets.* Circulation, 1997. **95**(10): p. 2387-2394.
409. Weyrich, A.S., Elstad, M.R., McEver, R.P., McIntyre, T.M., Moore, K.L., Morrissey, J.H., Prescott, S.M., and Zimmerman, G.A., *Activated platelets signal chemokine synthesis by human monocytes.* J Clin Invest, 1996. **97**(6): p. 1525-1534.
410. Dixon, D.A., Tolley, N.D., Bemis-Standoli, K., Martinez, M.L., Weyrich, A.S., Morrow, J.D., Prescott, S.M., and Zimmerman, G.A., *Expression of COX-2 in platelet-monocyte interactions occurs via combinatorial regulation involving adhesion and cytokine signaling.* J Clin Invest, 2006. **116**(10): p. 2727-2738.
411. Celi, A., Pellegrini, G., Lorenzet, R., De Blasi, A., Ready, N., Furie, B.C., and Furie, B., *P-selectin induces the expression of tissue factor on monocytes.* Proc Natl Acad Sci U S A, 1994. **91**(19): p. 8767-8771.
412. Stephen, J., Emerson, B., Fox, K.A., and Dransfield, I., *The uncoupling of monocyte–platelet interactions from the induction of proinflammatory signaling in monocytes.* J Immunol, 2013. **191**(11): p. 5677-5683.
413. Tsuchiya, S., Yamabe, M., Yamaguchi, Y., Kobayashi, Y., Konno, T., and Tada, K., *Establishment and characterization of a human acute monocytic leukemia cell line (THP‐1).* Int J Cancer, 1980. **26**(2): p. 171-176.
414. Rigbolt, K.T., Prokhorova, T.A., Akimov, V., Henningsen, J., Johansen, P.T., Kratchmarova, I., Kassem, M., Mann, M., Olsen, J.V., and Blagoev, B., *System-wide temporal characterization of the proteome and phosphoproteome of human embryonic stem cell differentiation.* Sci Signal, 2011. **4**(164): p. rs3.
415. Rappsilber, J., Mann, M., and Ishihama, Y., *Protocol for micro-purification, enrichment, pre-fractionation and storage of peptides for proteomics using StageTips.* Nat Protoc, 2007. **2**(8): p. 1896-1906.
416. Choe, L., D'Ascenzo, M., Relkin, N.R., Pappin, D., Ross, P., Williamson, B., Guertin, S., Pribil, P., and Lee, K.H., *8-plex quantitation of changes in cerebrospinal fluid protein expression in subjects undergoing intravenous immunoglobulin treatment for Alzheimer's disease.* Proteomics, 2007. **7**(20): p. 3651-3660.

417. Cox, J., Neuhauser, N., Michalski, A., Scheltema, R.A., Olsen, J.V., and Mann, M., *Andromeda: a peptide search engine integrated into the MaxQuant environment.* J Proteome Res, 2011. **10**(4): p. 1794-1805.
418. Huang da, W., Sherman, B.T., and Lempicki, R.A., *Systematic and integrative analysis of large gene lists using DAVID bioinformatics resources.* Nat Protoc, 2008. **4**(1): p. 44-57.
419. Thingholm, T.E., Jensen, O.N., Robinson, P.J., and Larsen, M.R., *SIMAC (sequential elution from IMAC), a phosphoproteomics strategy for the rapid separation of monophosphorylated from multiply phosphorylated peptides.* Mol Cell Proteomics, 2008. **7**(4): p. 661-671.
420. Lower, K.M. and Gecz, J., *Characterization of ARHGEF6, a guanine nucleotide exchange factor for Rho GTPases and a candidate gene for X‐linked mental retardation: Mutation screening in Börjeson‐Forssman‐Lehmann syndrome and MRX27.* Am J Med Genet, 2001. **100**(1): p. 43-48.
421. Yoshimura, S.-i., Gerondopoulos, A., Linford, A., Rigden, D.J., and Barr, F.A., *Family-wide characterization of the DENN domain Rab GDP-GTP exchange factors.* J Cell Biol, 2010. **191**(2): p. 367-381.
422. Côté, J.-F. and Vuori, K., *Identification of an evolutionarily conserved superfamily of DOCK180-related proteins with guanine nucleotide exchange activity.* J Cell Sci, 2002. **115**(Pt 24): p. 4901-4913.
423. Fukuda, M., *TBC proteins: GAPs for mammalian small GTPase Rab?* Biosci Rep, 2011. **31**(3): p. 159-168.
424. Kurachi, H., Wada, Y., Tsukamoto, N., Maeda, M., Kubota, H., Hattori, M., Iwai, K., and Minato, N., *Human SPA-1 gene product selectively expressed in lymphoid tissues is a specific GTPase-activating protein for Rap1 and Rap2 segregate expression profiles from a rap1GAP gene product.* J Biol Chem, 1997. **272**(44): p. 28081-28088.
425. Post, P.L., Bokoch, G.M., and Mooseker, M.S., *Human myosin-IXb is a mechanochemically active motor and a GAP for rho.* J Cell Sci, 1998. **111**(Pt 7): p. 941-950.
426. Fukui, K., Sasaki, T., Imazumi, K., Matsuura, Y., Nakanishi, H., and Takai, Y., *Isolation and characterization of a GTPase activating protein specific for the Rab3 subfamily of small G proteins.* J Biol Chem, 1997. **272**(8): p. 4655-4658.
427. Marklund, U., Brattsand, G., Osterman, O., Ohlsson, P., and Gullberg, M., *Multiple signal transduction pathways induce phosphorylation of serines 16, 25, and 38 of oncoprotein 18 in T lymphocytes.* J Biol Chem, 1993. **268**(34): p. 25671-25680.
428. Kamioka, Y., Fukuhara, S., Sawa, H., Nagashima, K., Masuda, M., Matsuda, M., and Mochizuki, N., *A novel dynamin-associating molecule, formin-binding protein 17, induces tubular membrane invaginations and participates in endocytosis.* J Biol Chem, 2004. **279**(38): p. 40091-40099.
429. Bai, S.W., Herrera-Abreu, M.T., Rohn, J.L., Racine, V., Tajadura, V., Suryavanshi, N., Bechtel, S., Wiemann, S., Baum, B., and Ridley, A.J., *Identification and characterization of a set of conserved and new regulators of cytoskeletal organization, cell morphology and migration.* BMC Biol, 2011. **9**(1): p. 54.
430. Eyers, C.E., McNeill, H., Knebel, A., Morrice, N., Arthur, S.J., Cuenda, A., and Cohen, P., *The phosphorylation of CapZ-interacting protein (CapZIP) by stress-activated protein kinases triggers its dissociation from CapZ.* Biochem J, 2005. **389**(Pt 1): p. 127-135.

431. Lafuente, E.M., van Puijenbroek, A.A., Krause, M., Carman, C.V., Freeman, G.J., Berezovskaya, A., Constantine, E., Springer, T.A., Gertler, F.B., and Boussiotis, V.A., *RIAM, an Ena/VASP and Profilin ligand, interacts with Rap1-GTP and mediates Rap1-induced adhesion.* Developmental cell, 2004. **7**(4): p. 585-595.
432. Belkina, N.V., Liu, Y., Hao, J.-J., Karasuyama, H., and Shaw, S., *LOK is a major ERM kinase in resting lymphocytes and regulates cytoskeletal rearrangement through ERM phosphorylation.* Proc Natl Acad Sci U S A, 2009. **106**(12): p. 4707-4712.
433. Sun, L., Deng, L., Ea, C.-K., Xia, Z.-P., and Chen, Z.J., *The TRAF6 ubiquitin ligase and TAK1 kinase mediate IKK activation by BCL10 and MALT1 in T lymphocytes.* Mol Cell, 2004. **14**(3): p. 289-301.
434. Moog-Lutz, C., Peterson, E.J., Lutz, P.G., Eliason, S., Cavé-Riant, F., Singer, A., Di Gioia, Y., Dmowski, S., Kamens, J., Cayre, Y.E., and Koretzky, G., *PRAM-1 is a novel adaptor protein regulated by retinoic acid (RA) and promyelocytic leukemia (PML)-RA receptor α in acute promyelocytic leukemia cells.* J Biol Chem, 2001. **276**(25): p. 22375-22381.
435. Wabnitz, G.H., Köcher, T., Lohneis, P., Stober, C., Konstandin, M.H., Funk, B., Sester, U., Wilm, M., Klemke, M., and Samstag, Y., *Costimulation induced phosphorylation of L‐plastin facilitates surface transport of the T cell activation molecules CD69 and CD25.* Eur J Immunol, 2007. **37**(3): p. 649-662.
436. Wu, Y., Zhan, L., Ai, Y., Hannigan, M., Gaestel, M., Huang, C.-K., and Madri, J.A., *MAPKAPK2-mediated LSP1 phosphorylation and FMLP-induced neutrophil polarization.* Biochem Biophys Res Commun, 2007. **358**(1): p. 170-175.
437. Hsu, J.-L., Huang, S.-Y., Chow, N.-H., and Chen, S.-H., *Stable-isotope dimethyl labeling for quantitative proteomics.* Anal Chem, 2003. **75**(24): p. 6843-6852.
438. Khosrovi-Eghbal, A., *Exploring the interaction environment of blood cells: proteomic analysis of platelet releasate and platelet-monocyte interaction*, in *Experimental Medicine*. 2012, University of British Columbia: Vancouver, Canada.
439. Qin, Z., *The use of THP-1 cells as a model for mimicking the function and regulation of monocytes and macrophages in the vasculature.* Atherosclerosis, 2012. **221**(1): p. 2-11.
440. Weng, S., Zemany, L., Standley, K.N., Novack, D.V., La Regina, M., Bernal-Mizrachi, C., Coleman, T., and Semenkovich, C.F., *β3 integrin deficiency promotes atherosclerosis and pulmonary inflammation in high-fat-fed, hyperlipidemic mice.* Proc Natl Acad Sci U S A, 2003. **100**(11): p. 6730-6735.
441. Shpilberg, O., Rabi, I., Schiller, K., Walden, R., Harats, D., Tyrrell, K., Coller, B., and Seligsohn, U., *Patients with Glanzmann thrombasthenia lacking platelet glycoprotein alpha(IIb)beta(3) (GPIIb/IIIa) and alpha(v)beta(3) receptors are not protected from atherosclerosis.* Circulation, 2002. **105**(9): p. 1044-1048.
442. Fine, K., Ashbrook, P., Brigden, L., Maldonado, J., and Didishelm, P., *Gel-filtered human platelets. Ultrastructure, function, and role of proteins in inhibition of aggregation by aspirin.* Am J Pathol, 1976. **84**(1): p. 11-24.

Appendices

Appendix A: Publication list

Zhang, C.-C. and Kast, J. **Applications of Current Proteomics Techniques in Modern Drug Design.** Curr. Comput. Aided Drug Des. 2010; 6(3):147-164.

Zhang, C.-C., Rogalski, J. C., Evans, D. M., Klockenbusch, C., Beavis, R. C., and Kast, J. ***In silico* Protein Interaction Analysis Using the Global Proteome Machine Database.** J Proteome Res. 2011; 10(2): 656-668.

Miao Q., **Zhang, C.-C.** and Kast, J. **Chemical Proteomics New Developments in Drug Design.** Expert Rev Proteomics. 2012; 9(3):281-91.

Zhang, C.-C., Lin, S.J., Rogalski, J. C., Liu, K., and Kast, J. **Development and Application of Quantitative Multiplexed Small GTPase Activity Assay Using Targeted Proteomics.** (Submitted)

Appendix B:

The 27 proteins identified for H2AFJ using *in silico* protein interaction analysis (sequence coverage≥18AA and log(e)≤-10 for H2AFJ, dataset size≤100 proteins, ProDis≥2 and frequency of occurrence≥20%).

f(%)	Accession	Description
100.0	H2AFJ	H2AFJ, H2A histone family, member J
74.0	sp|TRYP_PIG|	Trypsin precursor
71.2	KRT1	KRT1, Keratin, type II cytoskeletal 1
68.5	HIST4H4	HIST4H4, histone cluster 4, H4
61.6	ACTG1	ACTG1, actin, gamma 1
53.4	KRT10	KRT10, keratin 10
50.7	KRT9	KRT9, keratin 9
50.7	KRT2	KRT2, keratin 2
35.6	HIST1H2BB	HIST1H2BB, Histone H2B type 1-B
32.9	HIST1H1C	HIST1H1C, histone cluster 1, H1c
32.9	H3F3B	H3F3B, H3 histone, family 3B
30.1	VIM	VIM, Vimentin
27.4	sp|ALBU_BOVIN|	Serum albumin; BSA; Bos d 6; Flags: Precursor;
26.0	ENSP00000354403	H2BFS
26.0	KRT5	KRT5, keratin 5
24.7	HNRNPA2B1	HNRNPA2B1, Heterogeneous nuclear ribonucleoproteins A2/B1
24.7	sp|CAS1_BOVIN|	Alpha-S1-casein; Contains: Antioxidant peptide; Flags: Precursor;
24.7	H2AFV	H2AFV, Histone H2A.V
23.3	EEF1A2	EEF1A2, Elongation factor 1-alpha 2
23.3	HIST1H1B	HIST1H1B, histone cluster 1, H1b
23.3	HIST1H2BC	HIST1H2BC, histone cluster 1, H2bc
21.9	RPS13P8	RPS13P8, 40S ribosomal protein S13
21.9	H2AFX	H2AFX, Histone H2A.x
21.9	NPM1P21	NPM1P21, nucleophosmin
20.5	GAPDH	GAPDH, glyceraldehyde-3-phosphate dehydrogenase
20.5	KRT14	KRT14, keratin 14
20.5	TUBA1B	TUBA1B, tubulin, alpha 1b

Appendix C:

The 37 proteins identified for HIST1H2BB using *in silico* protein interaction analysis (sequence coverage≥18AA and log(e)≤-10 for HIST1H2BB, dataset size≤100 proteins, ProDis≥2 and frequency of occurrence≥20%).

f(%)	Accession	Description
100.0	HIST1H2BB	HIST1H2BB, histone cluster 1, H2bb
88.4	sp|TRYP_PIG|	Trypsin precursor
76.7	KRT1	KRT1, keratin 1
72.1	HIST4H4	HIST4H4, histone cluster 4, H4
69.8	KRT10	KRT10, keratin 10
69.8	KRT9	KRT9, keratin 9
65.1	KRT2	KRT2, keratin 2
58.1	KRT14	KRT14, keratin 14
53.5	sp|CAS1_BOVIN|	(P02662) Alpha-S1-casein precursor
51.2	KRT5	KRT5, keratin 5
51.2	GAPDH	GAPDH, glyceraldehyde-3-phosphate dehydrogenase
48.8	ACTG1	ACTG1, actin, gamma 1
44.2	sp|CASK_BOVIN|	(P02668) Kappa-casein precursor
39.5	sp|ALBU_BOVIN|	(P02769) Serum albumin precursor
37.3	ANXA2	ANXA2, annexin A2 pseudogene 1
37.2	VIM	VIM, vimentin
34.9	KRT16	KRT16, keratin 16
34.9	DCD	DCD, dermcidin
34.9	H2AFJ	H2AFJ, H2A histone family, member J
32.6	H3F3B	H3F3B, H3 histone, family 3B
30.2	sp|CASB_BOVIN|	(P02666) Beta-casein precursor
28.0	EEF1A2	EEF1A2, eukaryotic translation elongation factor 1 alpha 2
27.9	H2AFV	H2AFV, H2A histone family, member V
27.9	HRNR	HRNR, hornerin
27.9	sp|CAS2_BOVIN|	(P02663) Alpha-S2-casein precursor
27.9	BRD3	BRD3, bromodomain containing 3
25.6	HIST1H1C	HIST1H1C, histone cluster 1, H1c
23.3	KRT6C	KRT6C, keratin 6C
23.3	ENSP00000374990	IGHG1, immunoglobulin heavy constant gamma 1
23.3	FLG2	FLG2, filaggrin family member 2
23.3	ALB	ALB, albumin
21.0	KRT6A	KRT6A, keratin 6A
20.9	HIST1H4A	HIST1H4A, histone cluster 1, H4a
20.9	HIST1H1B	HIST1H1B, histone cluster 1, H1b
20.9	sp|K22E_HUMAN|	(P35908) Keratin, type II cytoskeletal 2 epidermal
20.9	S100A7	S100A7, S100 calcium binding protein A7
20.9	ACTB	ACTB, actin, beta

Appendix D:

The 73 proteins identified for H3F3B using *in silico* protein interaction analysis (sequence coverage≥18AA and log(e)≤-10 for H3F3B, dataset size≤100 proteins, ProDis≥2 and frequency of occurrence≥20%).

f(%)	HGNC	Description
100.0	H3F3B	H3F3B, H3 histone, family 3B
88.9	HIST4H4	HIST4H4, histone cluster 4, H4
88.9	sp|TRYP_PIG|	(P00761) Trypsin precursor (EC 3.4.21.4)
77.8	KRT1	KRT1, keratin 1
77.8	KRT10	KRT10, keratin 10
77.8	KRT9	KRT9, keratin 9
77.8	H2AFJ	H2AFJ, H2A histone family, member J
66.7	KRT2	KRT2, keratin 2
66.7	HIST1H2BB	HIST1H2BB, histone cluster 1, H2bb
66.6	RPS16	RPS16, ribosomal protein S16
55.6	HIST1H2BC	HIST1H2BC, histone cluster 1, H2bc
44.4	ACTG1	ACTG1, actin, gamma 1
44.4	H2AFV	H2AFV, H2A histone family, member V
44.4	KRT14	KRT14, keratin 14
33.3	VIM	VIM, vimentin
33.3	HIST1H1D	HIST1H1D, histone cluster 1, H1d
33.3	HIST1H2AB	HIST1H2AB, histone cluster 1, H2ab
33.3	HIST1H1B	HIST1H1B, histone cluster 1, H1b
33.3	RPS13	RPS13, ribosomal protein S13
33.3	RPL22	RPL22, ribosomal protein L22
33.3	H2AFX	H2AFX, H2A histone family, member X
33.3	sp|CAS1_BOVIN|	(P02662) Alpha-S1-casein precursor
33.3	H1F0	H1F0, H1 histone family, member 0
33.3	MYL6	MYL6, myosin, light chain 6, alkali, smooth muscle and non-muscle
33.3	RPS14	RPS14, ribosomal protein S14
33.3	RPS20	RPS20, ribosomal protein S20
33.3	UBA52	UBA52, ubiquitin A-52 residue ribosomal protein fusion product 1
33.3	DCD	DCD, dermcidin
33.3	HIST1H3A	HIST1H3A, histone cluster 1, H3a
33.3	sp|ALBU_BOVIN|	(P02769) Serum albumin precursor (Allergen Bos d 6) (BSA)
22.2	KRT8	KRT8, keratin 8
22.2	KRT77	KRT77, keratin 77
22.2	KRT19	KRT19, keratin 19
22.2	HNRNPC	HNRNPC, heterogeneous nuclear ribonucleoprotein C (C1/C2)
22.2	ENSP00000416110	40S ribosomal protein S18
22.2	TUBA1B	TUBA1B, tubulin, alpha 1b
22.2	ENSP00000202773	60S ribosomal protein L6
22.2	HNRNPU	HNRNPU, heterogeneous nuclear ribonucleoprotein U
22.2	HNRNPH1	HNRNPH1, heterogeneous nuclear ribonucleoprotein H1
22.2	DDX41	DDX41, DEAD (Asp-Glu-Ala-Asp) box polypeptide 41
22.2	FAU	FAU, Finkel-Biskis-Reilly murine sarcoma virus
22.2	RPS25	RPS25, ribosomal protein S25
22.2	RPL23A	RPL23A, small nucleolar RNA, C/D box 4A
22.2	RPS23	RPS23, ribosomal protein S23
22.2	SLC25A5	SLC25A5, solute carrier family 25
22.2	RPS19	RPS19, ribosomal protein S19
22.2	RPL11	RPL11, ribosomal protein L11
22.2	RPL27A	RPL27A, ribosomal protein L27a
22.2	RPL12	RPL12, ribosomal protein L12
22.2	BRD3	BRD3, bromodomain containing 3

22.2	KRT6C	KRT6C, keratin 6C
22.2	HIST2H2AA3	HIST2H2AA3, histone cluster 2, H2aa3
22.2	HIST2H2AB	HIST2H2AB, histone cluster 2, H2ab
22.2	MECP2	MECP2, methyl CpG binding protein 2
22.2	H1FX	H1FX, H1 histone family, member X
22.2	CSE1L	CSE1L, CSE1 chromosome segregation 1-like
22.2	sp|CASK_BOVIN|	(P02668) Kappa-casein precursor
22.2	ENSP00000374990	IGHG1, immunoglobulin heavy constant gamma 1
22.2	SEL1L	SEL1L, sel-1 suppressor of lin-12-like
22.2	ENSP00000374794	Immunoglobulin Kappa light chain V gene segment
22.2	RPLP2	RPLP2, ribosomal protein, large, P2
22.2	ENO1	ENO1, enolase 1
22.2	C19orf10	C19orf10, UPF0556 protein C19orf10 Precursor
22.2	SNRPD3	SNRPD3, small nuclear ribonucleoprotein D3 polypeptide 18kDa
22.2	ENSP00000378021	Peroxiredoxin-5, mitochondrial Precursor
22.2	TUBA8	TUBA8, tubulin, alpha 8
22.2	RPL31	RPL31, ribosomal protein L31
22.2	KRT5	KRT5, keratin 5
22.2	HRNR	HRNR, hornerin
22.2	HIST1H1C	HIST1H1C, histone cluster 1, H1c
22.2	H2AFY	H2AFY, H2A histone family, member Y
22.2	UHRF1	UHRF1, ubiquitin-like with PHD and ring finger domains 1
22.2	sp|PPIA_HUMAN|	(P62937) Peptidyl-prolyl cis-trans isomerase A

Appendix E:

The 72 proteins identified for PSMA1 using *in silico* protein interaction analysis (sequence coverage≥18AA and log(e)≤-10 for PSMA1, dataset size≤100 proteins, ProDis≥2 and frequency of occurrence≥20%).

f(%)	HGNC	Description
100.1	PSMA1	PSMA1, proteasome (prosome, macropain) subunit, alpha type, 1
66.7	HSPA8	HSPA8, heat shock 70kDa protein 8
66.7	TUBB3	TUBB3, melanocortin 1 receptor (alpha melanocyte stimulating hormone receptor)
50.0	FLNA	FLNA, filamin A, alpha
50.0	sp|ALBU_BOVIN|	(P02769) Serum albumin precursor (Allergen Bos d 6) (BSA)
50.0	FLNB	FLNB, filamin B, beta
50.0	PLEC1	PLEC1, plectin 1, intermediate filament binding protein 500kDa
50.0	DSP	DSP, desmoplakin
50.0	FASN	FASN, fatty acid synthase
50.0	VCL	VCL, vinculin
50.0	IQGAP1	IQGAP1, IQ motif containing GTPase activating protein 1
50.0	HARS	HARS, histidyl-tRNA synthetase
50.0	CDH13	CDH13, cadherin 13, H-cadherin (heart)
50.0	AHNAK	AHNAK, AHNAK nucleoprotein
50.0	SAE1	SAE1, SUMO1 activating enzyme subunit 1
50.0	CAD	CAD, carbamoyl-phosphate synthetase 2, aspartate transcarbamylase, and dihydroorotase
50.0	XRCC5	XRCC5, X-ray repair complementing defective repair in Chinese hamster cells 5
50.0	PRPF8	PRPF8, PRP8 pre-mRNA processing factor 8 homolog (S. cerevisiae)
50.0	SH3BGRL	SH3BGRL, SH3 domain binding glutamic acid-rich protein like
50.0	TUBB6	TUBB6, tubulin, beta 6
50.0	PGD	PGD, phosphogluconate dehydrogenase
50.0	NAP1L1	NAP1L1, nucleosome assembly protein 1-like 1
50.0	ANXA2	ANXA2, annexin A2 pseudogene 1
50.0	DDX18	DDX18, DEAD (Asp-Glu-Ala-Asp) box polypeptide 18
50.0	TRIM25	TRIM25, tripartite motif-containing 25
50.0	TAGLN2	TAGLN2, transgelin 2
50.0	DDT	DDT, D-dopachrome tautomerase
50.0	PPP2CB	PPP2CB, protein phosphatase 2 (formerly 2A), catalytic subunit, beta isoform
50.0	S100A4	S100A4, S100 calcium binding protein A4
50.0	HDGF	HDGF, hepatoma-derived growth factor (high-mobility group protein 1-like)
50.0	C3orf37	C3orf37, UPF0361 protein DC12
50.0	SFN	SFN, stratifin
50.0	KRT5	KRT5, keratin 5
50.0	ENO1	ENO1, enolase 1, (alpha)
50.0	GCN1L1	GCN1L1, GCN1 general control of amino-acid synthesis 1-like 1 (yeast)
50.0	SET	SET, SET nuclear oncogene
50.0	ENSP00000379748	PDCD6IP, Programmed cell death 6-interacting protein (PDCD6-interacting protein)
50.0	TBCA	TBCA, tubulin folding cofactor A
50.0	PAICS	PAICS, phosphoribosylaminoimidazole carboxylase, phosphoribosylaminoimidazole succinocarboxamide synthetase
50.0	MATR3	MATR3, matrin 3
50.0	ACOT7	ACOT7, acyl-CoA thioesterase 7
50.0	EHD2	EHD2, EH-domain containing 2
50.0	SAPS3	SAPS3, SAPS domain family, member 3
50.0	TPM1	TPM1, tropomyosin 1 (alpha)
50.0	ENSP00000351238	Peptidyl-prolyl cis-trans isomerase A (EC 5.2.1.8) (PPIase A)
33.3	P4HB	P4HB, prolyl 4-hydroxylase, beta polypeptide
33.3	MYH9	MYH9, myosin, heavy chain 9, non-muscle
33.3	RPLP2	RPLP2, ribosomal protein, large, P2
33.3	ANXA5	ANXA5, annexin A5
33.3	PLS3	PLS3, plastin 3 (T isoform)
33.3	ATP5A1	ATP5A1, ATP synthase, H+ transporting, mitochondrial F1 complex, alpha subunit 1, cardiac muscle

33.3	ENSP00000221801	rRNA 2'-O-methyltransferase fibrillarin (EC 2.1.1.-) (34 kDa nucleolar scleroderma antigen)
33.3	DNAJB1	DNAJB1, DnaJ (Hsp40) homolog, subfamily B, member 1
33.3	RPS8	RPS8, small nucleolar RNA, C/D box 55
33.3	ENSP00000202773	60S ribosomal protein L6 (TAX-responsive enhancer element-binding protein 107)(TAXREB107)(Neoplasm-related protein C140)
33.3	NME1	NME1, non-metastatic cells 1, protein (NM23A) expressed in
33.3	ACTN4	ACTN4, actinin, alpha 4
33.3	DYNC1I2	DYNC1I2, dynein, cytoplasmic 1, intermediate chain 2
33.3	PGK1	PGK1, phosphoglycerate kinase 1
33.3	PLIN3	PLIN3, perilipin 3
33.3	SPTAN1	SPTAN1, spectrin, alpha, non-erythrocytic 1 (alpha-fodrin)
33.3	S100A11	S100A11, S100 calcium binding protein A11
33.3	AHCY	AHCY, adenosylhomocysteinase
33.3	ENSP00000368515	RPL9P7, 60S ribosomal protein L9.
33.3	SKIV2L2	SKIV2L2, superkiller viralicidic activity 2-like 2 (S. cerevisiae)
33.3	PYGB	PYGB, phosphorylase, glycogen; brain
33.3	RPL13A	RPL13A, small nucleolar RNA, C/D box 32A
33.3	TXN	TXN, thioredoxin
33.3	GSTO1	GSTO1, glutathione S-transferase omega 1
33.3	TKT	TKT, transketolase
33.3	PA2G4	PA2G4, proliferation-associated 2G4, 38kDa

Appendix F:

The 88 proteins identified for all PSMA1, PSMA2, PSMA3, PSMA4, PSMA5, PSMA6 and PSMA7 using *in silico* protein interaction analysis (sequence coverage≥18AA and log(e)≤-10 for the protein of interest, dataset size≤350 proteins, ProDis≥2 and frequency of occurrence≥15%).

HGNC	Description
ACLY	ACLY, ATP citrate lyase
ACTB	ACTB, actin, beta
ACTG1	ACTG1, actin, gamma 1
ACTN4	ACTN4, actinin, alpha 4
ALDH1A1	ALDH1A1, aldehyde dehydrogenase 1 family, member A1
ALDOA	ALDOA, aldolase A, fructose-bisphosphate
ANXA2	ANXA2, annexin A2 pseudogene 1
APEH	APEH, N-acylaminoacyl-peptide hydrolase
ATP5A1	ATP5A1, ATP synthase, H+ transporting, mitochondrial F1 complex, alpha subunit 1, cardiac muscle
ATP5B	ATP5B, ATP synthase, H+ transporting, mitochondrial F1 complex, beta polypeptide
CA2	CA2, carbonic anhydrase II
CALM3	CALM3, calmodulin 3 (phosphorylase kinase, delta)
CAP1	CAP1, CAP, adenylate cyclase-associated protein 1 (yeast)
CCT2	CCT2, chaperonin containing TCP1, subunit 2 (beta)
CCT3	CCT3, chaperonin containing TCP1, subunit 3 (gamma)
CCT4	CCT4, chaperonin containing TCP1, subunit 4 (delta)
CCT5	CCT5, chaperonin containing TCP1, subunit 5 (epsilon)
CCT6A	CCT6A, chaperonin containing TCP1, subunit 6A (zeta 1)
CCT7	CCT7, chaperonin containing TCP1, subunit 7 (eta)
CCT8	CCT8, chaperonin containing TCP1, subunit 8 (theta)
CFL1	CFL1, cofilin 1 (non-muscle)
CLTC	CLTC, clathrin, heavy chain (Hc)
EEF2	EEF2, eukaryotic translation elongation factor 2
EIF4A1	EIF4A1, eukaryotic translation initiation factor 4A, isoform 1
EIF5A	EIF5A, eukaryotic translation initiation factor 5A-like 1
ENO1	ENO1, enolase 1, (alpha)
FASN	FASN, fatty acid synthase
FLNA	FLNA, filamin A, alpha
GAPDH	GAPDH, glyceraldehyde-3-phosphate dehydrogenase
HBA2	HBA2, hemoglobin, alpha 2
HBB	HBB, hemoglobin, beta
HSP90AA1	HSP90AA1, heat shock protein 90kDa alpha (cytosolic), class A member 1
HSP90AB1	HSP90AB1, heat shock protein 90kDa alpha (cytosolic), class B member 1
HSPA5	HSPA5, heat shock 70kDa protein 5 (glucose-regulated protein, 78kDa)
HSPA8	HSPA8, heat shock 70kDa protein 8
HSPD1	HSPD1, heat shock 60kDa protein 1 (chaperonin)
KPNB1	KPNB1, karyopherin (importin) beta 1
LDHA	LDHA, lactate dehydrogenase A
MYH9	MYH9, myosin, heavy chain 9, non-muscle
NACA	NACA, nascent polypeptide-associated complex alpha subunit 2
NAP1L1	NAP1L1, nucleosome assembly protein 1-like 1
NCL	NCL, nucleolin
PDIA3	PDIA3, protein disulfide isomerase family A, member 3
PFN1	PFN1, profilin 1
PKM2	PKM2, pyruvate kinase, muscle
PRDX1	PRDX1, peroxiredoxin 1
PRDX2	PRDX2, peroxiredoxin 2
PSMA1	PSMA1, proteasome (prosome, macropain) subunit, alpha type, 1
PSMA2	PSMA2, proteasome (prosome, macropain) subunit, alpha type, 2
PSMA3	PSMA3, proteasome (prosome, macropain) subunit, alpha type, 3

PSMA4	PSMA4, proteasome (prosome, macropain) subunit, alpha type, 4
PSMA5	PSMA5, proteasome (prosome, macropain) subunit, alpha type, 5
PSMA6	PSMA6, proteasome (prosome, macropain) subunit, alpha type, 6
PSMA7	PSMA7, proteasome (prosome, macropain) subunit, alpha type, 7
PSMB1	PSMB1, proteasome (prosome, macropain) subunit, beta type, 1
PSMB2	PSMB2, proteasome (prosome, macropain) subunit, beta type, 2
PSMB3	PSMB3, proteasome (prosome, macropain) subunit, beta type, 3
PSMB4	PSMB4, proteasome (prosome, macropain) subunit, beta type, 4
PSMB5	PSMB5, proteasome (prosome, macropain) subunit, beta type, 5
PSMB6	PSMB6, proteasome (prosome, macropain) subunit, beta type, 6
PSMB7	PSMB7, proteasome (prosome, macropain) subunit, beta type, 7
PSMD2	PSMD2, proteasome (prosome, macropain) 26S subunit, non-ATPase, 2
PSME1	PSME1, proteasome (prosome, macropain) activator subunit 1 (PA28 alpha)
PSME2	PSME2, proteasome (prosome, macropain) activator subunit 2 (PA28 beta)
PTGES3	PTGES3, prostaglandin E synthase 3 (cytosolic)
RAB1B	RAB1B, RAB1B, member RAS oncogene family
RAN	RAN, RAN, member RAS oncogene family
RPLP2	RPLP2, ribosomal protein, large, P2
RPS17	RPS17, ribosomal protein S17
RUVBL1	RUVBL1, RuvB-like 1 (E. coli)
ST13	ST13, suppression of tumorigenicity 13 (colon carcinoma) (Hsp70 interacting protein)
TCP1	TCP1, small nucleolar RNA, H/ACA box 29
TPI1	TPI1, triosephosphate isomerase 1
TPM3	TPM3, tropomyosin 3
TPM4	TPM4, tropomyosin 4
TUBB2C	TUBB2C, tubulin, beta 2C
TUT1	TUT1, terminal uridylyl transferase 1, U6 snRNA-specific
TXN	TXN, thioredoxin
UBA1	UBA1, ubiquitin-like modifier activating enzyme 1
UBA52	UBA52, ubiquitin A-52 residue ribosomal protein fusion product 1
USP5	USP5, ubiquitin specific peptidase 5 (isopeptidase T)
VCP	VCP, valosin-containing protein
XRCC5	XRCC5, X-ray repair complementing defective repair in Chinese hamster cells 5 (double-strand-break rejoining)
YWHAB	YWHAB, tyrosine 3-monooxygenase/tryptophan 5-monooxygenase activation protein, beta polypeptide
YWHAE	YWHAE, tyrosine 3-monooxygenase/tryptophan 5-monooxygenase activation protein, epsilon polypeptide
YWHAG	YWHAG, tyrosine 3-monooxygenase/tryptophan 5-monooxygenase activation protein, gamma polypeptide
YWHAQ	YWHAQ, tyrosine 3-monooxygenase/tryptophan 5-monooxygenase activation protein, theta polypeptide
YWHAZ	YWHAZ, tyrosine 3-monooxygenase/tryptophan 5-monooxygenase activation protein, zeta polypeptide

Appendix G:

The 33 proteins identified for talin1 using *in silico* protein interaction analysis (sequence coverage≥18AA and log(e)≤-10 for talin1, dataset size≤110 proteins, ProDis≥2 and frequency of occurrence≥20%).

f(%)	Accession	Description
100.0	TLN1	TLN1, talin 1
81.6	FLNA	FLNA, filamin A, alpha
77.3	MYH9	MYH9, myosin, heavy chain 9, non-muscle
69.8	THBS1	THBS1, thrombospondin 1
52.8	ACTN1	ACTN1, actinin, alpha 1
46.3	ACTG1	ACTG1, actin, gamma 1
45.4	FERMT3	FERMT3, fermitin family homolog 3
42.3	GAPDH	GAPDH, glyceraldehyde-3-phosphate dehydrogenase
40.6	ITGA2B	ITGA2B, integrin, alpha 2b
39.7	sp|TRYP_PIG|	Trypsin precursor
36.7	F13A1	F13A1, coagulation factor XIII, A1 polypeptide
35.8	GSN	GSN, gelsolin
35.4	PPBP	PPBP, pro-platelet basic protein
33.6	PKM2	PKM2, pyruvate kinase, muscle
33.2	PLEK	PLEK, pleckstrin
31.9	ENSP00000277829	Vinculin
30.5	MMRN1	MMRN1, multimerin 1
30.1	ACTB	ACTB, actin, beta
29.7	ITGB3	ITGB3, integrin, beta 3
29.7	TUBB1	TUBB1, tubulin, beta 1
28.8	KRT1	KRT1, keratin 1
28.4	ENSP00000309775	TAGLN2, Transgelin-2
28.4	PFN1	PFN1, profilin 1
27.9	TPM4	TPM4, tropomyosin 4
25.3	LIMS1	LIMS1, LIM and senescent cell antigen-like domains 1
24.9	CFL1	CFL1, cofilin 1
24.5	ZYX	ZYX, zyxin
23.6	TUBA4A	TUBA4A, tubulin, alpha 4a
23.6	FGA	FGA, fibrinogen alpha chain
23.2	GP1BA	GP1BA, glycoprotein Ib (platelet), alpha polypeptide
23.2	FGG	FGG, fibrinogen gamma chain
22.3	RAP1B	RAP1B, RAP1B, member of RAS oncogene family
20.1	ALDOA	ALDOA, aldolase A, fructose-bisphosphate

Appendix H:

The 50 proteins identified for FERMT3 using *in silico* protein interaction analysis (sequence coverage≥18AA and log(e)≤-10 for FERMT3, dataset size≤110 proteins, ProDis≥2 and frequency of occurrence≥20%).

f(%)	Accession	Description
100.0	FERMT3	FERMT3, fermitin family homolog 3
92.5	THBS1	THBS1, thrombospondin 1
90.3	FLNA	FLNA, filamin A, alpha
78.3	MYH9	MYH9, myosin, heavy chain 9, non-muscle
63.4	F13A1	F13A1, coagulation factor XIII, A1 polypeptide
59.7	ACTN1	ACTN1, actinin, alpha 1
58.2	ITGA2B	ITGA2B, integrin, alpha 2b
57.5	TLN1	TLN1, talin 1
54.5	TUBB1	TUBB1, tubulin, beta 1
54.5	sp|TRYP_PIG|	Trypsin precursor
53.7	GAPDH	GAPDH, glyceraldehyde-3-phosphate dehydrogenase
52.2	ACTB	ACTB, actin, beta
48.5	ACTG1	ACTG1, actin, gamma 1
45.5	ITGB3	ITGB3, integrin, beta 3
44.8	MMRN1	MMRN1, multimerin 1
44.0	PKM2	PKM2, pyruvate kinase, muscle
43.2	LIMS1	LIMS1, LIM and senescent cell antigen-like domains 1
41.1	GSN	GSN, gelsolin
36.6	FGA	FGA, fibrinogen alpha chain
35.1	TUBA4A	TUBA4A, tubulin, alpha 4a
35.1	RAP1B	RAP1B, RAP1B, member of RAS oncogene family
35.1	PLEK	PLEK, pleckstrin
32.8	TPM4	TPM4, tropomyosin 4
31.4	ZYX	ZYX, zyxin
30.6	CFL1	CFL1, cofilin 1
30.6	PPBP	PPBP, pro-platelet basic protein
30.6	PFN1	PFN1, profilin 1
29.8	FGG	FGG, fibrinogen gamma chain
29.1	GP1BA	GP1BA, glycoprotein Ib (platelet), alpha polypeptide
28.4	SDPR	SDPR, serum deprivation response
28.4	KRT1	KRT1, keratin 1
26.9	VCL	VCL, vinculin
26.9	RSU1	RSU1, Ras suppressor protein 1
26.2	MYL6	MYL6, myosin, light chain 6, alkali, smooth muscle and non-muscle
26.1	TUBA1B	TUBA1B, tubulin, alpha 1b
26.1	MYL12A	MYL12A, myosin, light chain 12A, regulatory, non-sarcomeric
25.3	WDR1	WDR1, WD repeat domain 1
24.7	PARVB	PARVB, parvin, beta
24.6	YWHAE	YWHAE, tyrosine 3-monooxygenase/tryptophan 5-monooxygenase activation protein, epsilon polypeptide
24.6	ENSP00000277829	Vinculin
23.9	LDHB	LDHB, lactate dehydrogenase B
23.9	ENSP00000309775	TAGLN2, Transgelin-2
22.4	PF4	PF4, platelet factor 4
22.4	ALDOA	ALDOA, aldolase A, fructose-bisphosphate
22.3	TAGLN2	TAGLN2, transgelin 2
21.6	ACTN4	ACTN4, actinin, alpha 4
21.6	ENSP00000322781	No Description
20.9	TPM3	TPM3, tropomyosin 3
20.8	STOM	STOM, stomatin
20.1	VWF	VWF, von Willebrand factor

Appendix I:

The 72 proteins identified for Rap1b using *in silico* protein interaction analysis (sequence coverage≥18AA and log(e)≤-10 for Rap1b, dataset size≤110 proteins, ProDis≥2 and frequency of occurrence≥20%).

f(%)	Accession	Description
100.0	RAP1B	RAP1B, RAP1B, member of RAS oncogene family
84.0	FLNA	FLNA, filamin A, alpha
81.1	TLN1	TLN1, talin 1
79.7	THBS1	THBS1, thrombospondin 1
79.7	FERMT3	FERMT3, fermitin family homolog 3
68.1	GAPDH	GAPDH, glyceraldehyde-3-phosphate dehydrogenase
66.7	MYH9	MYH9, myosin, heavy chain 9, non-muscle
65.2	TUBB1	TUBB1, tubulin, beta 1
62.3	F13A1	F13A1, coagulation factor XIII, A1 polypeptide
62.3	ITGB3	ITGB3, integrin, beta 3
60.9	ACTG1	ACTG1, actin, gamma 1
60.8	PKM2	PKM2, pyruvate kinase, muscle
57.9	ITGA2B	ITGA2B, integrin, alpha 2b
55.1	TAGLN2	TAGLN2, transgelin 2
55.1	LIMS1	LIMS1, LIM and senescent cell antigen-like domains 1
53.6	CFL1	CFL1, cofilin 1
53.5	FGG	FGG, fibrinogen gamma chain
52.2	ACTB	ACTB, actin, beta
50.7	GSN	GSN, gelsolin
50.7	PFN1	PFN1, profilin 1
49.3	sp|TRYP_PIG|	Trypsin precursor
49.3	ACTN1	ACTN1, actinin, alpha 1
47.8	FGA	FGA, fibrinogen alpha chain
46.4	MYL12A	MYL12A, myosin, light chain 12A, regulatory, non-sarcomeric
46.4	PPBP	PPBP, pro-platelet basic protein
46.4	PLEK	PLEK, pleckstrin
44.9	LDHB	LDHB, lactate dehydrogenase B
43.4	TUBA4A	TUBA4A, tubulin, alpha 4a
42.0	TUBA1B	TUBA1B, tubulin, alpha 1b
39.1	PF4	PF4, platelet factor 4
37.6	MYL6	MYL6, myosin, light chain 6, alkali, smooth muscle and non-muscle
36.2	ALDOA	ALDOA, aldolase A, fructose-bisphosphate
36.2	HBB	HBB, hemoglobin, beta
34.8	TPM4	TPM4, tropomyosin 4
33.3	MMRN1	MMRN1, multimerin 1
30.4	GP9	GP9, glycoprotein IX
30.4	SDPR	SDPR, serum deprivation response
30.4	ENSP00000309775	TAGLN2, Transgelin-2
29.0	MYL9	MYL9, myosin, light chain 9, regulatory
29.0	YWHAZ	YWHAZ, tyrosine 3-monooxygenase/tryptophan 5-monooxygenase activation protein, zeta polypeptide
29.0	GP1BA	GP1BA, glycoprotein Ib
28.9	CSRP1	CSRP1, cysteine and glycine-rich protein 1
27.5	ZYX	ZYX, zyxin
27.5	FGB	FGB, fibrinogen beta chain
27.5	WDR1	WDR1, WD repeat domain 1
27.5	PDIA3	PDIA3, protein disulfide isomerase family A, member 3
27.4	CAP1	CAP1, CAP, adenylate cyclase-associated protein 1
26.1	RAC2	RAC2, ras-related C3 botulinum toxin substrate 2
26.1	KRT1	KRT1, keratin 1
26.1	YWHAE	YWHAE, tyrosine 3-monooxygenase/tryptophan 5-monooxygenase activation protein, epsilon polypeptide

26.1	RSU1	RSU1, Ras suppressor protein 1
24.6	PPIB	PPIB, peptidylprolyl isomerase B
24.6	HBA2	HBA2, hemoglobin, alpha 2
24.6	GP1BB	GP1BB, glycoprotein Ib (platelet), beta polypeptide
24.6	ENSP00000277829	Vinculin
24.6	PARVB	PARVB, parvin, beta
23.2	KRT9	KRT9, keratin 9
23.2	ENSP00000259925	Tubulin beta chain
23.2	TPM3	TPM3, tropomyosin 3
23.1	CNN2	CNN2, calponin 2
23.1	STOM	STOM, stomatin
21.7	ARPC3	ARPC3, actin related protein 2/3 complex, subunit 3, 21kDa
21.7	RAB7A	RAB7A, RAB7A, member RAS oncogene family
21.7	ARHGDIB	ARHGDIB, Rho GDP dissociation inhibitor (GDI) beta
21.7	CDC42	CDC42, cell division cycle 42
21.7	ACTN4	ACTN4, actinin, alpha 4
21.7	RAB11B	RAB11B, RAB11B, member RAS oncogene family
21.7	VCL	VCL, vinculin
21.7	ENSP00000265995	PDLIM1, PDZ and LIM domain protein 1
20.3	DUSP3	DUSP3, dual specificity phosphatase 3
20.3	ENSP00000322781	No Description
20.3	MTPN	MTPN, leucine zipper protein 6

Appendix J:

a. The 12 proteins identified in the integrin β 1 complexes in activated and formaldehyde treated platelets by LC-MS/MS (Experiment 1). Proteins were identified by the GPM and confirmed by MASCOT.

Protein information		GPM information						Mascot
Accession	Description	log(e)	log(I)	% (measured)	% (corrected)	unique	total	Score
ITGB1	integrin, beta 1	-162	5.16	18	36	17	32	582
ITGA2	integrin, alpha 2	-114.7	4.85	14	30	13	17	329
ITGA6	integrin, alpha 6	-364.4	5.45	35	49	32	51	1518
ITGA2B	integrin, alpha 2b	-43.5	4.35	5.5	10	5	8	284
ITGB3	integrin, beta 3	-6.6	3.9	1.4	2	1	2	104
ACTG1	actin, gamma 1	-2.9	3.71	2.4	3	1	2	55
TLN1	talin 1	-243.8	5.18	13	17	25	39	1215
FERMT3	fermitin family homolog 3	-11	3.61	1.8	2	1	2	76
FLNA	filamin A, alpha	-79.9	4.63	4.2	6	10	12	247
VCL	vinculin	-4	3.53	0.9	1	1	1	55
DCD	dermcidin	-3.5	3.54	9.1	16	1	1	47
TUFM	tu translation elongation factor, mitochondrial	-2.1	3.58	1.3	2	1	1	30

b. The 12 proteins identified in the integrin β 1 complexes in activated and formaldehyde treated platelets by LC-MS/MS (Experiment 2). Proteins were identified by the GPM and confirmed by MASCOT.

Protein information		GPM information						Mascot
Accession	Description	log(e)	log(I)	% (measured)	% (corrected)	unique	total	Score
ITGB1	integrin, beta 1	-261.7	5.74	30	59	27	65	1237
ITGA2	integrin, alpha 2	-316.7	5.48	26	55	29	61	1603
ITGA6	integrin, alpha 6	-580.2	6.1	48	68	47	111	3377
ITGA2B	integrin, alpha 2b	-91.3	4.76	11	19	9	15	551
ITGB3	integrin, beta 3	-62.6	4.71	11	17	7	11	319
ACTG1	actin, gamma 1	-23.8	4.51	9.1	10	4	6	147
TLN1	talin 1	-243.8	5.18	13	17	25	39	1215
FERMT3	fermitin family homolog 3	-415.2	5.38	22	30	39	57	1758
FLNA	filamin A, alpha	-242	5.12	11	16	24	33	975
VCL	vinculin	-34.1	4.28	4.9	6	5	5	131
DCD	dermcidin	-2.9	3.5	9.1	16	1	1	56
TUFM	tu translation elongation factor, mitochondrial	-2.3	4.27	1.3	2	1	3	39

Appendix K:

The seven and 18 proteins for integrin β1 using *in silico* protein interaction analysis with frequency of occurrence of ≥20% and ≥10% respectively (sequence coverage≥18AA and log(e)≤-10 for integrin β1, dataset size≤50 proteins and ProDis≥2).

f(%)	Accession	Description
100.0	ITGB1	ITGB1, integrin, beta 1
45.2	ITGA5	ITGA5, integrin, alpha 5
27.5	ITGA6	ITGA6, integrin, alpha 6
27.5	ITGA2B	ITGA2B, integrin, alpha 2b
27.4	FLNA	FLNA, filamin A, alpha
25.8	ACTG1	ACTG1, actin, gamma 1
21.0	ITGA2	ITGA2, integrin, alpha 2
21.0	ITGB3	ITGB3, integrin, beta 3
19.3	THBS1	THBS1, thrombospondin 1
16.2	ITGA4	ITGA4, integrin, alpha 4
14.5	GP1BA	GP1BA, glycoprotein Ib
14.5	MMRN1	MMRN1, multimerin 1
12.9	DCD	DCD, dermcidin
12.9	TLN1	TLN1, Talin-1
12.9	FERMT3	FERMT3, fermitin family homolog 3
12.9	MYH9	MYH9, myosin, heavy chain 9, non-muscle
11.3	VIM	VIM, vimentin
11.3	EEF1A2	EEF1A2, eukaryotic translation elongation factor 1 alpha 2
11.3	AHNAK	AHNAK, AHNAK nucleoprotein

Appendix L:

The 28 human integrin β1 interaction partners obtained using the STRING database with the confidence score cutoff>0.950, based on the active prediction methods of "Experiments" and "Databases".

Confidence score	Accession	Description
0.999	ITGA3	Integrin alpha-3 precursor
0.999	ITGA6	Integrin alpha-6 precursor
0.999	ITGA1	Integrin alpha-1 precursor
0.999	ITGA2	Integrin alpha-2 precursor
0.999	ITGA9	Integrin alpha-9 precursor
0.999	ITGA11	Integrin alpha-11 precursor
0.999	ITGA5	Integrin alpha-5 precursor
0.999	ITGA8	Integrin alpha-8 precursor
0.999	ITGAV	Integrin alpha-V precursor
0.999	ITGA4	Integrin alpha-4 precursor
0.999	ITGA10	Integrin alpha-10 precursor
0.998	ITGA7	Integrin alpha-7 precursor
0.996	CD9	CD9 antigen
0.994	FLNA	Filamin-A
0.983	ILK	Integrin-linked protein kinase
0.966	PRKCA	Protein kinase C alpha type
0.961	CRKL	Crk-like protein
0.961	FN1	Fibronectin precursor
0.961	TLN1	Talin-1
0.961	VCAM1	Vascular cell adhesion protein 1 precursor
0.961	FLT4	Vascular endothelial growth factor receptor 3 precursor
0.961	ACTN4	Alpha-actinin-4
0.961	PXN	Paxillin
0.961	ACTN1	Alpha-actinin-1
0.959	PTK2	Focal adhesion kinase 1
0.957	LAMA1	Laminin subunit alpha-1 precursor
0.957	SPP1	Osteopontin precursor
0.957	COL1A1	Collagen alpha-1(I) chain precursor

Appendix M:

The 57 human integrin β 1 interaction partners obtained using BioGRID.

Interactor	Experimental System	Author	Pubmed ID
ACTN1	Reconstituted Complex	Otey CA (1990)	2116421
CANX	Affinity Capture-Western	Lenter M (1994)	8163531
CD151	Affinity Capture-Western	Mazzocca A (2002)	12175627
CD36	Affinity Capture-Western	Miao WM (2001)	11238109
CD46	Affinity Capture-Western	Lozahic S (2000)	10741407
CD46	Affinity Capture-Western	Lozahic S (2000)	10741407
CD47	Affinity Capture-Western	Chung J (1999)	10397731
CD63	Affinity Capture-Western	Mazzocca A (2002)	12175627
CD81	Affinity Capture-Western	Serru V (1999)	10229664
CD81	Affinity Capture-Western	Mazzocca A (2002)	12175627
CD9	Affinity Capture-Western	Radford KJ (1996)	8630057
CD9	Affinity Capture-Western	Mazzocca A (2002)	12175627
COL1A1	Co-purification	Staatz WD (1990)	2156854
FBXO2	Affinity Capture-Western	Yoshida Y (2002)	12140560
FHL2	Two-hybrid	Wixler V (2000)	10906324
FHL2	Affinity Capture-Western	Wixler V (2000)	10906324
FLNA	Two-hybrid	van der Flier A (2002)	11807098
FLNA	Reconstituted Complex	van der Flier A (2002)	11807098
FLNA	Two-hybrid	Loo DT (1998)	9722563
FLNA	Reconstituted Complex	Loo DT (1998)	9722563
FLNA	Affinity Capture-Western	Loo DT (1998)	9722563
FLNB	Two-hybrid	van der Flier A (2002)	11807098
FLNB	Reconstituted Complex	van der Flier A (2002)	11807098
FLT4	Affinity Capture-Western	Wang JF (2001)	11553610
GNB2L1	Affinity Capture-Western	Liliental J (1998)	9442085
GNB2L1	Affinity Capture-Western	Lee HS (2002)	12435334
ILK	Affinity Capture-Western	Hannigan GE (1996)	8538749
ITGA10	Affinity Capture-Western	Camper L (1998)	9685391
ITGA3	Reconstituted Complex	Dorfleutner A (2004)	15254262
ITGA6	Affinity Capture-Western	Schaapveld RQ (1998)	9660880
ITGA8	Affinity Capture-Western	Schnapp LM (1995)	7768999
ITGA9	Affinity Capture-Western	Palmer EL (1993)	8245132
ITGB1BP1	Reconstituted Complex	Chang DD (1997)	9281591
ITGB1BP1	Affinity Capture-Western	Chang DD (1997)	9281591
ITGB1BP1	Reconstituted Complex	Chang DD (2002)	11741908
LAMA1	Reconstituted Complex	Ettner N (1998)	9688542
LGALS8	Affinity Capture-Western	Hadari YR (2000)	10852818
LGALS8	Reconstituted Complex	Hadari YR (2000)	10852818
MAP4K4	Two-hybrid	Poinat P (2002)	11967148
MAP4K4	Reconstituted Complex	Poinat P (2002)	11967148
MAP4K4	Affinity Capture-Western	Poinat P (2002)	11967148
NME1	Affinity Capture-Western	Fournier HN (2002)	11919189
NME1	Two-hybrid	Fournier HN (2002)	11919189
PRKCA	Affinity Capture-Western	Lee HS (2002)	12435334
PRKCA	Affinity Capture-Western	Parsons M (2002)	12138200
PTK2	Reconstituted Complex	Schaller MD (1995)	7657702
PXN	Reconstituted Complex	Schaller MD (1995)	7657702
PXN	Affinity Capture-Western	Chen LM (2000)	10804218
RAB8B	Affinity Capture-Western	Lau AS (2003)	12639940
SLC3A2	Affinity Capture-Western	Rintoul RC (2002)	12181350
TGOLN2	Affinity Capture-Western	Wang J (2000)	11208159
TLN1	Protein-peptide	Martel V (2001)	11279249
TSPAN4	Affinity Capture-Western	Tachibana I (1997)	9360996
TSPAN4	Affinity Capture-Western	Tachibana I (1997)	9360996
YWHAB	Affinity Capture-Western	Han DC (2001)	11313964
YWHAB	Two-hybrid	Han DC (2001)	11313964
YWHAB	Reconstituted Complex	Han DC (2001)	11313964